The Sonic Hedgehog and Wnt Signalling Pathways in Interstitial Lung Disease and $CD4^+$ T cell activation

Gareth Alexander Stewart

A thesis submitted for the degree of Doctor of Philosophy

University of Edinburgh, 2003
Edinburgh University Medical School

Abstract

The Sonic Hedgehog (Shh) signalling pathway plays an important role in lung development where it promotes branching morphogenesis through epithelial-mesenchymal interactions. Increased Shh expression promotes epithelial and mesenchymal proliferation *in vitro* and *in vivo*. TGFβ is also expressed in embryonic lung where it acts to inhibit branching morphogenesis. TGFβ overexpression results in lung hypoplasia, a similar phenotype to that seen in $Shh^{-/-}$ mutants; suggesting that Shh and TGFβ have opposing roles. Evidence to date would suggest that although TGFβ and Shh may not directly interact in lung development, they probably have common targets and may function in a shared regulatory circuit.

Interstitial lung disease (ILD) is the end result of a multiplicity of pathological processes. It has been recently proposed that the commonest form, Idiopathic Pulmonary Fibrosis (IPF) or Usual Interstitial Pneumonia (UIP), is due to abnormal wound healing in the lung, characterized by epithelial-fibroblast interactions; a process similar to foetal lung branching and epithelialization. TGFβ has been strongly linked with ILD in both animal models and human disease. Based on the link between TGFβ and Shh in lung morphogenesis, the initial aim of this thesis was to determine whether or not Shh signalling was upregulated in ILD. The work presented confirms that Shh and TGFβ expression are increased in the airway epithelium of fibrotic but not non-fibrotic lung both in the murine FITC model of ILD and in biopsy sections from patients with IPF. Expression of Patched (Ptc), the Shh receptor, is unchanged in epithelial cells. Notably, Ptc is present both in alveolar macrophages and lymphocytic infiltrates. However, there is no discernible difference in the fibrotic response in the lungs of mice containing heterozygous mutations of *Gli2* and *3*, used as models of dysregulated Shh signalling, nor in mice treated with intra-tracheal SPC-Shh cDNA.

The Shh pathway has recently been shown to play a role in thymocyte development. The findings presented demonstrate that both Shh and Ptc are expressed in human T

cells. In addition, upregulation of Shh signalling enhances and blocking of endogenous Shh inhibits T cell receptor mediated T cell activation, respectively; as determined by proliferation, cytokine production and CD25 and CD69 expression.

Wnt signalling is also thought to play a role in lung branching morphogenesis. It is known to interact both with Shh signalling and TGFβ. However, using presently available antibodies, there is no evidence of upregulation of Wnt signalling in ILD. In an attempt to drive the Wnt Pathway, a replication-deficient adenovirus expressing *Dvl1* (Ad5-MCMV-Dvl1) was successfully rescued. Although the virus drives *Dvl1* mRNA and protein expression *in vitro* and *in vivo*, it does not consistently mimic Wnt signalling, nor does it appear to affect Shh or TGFβ signalling. Furthermore such Dvl1 overexpression has little effect on cell proliferation either *in vitro* or *in vivo*, and does not cause lung fibrosis in mice.

Thus Shh signalling appears to be upregulated in fibrotic lung in mice and humans. However the work presented does not define whether or not the pathway plays a specific role in the pathogenesis of ILD. There is also no evidence relating Wnt signalling or Dvl1 upregulation to ILD. Finally, Shh is shown to influence TCR mediated signalling and clonal expansion. It may be that damaged epithelial cells and the immune system communicate via this pathway.

Declaration

I hereby declare that this thesis has been composed solely by myself and has not been accepted in any previous application for candidature for a higher degree. All work presented in this thesis, was, unless acknowledged, initiated and executed by myself. All sources of information in the text have been acknowledged by reference.

Acknowledgements

I would like to thank Professor Jonathan R. Lamb and Dr Sarah E.M. Howie for their supervision, help and advice during my thesis. I would also like to thank Professor Chris Haslett for introducing me to the lab and the Medical Research Council who funded my PhD thesis project, as a MRC Clinical Training Fellow.

Many thanks to everyone in the Lamb and Rayne labs, past and present, especially Drs Susannah Lindey and Nigel Savage for their friendship and guidance, and Dr Jean-Michel Sallenave for his tuition in adenoviral construction and delivery. I am grateful to Professor Jack Gauldie, and his lab, for amplifying and banding the Ad5-MCMV-Dvl1, and for providing the control adenovirus. Thanks also to Mrs Anne Grant and Mrs June Stewart for their expert histology and immunohistochemistry preparations.

I would also like to thank Dr Roel Nusse for the Dvl1 polyclonal anibody, and Dr C.C.Hui and Professor A.Joyner for the *Gli2*$^{+/-}$ and *Gli3*$^{+/-}$ mice respectively. Thanks to Dr Gerard Hoyne for all his ideas and his help with the *in vivo* experiments.

I would like to thank my family and friends for their support and encouragement. Finally, I would particularly like to thank Ciara McNamara for her love, patience and understanding over the past four years.

Dedication

For my Parents

Contents

Chapter 1

Chapter 2

Chapter 3

Chapter 4

Chapter 5

List of Figures

List Of Tables

Abbreviations

^{3}H-TdR	Tritiated Thymidine
Ab	Antibody
Ad	Adenovirus
APC	Antigen Presenting Cell
APC	Adenomatous polyposis coli
Arm	Armadillo
ATCC	American Type Culture Collection
BAL	Immunohistochemistry
BCC	Basal cell carcinoma
BCNS	Basal cell nevus syndrome
BM	Basement Membrane
Bmp	Bone morphogenetic protein
bp	Base pairs
C-	Carboxy terminus
Ca^{2+}	Calcium ion
CAT	Chloramphenicol acetyltransferase
CBP	CREB binding protein
CD	Cluster of differentiation
cDNA	Complementary DNA
CFA	Cryptogenic fibrosing alveolitis
Ci	Cubitus interruptus
CMV	Cytomegalovirus
CNS	Central nervous system
ConA	Concanavalin A
Cos-2	Costal-2
CPE	Cytopathic effect
CRD	Cysteine rich domain
CT	Computerised tomography
CtBP	C-terminal Binding Protein

DC	Dendritic Cell
DEP	Dishevelled-EGL-10-Pleckstrin
DEPC	Diethylpryocarbonate
Dhh	Desert hedgehog
DIP	Desquamative interstitial pneumonia
DIX	Dishevelled-Axin
Dkk	Dickkopf
DMEM	Dulbecco's minimal essential medium
DNA	Deoxynucleic acid
Dpp	Decapentaplegic
Dsh	Dishevelled
Dvl	Dishevelled (murine or human)
E	embryonic days
E	Early
ECACC	European Collection of Cell Cultures
ECM	Extracellular Matrix
ELISA	Enzyme Linked ImmunoSorbant Assay
FAP	Familial adenomatous polyposis
FCS	Foetal calf serum
FGF	Fibroblast growth factor
FITC	Fluorescein isothiocyanate
Fu	Fused
Fz	Frizzled
g	Gravitational force
GAPDH	Glyceraldehyde-3-phosphate dehydrogenase
GBP	GSK-3 Binding Protein
GCPS	Greig's cephalopolysyndactyly syndrome
gm	Gram
GM-CSF	Granulocyte-macrophage colony stimulating factor
GSK	Glycogen synthase kinase
H&E	Haematoxylin and eosin
Hh	Hedgehog

Hip	Hedgehog-interacting protein
HMG	High mobility group
HPE	Holoprosencephaly
HRP	HorseRadish Peroxidase
hrs	Hours
ICAM	Intercellular adhesion molecule
ICC	Immunocytochemistry
ICOS	Inducible co-stimulator molecules
IFN	Interferon
Ihh	Indian hedgehog
IL	Interleukin
ILD	Interstitial lung disease
IPF	Idiopathic pulmonary fibrosis
ITAM	Immunoglobulin family tyrosine-based activation motif
J	Joule
JAK-STAT	Janus kinase-signal transducers and activators of transcription
JNK/SAPK	C-Jun N-terminal kinase/stress-activated protein kinase
kb	Kilobases
kDa	Kilodaltons
L	Late
LB	Luria-Bertani
Lef	Lymphoid-enhancer factor
LFA	Lymphocyte function-associated antigen
LL	Lower left
LPS	Lipopolysaccharide
LR	Lower right
LRPs	Low density lipoprotein receptor-related proteins
mAb	Monoclonal Antibody
MB	Medulloblastoma
MCMV	Murine cytomegalovirus
MCP1	Monocyte chemoattractant protein1
MEM	Minimal essential medium

mg	milligram
MHC	Major Histocompatibility Complex
ml	Millilitre
moi	Multiplicity of infection
mRNA	Messenger RNA
mu	Map units
N-	Amino terminus
NFAT	Nuclear factor of activated T cells
ng	nanogram
NK	Natural killer
nm	Nanometres
°C	Degrees centigrade
PBMCs	Peripheral Blood Mononuclear Cells
PBS	Phosphate Buffered Saline
PCR	Polymerase chain reaction
pfu	Plaque forming units
pg	picogram
PHA	Phytohaemagglutinin
PI	Propidium iodide
PKA	Protein kinase A
PKC	Protein kinase C
Ptc	Patched
RGS	Regulator of G-protein Signalling
RMS	Rhabdomyosarcoma
RNA	Ribonucleic acid
rpm	Revolutions per minute
RT	Room temperature
RT-PCR	Reverse transcription PCR
SCF	Subcellular fractionization
sFRPs	Secreted frizzled-related proteins
Shh	Sonic hedgehog
Smo	Smoothened

SP-C	Surfactant protein-C
Su(Fu)	Suppressor of fused
Tc	Cytotoxic T cell
Tcf	T-cell factor
TCR	T Cell Receptor
TGFβ	Transforming growth factor beta
Th	Helper T cell
Th1	T helper 1
Th2	T helper 2
TLR	Toll-like receptor
Tm	Annealing temperature
TNF	Tumour Necrosis Factor
Tr	Regulatory T cell
UIP	Usual interstitial pneumonia
UL	Upper left
UR	Upper right
Wg	zeste-white-3
μCi	Microcurie
μg	micogram
μl	Microlitre
μm	Micron

Chapter 1

Introduction

1.1 Aims of Thesis

The aims of the research reported in this PhD thesis were to investigate the role of the Sonic hedgehog (Shh) and Wnt (Wnt) signalling pathways in the pathogenesis of Interstitial Lung Disease (ILD), and the effects of Shh signalling on human $CD4^+$ T cell activation. As will be discussed, both of these pathways play a role in branching morphogenesis of the developing lungs. Upregulation of either is associated with increased cell proliferation, and they are known to interact both with each other and with the profibrotic cytokine TGFβ. Furthermore, they are emerging as potential mediators in an increasing number of cell functions and disease processes in mature species. Such features prompted the study described.

This introduction begins with quite detailed descriptions of the Shh and Wnt signalling pathways, with particular reference to their roles in lung development, cell proliferation, disease processes and interactions with genes such as *TGFβ*. Recent work relating Shh to the developing immune system is also discussed. The clinical features, pathogenesis and management of ILD are then addressed, followed by an introduction to the FITC rodent model of pulmonary fibrosis. A brief summary of T cell receptor mediated T cell activation precedes a concluding description of the rationale behind, and application of, adenoviral gene therapy.

1.2 The Sonic Hedgehog Signalling Pathway

1.2.1 THE HEDGEHOG PATHWAYS

1.2.1.1 The Hedgehog (Hh) Pathway in *Drosophila*

Hh was first identified as one of the segment polarity genes in *Drosophila*, which are so called because mutations in these genes disrupt the pattern and polarity of the larval segments [1]. The larval cuticle becomes covered in spiky processes called denticles in *Hh* homozygotes [2]; thus the name "hedgehog". *Drosophila* only have a single *Hh* gene, which is expressed in the posterior cells of each segment and activates expression of the Wnt family gene *wingless* (*wg*) in the adjacent anterior cells [3]. *Hh* induces the expression of secondary signals, *wg* and *decapentaplegic* (*dpp*, a member of the TGFβ superfamily) during postembryonic limb formation [4,5], which function as morphogens required in pattern formation [6,7]; a morphogen being an organizing molecule that emanates from a localized source and diffuses away to form a concentration gradient. Indeed *Hh* itself is thought to act as a morphogen [8,9], eliciting differential responses at different concentrations.

Hh encodes a 46kDa native protein that initially undergoes signal peptide cleavage to a 39kDa form, followed by an autoproteolytic cleavage into a 19kDa amino-terminal peptide (N-Hh) and a 26kDa carboxy-terminal peptide (C-Hh) [10]. This second cleavage is dependant upon a conserved domain within the carboxy-terminus [10,11]. The N-Hh remains associated with the cell surface whilst the C-Hh diffuses from the cell. Only the N-Hh peptide has been shown to have signalling activity [11,12]. This association of N-Hh is dependent on its covalent attachment to a cholesterol moiety in the membrane, which is catalysed by intramolecular cholesterol transferase activity of C-Hh [13,14]. It would appear that active signalling requires cleavage and binding to cholesterol [13]. Why hedgehog undergoes cholesterol modification is unclear. It has been suggested that it may be involved in directing intracellular transport within epithelia [15]. In addition, cholesterol may affect the movement of Hh,

which may in turn influence long-range signalling [16]. Cell culture studies have also produced evidence for a degree of palmitoylation of hedgehog [17].

Hh interacts with a receptor complex comprising Patched (Ptc) and Smoothened (Smo) [18]. *Ptc* is a segment polarity gene encoding a twelve-transmembrane protein with two large extracellular loops [19,20]. In vertebrates, Ptc has been shown to bind to the Sonic Hedgehog protein (Shh) with high affinity [18,21], a function dependant on the extracellular domains [21]. *Smo*, another segment polarity gene, encodes a seven-transmembrane protein that shares homology with G protein coupled receptors [22]. In contrast to Ptc, there is no *in vitro* evidence of physical interaction between vertebrate Smo and Hh proteins [18]. It would therefore appear that Ptc and not Smo is the Hh receptor. However, whilst remaining constitutively active in the combined absence of Ptc and Hh [23], Hh signalling is dependent on Smo [22,24]. In the absence of the Hh ligand, Ptc inhibits Smo signalling, through modification of the Smo protein [25], and thus prevents constitutive activation of the Hh pathway [26]. Hedgehog binding to Ptc represses its activity leading to the derepression of Smo and ligand independent Hh signalling by Smo [26](Figure 1.1). This is most likely due to a conformational change rather than dissociation of the Ptc-Smo receptor complex, as the association of the two proteins is unaffected by Hh signalling [18].

Paradoxically Hh signalling induces expression of its own receptor, Ptc [14,27]. It has been shown that the absence of Ptc causes the Hh signal to spread further from its source, whereas upregulating Ptc restricts movement [28]. This would imply that Hh is normally sequestered by Ptc; a feature that would allow Hh to restrict its own movement, which may have further implications on short and long-range signalling. Therefore Ptc serves both to antagonise Hh signalling through inhibition of Smo signalling and sequestration of Hh itself.

So how does Hh control transcription in *Drosophila*? A crucial element is Cubitus-Interruptus (Ci), a zinc finger transcription factor homologous to the vertebrate Gli factors [29]. However, unlike *Gli*'s in vertebrates [30], *Ci* transcription is independent of Hh signalling [31]; control is therefore post-transcriptional. Ci, which is subject to

proteolytic cleavage [32], exists as either a full length (Ci-155) or a truncated form (Ci-75). Importantly Ci-155 overexpression has been shown to activate Hh targets such as *dpp*, *Ptc* and *wg* [33-36], whilst Ci-75 can act as a transcriptional repressor [32]. It is therefore not surprising that Ci-75 is predominant in cells in the absence of Hh signalling. Following Hh induction Ci cleavage is blocked with a resultant accumulation in the Ci-155 form before its transport to the nucleus [37]. The transcriptional activation domain [34] and binding site for CREB binding protein (CBP), necessary for Hh target gene activation [38], are lost during cleavage from Ci-155 to Ci-75 [32,34](Figure 1).

A model proposed by P.W.Ingham [39](Figure 1.1) suggests that Hh signalling may be modulating Ci phosphorylation, preventing Ci ubiquitination and cleavage (to Ci-75) by the proteasome pathway [40]. Indeed a number of protein kinase A (PKA) phosphorylation sites have been identified in vertebrate Gli proteins [38,41]. In addition PKA is inactivated in a number of wing duplication mutations [27](phenotype consistent with Hh activation), and mutations of likely Ci phosphorylation sites result in increased Ci-155 stability and activity [41]. These observations imply that PKA controls Ci phosphorylation, under the regulation of Hh signalling. However as upregulation of PKA does not suppress Hh signalling it seems more likely that PKA is working in parallel, rather than downstream of, Hh [42].

Ci is normally found as part of a large high molecular weight complex along with the kinase related protein, costal-2 (Cos2)[43], and the serine-threonine kinase, fused (Fu)[44]. This complex docks at microtubules, possibly through the action of Cos2. This association allows targeting of Ci to the proteasome for cleavage to take place. Moreover the binding of this complex to the microtubule is controlled by Hh signalling, the complex detaching upon Hh activation [44]. Thus Hh signalling prevents association of the complex to the proteasome and cleavage into Ci-75 (Figure 1.1). How Hh causes this dissociation is unknown. As Fu is epistatically upstream of Cos2, Smo may directly activate Fu, which in turn may inhibit Cos2 [45]. When a fourth component of the complex, Suppressor of Fused [Su(Fu)] protein is eliminated, Fu activity is no longer necessary [46]. Thus, although Su(Fu) antagonises

Fu activity, Hh signalling can function normally when neither is present. Su(Fu) binds cytoplasmic Ci-155. Loss of Su(Fu) enhances ectopic Hh target gene expression, in keeping with its role as an antagonist of Ci-155 function [42]. However, Su(Fu) has paradoxical effects: while antagonising Ci-155 function, it also increases cellular Ci-155 independently of Ci proteolysis. To explain this it has been suggested that Su(Fu) prevents the maturation of Ci-155 from its stable cytoplasmic inactive form into a nuclear active one [42].

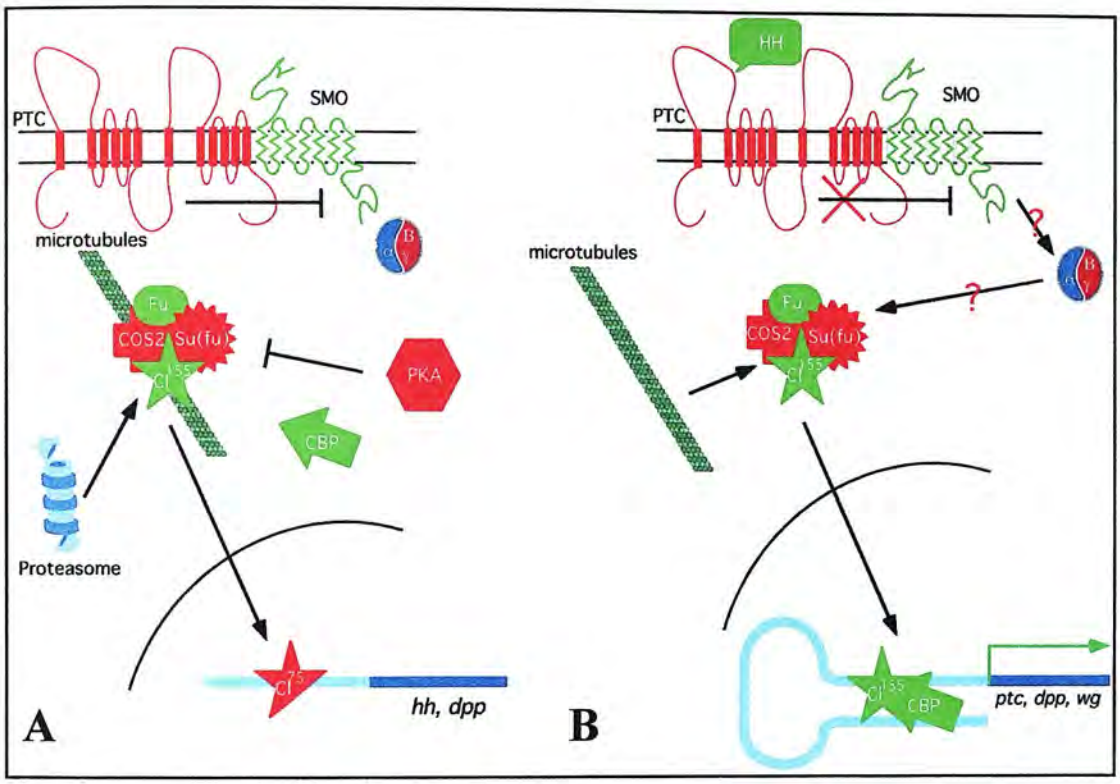

Figure 1.1: The Hedgehog Signalling Pathway in *Drosophila.* Figure taken from review article by P.W. Ingham "Transducing Hedgehog: the story so far" (1998) [39]

Negatively acting components are shown in red, positively acting components in green. **Note:** in above figure patched is represented as PTC and ptc, hedgehog as HH and hh, and smoothened as SMO.

(A) In the absence of Hh (or HH) induction, the activity of Smo (or SMO) is inhibited by Ptc (or PTC) probably through their physical association. Full-length Ci forms a complex with Fu, Cos-2 and Su(fu), via which it associates with microtubules. This association leads to targeting of Ci to the proteasome where it is cleaved to release the transcriptional repressing form Ci^{75}. The phosphorylation of Ci^{155} promotes its cleavage, either by promoting association with the Cos-2-Fu or by promoting ubiquitination (or both). Although Ci^{75} translocates to the nucleus, it is also found in association with Fu and Cos-2. It is not clear whether it dissociates from the complex prior to translocation; there is, however, no evidence that Cos-2 enters the nucleus. The intracellular distribution of Fu protein has not been determined. **(B)** When Hh binds to Ptc, the inhibitory effect on Smo is suppressed. The resulting activation of Smo leads, by an unknown mechanism (but possibly via a heterotrimeric G protein signal), to the dissociation of the Fu-Cos-2-Ci complex from microtubules. Cleavage of Ci^{155} is blocked; this or a related form of Ci then presumably enters the nucleus to activate transcription of *Ptc*, *wg*, *dpp* and other unidentified target genes in association with CREB binding protein (CBP).

1.2.1.2 The Sonic Hedgehog Pathway

Many of the features of Hedgehog Signalling described in *Drosophila* are preserved in mammals. There are three Hh homologues in mammals: Sonic hedgehog (Shh), Desert hedgehog (Dhh) and Indian hedgehog (Ihh). Dhh is largely expressed in testes where it regulates spermatogenesis, and it organizes the perineurium around peripheral nerves; whilst Ihh coordinates chondrocyte maturation and proliferation during endochondral skeleton development [47-49]. However Shh is the best known of the mammalian homologues; it is produced in many tissues with organizing properties, including the CNS, limbs, eye [48,50-54] and, of particular relevance to this thesis, the lungs [55,56]. Like other hedgehog proteins, Shh undergoes autoproteolytic cleavage into an amino-terminal (N-Shh) peptide responsible for activity, and a carboxy-terminal (C-Shh) containing all auto-processing machinery [57]. As in *Drosophila* N-Shh remains membrane associated, by a palmitic acid at its N-terminus [17]and cholesterol at its C-terminus [13,14]. Palmitoylation results in a 30-fold increase in potency [17]. Other properties of Hh relating to short and long-range signalling also apply to Shh.

Shh also acts through a Ptc-Smo receptor complex. In fact much of the biochemical characterization of Hh-Ptc-Smo interactions has been carried out in mammals and vertebrates [18,21]. Two Ptc homologues have been identified in mammals, known as Ptc (or Ptc1) and Ptc2 [58-60]. Whilst mouse Ptc1 and Ptc2 share only 56% identity, their basic structure is similar; greatest variation is noted at the amino- and carboxy-termini. Both are differentially expressed during epidermal development and *Ptc2* is co-expressed with *Shh* in epithelial cells. Although they may have different functions both *Ptc* genes are modulated by Shh signalling [59].

Similarities between Hh and Shh signalling also exist in the cytoplasm. Shh counteracts PKA activity [61], and Fu and Su(Fu) homologues have been isolated and linked to the Shh pathway [62-65]. In addition, Shh signalling is related to Ci homologues, the Gli factors; as discussed below.

Target genes of Hh signalling appear to be conserved. Shh activates *Bmp2* (Bone morphogenetic protein 2) and *Bmp4* (*dpp* vertebrate homologues), as well as transcription of its own receptor *Ptc* [60,66-70].

1.2.1.3 The Gli's

Three homologues of *Ci* (*Gli1*, *Gli2* and *Gli3*) have been identified in humans and mice [71,72]. The Gli proteins share high homology in their five zinc finger domains, but limited homology outside of this region [73]. Their partial redundancy and often overlapping domains of expression has made it difficult to define precisely their individual features and functions. Unlike *Ci* in *Drosophila*, the *Gli* genes are transcriptionally regulated by Shh protein. Ectopic Shh expression induces *Gli1* but represses *Gli3* [30,74-77]. *Xenopus Gli2* is induced by Shh in the CNS, but this is not the case in mouse lungs [56,78].

As in Ci control there are post-transcriptional interactions between Shh and Gli's. Biochemical studies have indicated that mouse Gli2 and Gli3 have activator and repressor activities, like Ci, whereas Gli1 only has activator function and may not be processed post-transcriptionally [79,80]. It therefore follows that Gli1 functions solely as an activator in Hh signalling [81]. Gli2 has been shown to act as a repressor in floor plate induction [78] and as an activator in transgenic flies and frog embryos [78,81]. Gli3 has been shown to repress *Shh* expression, and its inductive activity may be independent of Shh [30,78,82,83]. Together these results indicate that the Gli proteins form a regulatory network that responds to Hh signalling and that Gli proteins have distinct properties.

Somewhat surprisingly mice that lack *Gli1* function are phenotypically normal. Gli1 function is dispensable in mice if both copies of the *Gli2* gene are present [84]. It would appear that Gli2 can compensate for the absence of Gli1, possibly by mimicking Gli1 as a regulated activator [81]. Mice with homozygous *Gli2* mutations die at birth, have numerous skeletal defects [85] and abnormal lungs [86]. They have similarities to *Shh* mutant mice suggesting that *Gli2* functions downstream of *Shh* [87]. It has recently

been shown that a low level of Gli1 can rescue all Shh signalling events in Gli2 mutants [88]; why endogenous compensation does not normally occur is less clear. *Gli3* mutant mice have many abnormalities including CNS and lung defects, and polydactyly [74,89,90]. Aspects of these phenotypes are similar to Shh gain of function effects, and *Shh* expression is upregulated [78,83], implying a role for Gli3 in repressing *Shh*. *Gli2/Gli3* double mutants have more extreme skeletal and lung defects than either homozygous phenotype, indicating overlapping functions of *Gli2* and *Gli3* [85,86]

1.2.1.4 Hedgehog-interacting protein (Hip)

In 1999, Chuang and McMahon [91] isolated a 2.7 kilobase clone, which bound to Shh, Ihh and Dhh in a mouse limb bud cDNA library screen. As the 700 amino acid protein encoded by this cDNA bound all three mammalian Hedgehog proteins, the gene was called *Hedgehog-interacting protein* (*Hip*). Hip is a transmembrane glcoprotein, which directly interacts with N-Shh. In the developing mouse *Hip* is well placed to participate in Shh signalling, as it is consistently expressed in mesenchyme adjacent to Shh expressing epithelium, in several organs including the lungs. *Hip*, like *Ptc*, is a general transcriptional target of Hh signalling. It appears that upregulation of *Hip* by Hh signals attenuates further Hh signalling [91].

1.2.2 THE SHH PATHWAY IN LUNG DEVELOPMENT

Mammalian lung morphogenesis begins as a ventral outpouching of the foregut endoderm into the surrounding splanchnic mesoderm. Primitive buds produce the left and right primary bronchi before primary bronchial buds divide asymmetrically giving rise to 2 left and 3 right secondary bronchi (later lobar bronchi) in humans; 1 left and 4 right in mice. These secondary bronchi branch further within the pulmonary mesenchyme to complete lung formation. Branching morphogenesis of the lung buds is dictated by epithelial-mesenchymal tissue interactions. Morphogens and growth factors such as Shh are thought to control these processes.

1.2.2.1 Shh

Shh is expressed in the trachea and lung endoderm in the developing mouse lung [55], at low levels throughout the epithelium with higher levels in the growing distal buds [56,92,93]. Shh mutant (*Shh*$^{-/-}$) mice display serious foregut defects, with failure of separation of the trachea and oesophagus into distinct tubes and hypoplastic lung buds [55,94]. Each bud appears as a single lobe with loss of the normal extensive network of air sacs and no sign of either epithelial branching or mesenchymal proliferation. Proximal-distal lung epithelial differentiation is preserved, indicating that Shh is specifically associated with branching morphogenesis [94]. Mesenchymal *Ptc*, *Gli1* and *Gli3* expression is downregulated in *Shh*$^{-/-}$ mice. Shh overexpression, under the control of a Surfactant Protein-C (SP-C) enhancer/promoter, results in an increase in interstitial tissue due to increased proliferation of both epithelial and mesenchymal cells, with the absence of functional alveoli. Cell differentiation is maintained and *Ptc* expression is increased in these Shh transgenic mice, which die soon after birth, presumably due to respiratory failure [56].

In addition to the above evidence linking Shh with branching morphogenesis, it also seems to play a role in establishing left/right asymmetry of the lungs, and in separation of trachea and oesophagus [95,96].

1.2.2.2 Ptc

Ptc represses the transcription of Shh induced genes, including *Gli1* and *Ptc* itself. Derepression takes place on Shh binding. *Ptc* is expressed at high levels in the developing lung mesenchyme, adjacent to terminal buds where Shh is expressed, and at low levels in the distal epithelium. *Ptc* (*Ptc1*) null mutant mice die between embryonic days (E) 9.0 and 10.5 due to neural and cardiac defects, just at the time when lung development begins [97]. *Ptc* and *Shh* mRNA levels decline towards birth [56]. As already described, *Ptc* is upregulated when Shh is overexpressed and downregulated in the lung mesenchyme of Shh$^{-/-}$ mice [55,94].

1.2.2.3 Gli Family Members

All three of the *Gli's* are expressed in lung mesoderm at higher levels distally than proximally, and not in the endoderm. Expression falls as development proceeds. Shh overexpression results in *Gli1* upregulation with no effect on either *Gli2* or *Gli3* expression [74].

As already mentioned *Gli1*$^{-/-}$ mutants are viable and normal [84]. *Gli2*$^{-/-}$ mutants die at birth with severe skeletal and neural defects. The lungs appear together as a single smaller lobe, and primary branching is defective in the right lung. There is normal separation of the hypoplastic trachea and oesophagus, a reduction in mesenchymal proliferation and normal terminal cell differentiation. As discussed, the *Gli2*$^{-/-}$ phenotype is very similar to *Shh*$^{-/-}$ mice, except trachea and oesophagus fail to separate in the latter. In *Gli2*$^{-/-}$ mouse lungs *Ptc* and *Gli1* expression are reduced; *Shh* is unaffected. Though Gli3 is normally regarded as a repressor of Shh signalling it is unclear whether this holds for lung development [86,98]. Gli3 (*Gli3*$^{-/-}$) mutant mice, though viable, have smaller lungs with altered lobe shape [74]. Expression of *Shh*, *Ptc*, *Gli1* and *Gli2* is unchanged in these mice, suggesting that *Gli3* may have more of a supporting role in lung development rather than being crucial itself.

Gli1$^{-/-}$/*Gli2*$^{+/-}$ double mutants normally develop multiple defects, small lungs and die soon after birth. *Gli1*$^{+/-}$/*Gli2*$^{-/-}$ mutants have smaller lungs than *Gli2*$^{-/-}$ mice but do form 2 lung buds. *Gli1*$^{+/-}$/*Gli2*$^{+/-}$ mice lung lobes appear normal, whilst *Gli1*$^{-/-}$/*Gli2*$^{-/-}$ mutants have 2 very small lobes, with branching. These various phenotypes imply that Gli1 and Gli2 have overlapping functions during lung development. *Gli2*$^{+/-}$ /*Gli3*$^{+/-}$ double mutants are viable with no obvious defects. *Gli2*$^{-/-}$/*Gli3*$^{+/-}$ mice develop hypoplastic lungs with failure of separation of right and left lobes, and the trachea and oesophagus do not separate. *Gli2*$^{-/-}$/*Gli3*$^{-/-}$ mutants die at about E10.5 with no trachea, oesophagus or lung. These phenotypes illustrate the ability of *Gli3* to compensate when *Gli2* is absent [86].

1.2.2.4 Shh and Bmp4

As described, Shh is able to activate *Bmp4*. In the developing lung *Bmp4* is highly expressed in the distal lung tips, as is *Shh*. However, whereas *Shh* is confined to epithelial cells, *Bmp4* is also expressed in the adjacent mesenchyme. *Bmp4* overexpression in distal lung epithelium results in smaller lungs with reduced epithelial branching and fewer, dilated air sacs [92]. *Shh* expression is unaffected. In addition *Shh* and *Bmp4* overexpression produce different phenotypes, and *Bmp4* expression is not significantly altered in *Shh*$^{-/-}$ mutants [55,94]. This argues against Bmp4 being a direct mesenchymal target for Shh during mouse lung development. As *Bmp4*-deficient mice die before lung bud formation they offer little more information on the role of Bmp4 in lung development [99]. However overexpression of the Bmp antagonist Noggin in distal lung epithelium results in a reduction in distal epithelial and an increase in proximal cell types [100], suggesting a role for Bmp4 in controlling proximal-distal endoderm differentiation. *Shh* expression is unaffected, which again is against a direct Shh-Bmp4 interaction in lung development.

1.2.2.5 Shh and Fibroblast Growth Factors

Fibroblast growth factors (FGF) are essential components in lung development. FGF10 is expressed at high levels in the distal lung mesenchyme and plays a strong role in branching morphogenesis [56,92], with *FGF10* mRNA expression increasing towards birth. FGF10 null mutants die at birth with lung and limb defects [101,102]; right and left primary lung buds fail to form. A similar phenotype is displayed when the proposed FGF10 receptor, *FGFR2*, is knocked out [103]. Shh has been shown to inhibit *FGF10* expression *in vitro* and *in vivo* [104,105]. However other evidence linking the two directly is conflicting [101,102], prompting Tuyl and Post [106] to suggest that Shh and FGF10 actually function in parallel pathways in lung development.

FGF7 has been shown to play a role in lung branching [107]. *FGF7* null mutants appear normal implying that any function played by *FGF7* in lung development can be maintained in its absence [108]. Like *FGF10*, *FGF7* expression increases through

gestation [56,105,109]. Shh induces *FGF7* expression *in vitro*, and *Shh* and *Ptc* signals are reduced around sites of FGF7 bead implantation in whole organ lung cultures. These findings are suggestive of a negative regulatory loop involving FGF7 and Shh. Lebeche *et al* [104] have suggested that FGFs, Shh, Bmp4 and TGFβ1 form a regulatory circuit in lung development.

1.2.2.6 Shh and TGFβ

TGFβ1, 2 and 3, and the TGFβ type I and II receptors, are expressed in embryonic and foetal lung [110-112]. TGFβ1 and 2 both inhibit branching morphogenesis [112,113]. TGFβ3 null mutant mice develop an immature lung phenotype with excessive mesenchyme later in gestation and often die shortly after birth [114]. In contrast TGFβ1 null mutant mice display a normal neonatal lung phenotype, which has been attributed to maternal transplacental rescue. *TGFβ1* overexpression, under control of the SP-C promoter, results in a neonatal lethal phenotype characterised by general lung hypoplasia with decreased saccule formation and epithelial differentiation [115]. Blocking TGFβ type II receptor signalling stimulates lung morphogenesis and blocking the TGFβ type I receptor reduces the number of new branch points in mouse lung in culture, resulting in lungs with long, tubular airways without branch points [112]. TGFβ1 and TGFβ2, like Shh, inhibit *FGF10* expression *in vitro* [104]. Although TGFβ and Shh may have not been directly linked in lung development, they probably have common targets and may interact in a shared regulatory circuit as suggested above [104].

1.2.3 THE SHH PATHWAY AND CELL PROLIFERATION

Shh signalling is associated with proliferation of many cell types. With particular relevance to the subject matter of this thesis, only epithelial cells and immune system precursors are discussed.

1.2.3.1 Shh overexpression in epithelial cells *in vitro*

As described by Parisi *et al* [116], Hh signalling appears to control epithelial cell proliferation both in *Drosophila* and in vertebrates. In 1997 Fujita *et al* [117] analysed the Shh pathway in human lung squamous carcinoma cells (LK-2). They showed that upregulation of the Shh pathway, induced by adding a His-tag fusion protein of the amino-terminus of rat Shh (N-Shh) to the system, stimulated cell growth; N-Shh being the active component of Shh signalling as described. In addition, an antibody against the amino-terminus of Shh (anti-Shh-N) inhibited growth. They concluded that Shh signalling allowed LK-2 cells to promote their own growth through an autocrine mechanism. Shh signalling has also been shown to augment the proliferative capacity of primary human keratinocytes, possibly by opposing cell cycle arrest [118].

1.2.3.2 Shh overexpression *in vivo*

Shh overexpression *in vivo*, under control of the SP-C promoter, results in increased epithelial and mesenchymal cell proliferation in the developing lung [56]. The pathway appears to exert similar effects in other tissues as well. For example, Shh signalling has been shown to stimulate epithelial proliferation and increase cell survival in the developing tooth [119]. Furthermore, in the skin the upregulation of Shh results in epidermal hyperplasia and stimulates hair growth by inducing resting hair follicles to enter anagen, the growth phase in mature follicles [118,120].

1.2.3.3 The Shh Pathway in the Immune System

Using similar approaches to those employed in *in vitro* epithelial cell cultures, the Shh pathway has recently been studied with respect to the developing immune system. Outram *et al* studied the mammalian Hh pathways in mouse foetal and adult thymus [121]. They showed that many components of the pathways were present in whole thymus, including *Shh*, *Ihh* (*Dhh* was not detected), *Ptc*, *Smo*, *Hip*, *BMP4* and

the *Gli's*. Following cell sorting, *Shh* was found only to be present in the epithelial cells, and *Smo* and *Ptc* were detectable on the thymocyte populations. They manipulated Shh signalling in thymic explant cultures by adding either a neutralizing anti-Shh monoclonal antibody 5E1 [122] or a modified (for optimal activity [17]) human recombinant Shh peptide (Octyl N-Shh). Their findings suggested that the 5E1 antibody, which blocked Shh signalling, increased thymocyte differentiation from double negative to double positive, whereas the Shh peptide arrested thymocyte development at the double negative stage. Therefore, it appears that Shh signalling plays a role in thymocyte development.

Detmer *at al* [123] confirmed the presence of *Ptc* and *Smo* in a range of human leukaemia cell lines and *Ptc* expression in normal marrow. They demonstrated that blocking Shh signalling with cyclopamine, a known specific antagonist of Hh signalling [124], inhibited erythroid colony formation and maturation. In the same system, the addition of a N-Shh peptide had the opposite effect, causing increased proliferation as indicated by larger colony size. They postulated that Hh signalling regulated haematopoietic differentiation, and that aberrant signalling may contribute to the development of leukaemia.

Subsequent work carried out by Bhardwaj *et al* [125] employed the same 5E1 blocking antibody and Octyl N-Shh peptide as above [121], but in the context of human haematopoietic stem cells. It had already been shown that Bmp4, an established target of Shh signalling, induced haematopoietic commitment in Xenopus embryos [126] and that human Bmp's could increase human stem cell survival [127]. Bhardwaj *et al* [125] showed that *Shh*, *Ptc* and *Smo* are expressed in highly purified primitive human blood cells, the precursors of myeloid and lymphoid blood cells [128]. In addition, blocking endogenous Shh (with the 5E1 antibody) inhibited cytokine-induced proliferation of these haematopoietic progenitor cells, maintaining them in an undifferentiated state. On the other hand, adding exogenous Shh (Octyl N-Shh) augmented proliferation without affecting differentiation. They concluded that these effects were mediated through Bmp4 induction.

1.2.4 THE SHH PATHWAY IN DISEASE

Dysregulation of the Hh pathway is associated with a number of human diseases, syndromes and malformations. Sporadic and inherited mutations of the *Shh* gene have been shown to cause holoprosencephaly (HPE), a common dominant syndrome affecting the head and face; which is also caused by other gene mutations affecting Gli function [82,129]. HPE also develops when Shh function is lost and in farm animals exposed to the Shh antagonist, cyclopamine [124,130]. Smith-Laemli-Opitz syndrome patients, who are deficient in cholesterol biosynthesis, develop similar features [131].

Sporadic basal-cell carcinoma (BCC) is the most common skin cancer in Caucasians. Mutations inactivating *Ptc* (*Ptc1*), and *Smo* mutations rendering it insensitive to *Ptc* repression, have been detected in BCC [68,132,133]. A majority of BCCs show *Gli1* expression, which may be involved in their formation and may be induced by the above mutations [134]. *Ptc* mutations have been associated with the familial basal cell nevus syndrome (BCNS or Gorlin's syndrome) [135]. A further two sporadic tumours in BCNS, medulloblastoma (MB) and rhadomyosarcoma (RMS), may also be due to *Ptc* mutations. They are certainly seen in mice with *Ptc* mutations, in which *Gli* is expressed constituitively [68,97,136].

Gli3 loss or misfunction results in several human syndromes. *Gli3* happloinsufficiency causes Greig's cephalopolysyndactyly syndrome (GCPS), characterized by many abnormalities including syndactyly, polydactyly, and facial and CNS defects [137]. Mice with extra-toes (Xt^J), in which *Gli3* is mutated, develop a similar phenotype [90]. Gli3 protein truncations also result in Pallister-Hall syndrome [138] and postaxial polydactyly type A [139], which both share phenotypic features with GCPS. Indeed mutations of the Creb-binding protein (CBP) also result in defects similar to GCPS, in the Rubinstein-Taybi syndrome [140].

A number of human diseases associated with the Shh pathway, including some not discussed above, are listed in Figure 1.2 [141].

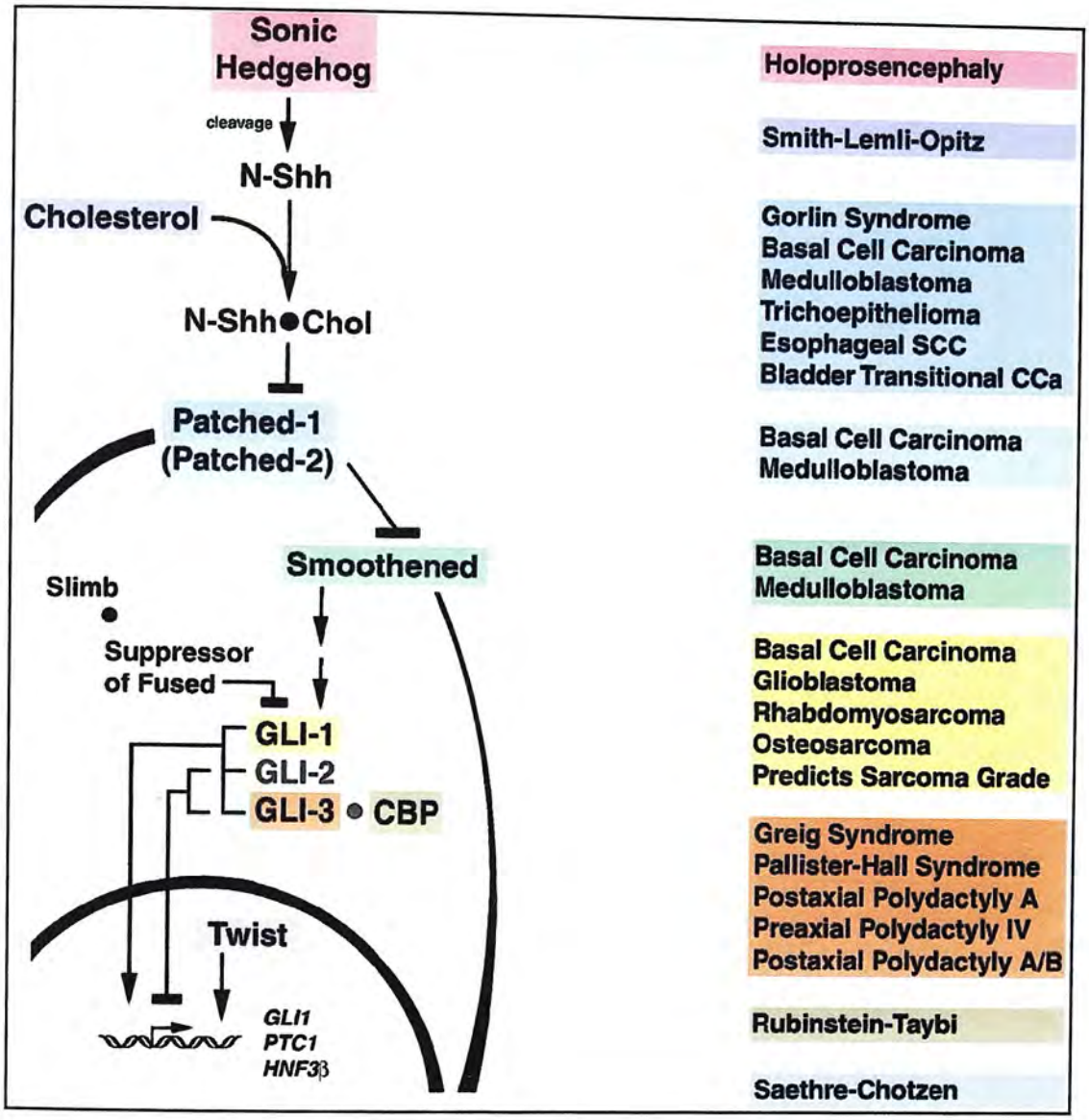

Figure 1.2: The Human Sonic Hedgehog Signalling Pathway and related diseases. Figure taken, with permission, from review article by E.H. Villavicencio et al "The Sonic Hedgehog-Patched-Gli Pathway in Human Development and Disease" (2000) [141]

Human Shh-Ptc-Gli pathway (*left*) and its links to human diseases (*right*). The association of the human disease with malfunction of a given element in the pathway is indicated by the matching colours of the boxes. The placement of the elements of the pathway, as well as their role as a repressor (*bars*) or as an activator (*arrows*), has been demonstrated in humans. The exceptions are that interaction between human *Gli3* and CBP was demonstrated using mouse CBP, human *Gli* genes were tested in frog and mouse cells, and mouse Gli2 protein function is shown for completeness, although human *Gli2* has not been fully characterized.

1.3 The Wnt Signalling Pathways

1.3.1 WNTS AND THEIR RECEPTORS

1.3.1.1 Wnts

The term Wnt is an acronym for the orthologous genes *wingless* (*wg*), from *Drosophila*, and *Wnt1* (previously *int-1*) from mouse [142,143]. The gene family is large: there are currently more than 20 Wnt isoforms. They encode secreted glycoproteins, usually 350-400 amino acids in length, which in general appear to act as morphogens [7,144]. Wnt genes are developmental molecules, regulating a variety of processes such as cell fate specification, cell migration and cell polarity [145]. *Wg*, a segment polarity gene in *Drosophila*, plays a role in controlling a range of developmental events from organization and patterning of the nervous system to tissues such as the wing and the larval cuticle. Whilst the cuticle of a wild type larva displays denticle belts alternating with naked regions, the cuticle of a *Wg* mutant larva is completely covered with denticles [1]. Embyros mutant for downstream, cooperative genes show a similar phenotype whilst mutant embryos with genes inhibitory to Wnt signalling, such as *zeste-white 3* (*zw3*), have the 'opposite' phenotype, namely a naked cuticle [146].

Wnt1 was identified as a site of insertion of mammary tumour virus in mice where it leads to epithelial hyperplasia and, occasionally, to adenocarcinomas in the mouse mammary gland [145]. Injection of *Wnt1* mRNA into blastomeres of *Xenopus* embryos leads to duplication of body axis [147]; a property which is shared by many, but not all, members of the Wnt family. This distinction has lead to a division of Wnts into 2 functional classes: Wnt1 (eg Wnt1/3a/8/8b), which induce axis duplication, and Wnt5a (eg Wnt4/5a/11), which do not, but do regulate morphogenetic cell movements [148]. Importantly however, Wnt5a can induce axis duplication if co-injected with an appropriate receptor (frizzled) [149] implying that specificity of signalling is not solely dependent on the Wnt ligand.

Wnts have been shown to stimulate three distinct signal transduction pathways; a β-catenin dependent pathway, a pathway activating protein kinase C (PKC) through raising intracellular Ca^{2+}, and a rho GTPase mediated pathway. It has been suggested that the Wnt1 class signal through the Wnt/β-catenin pathway and the Wnt5a class through the Wnt/Ca^{2+}dependent pathway [150].

1.3.1.2 Wnt Receptors

The diversity of responses seen with different Wnt ligands is to some extent due to the repertoire of cell surface receptors. The *Frizzled* (*Fz*) gene family have been shown to function as Wnt receptors [151-153], encoding seven-transmembrane proteins with an amino-terminal cysteine-rich domain (CRD) that binds Wnt with high affinity [154]. Like Wnts themselves there are many *Fz* genes including *Smo*, a component of the receptor complex in Hh signalling. Their overall structure resembles that of G protein-coupled receptors. Though the evidence in favour of Fzs as Wnt receptors is strong, other cell surface and extracellular molecules have been implicated.

Heparin-sulfate proteoglycans are positive regulators of Wnt signalling in *Drosophila* [155], probably functioning to facilitate ligand-receptor interactions or ligand movement. In addition, low density lipoprotein receptor-related proteins (LRPs) play essential roles in receiving Wnt signal [156-158]. Unlike proteoglycans, LRPs are essential for Wnt signalling. In the absence of the *Drosophila* LRP homolog, Arrow, Fz cannot activate the signal transduction cascade [158]. LRP6 and Fz extracellular domains interact in the presence of Wnt1, in keeping with their function as co-receptors [157].

There are also secreted Wnt antagonists known as secreted Frizzled-related proteins (sFRPs). As their name suggests they share homology with Fz receptors, containing a similar CRD domain but not the membrane spanning or intracellular sequences. Frzb1 (or sFRP3) binds Wnt directly and is capable of blocking axis duplication in

Xenopus i.e. blocking Wnt signalling [159-161]. Several different sFRPs are expressed in a broad range of tissues during development where they appear to be able to selectively block specific Wnts [162,163]. They have been shown to bind to members of the Wnt1 class but not, to date, to Wnt5a.

Two other unrelated secreted proteins, Wnt inhibitory factor-1 (WIF-1) and Cerberus, bind to Wnts directly to inhibit their activity [164,165]. Members of the Dickkopf (Dkk) family influence the efficacy of Wnt signalling but, unlike other antagonists, do not bind Wnts directly [166-168].

1.3.2 THE WNT/BETA-CATENIN PATHWAY

β-catenin is central to the function of the Wnt/β-catenin pathway. It is normally found in two pools within the cell: one at the membrane associated with Cadherin and the other in the cytoplasm [169]. In the absence of Wnt signals β-catenin is ubiquitinated and degraded by the proteasome pathways. Wnt binding and activation prevents this ubiquitination, raising cytoplasmic β-catenin levels. This free signalling pool of β-catenin enters the nucleus and forms a complex with members of the Tcf/Lef family, which regulates target gene expression (see Figure 1.3). This whole process is driven by a series of interactions between several intracellular proteins as described below.

Four proteins (labelled the "destruction complex" [170]) promote β-catenin degradation to maintain steady state low levels: GSK-3, Axin, APC and β-TrCP/Slimb. Axin and APC bind β-catenin and GSK-3 to facilitate phosphorylation of β-catenin by GSK-3. This promotes binding to β-TrCP/Slimb, which allows ubiquitination to take place (see Figure 1.3).

1.3.2.1 The "Destruction Complex"

Glycogen Synthase Kinase 3 (GSK-3), a serine–threonine kinase, acts as a negative regulator of the Wnt/β-catenin pathway. Null mutations of *GSK-3* and its *Drosophila* homolog, *zeste-white 3* (*zw3*), result in nuclear accumulation of β-catenin (Armadillo) and activation of the Wnt/β-catenin pathway [171-174]. GSK-3 phosphorylates several highly conserved serine and threonine sites in β-catenin, contributing to its targeting to the proteasome for degradation [174].

Axin interacts with APC, β-catenin, GSK-3 and Dishevelled. It possesses 2 conserved domains, an amino-terminal RGS (Regulator of G-protein Signalling) and a carboxy-terminal DIX domain (found in Axin and Dishevelled [145]). The RGS domain allows binding to APC, a central region to β-catenin and GSK-3, and the carboxy terminus facilitates interactions with Dishevelled. Axin acts as a bridge between GSK-3 and β-catenin, allowing GSK-3-dependent phosphorylation and degradation of β-catenin [175-177]. Axin is itself a target for GSK-3 phosphorylation, which improves the effectiveness of its binding to β-catenin [178,179].

APC binds to β-catenin, GSK-3 and Axin. It was originally identified as a tumour suppressor protein. It also appears to act as a negative regulator of β-catenin, facilitating its phosphorylation and degradation in a similar manner to Axin [180,181]. However, APC overexpression in *Xenopus* mimics Wnt activation suggesting that APC can also function as a positive regulator [182].

Phosphorylated β-catenin specifically binds to β-TrCP/Slimb, a component of the SCF ubiquitin ligase complex. Interaction with this complex results in β-catenin ubiquitination and proteolysis by the 26S proteasome [183-185]. In *Drosophila*, loss of β-TrCP/Slimb causes accumulation of high levels of Armadillo (*Drosophila* homolog of β-catenin) and Wnt activation, consistent with β-TrCP/Slimb's role as another negative regulator of the Wnt/β-catenin pathway [40].

1.3.2.2Dishevelled (Dsh)

Dsh is the most upstream intracellular component of the Wnt/β-catenin pathway. Its mode of interaction with the Wnt/Wg receptors is poorly understood. It is a phosphoprotein absolutely required for Wg signalling [186], which becomes more highly phosphorylated when signalling is activated, when it appears to be recruited to the cell membrane. Dsh overexpression, in the absence of Wg, leads to its hyperphosphorylation and Arm accumulation, thus mimicking Wg signalling [187-189].

Dsh binding to Axin facilitates its interaction with zw3/GSK-3 [190,191]. It is thought to downregulate zw3/GSK-3 activity via direct phosphorylation, and possibly indirectly through inhibition of Axin-stimulated effects [192].

1.3.2.3 GSK-3 Binding Protein (GBP)

GBP and its mammalian ortholog Frat1, like Dsh, act as positive regulators of the Wnt/β-catenin pathway. Overexpression of GBP/Frat1 in *Xenopus* induces axis duplication, thereby mimicking Wnt/β-catenin signalling [193]. GBP expression also stabilizes β-catenin, probably through inhibition of GSK-3 activity. Dsh and GBP have been shown to interact *in vitro* and *in vivo*. They have been identified in a common, Wnt1 dependent, complex along with Axin and GSK-3 [191].

It is therefore generally accepted that Dsh and GBP, activated by Wnt, inhibit GSK-3-mediated β-catenin phosphorylation thereby stimulating β-catenin signalling and function (see Figure 1.3)

1.3.2.4 Targets and Regulation

Following stabilisation cytoplasmic β-catenin migrates to the nucleus where it binds to members of the Tcf/Lef family of transcription factors to form a complex, which stimulates target gene expression [194]. Tcf1 (T-cell factor 1) was first cloned as a gene encoding a T-cell-specific DNA-binding protein [195,196]. Lef1 (lymphoid-enhancer

factor 1) is expressed by both B and T cell precursors [197]. While there are several mammalian Tcfs, *Pangolin*, most closely related to *Tcf1*, appears to be the only *Tcf* gene in the *Drosophila* genome [198,199]. Each Tcf contains a single DNA-binding high mobility group (HMG) domain.

The mechanism of β-catenin activated transcription remains unclear. Two regions of β-catenin have been shown to influence transcription, one at the amino-terminus and one at the carboxy-terminus [198,200,201]. In the absence of Wnt signalling, Tcf/Lef proteins can prevent transcription of Wnt target genes [202,203]. To act as repressors in this manner they appear to require interactions with co-repressors such as Groucho and CtBP (C-terminal Binding Protein) [204,205].

There are many targets of Wnt signalling including developmental genes (*siamois*, *twin* and *ultrabithorax* [202,203,206-208]), cell growth regulators (*c-myc* and *cyclin-D1* [209-211]) and the metalloproteinase, *matrilysin* [212]. Further examples are listed in Table 1.

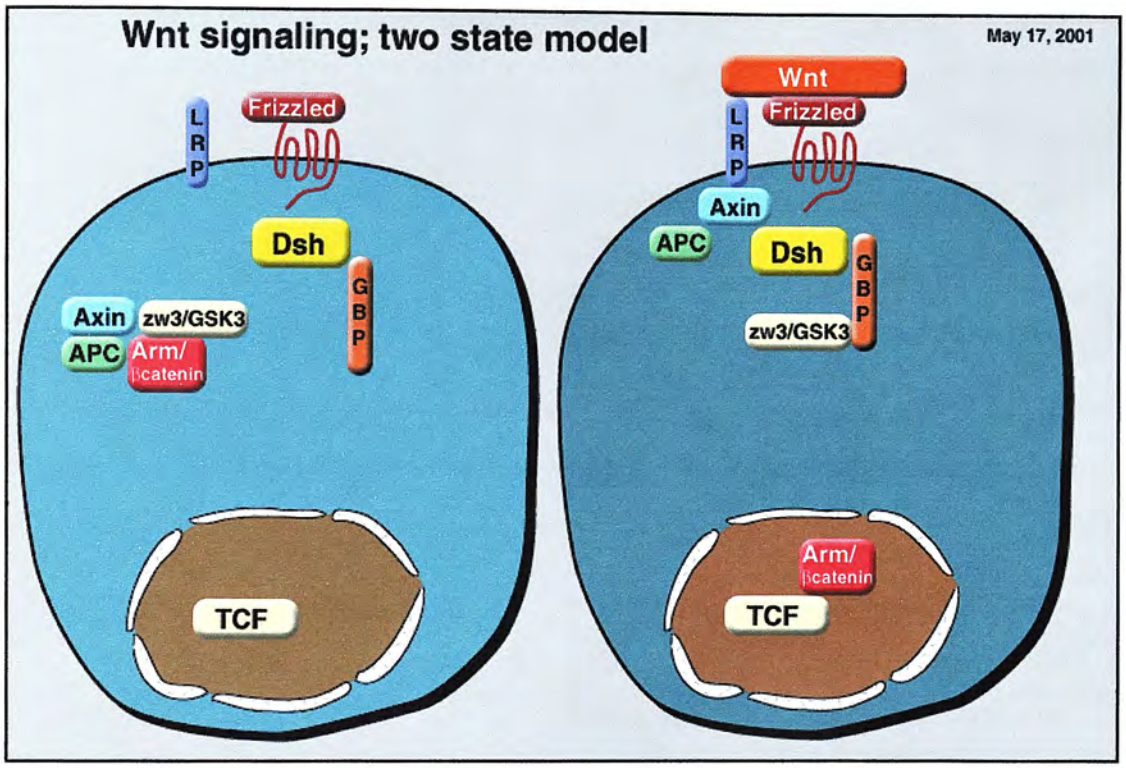

Figure 1.3: The Wnt Signalling Pathway. Taken, with permission, from "The Wnt gene homepage" maintained by Roel Nusse

(www.ana.ed.ac.uk/rnusse/wntwindow.html)

Left panel: In the absence of Wnt signalling Axin, APC and zw3/GSK3 contribute to Arm/β-catenin ubiquitination

Right panel: Upon Wnt binding to Frizzled and LRP, Arm/β-catenin is released form the "destruction complex" (see text). Cytoplasmic β-catenin then migrates to the nucleus where it binds to members of the Tcf/Lef family of transcription factors to form a complex, which in turn stimulates target gene expression

Abbreviations: LRP: low density lipoprotein receptor-related proteins; Dsh: Dishevelled; GBP:GSK-3 Binding Protein; APC: Adenomatous Polyposis Coli; zw3/GSK3: zeste-white 3/Glycogen Synthase Kinase 3; TCF:T cell factor; Arm: Armadillo

Gene	Organism	Effect	Gene	Organism	Effect
CD44	Human	up	**Bmp4**	Xenopus	down
c-jun	Human	up	**Connexin30**	Xenopus	
c-myc	Human	up	**Connexin43**	Xenopus	up
Cyclin D	Human	up	**engrailed-2**	Xenopus	up
fra-1	Human	up	**fibronectin**	Xenopus	up
MMP-7	Human	up	**myogenic bHLH**	Xenopus	up
PPARdelta	Human	up	**Retinoic acid**	Xenopus	
Tcf-1	Human	up	**Siamois**	Xenopus	up
uPAR	Human	up	**Twin**	Xenopus	up
Brachury	Mouse	up	**Xnr3**	Xenopus	up
Cdx1	Mouse	up	**Dfrizzled2**	Drosophila	down
Cyclooxygenase2	Mouse	up	**Dpp**	Drosophila	down
MBTEB2	Mouse	up	**Engrailed**	Drosophila	up
Periostin	Mouse	down	**Shavenbaby**	Drosophila	down
SFRP-2	Mouse	up	**stripe**	Drosophila	down
Stra6	Mouse	up	**ubx**	Drosophila	either
WISP	Mouse	up	**Wingless**	Drosophila	either
Wrch-1	Mouse	up	**Dharma/bozozok**	Zebrafish	up
Connexin43	Mouse,Rat	up	**nacre**	Zebrafish	up
ret	Rat	up	**BetaTrCP**		up

Table 1: Target Genes of Wnt/β-catenin Signalling

Table lists identified target genes of Wnt/β-catenin Signalling Pathway. In each case the gene, organism and the effect of increased pathway activity on expression (up or down-regulated) is listed. Table adapted, with permission, from "The Wnt gene homepage" maintained by Roel Nusse

(www.ana.ed.ac.uk/rnusse/wntwindow.html)

1.3.3 WNT/CA^{2+} PATHWAY

Less is known about this Wnt dependent pathway. As already described members of the Wnt1 class signal preferentially through the Wnt/β-catenin pathway and Wnt5a through the Wnt/Ca^{2+} pathway [150]. In addition, Wnt5a factors have been shown to antagonise the function of Wnt1 factors [213], implying an antagonistic effect of the Wnt/Ca^{2+} on the Wnt/β-catenin pathway.

It appears that Fzs are capable of discriminating between different Wnt ligands, thus determining which downstream pathway is activated in the cell. There are also two functionally distinct classes of Fzs, which allow activation of either the Wnt/β-catenin or the Wnt/Ca^{2+} pathway. It is possible that Fzs activating the Wnt/Ca^{2+} pathway do so through G-protein interactions, though it is unclear whether G-proteins play a direct or indirect role in signalling [214]. Besides modulating adhesion and cell movements, the function this pathway plays in embryonic development is unclear.

1.3.4 DISHEVELLED

It has been recently shown that Dsh functions in at least two distinct signalling pathways. As already described it is required for Wg signalling. However it also plays a role in epithelial planar polarity (tissue polarity). *Dsh* null mutations in *Drosophila* have phenotypes consistent with loss of Wg signalling [215], but the first mutant reported (*Dsh^1*) displayed planar polarity defects characterized by misorientation of cells within epithelia in the wings, thorax and eyes. The random arrangement of the hairs on the wing and thorax prompted the phenotype to be named Dishevelled [216].

By genetic epistasis analysis *Dsh* has been placed downstream of *Fz* in polarity signalling [215,216]. Significantly, manipulation of other members of Wg signalling, such as zw-3, Arm and Pangolin, does not affect planar polarity. The planar polarity

signalling pathway downstream of Fz actually consists of Dsh and small GTPases of the Rho family, leading to activation of the c-Jun N-terminal kinase/stress-activated protein kinase (JNK/SAPK) cascade [188,217,218]. Thus, a pathway distinct from the Wnt/β-catenin and Wnt/Ca^{2+} pathways has emerged.

There are presently 3 murine and 3 human *Dsh* homologues referred to as (mouse or human) *Dvl1* to *3* [219-221]. There is 40-50% amino acid identity between *Drosophila Dsh* and any of the murine *Dvls*, and 60-70% identity amongst murine *Dvls*. All Dishevelled genes (including vertebrate and invertebrate homologues) have three highly conserved domains. An amino-terminus DIX (Dishevelled-Axin) domain also found in Axin, a central PDZ domain and a carboxy-terminus DEP (Dishevelled-EGL-10-Pleckstrin) domain, which can also be found in factors involved in G protein signalling [222-224]. The DEP domain is essential for polarity signalling, whereas the DIX domain is dispensable. Conversely the DIX domain is crucial for Wg signalling, in which most of the DEP domain is dispensable [188,217,225]. Therefore Dsh may preferentially activate one or other of these downstream pathways through its DEP and DIX domains, though how this is controlled is not known.

Dvl1 null mutants have no obvious anatomical abnormalities and are viable and fertile. However, they display abnormal social behaviour and several neurological defects [226]. Mutations in the other mouse *Dvl* genes have not yet been reported and thus phenotypic effects remain unknown.

1.3.5 THE WNT PATHWAY IN LUNG DEVELOPMENT

1.3.5.1 The Wnt Pathway and the lungs

Whilst the most common sites for Wnt expression in mouse embryos are the limbs and central nervous system [227,228], many are expressed in both embryonic and adult lung tissue [227,229-234]. Similar expression has also been noted in human lung tissue [235-237]. In common with related growth and differentiation factors, such as FGFs, TGF-β

and Hh proteins, Wnts appear to be particularly important in controlling epithelial-mesenchymal interactions involved in branching morphogenesis. Notably, though *Wnt2* is present in both adult and embryonic tissue, expression is higher in the latter in keeping with a particular association between Wnt signalling and organogenesis. *Wnt2* and *Wnt11* are predominantly expressed in the developing lung mesenchyme, consistent with Wnt signalling from mesenchymal cells to adjacent epithelium during morphogenesis [229-231]. However no *Wnt* mutations to date have resulted in abnormal lung development, which may be due to functional redundancy and overlap between the many *Wnts*.

The three murine *Dvl* genes are widely expressed throughout the embryo and the adult mouse, including the lungs, with maximal expression in the central nervous system [219-221]. There is considerable overlap in this expression suggesting they have redundant functions.

1.3.5.2 Wnt and Hedgehog Signalling

Wg is a target of Hh signalling [3], and *Wnt5A* expression is dependent upon Shh in the developing hair follicle [238]. It also appears that *Wg* maintains *Hh* expression in *Drosophila* [239], and it has been proposed that *Wnt7A*, *10A* and *10B* may regulate *Shh* in the developing limb and hair follicle [228,238]. Thus the two pathways are capable of upregulating each other, suggestive of a paracrine signalling loop between epithelial and mesenchymal cells: Hh signalling from epithelium to mesenchyme and Wnt from mesenchyme to epithelium.

1.3.5.3 Wnt and TGFβ

Several studies, in *Xenopus* and *Drosophila*, have shown that cooperation between the TGFβ and Wnt/Wg signalling pathways plays a role in development [203,240,241]. Smads are signal transduction molecules critical for transmitting TGFβ signals form the cell surface to the nucleus [242]. Smad4 is known as a common mediator Smad as it is required for all TGFβ superfamily signalling and Smad3 is specifically associated

with TGFβ receptors [243]. It has recently been shown that Smad4 interacts directly with Tcf/Lef1 and indirectly with β-catenin, and activation of the Wnt pathway alone enhances the Smad4/ β-catenin interaction [244]. Subsequent to this, interactions between Smad3 and both Tcf/Lef1 and Axin have also been demonstrated [245,246]. In addition, TGFβ-Wnt cooperation may also mediate carcinogenesis. When both signalling cascades are altered there is an associated increase in progression of benign adenomatous polyps to invasive carcinomas [247]. Thus, it is possible that these pathways may play combined roles in other TGFβ related disease processes, such as interstitial lung disease (ILD). This possible association prompted the experimental work presented in Chapter 5.

1.3.6 THE WNT PATHWAY AND CELL PROLIFERATION

Wnt1 promotes proliferation of epithelial cells and fibroblasts both *in vivo* and *in vitro* [248-251]. Expression of other Wnts, such as Wnt5A and Wnt11, has also been associated with increased epithelial cell proliferation [252,253]. In the immune system Wnt proteins can stimulate pro-B cell proliferation via Lef1 [254]. In addition, Wnt signalling promotes anti-apoptotic effects, in that Wnt1 inhibits chemotherapy-induced apoptosis through β-catenin/Tcf mediated transcription [255]. Furthermore, ectopic β-catenin expression has been shown to inhibit apoptosis, and APC overexpression (inhibiting β-catenin accumulation and Wnt signalling) induces apoptosis in human colorectal cancer cells [256,257].

However, it has been reported that the pathway can, in some circumstances, induce pro-apoptotic effects. β-catenin and Tcf expression have been shown to promote apoptosis in *Drosophila*, mouse and human cells [258-261]. Related to this, *Kim et al* [261] showed that the apoptotic effect in NIH 3T3 fibroblasts was independent of Lef1; implying that β-catenin may be interacting with other unknown proteins in this respect. Finally, and of most relevance to this thesis, Stovel *et al* [262] have recently

demonstrated that overexpression of *Dvl* genes in COS-1 and C57MG cells results in an APC-dependent apoptosis.

The role of Wnt signalling in cell proliferation and apoptosis therefore remains ambiguous. It is likely that other, as yet unknown, mechanisms are also involved.

1.3.7 THE WNT PATHWAY IN DISEASE

1.3.7.1 Wnt Pathway and Cancer

As described, *Wnt1* was originally identified as a preferred integration site for mouse mammary tumour virus in breast carcinomas [142]. *Wnt1* transgenic mice develop mammary epithelial hyperplasia and adenocarcinoma [263,264], and Wnt1 is capable of transforming mammary epithelial cell lines *in vitro* [265,266]. Though none have been identified to date it is likely that Wnt1 mutations act as oncogenes in humans. Germline APC mutations are associated with familial adenomatous polyposis (FAP), which results in colorectal polyps early in adult life [267,268]. Somatic APC mutations are linked with >80% of sporadic colorectal adenomas and carcinomas [269,270]. In addition, APC mutations have been implicated in aggressive fibromatosis and as a genetic modifier of BRCA penetrance for breast cancer [271,272]. β-catenin has been found to be highly mutable in a range of human cancers including endometrial, hepatocellular and ovarian carcinoma, medulloblastoma, synovial sarcoma and prostatic tumours [170].

1.3.7.2 Wnt and Lung Disease

There are at present only a few preliminary studies linking Wnt signalling with diseases of the lung. Differential display analysis has confirmed the presence of *sFrp1* in emphysema but not in normal human lung tissue. In addition, mouse *sFrp1* was detectable in the lungs of both transgenic and smoke-induced emphysema models but not in normal adult mouse lung [273]. It has also been suggested that the

observed apoptosis in emphysema is secondary to *sFrp1* expression, though this has not as yet been proven [274].

Further more recent studies suggest that β-catenin may play a role in the pathogenesis of pulmonary fibrosis, and in airway epithelial repair [275,276]. These preliminary observations were based on immunohistochemistry findings in mouse model systems. In the former, β-catenin expression appeared to be downregulated in the 'small airway epithelial cells' of mice with bleomycin-induced fibrosis [275]. Finally, in non-small cell lung cancer, high β-catenin expression was identified as a significant and independent favourable prognostic factor, suggesting that, in these tumours, β-catenin activation does not have the same oncogenic potential as it has in other tumours such as colonic carcinomas or hepatomas [277].

1.4 Interstitial Lung Disease

1.4.1 EPIDEMIOLOGY AND CLINICAL FEATURES

Interstitial lung disease (ILD), or pulmonary fibrosis, is the end result of a multiplicity of pathological processes, from infections to autoimmune diseases. It can be associated with connective tissue diseases, dust or particle exposure, vasculitides and drug toxicity amongst others. However in the largest single group of patients with ILD the aetiology is unknown; hence the name idiopathic pulmonary fibrosis (IPF), or crytogenic fibrosing alveoilitis (CFA).

Patients with IPF most commonly present between the ages of 50 and 70 years. It is more common in men with an annual incidence (in the USA) of 10 per 100,000 compared with 7 per 100,000 women [278]. Up to 3% of cases appear to cluster in families, suggesting a genetic susceptibility in some patients [279]. Although several polymorphisms have been observed, there is no clear evidence of a specific genetic abnormality [280]. Up to 75% of patients with IPF are current or former smokers and smoking has been epidemiologically linked with IPF, as a potential independent risk factor [281,282]. Several viral infections, especially those caused by the herpes virus family, have been implicated but the evidence in support of a viral aetiology is inconclusive [283-285]. In addition, despite some associations with metal or dust exposure, no industrial or environmental factor has been clearly linked to IPF [286].

Patients with IPF typically present with a history of exertional dyspnoea and a non-productive cough [287]. Many have symptoms for at least 6 months before diagnosis. On examination up to 50% have finger clubbing and lower zone inspiratory crackles are audible on chest auscultation [288]. Late in the course of the disease there may also be clinical features of pulmonary hypertension and cor pulmonale. The typical chest radiograph reveals bilateral lower zone peripheral reticular opacities, progressing to peripheral honeycombing [289]. Pulmonary function tests reveal a restrictive impairment with a reduced carbon monoxide diffusing capacity [290]. High resolution

computerised tomography (CT) is used to image the lungs in greater detail. CT appearances have been shown to correlate with physiological impairment and fibrosis on lung biopsy [291].

1.4.2 PATHOGENESIS

1.4.2.1 Pathology

The clinical label "idiopathic pulmonary fibrosis" is now reserved for a specific group of patients with what is now termed usual interstitial pneumonia (UIP). Histologically, UIP is characterized by a heterogeneous appearance comprising alternating areas of normal lung, interstitial inflammation, fibroblastic foci, dense fibrosis and "honeycomb lung", with a predilection for the peripheral subpleural parenchyma [292]. Honeycombing refers to densely fibrotic lung with macroscopically characteristic visible spaces. Areas of scarring may be associated with significant smooth muscle proliferation. The pleomorphic cellular infiltrate is largely composed of monocytes and lymphocytes, which may form focal aggregates, and relatively few granulocytes. There is alveolar wall thickening due to collagen deposition and loss of type I alveolar epithelial cells (pneumocytes), with what appears to be a compensatory hyperplasia of the type II pneumocytes (Figure 1.4 A and B)[293].

Other idiopathic interstitial pneumonias display particular distinguishable histologic features. Desquamative interstitial pneumonia (DIP) is notable for the cellular appearance of biopsies due to marked alveolar macrophage accumulation and pneumocyte hyperplasia. Fibroblastic foci and honeycombing are less prominent features than in UIP [294]. Acute interstitial pneumonia involves a diffuse fibroproliferative response to alveolar injuries, with significant type II pneumocyte hyperplasia, diffuse fibroblast and myofibroblast proliferation and alveolar septal collapse with intra-alveolar exudates and hyaline membranes [295]. Nonspecific interstitial pneumonia is characterized by varying degrees of fibrosis and inflammation evenly distributed throughout the lung [296].

1.4.2.2 Original Hypothesis

A long held hypothesis of "inflammatory fibrosis" states that chronic inflammation leads to lung injury and fibrogenesis, resulting in end-stage fibrotic scar [297]. A recent review by Selman *et al* [292] argues that this may not be the case, suggesting an alternative hypothesis.

Following an extensive literature review Selman *et al* [292] found little evidence that inflammation is most prominent in the early stages of UIP, as had previously been believed. In addition, the inflammatory component of UIP is usually mild, being most closely associated with collagen deposition or honeycombing [298]. They also found evidence that that inflammation is not absolutely necessary for fibrosis. Interleukin-10 deficient mice displayed more pronounced inflammation but less fibrosis than wild type controls when treated with silica [299], and hyperoxia induced mouse epithelial injury is sufficient to induce fibrosis in the absence of ongoing inflammation [300]. Most inflammatory markers have shown no real correlation with disease stage or prognosis in IPF, including bronchoalveolar lavage (BAL) cell constituents, gallium scanning and circulating immune complexes [301-304]. Finally, in contrast with other potentially fibrotic lung disorders, anti-inflammatory therapy (glucocorticosteroids being the mainstay) yields only marginal or no responses in patients with UIP [305-307].

1.4.2.3 Emerging Hypothesis

It has recently been proposed that UIP is actually due to abnormal wound healing in the lung, distinguished by the absence of adequate reepithelialization and abnormal myofibroblast behaviour, and characterized by epithelial-fibroblast interactions [292].

In UIP the reeipthelialization of the alveolar epithelium appears to be inadequate. The type II pneumocytes have a reduced capacity to restore damaged type I cells, resulting in abnormal phenotypes, pulmonary surfactant abnormalities and alveolar

collapse [308-310]. In IPF the alveolar epithelial cells have been shown to strongly express greater quantities of procoagulants and antifibrinolytics such as tissue factor and plasminogen activator inhibitor-1 and –2 [311-313], thereby impairing cell movement in the extra cellular matrix fibrin and impeding repair. Epithelial cells in IPF also express several profibrotic cytokines and growth factors such as platelet-derived growth factor, TGFβ_1 and tumour necrosis factor-α (TNFα) [314-316].

It has been shown that the extent of fibroblastic foci within the injured lung is related to the progression to dense fibrosis [298,317]. Probably largely driven by factors released from the epithelial cells, the fibroblasts progress through migratory and proliferative to a final profibrotic phenotype (myofibroblast) [317]. It has also been shown that lung fibroblasts and myofibroblasts from patients with IPF induce *in vitro* alveolar cell death [318]. Another proposed contributing factor to the failure of reepithelialization in IPF is excessive alveolar cell apoptosis, particularly in areas adjacent to these myofibroblast foci [319].

The basement membrane (BM) plays a role in maintaining the alveolar epithelium, and its disruption is important in lung fibrosis pathogenesis [320], as fibroblast and myofibroblast migration into alveolar spaces occurs through disrupted BM [317]. How BM disruption occurs is unknown, though it has been suggested that myofibroblasts may play a role [321].

As already inferred fibroblasts and myofibroblasts are crucial in the synthesis, deposition, and remodelling of extracellular matrix (ECM). Excess deposition of ECM including fibrillar collagens, fibronectin, elastic fibres, and proteoglycans is the hallmark of the aberrant tissue remodelling in IPF [322,323].

1.4.2.4 Cytokines in ILD

It has been suggested that an imbalance in cytokines, with a shift toward T helper2 (Th2) type, contributes to fibrogenesis. Th1 and Th2 cytokines are not only produced by their respective $CD4^+$ T helper subsets; they are also released by other cell types

such as fibroblasts, macrophages and mast cells. Type 1 cytokines include interferon gamma (IFNγ), TNFβ, and the interleukins, IL2, IL12 and IL18, while Type 2 cytokines include IL4, IL5, IL10, IL13 and monocyte chemoattractant protein1 (MCP1). Several of these will be discussed further in Section 1.6.

IL4 has been shown to promote fibroblast proliferation, collagen gene expression and collagen synthesis [324-326]. IL13 and MCP1 increase *in vitro* type 1 procollagen production, and IL10 is capable of suppressing type 1, thus favouring type 2 cytokines [327,328]. In contrast the type 1 cytokine, IFNγ, inhibits fibroblast proliferation and collagen deposition as well as inhibiting TGFβ synthesis and action [329-331]. Other type 1 cytokines appear to promote IFNγ production [332].

These findings are further strengthened by animal studies. IL4 is raised in a rat model of radiation-induced lung fibrosis, and both IL5 and MCP1 in a mouse bleomycin model [333-335]. Furthermore blocking either IL5 or MCP1 reduces inflammation and fibrosis [336,337]. Type 2 cytokines are not necessarily produced in isolation. In a mouse model of silicosis lymphocyte IFNγ production is increased consistent with a type 1 cytokine role in fibrosis [338]. In human studies, expression of the type 2 cytokines IL4, IL5, IL13 and MCP1 was increased in cells (including fibroblasts, alveolar macrophages and lymphocytes), BAL and serum from patients with fibrotic disease [339-343]. Proportionally more mononuclear cells in the lungs of patients with IPF stained positively for IL4 and IL5 (>50%) than IFNγ (<7%), as assessed by immunohistochemistry [344]. Therefore, evidence for predominant type 1 cytokine activity in the granulomatous diseases, sarcoidosis and hypersensitivity pneumonitis, goes against the grain somewhat though it serves to remind us that it is likely that type 1 cytokines may also play some role in ILD [345-348].

Of the three TGFβ isoforms, $TGF\beta_1$ has been most widely studied in the context of fibrogenesis. TGFβ is produced by T cells, monocytes/macrophages, platelets, fibroblasts and epithelial cells, and influences both immune and structural cells. It is capable of suppressing monocyte function and of inhibiting B and T cell proliferation

[349]. Notably, TGFβ and IFNγ appear to be mutually antagonistic [350]. TGFβ is known to be a strong stimulator of ECM production including collagen, proteoglycans and fibronectin [351], and is capable of inducing a myofibroblast phenotype in fibroblasts *in vitro* [352]. *In vivo*, TGFβ expression is increased in a variety of mouse models and in human ILD [353-357]. Using adenovirus vectors, it has been shown that transient overexpression of the active form of $TGF\beta_1$ in rat lungs induces a myofibroblast phenotype and a severe irreversible fibrogenesis in the pulmonary interstitium and pleura. Moreover, similar overexpression of the full-length latent $TGF\beta_1$ protein does not induce fibrosis, implying that the state of TGFβ activation is crucial [358]. How this activation might occur *in vivo* is not fully understood.

In addition it seems that other profibotic molecules, such as TNFα and granulocyte – macrophage colony-stimulating factor may mediate their fibrogenic effects through TGFβ upregulation [359].

1.4.2.5 CD40-CD40L

CD40 is a member of the TNFα receptor superfamily initially identified on B lymphocytes and its ligand, CD40L, is found on activated T lymphocytes [360]. CD40-CD40L interactions are known to stimulate T lymphocyte cytokine production (IL4, IL6, IFNγ), B lymphocyte antibody production and fibroblast activation [361,362]. CD40 is also expressed on macrophages, dendritic cells, fibroblasts, epithelial and endothelial cells [363-366], and CD40L is also found on mast cells, eosinophils and activated platelets [367].

Therefore following injury CD40-CD40L interaction promotes production of proinflammatory cytokines and the profibrotic prostaglandin E_2 [368], cell adhesion molecule expression and fibroblast activation. Therapeutically blocking this interaction, with an anti-CD40L antibody (MR1), has been shown to protect mice from radiation-induced lung injury and fibrosis [369].

1.4.2.6 Lymphocytes

The number of T lymphocytes is increased in the BAL of patients with IPF when compared with normal controls. T lymphocyte infiltration is also characteristic. Although all subsets are represented, a relative increase in the number of $CD8^+$ T cells has been correlated with a poorer prognosis [370]. The potential role of $CD4^+$ T cells in ILD pathogenesis with particular respect to Th2 cytokine production has already been discussed.

The total number of B lymphocytes is also increased in IPF, and B-lymphocytic follicles with germinal centres have been identified in biopsy sections [371]. IgG levels are increased in the BAL of IPF patients, suggesting there is active local immunoglobulin production [372,373], against an as yet unknown antigen(s). Wallace *et al* did however identify a 70-90kDa cytoplasmic protein present in alveolar epithelial lining cells, which is recognised by autoantibodies from the plasma of IPF patients [374,375].

1.4.3 TREATMENT AND PROGNOSIS

1.4.3.1 Anti-inflammatory therapy

In early reports addressing the use of corticosteroids and cytotoxic agents in the management of IPF response rates of 10-40% were noted [288,376,377]. However, other idiopathic interstitial pneumonias than UIP, which are generally more responsive to steroid therapy, were not excluded in such studies. When they are, and UIP is looked at in isolation, there is little evidence of a meaningful response to anti-inflammatory drugs [378-380]. Therefore current evidence does not support the use of anti-inflammatory drugs in IPF/UIP. However a trial of therapy is often attempted particularly in cases in which features of other idiopathic interstitial pneumonias than UIP are identified.

Current British Thoracic Society Guidelines for the treatment of IPF [381] recommend initial combined therapy with the corticosteroid, prednisolone, and azathioprine or cyclophosphamide. If there is an objectively measurable response therapy should be continued with steady reduction in prednisolone dose. If not, alternative therapies such as colchicines should be considered. Referral for lung transplantation should be considered shortly after failure of first line treatment. Lung transplantation has emerged as a viable option for IPF patients over recent years [382].

1.4.3.2 Anti-fibrotic therapy

Therapies aimed at directly inhibiting fibrogenesis have also been applied to IPF. Colchicine has been shown to increase expression of collagen–degrading enzymes and suppress fibroblast growth factors *in vitro* [383]. However, though initial studies using colchicine therapy seemed promising [384], as with anti-inflammatory drugs it appears to offer no benefit when given to patients with confirmed UIP [306,307]. The collagen cross-link inhibitor pencillamine is equally ineffective [306]. Other potential anti-fibrotic therapies include pirfenidone, a growth factor inhibitor shown to have some effect in animal studies and a preliminary IPF trial [385,386]; relaxin, which inhibits fibrogenesis in mice and has improved lung function in patients with systemic sclerosis [387,388]; and suramin, which has shown some benefits in rabbit models [389]. Futhermore, inhibitors of fibroblast mitogenic peptides such as endothelin1 and angiotensin II have also been considered [390,391].

Consistent with the "emerging hypothesis" for the pathogenesis of IPF new therapies aimed at enhancing reepithelialization are being tried, including N-Acetylcysteine [392] and Keratinocyte growth factor [393].

1.4.3.3 Anti-cytokine therapy

In an attempt to manipulate the type 1-type 2 cytokine balance IFNγ has been used to treat fibrotic disease in mice, with some success [394]. More recently IFNγ–1b has been shown to improve lung capacity and oxygenation, and reduce mRNA levels of the

profibrotic cytokines TGFβ and connective tissue growth factor, in patients with IPF [350]. IFNγ therapy has also proved efficacious in patients with systemic sclerosis induced pulmonary fibrosis [395]. As a result of such success a multicentre trial of IFNγ in IPF treatment has been commenced. IL12 therapy has also proved successful in reducing the severity of bleomycin-induced fibrosis [396].

As a precautionary note, skewing the cytokine profile towards type 1 responses may cause its own problems. Though not as yet encountered in human studies there is a theoretical risk of inducing type 1 associated disease such as autoimmune disease.

There has been some preliminary work on anti-TGFβ therapy for lung fibrosis in animals, but none as yet in humans. In rodents, anti-TGFβ antibodies and TGFβ–soluble receptors have been shown to reduce bleomycin-induced fibrosis [397,398]. Overexpression of decorin, a proteoglycan known to block TGFβ activity [399], can also inhibit fibrogenesis in the bleomycin model [400]. As with anti-cytokine therapy side-affects of generally blocking TGFβ could potentially arise, particularly in view of its many biological functions. In both cases targeted localised inhibition may be preferable.

1.4.3.4 Prognosis

IPF is a progressive disease from which 40% of patients die with respiratory failure. End-stage disease is characterized by severe pulmonary hypertension with cor pulmonale (secondary right heart failure). The median survival is less than 3 years [401]. Poor prognostic factors include older age, poor lung function at presentation and advanced fibrosis [402]. There is also an, as yet unexplained, increase in the incidence of bronchogenic carcinoma in IPF patients [403].

1.4.4 FITC MODEL OF ILD

As discussed, most IPF patients have symptoms for more than 6 months, and the average duration of symptoms is 24 months, before diagnosis [292]. As a result of the insidious onset and late presentation it is impossible to study the initial events in human disease. It is in this respect that animal models have proved most useful. There are presently a range of models of lung fibrosis, some of which have already been mentioned, including those induced by bleomycin, metals, reactive chemicals and dusts [404-407]. In one such rodent ILD model, a single intra-tracheal administration of the fluorescent hapten fluorescein isothiocyanate (FITC) resulted in a patchy fibrosis, which was localised to areas of FITC deposition (Roberts *et al* [408]). Since this model was used in the experiments reported in this thesis I will describe it in detail.

Following FITC instillation rodents initially develop an acute inflammatory response characterized, at 3 days, by a diffuse interstitial and alveolar mononuclear cell and neutrophil infiltrate, significant airway epithelial cell hyperplasia and alveolar oedema. By 5 months, a focal, patchy, peribronchial interstitial fibrosis and predominantly mononuclear infiltrate are evident. FITC fluorescence can be co-localized to areas of fibrosis by confocal microscopy (Figures illustrating this are included in Chapter 3). The BAL differential cell counts from the original paper [408] confirmed a shift from a baseline control of predominantly macrophages/monocytes to a marked relative increase in neutrophils by 24 hrs post-FITC. Lymphocytes become apparent from day 7 and persist thereafter (Figure 1.4C). Specific anti-FITC antibodies are detectable in the serum of treated rats from 7 days to 6 weeks following FITC instillation. This fibrosis model was reproduced by Christensen *et al* [409], who also confirmed that the levels of hydroxyproline, a surrogate marker of collagen deposition, in FITC treated mice were nearly double that of controls; a similar relative increase as that found in bleomycin-induced fibrosis [410]. They also showed that FITC-induced fibrosis, as measured at 3 weeks, did not appear to be T cell dependent. Data concerning the potential role of T cells in the bleomycin model is conflicting [410-412].

Roberts *et al* [408] proposed a mechanism in which intra-tracheal FITC is cytotoxic to the airway epithelial cells, resulting in epithelial cell shedding, and a compensatory hyperplasia. The FITC is then able to bind to exposed proteins such as elastin through the breached epithelium, inducing chronic inflammation and fibrosis.

Both groups have suggested potential advantages of the FITC model of ILD over other animal models [408,409]. As FITC can be visualised by its fluorescence its association with the observed pathology can be easily assessed. The patchy distribution of the fibrosis in the FITC model is more reminiscent of the pattern seen in IPF, though the peribronchial distribution is not. In addition, the chronic persistent inflammation characteristic of FITC-induced fibrosis may allow further analysis of links between such inflammation and fibroblast biology.

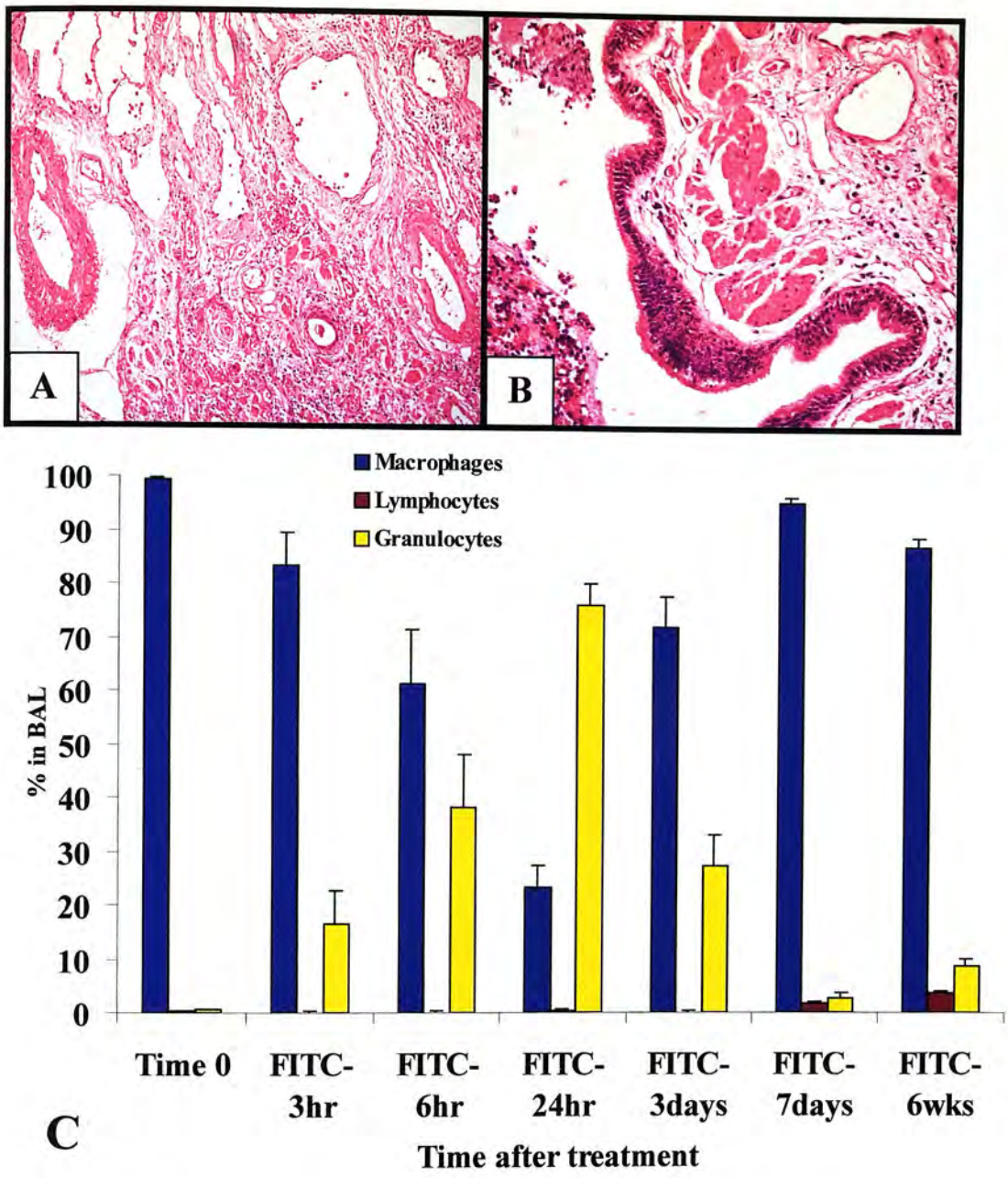

Figure 1.4: Interstitial Lung Disease histology and BAL differential

Haematoxylin & Eosin stains of biopsy sections from a patient with Idiopathic Pulmonary Fibrosis. **A)** Normal alveoli are seen adjacent to areas of fibrosis with markedly thickened alveolar walls, inflammatory infiltrate and ECM deposition. **B)** Note marked airway epithelial hyperplasia.

C) Differential bronchoalveolar lavage fluid (BALF) cell count in FITC treated mice. As indicated, the blue bars represent the percentage of macrophages, the maroon of lymphocytes and the yellow of granulocytes. Data represent mean and standard error the mean; 4-7 mice at each time-point. Taken from original FITC paper by Roberts *et al.*

1.5 Human T Cell Activation

In this section it is not my intention to review T cell biology in its entirety, but to discuss the areas that relate to the experimental work of this thesis.

T cell activation, clonal expansion and the induction of effector function are essential events in the efficient response of the immune system. Optimal activation is dependent on at least two signals following contact and adhesion between the APC (antigen presenting cell) and T cell. The first signal is mediated through recognition of antigenic peptide/MHC (major histocompatability complex) complexes on the cell surface of APCs by the T cell receptor (TCR). The second signal(s) is provided by ligation of co-stimulatory receptors (eg CD28) expressed on T cells and by ligands expressed on APCs.

1.5.1 T CELL RECEPTOR MEDIATED ACTIVATION

1.5.1.1 Antigen Presentation

Of the APCs, which include B cells and macrophages, dendritic cells (DCs) are particularly important in activating primary naïve T cells. DCs normally reside throughout all non-lymphoid tissues in a resting, so-called immature state. In response to inflammatory stimuli or pathogens, they migrate to the T cell areas of secondary lymphoid organs where they switch from an antigen capturing to an antigen presenting mode [413,414]. During this so-called DC maturation they assemble peptide-MHC complexes, upregulate co-stimulatory molecules such as B7.1 and B7.2, and release cytokines such as IL12, IL18 and IL4 [415-418]. Mature DCs have a finite life span, surviving for only a few days after reaching lymph nodes and for up to 48 hours after interacting with antigen-specific naïve T cells [419,420].

Immature DCs efficiently capture exogenous antigens and, upon maturation, load the antigenic peptides onto newly synthesized MHC class II molecules, which accumulate on the cell surface for in excess of 100 hours thereby maximising presentation [415,421-423]. DCs process and present on MHC class I molecules viral proteins that are either synthesized intracellularly or taken up from apoptotic cells [416,424]. These peptide-MHC class I complexes have only relatively short half-lives (~ 10 hours) and therefore must be continually replenished using internal antigen sources to facilitate presentation.

1.5.1.2 T Cell Receptor Mediated Activation

The TCR is a complex machine that allows the T cell to monitor and, when appropriate, respond to the presentation of antigen. TCR signalling is sustained for as long as the T cell is in contact with the APC, ceasing immediately after the antigen is removed [425,426]. Variable TCR αβ and γδ receptors are associated with the invariant CD3 γ, δ, ε and ζ proteins to from the TCR-CD3 complex. TCR mediated antigen recognition results in downstream activation of a number of intracellular signalling pathways, some associated with cytokine gene expression. The CD3 chains are responsible for TCR associated signal transduction, though they do not in themselves possess intrinsic enzymatic activity. They influence activation signals, including IL2 production, which is a key event in T cell activation, through cytoplasmic tail motifs, ITAMs (immunoglobulin family tyrosine-based activation motif) [427-429]. However, binding of the TCR to the antigen-MHC complex is not sufficient in itself to induce T cell activation. As discussed later, co-stimulation is also required.

CD4 and CD8, which are co-receptors on the T cell, appear to have both cell adhesion and signalling functions [430]. $CD4^+$ T cells (T helper or Th cells) only recognise antigen presented with MHC class II, and endogenous antigens complexed with MHC class I molecules activate $CD8^+$ (Tc) cytotoxic T cells. As MHC class I molecules are expressed on almost all nucleated cells, any such cell infected with a virus or intracellular pathogen can present the antigen with class I and thus be removed by cytotoxic attack. In contrast to this specific $CD8^+$ cell targeting, $CD4^+$

activation leads to production of cytokines, which activate a wide range of cells around them. To keep this reaction in check MHC class II molecule expression is therefore limited only to the APCs [431].

After the first round of mitosis, activated T cells divide every ~10 hours. As they divide, under continuous TCR and cytokine stimulation, they progressively differentiate and acquire the ability to produce effector cytokines [432,433]. Polarization towards either Th1 or Th2 is directed by IL12 and IL4 respectively [417,434-436], as well as by the strength and duration of TCR stimulation [437-439].

1.5.1.3 T Cell Synapse

T cell activation requires a long physical coupling between APCs and T cells. Two adhesion pathways capable of maintaining this avidity are the CD2 pathway and the lymphocyte function-associated antigen (LFA)-1/intercellular adhesion molecule (ICAM) pathway. While the issue of the former remains controversial and poorly understood, the role of the αLβ2 integrin (LFA-1) pathway appears to be more straightforward.

Activation of local LFA-1 integrins is one of the first consequences of TCR activation. These integrins do not display significant affinity for their ICAM ligands and have limited cytoskeleton contact in resting T cells. Upon TCR signalling, they reveal a high-affinity binding site for ICAM and strengthen their linkage to the cytoskeleton by actin fasciculation. They converge, forming focal contact areas, thereby increasing their affinity and T cell avidity for the APC, and ensuring binding of the two cellular partners. LFA-1 also delivers a strong co-activation signal within the T cell, which appears to the initial 'second signal'. The area of cell contact, in which signalling and adhesion molecules accumulate, is termed the T cell synapse [440].

Co-stimulation occurs independently of antigen recognition. It is critical to allow full T cell activation, sustain cell proliferation, prevent anergy, and induce effector function and differentiation into memory cells. Co-stimulator receptors include CD28, ICOS (inducible co-stimulator molecules, which are related to CD28 [441]), and members of the TNFR (TNF receptor) family, including CD40L [442].

1.5.2.1 CD28

CD28 was the first co-stimulatory receptor characterized in resting T cells, and is the best-understood [443]. It is a homodimeric glycoprotein expressed on 95% of $CD4^+$ and approximately 50% of $CD8^+$ T cells [444], and its ligation has been shown to activate PLCγ1 and $[Ca^{2+}]_i$ mobilization [440]. Upon interaction with its ligands B7.1 (CD80) and B7.2 (CD86) expressed on APCs, CD28 increases IL2 production and T cell proliferation [444,445]. Generally CD28 engagement does not have a physiological effect in the absence of TCR signalling. The importance of CD28-mediated co-stimulation has been demonstrated in a variety of model systems *in vitro* and *in vivo*. Most notably, the absence of CD28 function, either by blockade, CD28-deficiency or deficiency of CD28 ligands, results in a greatly reduced ability to respond to protein antigens, parasites and some viruses, and to generate germinal centres and mediate B cell help. Blocking CD28-mediated co-stimulation can prevent systemic and tissue-specific autoimmune disease, and graft rejection [446-448]. However, some T cell responses appear to be CD28 co-stimulation independent, which of course does not exclude other routes of co-stimulation [438,442,449].

1.5.2.2 Inducible co-stimulator molecules (ICOS)

CD28 does not account for all co-stimulatory function in T cells. One recently discovered alternative co-stimulator is ICOS, which is structurally related to CD28 but does not bind to B7.1 or B7.2. The ligand for ICOS (ICOSL) is a novel B7 family member expressed on APCs [441]. ICOS is either absent or expressed at very

low levels in naïve T cells, but is upregulated upon stimulation, implying that its co-stimulatory role may be more important for memory and effector cells [450]. Indeed, its co-stimulation promotes production of effector cytokines (IFNγ, TNFα, IL4, IL5, IL10) but not so much IL2 [451,452]. APCs show differential regulation of B7.1, B7.2 and ICOSL, which may allow specificity in eliciting responses from naïve or memory T cells [453-455]. Significantly, the inflammatory agents LPS and TNFα can induce ICOSL expression *in vitro*, whereas CD28 ligands are not induced [453]. Therefore, inflamed tissues may be able to stimulate antigen-experienced T cells, but not naïve cells, as a result of the differential regulation of the ligands for CD28 and ICOS.

1.5.2.3 Negative regulators of co-stimulation

There are also negative regulators of co-stimulation, which include the CTLA-4 and PD-1 receptors, both of which share homology with CD28 and ICOS. The interaction between negative signals and positive signals, such as those described above, appears to be a critical aspect of the regulation of T cell function. CTLA-4 is the best studied inhibitory receptor and was the second member of the CD28 family to be identified. Like CD28, it also binds to B7.1 and B7.2, though with significantly higher affinity. Naïve (resting) T cells express little surface CTLA-4, but levels are increased upon activation. CTLA-4 inhibits T cell proliferation and IL2 synthesis in response to anti-CD3 and anti-CD28 antibodies, suggesting a model in which the regulation of CTLA-4 and B7 levels is responsible for setting the activation threshold of T cells. CD28 co-stimulation upregulates CTLA-4 expression, such that co-stimulation itself is a self-limiting process [456,457]. CTLA-4 can interfere with T cell activation both by outcompeting CD28 for B7 binding and by inducing its own inhibitory signals [458-460].

1.5.3 CYTOKINES

Cytokines are small molecular weight regulatory proteins, secreted by lymphocytes and other cells associated with immune activity, with a variety of roles in regulating the kinetics as well as qualitative and quantitative aspects of immune and

inflammatory responses. They are often produced transiently and exert effects on cells near to their source by binding to specific cell surface receptors. In 1986, Mosmann *et al* [461] first proposed a new paradigm in which T helper (Th, $CD4^+$) cells could be classed into two reciprocally inhibitory populations depending on their cytokine profiles. The so-called Th1 cytokines, including IFNγ and IL2, stimulate cytotoxic cells and macrophages leading to cell mediated immunity, protecting against viruses and bacteria. Th2 cytokines, including IL4, IL5, IL10 and IL13, stimulate B cells and antibody production, activating defence mechanisms against parasites and allergic inflammation [461,462]. However, this Th1/Th2 classification has been challenged in recent years. It has been suggested that it represents an oversimplification in that many immune responses can involve a combination of both classes of cytokines [463]. The cytokines applicable to this thesis are each discussed in more detail below.

1.5.3.1 Interferon γ (IFNγ)

Interferons are a major class of cytokine that play a complex and central role in the resistance of mammalian hosts to pathogens. There are type 1 (interferon α and β), produced by virally infected cells, and type 2 (interferon γ) interferons, produced by T cells and by natural killer (NK) cells. The former bind to a common receptor and increase MHC class I expression on the infected cells, thereby facilitating Tc ($CD8^+$) targeting [431].

IFNγ was first identified in PHA (phytohaemagglutinin)-activated lymphocyte supernatants as a distinctive antiviral agent, although this is only part of the function of this pleiotropic cytokine [464]. This Th1 cytokine also activates macrophage and neutrophil intracellular killing, stimulates NK cell function and enhances MHC class II, as well as MHC class I expression, on APCs [431].

In T cells the main inducer of IFNγ is cross-linking of the TCR complex [465]. Its production is also induced by IL2, IL12, IL15, TNF, and by other interferons [466-468]. IFNγ binds to a different receptor to that of the type 1 interferons, most highly

expressed outside the lymphoid system [469]. Elucidation of the IFN-signalling mechanism led to the discovery of the JAK-STAT (Janus kinase-signal transducers and activators of transcription) pathway [470], which is also employed by more than 30 members of the cytokine superfamily [471]. Upon receptor binding, JAK-1 and JAK-2 are phosphorylated and modulate signal-transducing peptides, with eventual target gene activation due to binding of STAT-1 to DNA elements [472].

1.5.3.2 Interleukin 2 (IL2)

Originally described as T cell growth factor [473], the function of IL2 extends beyond lymphocyte activation and population expansion, though T cells still appear to be its major target. This Th1 cytokine also stimulates growth of B cells, NK cells and lymphokine-activated killer cells. IL2 knockout mice do not develop lymphopaenia or immune deficiency, suggesting that IL2 is not required for lymphopoiesis. However, these mice do develop a syndrome of generalized inflammatory disease involving multiple organs, often with a severe colitis [474].

T cell growth and clonal expansion is a tightly regulated process determined by the concentration of IL2 available to the cell and the level of IL2 receptor (IL2R) expression on the cell [465]. Accordingly, a primary focus in T cell activation studies is on the receptors and intracellular mechanisms that control expression of the *IL2* gene and genes encoding the IL2R. IL2 is a 15kDa glycoprotein encoded by a single gene whose transcriptional activity is rapidly increased in activated T cells [475,476]. A transcriptional enhancer at the initiation site of this gene has been shown to interact with transcriptional factors such as AP-1, NFκB and Oct-1 [477]. There are also binding sites for a unique lymphocyte-specific transcriptional complex termed NFAT (nuclear factor of activated T cells), which appears to determine the T cell specificity and inducibility of expression of *IL2* [478].

1.5.3.3 Interleukin 5 (IL5)

IL5 is a T cell derived Th2 cytokine involved in the pathogenesis of atopic diseases. Though predominantly produced by $CD4^+$ T cells, it is also expressed by mast cells and $CD8^+$ cells. IL5 specifically plays a role in the differentiation, recruitment and survival of eosinophils, which are known to mediate allergic and asthmatic symptoms [479,480]. It also increases basophil numbers and can prime them for histamine release and leukotriene production. In addition, IL5 can augment IL2 dependent differentiation and proliferation of T cells themselves, though IL5 receptors have not been identified on T cells a yet [481].

The IL5 receptor consists of a specific α subunit (IL5Rα) and a β subunit common to IL13 and GM-CSF [482]. The α subunit is restricted to eosinophils and basophils in humans, and binds IL5 with low affinity in isolation, and high affinity in association with the β subunit. IL5, IL3 and GM-CSF are associated with similar intracellular signalling events, including activation of protein kinase C, ras, raf, and mitogen activated kinase [481].

1.5.3.4 Interleukin 10 (IL10)

IL10 is a major regulatory cytokine of inflammatory responses, originally described as a mouse Th2 cytokine, inhibiting Th1 cytokine synthesis [483]. Since then, however, there has been increasing evidence that it acts as a general inhibitor of proliferative and cytokine responses of both Th1 and Th2 cells *in vitro* and *in vivo*. IL10 is secreted by monocytes, NK cells, T cells (Th1 and Th2 $CD4^+$, and $CD8^+$), mast cells and B cells [484-487]. It has been shown to play a pivotal role in the establishment of peripheral T cell anergy, a state of immune inactivation characterized by abolished proliferative and cytokine responses, in mice, in which its administration before allergen treatment induced antigen-specific T cell tolerance [488,489]. In addition, IL10 derived regulatory ($CD4^+$) T cells have been identified in humans and mice. These cells produce IL10, but not IL2 nor IL4, which suppresses antigen-specific T cell response *in vitro* and prevents antigen-induced colitis [490]. Furthermore, IL10 inhibits

DC maturation, characterized by a decreased expression of MHC class II molecules, and drives their function towards tolerance induction of both Th1 and Th2 T cells [491,492].

The IL10 receptor (IL10R) is composed of at least two subunits, which are members of the interferon receptor family [493]. The best characterized intracellular signalling pathway is the JAK-STAT system, in which the IL10/IL10R interaction engages JAK-1 and Tyk2, and transcription is activated by STAT-1, STAT-3 and STAT-5 [494-497].

1.5.4 T CELL SURFACE ACTIVATION MARKERS

The changes that occur on the T cell surface during an immune response are multiple but it is particularly well characterized that activated T cells synthesize and express new receptor molecules of which the best studied examples are CD69, transferrin receptors, and receptors for cytokines such as IL2 (CD25). Those applicable to this thesis are discussed.

1.5.4.1 CD69

CD69, also known as activation inducer molecule, is one of the earliest cell surface antigens expressed by activated T cells, detectable within 1 hour of TCR-CD3 ligation. Furthermore, it is expressed in response to alternative modes of activation mediated by either CD2 or CD28. CD69 exists as a cytoplasmic pool in non-activated T cells, which can be mobilized upon activation. Once expressed, it acts as a co-stimulatory molecule for T cell activation and proliferation. Its expression can also be induced *in vitro* in B cells, NK cells, macrophages and granulocytes. Although a specific ligand has not identified, its wide distribution and the induction of intracellular signalling upon CD69 cross-linking imply a role in haematopoietic cell functions [498-500].

CD69 generated signals include Ca^{2+} influx and PLA2 activation, as well as cooperation with lymphokine gene expression and cell division [501-506]. Futhermore, it has been shown that accumulation of GTP-bound ras plays a central role in TCR-CD3 mediated CD69 expression [507,508].

1.5.4.2 CD25 (IL2Rα)

The IL2 receptor (IL2R) consists of 2 signalling units, IL2Rβ (CD122) and γ_c (CD132), and a variably expressed IL2Rα subunit (CD25), which regulates IL2 affinity [509]. Although signalling can occur in the absence of CD25, it is necessary for normal immune function, as demonstrated by the autoimmunity, colitis and premature mortality in $CD25^{-/-}$ mice [510], and by the severe combined immunodeficiency in a patient with CD25 deficiency [511]. The presence of CD25 appears to increase the binding affinity of the IL2R for IL2, thus allowing responsiveness to the low IL2 concentrations physiologically produced *in vivo*. CD25 expression is induced by a range of stimuli, including antigens/mitogens and cytokines, such as IL2 [473]. Its expression is not only important for maximal T cell proliferation, but also seems to contribute to activation-induced cell death [510].

The *CD25* gene contains at least three regulatory regions. The first two (I and II) are essential for mitogen-induced CD25 expression, but are insufficient for IL2 regulation of *CD25* [512]. This is dependent on region III, which binds both STAT-5 and ELF-1 in this respect [513,514]. Upon IL2 binding, JAK-1 and JAK-3 phosphorylate the IL2R chains with eventual activation of target genes by STAT-5 (A+B) [515]. STAT-5A is essential for IL2 induced *CD25* expression but not for that induced by anti-CD3. Furthermore, proliferation at physiological IL2 levels is dependent on IL2-induced *CD25* expression, and antigen-mediated CD25 induction in the absence of IL2 induction is insufficient for normal T cell proliferation or clonal expansion *in vivo* [516].

$CD4^+CD25^+$ expression has also been recently associated with a regulatory T cell (Tr cell) phenotype. Increasing evidence suggests that Tr cells may be acting to down-

regulate other T cell responses, including those that are directed against self, thereby helping to maintain peripheral tolerance [517-519]. Such $CD4^+CD25^+$ T cells are unresponsive to stimulation with anti-CD3 antibody, anti-CD3 and anti-CD28 antibodies used together, high IL-2 concentration, and con A in the presence of T cell-depleted spleen cells as a source of APCs. In addition they suppress proliferation of $CD4^+CD25^-$ cells cultured *in vitro* in the presence of APCs and soluble anti-CD3 antibody, and inhibit induction of *IL-2* mRNA. This is mediated by a cytokine-independent (neither IL-10 nor TGF-β), cell-cell contact-dependent mechanism [520].

1.6 Adenoviral Gene Delivery

1.6.1 VECTORS USED FOR GENE DELIVERY AND GENE THERAPY

A variety of gene transfer vectors can be used to deliver the therapeutic gene to the relevant target cell. They are traditionally classified as either viral or non-viral. Viral vectors exploit the sophisticated and efficient cellular entry characteristics of the viruses specifically to deliver DNA to host nuclei. There are a range of viral vectors including retroviruses, adenoviruses, adeno-associated viruses and herpes simplex virus. Most experience to date has been with retroviruses and adenoviruses.

Recombinant retroviruses are the most long-standing vectors used [521]. Viral DNA is integrated into the host genome facilitating stable expression thus circumventing the need for re-administration [522]. However large-scale retroviral production is technically difficult and they can only achieve gene transfer to dividing cells, which largely precludes their use in the terminally differentiated surface bronchial epithelium [523].

Adenoviruses are ideal candidates for gene delivery to the lungs, in that they are capable of efficiently transfecting non-dividing cells and they have a natural tropism for respiratory epithelium. They have a higher, *in vitro* and *in vivo*, transfection efficiency than many of the other vectors, including naked DNA (as used in this thesis). They can also be concentrated to produce high titres; up to 10^{12} plaque forming units (pfu)/ml compared with only 10^{6} pfu/ml for retroviruses. As the adenoviral DNA is episomal, thus not integrating into the host chromosome, transgene expression is only transient making re-administration necessary for long-term therapy. However, the resultant risk of insertional mutagenesis is much less of a concern than it is for retroviral vectors. A major disadvantage of adenoviral vectors is the induction of a significant host immune response. A T cell-mediated response against adenoviral proteins causes a local inflammatory reaction that can result in lysis of the transduced cells and a shorter duration of adenoviral-mediated transgene

expression. Another concern is the development of virus-neutralizing antibodies, which eliminate the virus upon repeated administration [524]. Overcoming these immune mechanisms has become a priority in adenoviral gene therapy.

Non-viral vectors include ligand-DNA conjugates, naked DNA and, of most interest, liposomes. Cationic liposomes form artificial membranes that complex with DNA and confer transfection of DNA into cells by endocytosis. They are easy to produce and administer and do not appear to induce immune responses, nor carry the risk of mutagenesis associated with viral vectors. Liposome-mediated gene transfer is limited by aggregation and destruction of a majority of the DNA in endosomes during transfer from the cytoplasm to the nucleus. DNA reaching the nucleus is often only transiently and weakly expressed [525].

Several approaches have been adopted to address some of the disadvantages of present vectors. For example viral proteins used to evade endosomal ingestion have been fused to liposomes to allow more efficient gene delivery [525]. Cell and tissue specific promoters facilitating specific targeting are now available [526,527], as are inducible promoters allowing transgene expression to be controlled at will [528,529]

In an attempt to make adenoviruses less immunogenic, Ad vectors ('gutted viruses') in which almost the entire viral genome has been deleted have been constructed [530-532]. This also frees up to 30 kb for DNA insertion, allows longer transgene expression and re-administration [533]. Host immunity to Ad vectors has also been modulated by a variety of agents resulting in increased and prolonged transgene expression [534-539].

1.6.2 ADENOVIRUSES

1.6.2.1 Wild type Adenoviruses

Adenoviruses (Ad) are a frequent cause of acute upper respiratory tract infections. They were first isolated in 1953 by investigators trying to establish cell-lines from

adenoidal tissue of children removed during tonsillectomy and from military recruits with febrile illnesses. Ad are non-enveloped, icosahedral particles with a diameter of approximately 70-100nm (see Figure 1.5A). They are composed of a linear, double-stranded DNA core surrounded by a protein shell composed of 252 subunits, called caspsomeres. Fibres that extend from the 12 vertices of the outer capsid mediate adenoviral attachment to cells. To date more than 49 serotypes of human Ad have been identified and classified into six distinct subgroups (A-F). The most studied adenoviruses are the group C serotypes 1, 2, 5, and 6. Ad types 2 and 5 have been most commonly used to prepare recombinant Ad vectors. The latter was used in this thesis.

Uptake of the adenovirus particle initially involves an interaction of the fibre protein with a range of cellular receptors, which include the MHC class I molecule and the coxsackievirus-adenovirus receptor [540,541]. The penton base protein then binds to the integrin family of cell surface heterodimers allowing internalisation via receptor-mediated endocytosis [542-544]. Most cells express primary receptors for the adenovirus fibre coat protein, however internalisation is more selective. Penetration involves phagocytosis into vacuoles, after which the toxic activity of the pentons is responsible for rupture of the phagocytic membrane and release of the particle into the cytoplasm. The core migrates to the nucleus where the DNA enters through nuclear pores, whereupon it is converted into a virus DNA-cell histone complex (see Figure 1.5B)

The adenoviral genome is approximately 36 kilobases (kb), conventionally represented as 100 map units (1 map unit = 360 bp). Viral gene expression occurs in a sequential cascade. Adenoviral genes are grouped as early (E) genes whose expression precedes viral DNA replication and the transcription of the late (L) genes, which takes place 6 to 8 hours after infection. The E genes encode regulatory proteins for viral replication and the L genes encode structural proteins necessary for assembly of progeny virions [545].

1.6.2.2 Adenoviral Vector Construction

The E1A and E1B products of the E1 gene are the first viral proteins produced after infection and are critical for adenoviral replication, which occurs in the nucleus of the host cell. Their deletion results in replication-deficient viruses, which have been used as adenoviral vectors [546]. These viruses can be propagated in transformed helper cell lines, such as the 293 line prepared from human embryonic cells, that express the E1 gene products [547]. The E3 gene product functions in abrogating the host immune response to the virus. It is not required for viral growth in tissue culture, and E3-deleted viruses appear to be fully infectious. Up to 3.2 and 3.1 kb of the E1 and E3 region, respectively, can be deleted [546], and ~105% of the wild-type genome can be effectively packaged into Ad virions [548], thus allowing for the insertion of a further ~2 kb of foreign DNA, without effecting viral growth rate or titre. Therefore E1/E3-deleted Ad vectors allow packaging of ~8.1-8.2 kb of foreign DNA [546].

A number of strategies of adenoviral vector construction have been employed. The homologous recombination method, as relevant to this thesis, was developed by Bett *et al* in 1994 [546]. This method uses two plasmids containing overlapping fragments that recombine. The first plasmid contains most of the viral genome in circular form, minus the DNA packaging signals and the E1 region. In this thesis pBHG10, an E1/E3-deleted Ad 5 plasmid, was used [549]. The second plasmid contains the left 100 to 150 bp of repeated DNA sequence (inverted terminal repeat), packaging signal, and sequence overlapping the first plasmid: pDK6, which contains the murine cytomegalovirus promoter (MCMV), was used in the construction of Ad5-MCMV-Dvl1. MCMV is a particularly efficient promoter of adenoviral-mediated transgene expression in rodent lungs [550]. After the gene of interest (Dvl1in this case) has been cloned into the second plasmid (pDK6), the two plasmids are co-transfected into the E1-transformed 293 cells (see Figure 1.5C). The resultant virus produced by homologous recombination in 293 cells is then isolated through plaque purification. This process is limited by the low frequency of the recombination event and the laborious plaque purification procedure necessary to select the desired recombinant adenovirus.

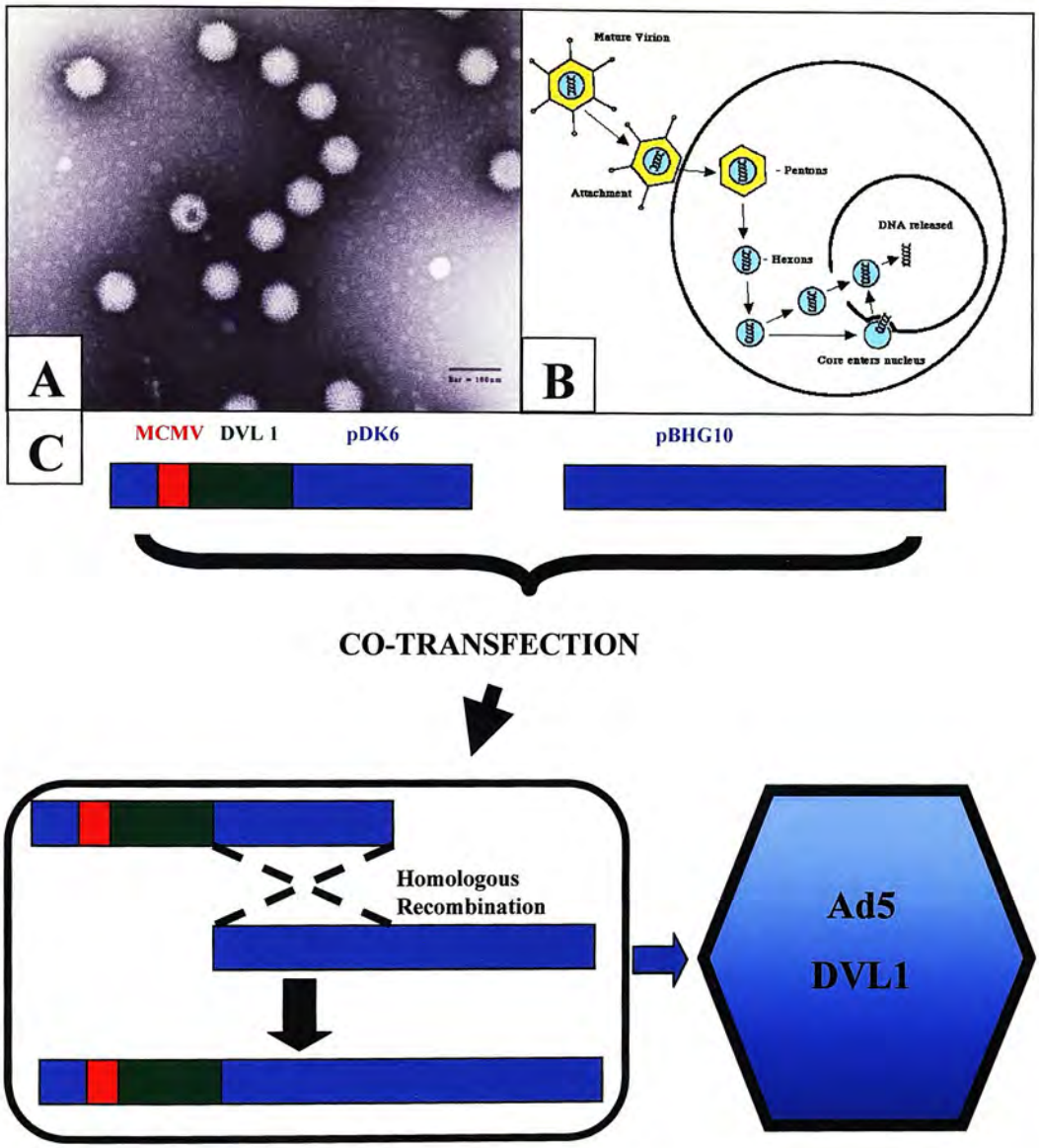

Figure 1.5: Adenoviral Gene Therapy. A & B:Taken from University of Leicester BS335 Virology (http://www-micro.msb.le.ac.uk/335/BS335.html)

A) Negatively-stained electron micrograph of adenoviral particles. The thin fibres protruding from each vertex of the icosahedral particles are just visible

B) Uptake of the adenovirus particle initially involves interaction of the fibre proteins with cellular receptors. The penton base protein then binds to integrins allowing internalisation via receptor-mediated endocytosis. Penetration involves phagocytosis, after which the toxic activity of the pentons is responsible for rupture of the phagocytic membrane and release of the particle into the cytoplasm. The core migrates to the nucleus where the DNA enters through nuclear pores, whereupon it is converted into a virus DNA-cell histone complex

C) After the gene of interest (Dvl1 in this thesis) has been cloned into pDK6, containing the MCMV promoter, this is co-transfected with pBHG10, an E1/E3-deleted Ad 5 plasmid, in the E1-transformed 293 cells The resultant virus produced by homologous recombination is then isolated through plaque purification.

Chapter 2

Materials and Methods

2.1 Materials

All reagents were purchased from Sigma (Poole, Dorset, U.K.) unless otherwise stated.

Cell Culture Media for 293 Cells

50ml 10X MEM (Eagle w/o sodium bicarbonate) with 10% foetal calf serum (FCS) (F-9665), 100IU/ml penicillin/100μg/ml streptomycin (Gibco, Paisley, U.K. 15070-071), 2mM L-Glutamine (Gibco, Paisley, U.K., 25033-010), 15ml 7.5% sodium bicarbonate (Gibco) and 375ml autoclaved dH_20. Kept at 4°C.

10X Citrate Saline

50gm KCl, 22gm Na-Citrate.$2H_20$; made up to 500ml with dH_20. Diluted 1/10 and filter-sterilized (0.22μ) for 1X Citrate Saline.

10X HEBS Buffer

8gm NaCl, 5.46 gm HEPES (sodium salt), 0.36gm KCl, 0.2gm Na_2HPO_4; made up to 100ml with dH_20. and filter-sterilized (0.22μ). Diluted with dH_20 to 2X HEBS and pH adjusted to 7.1.

Agarose Overlay for DNA Co-transfection (adenovirus)

A) 1gm agarose dissolved in 100ml dH_20

B) 16.8ml 10X MEM (Eagle w/o sodium bicarbonate), 61.2ml dH_20, 6ml 7.5% sodium bicarbonate (Gibco), 10% foetal calf serum (FCS) (F-9665), 2ml 5% yeast extract (Difco 0127-17), 100IU/ml penicillin/streptomycin (Gibco, Paisley, U.K. 15070-071), 2mM L-Glutamine (Gibco, Paisley, U.K., 25033-010), 2μl/ml fungizone; filter-sterilized (0.22μ).

A + B made freshly, mixed and incubated at 44°C before pouring.

PBS^{2+} (adenovirus dilution)

A) 80gm NaCl, 2g KCl, 11.5 Na_2HPO_4, 2g KH_2PO_4/ litre of dH_20

B) 1gm $CaCl.2H_20$ / 100ml dH_20

C) 1gm $MgCl_2.6H_20$ / 100ml dH_20

For 1L of $PBS2^+$: 880ml dH_20 + 100ml A + 10ml B + 10ml C.

Pronase

Pronase (Protease) dissolved at 5mg/ml in 0.01M Tris-HCl pH 7.5, 15 minute incubation at 56°C and 60 minutes at 37°C

Pronase-SDS

0.5mg/ml Pronase (as above), 0.01M EDTA, 0.5% SDS, 8.3mM Tris-HCl pH 7.5; freshly made.

Complete Human RPMI Culture Media

500ml RPMI 1640 (R-0883) with 5% human AB serum [heat inactivated] (H-1513), 100IU/ml penicillin/100μg/ml streptomycin (Gibco, Paisley, U.K. 15070-071), 2mM L-Glutamine (Gibco, Paisley, U.K., 25033-010). Kept at 4°C.

Complete DMEM Culture Media

500ml DMEM (D-5921) with 5-10% foetal calf serum (FCS) (F-9665), 100IU/ml penicillin/100μg/ml streptomycin (Gibco, Paisley, U.K. 15070-071), 2mM L-Glutamine (Gibco, Paisley, U.K., 25033-010). Kept at 4°C.

Avertin (Tribromoethanol anaesthetic)

2.5gm 2,2,2-tribromoethanol (Aldrich T4840-2), 5ml 2 methyl-2-butanol (tertiary amyl alcohol; Sigma A1685); made up to 200 ml with dH_2O.

LB Medium

Ten LB media capsules (Sigma L-7275) in 500ml dH_2O; autoclaved. Ampicillin at 50μg/ml if required.

LB Agar

Ten LB agar capsules (Sigma L-7025) in 500ml dH_2O; autoclaved. Ampicillin at 50μg/ml if required.

6X PCR Loading Buffer

0.25% weight/volume of bromophenol blue and 40% weight/volume of sucrose in distilled water. Stored at 4°C.

TE Buffer

10mM Tris-HCl (pH 8), 1mM EDTA

8% SDS-PAGE Gel (200mls)

67.8ml dH_2O, 53.2ml 30% acrylamide/bis-acrylamide mix (A-3699), 75ml 1M Trizma Base pH 8.8 (T-1503), 2ml 10% SDS (L-4509). Kept at 4°C. Polymerisation of 5mls gel mixture catalysed by addition of 5μl TEMED (T-9281) and 50μl 10% APS (A-3678).

15% SDS-PAGE Gel (200mls)

21ml dH_2O, 100ml 30% acrylamide/bis-acrylamide mix (A-3699), 75ml 1M Trizma Base pH 8.8 (T-1503), 2ml 10% SDS (L-4509). Kept at 4°C. Polymerisation of 5mls gel mixture catalysed by addition of 5μl TEMED (T-9281) and 50μl 10% APS (A-3678).

5% Stacking Gel (100mls)

68ml dH_2O, 17ml 30% acrylamide/bis-acrylamide mix (A-3699), 12.5ml 1M Trizma Base pH 6.8 (T-1503), 1ml 10% SDS (L-4509). Kept at 4°C. Polymerisation of 5mls gel mixture catalysed by addition of 5μl TEMED (T-9281) and 50μl 10% APS (A-3678).

SDS-Tris Glycine Electrophoresis Buffer

25mM Trizma Base (T-1503), 250mM Glycine (G-7403), 0.1% SDS (L-4509). Kept at room temperature.

Methanol Based Transfer Buffer (1L)

14.4gm Glycine (G-7403), 3gm Trizma Base (T-1503), 200ml methanol (M-1770); dH_2O to make up to 1L. Made fresh.

Western Blot Nitrocellulose Wash Buffer (TBS Tween)

0.5M Tris-HCl (pH7.6) made up to 2L with dH_2O. Diluted 1/10 in 0.85% NaCl with 0.05% Tween-20 (P-7949). Kept at room temperature.

Western Blot Blocking Buffer

Western blot nitrocellulose wash buffer with 5% 'Marvel' dried skimmed milk powder.

Whole Organ Lysis Buffer

1% NP40 (BDH 56009) in PBS (D-8662); 1 protease inhibitor tablet (Roche 1836170) / 10ml. Made fresh.

Cytoplasmic Lysis Buffer

50mM sodium fluoride, 5mM tetra sodium pyrophosphate, 1mM sodium orthovanadate (pH 10), 10mM β-glyceropyrophosphate, 0.5% NP40 (BDH 56009), 2mM EDTA, 20mM Na_2HPO_4, 20mM NaH_2PO_4; made up to 10ml with dH_2O and 1 protease inhibitor tablet (Roche 1836170) added. Stored at –20°C.

Nuclear Lysis Buffer

50mM sodium fluoride, 5mM tetra sodium pyrophosphate, 1mM sodium orthovanadate (pH 10), 10mM β-glyceropyrophosphate, 0.5% NP40 (BDH 56009), 2mM EDTA, 20mM Na_2HPO_4, 20mM NaH_2PO_4, 300mM NaCl; made up to 10ml with dH_2O and 1 protease inhibitor tablet (Roche 1836170) added. Stored at –20°C.

Physiological Buffer

10mM Tris-HCl (pH 7.4), 140mM NaCl, 5mM EDTA, 2mM dithiothreitol, 1mM phenylmethylsulfonyl fluoride, 1μg aprotonin/ml, 2μg leupeptin/ml, 2μg pepstatin/ml. Stored at –20°C.

Recombinant Mouse Sonic Hedgehog Peptide

The recombinant mouse Sonic Hedgehog amino-terminal peptide (R&D Systems, UK; 461-SH) was reconstituted in filter-sterilised PBS (D-8537) containing 0.2% endotoxin free BSA (A-4919), to a final concentration of 50μg/ml. Aliquots were prepared and stored at -20°C for up to 3 months.

Anti-Sonic Hedgehog Antibody

The neutralising anti-Sonic Hedgehog antibody 5E1 (Developmental Studies Hybridoma Bank, USA) was purified from hybridoma supernatants using Protein G columns (Amersham Pharmacia Biotech, UK) as per standard protocols.

Fluorescein Isothiocyanate (FITC)

FITC powder (Sigma F-7250) was resuspended at 2mg/ml in sterile PBS (D-8537) and 50μl was given intra-tracheally to each mouse. For latter experiments with the larger *Gli* mutant mice FITC was given at 7μg/gm.

Red Blood Cell Lysis Buffer

1mM NH_4HCO_3 and 114mM NH_4Cl. Kept at 4°C.

MACS Buffer

0.5% BSA (A-2153) in PBS (D-8537). Kept at 4°C.

FACS Fixing Buffer

2% paraformaldehyde (P-6148) in PBS (D-8537). Kept at 4°C.

FACS Wash

0.1% sodium azide, 0.2% BSA (A-2153) in PBS (D-8537). Kept at 4°C.

ELISA Binding Buffer

Carbonate-Bicarbonate buffer (C-3041). 1 capsule dissolved in 100ml of distilled water yields a 50mM Carbonate-Bicarbonate buffer, pH 9.6. Kept at 4°C.

ELISA Wash Buffer

PBS tablets (Oxoid BR14) diluted in water (1 tablet/100ml distilled water) containing 0.05% Tween-20 (P-7949). Kept at room temperature.

ELISA Blocking Buffer

ELISA washing buffer containing 1% BSA (A-9418). Freshly prepared.

ELISA Substrate Solution

ELISA ethanolamine buffer (Don Whitley Scientific, Shipton, U.K. E-016) containing 1mg/ml pNPP (N-2770). Made fresh.

2.2 Methods

2.2.1 ADENOVIRUS CONSTRUCTION

The construction and application of the recombinant adenovirus, Ad5-MCMV-Dvl1 (Dishevelled1), is discussed below and presented in detail in Chapter 5. It is important to note that the facilities for large scale virus production and purification were not available locally. These steps were very kindly carried out by staff in Professor Jack Gauldie's laboratory, Department of Pathology, McMaster University, Ontario, Canada. All the protocols described were based on those used by Professor Gauldie's lab.

2.2.1.1 DNA Co-transfection

Details of the construction of pDK6-Dvl1 are given below and in Chapter 5. This new construct and pBHG10 were co-transfected into 293 cells [human embryonic kidney cell line (European Collection of Cell Cultures [ECACC], Salisbury, UK)] to rescue *Dvl1* cDNA in the adenovirus genome. The co-transfections were carried out in 60mm tissue culture dishes. 293 cells were grown to 70-80% confluence in these dishes, media was removed and replaced with 5ml of fresh media per dish. The DNA (10μg of both pDK6-Dvl1 and pBHG10 per dish) was added to 2X HEBS (500μl per dish) in a 15ml Falcon tube and mixed well. 250mM $CaCl_2$ (500μl per dish) was added very slowly with gentle agitation, during which a cloudy precipitate was noted. This mixture was incubated for 15 minutes at room temperature, 1ml was added to each of the 293 cell dishes (containing 5ml of fresh medium) and gently mixed. The dishes were then incubated overnight (~16 hours). Normally between 4 and 8 dishes were transfected at one time. The following day an agarose/media overlay was freshly made and maintained at 44°C. The medium from each dish was gently aspirated and 10ml of overlay was very slowly added to each. The dishes were then returned to the humidified 37°C incubator with 5% CO2. Culture dishes were examined daily thereafter for the development of plaques (which took 1 to 2 weeks).

Plaques were characterized by slowly increasing localised areas of cell clearing beneath the overlay, due to the cytopathic effect of the replicating virus. Once identified a plaque, was repeatedly 'stabbed' with a P1000 tip (Gilson) and the samples were resuspended in PBS^{2+} before storage at -80°C.

2.2.1.2 Amplification

293 cells were grown to near confluence in 60mm culture dishes and the media gently removed. Virus was released from the plaque 'stabs' by repeated freeze-thawing between liquid nitrogen and a 37°C water bath. An aliquot was then added to 293 cells (in a 60mm tissue culture dish) in a 500µl volume and the cells were returned to the incubator for 45-60 minutes with gentle 'swirling' intermittently, before fresh media was added. The viral associated cytopathic effect (CPE) was observed within a few days, characterized by the cells rounding up and detaching from the dish. Once complete CPE was evident (all cells rounded up) the contents of each dish were transferred to a 15ml Falcon tube and centrifuged at 300g for 10 minutes at room temperature. The supernatant, which contained adenovirus, was removed and stored at -80°C for later use. The cell debris/pellet and any remaining cells in the dishes were resuspended in freshly prepared Pronase-SDS solution and incubated overnight at 37°C. DNA was then extracted as follows. 500µl of the overnight Pronase-SDS digestion was added to 500µl of water-saturated phenol and mixed before centrifugation at 12,000g for 10 minutes at 4°C. The aqueous (top) layer was removed and mixed with 1ml of 96% ethanol before a further centrifugation at 12,000g for 10 minutes at 4°C. The pellet was washed twice in 96% ethanol with repeat centrifugations, dried and resuspended in 50µl of TE, pH 8. DNA was quantified and analysed by Southern blotting as described.

A second plaque purification step, to minimise potential contaminating wild type adenovirus, was performed once Dvl1 expression had been confirmed in the original plaques. Essentially the protocol was the same as that used for titration, described below. A single discrete plaque was identified and virus acquired, as above, was used for large scale preparation.

2.2.1.3 Titration

The adenovirus was titrated by a plaque assay giving the viral concentration in plaque forming units per ml (pfu/ml). To do this, serial dilutions of the virus were made in PBS^{2+} and 200µl of each was added to near-confluent 293 cells in 60mm dishes, with at least duplicate dishes of each dilution. These were incubated for 45-60 minutes with gentle 'swirling' at room temperature. 10ml of overlay (as in cotransfection) were added slowly to each dish before being returned to the incubator. The number of discrete plaques was counted after 5-7 and 10-14 days. The optimal dilution at which discrete plaques were appreciable was chosen. The concentration (in plaque forming units per ml or pfu/ml) was calculated as: the number of plaques x 1/0.2 x dilution factor.

2.2.1.4 Large Scale Virus Production using Spinner Culture (in Canada)

To allow the adenovirus to be produced on a larger scale 293N3S (a variant of 293 cells which grow in suspension) cells were used in spinner cultures. The cells were initially grown in 3-litre spinner flasks (Bellco Biotechnology) to a confluency of $2x10^5$ cells/ml. They were then transferred to three 1-litre centrifuge bottles (Nalgene) and centrifuged at 1500g for 45 minutes at room temperature (MSE centrifuge). The supernatant was saved (as 'conditioned medium'), and the pellet resuspended in 300ml of virus inoculum medium and transferred to a 1 litre spinner flask. Viral supernatant, as taken during amplification, was added at a concentration of 2 pfu/cell and incubated for 90 minutes in a 37°C 'warm room'. The whole volume was then transferred to a 3-litre spinner flask along with 1500ml of 'conditioned medium' and 1200ml of fresh medium. Infection was allowed to proceed until inclusion body staining was >90% (see below). Cells were harvested by transferring to three 1-litre centrifuge bottles and centrifuging as before. The supernatant was saved and the pellet resuspended in 15ml of 0.1M TrisHCl (pH 8), ready for banding.

2.2.1.5 Purification (Banding) of Adenovirus using CsCl Gradient (in Canada)

The virus suspension, from spinner culture, was added to 5% sodium deoxycholate at a ratio of 10:1 and incubated for 30 minutes at room temperature (RT), with occasional mixing. 1/100th volume of 2M $MgCl_2$ and 1/200th volume of 10mg/ml DNase I were then added, and incubated for 45 minutes at 37°C, with gentle periodic mixing. The virus was then ready for banding and fractionation. Briefly, the viral suspension was mixed with saturated CsCl and centrifuged at 14,000g for 18 hours at 4°C. The band, containing the recombinant adenovirus, was collected and mixed with 'top-up' solution before a second similar centrifugation. The viral band was again collected and PD-10 column chromatography performed to remove the CsCl. The purified adenovirus was then aliquoted, titred and stored at -80°C until use.

2.2.1.6 Inclusion Body Staining (in Canada)

Inclusion bodies are densely staining nuclear bodies resulting from accumulation of large amounts of virus and viral products at late points in infection. They are used to monitor adenoviral infection.

5ml aliquots of infected spinner culture were centrifuged (Beckman TJ-6 centrifuge) at 1500g for 10 minutes at room temperature (RT). The pellet was resuspended in 0.5ml of 1% sodium citrate and incubated for 10 minutes at RT. 0.5ml of Carnoy's fixative was added and fixed 10 minutes at RT. This was resuspended in 1ml of 1% sodium citrate and centrifuged at 1500g for 10 minutes at RT, and the pellet resuspended in 150µl of 1% sodium citrate. A drop of this suspension, containing fixed cells, was placed on a microscope slide, dried for 60 minutes, a drop of orcein and a cover-slip were added. Inclusion bodies were identified and counted by microscopy.

2.2.1.7 Adenovirus Transfections

In vitro transfections were carried out in all of the adherent cell lines listed below. For each the quantity of virus added was expressed as a multiplicity of infection (moi), which is the ratio of the number of pfu's of virus to the number of cells within the well. The number of cells in a particular size of well/dish were pre-determined by preliminary experiments, in which the cells were grown to the same confluency at which transfection would be performed, trypsinized and counted; several counts were averaged. Hence, an estimation of the cell number at transfection was obtained and a specified moi calculated.

In transfections the cells were grown to 80-90% confluency in most cases (although occasional transfections were carried out in less confluent cells eg 50%), media removed and adenovirus added. The samples were then returned to the incubator for 45-60 minutes, with occasional swirling, before the cells were gently washed and fresh media added. Cells were harvested at time-points from 6-72 hours for a variety of assays as discussed in Chapter 5. *In vivo*, the adenoviruses were administered intra-tracheally, as described (Section 2.2.3.2 below), at a range of pfu's.

2.2.1.8 Safety

All adenovirus work, including *in vivo* administration, was carried out in Class II safety cabinets. Mice were always housed in isolators following adenoviral treatment. All equipment in contact with adenovirus was thoroughly bleached (Mini-Haz tabs, Guest Medical, UK, H8875) and the area was treated with germicidal ultraviolet light.

2.2.2 CELL CULTURE

2.2.2.1 Cell lines

The cell lines used included mouse Clara cells (mt-CC1-2, gift from Franco DeMayo, Baylor College of Medicine, Houston, USA), mouse Swiss 3T3 fibroblasts and human A549 cells (ECACC), and rat-1 fibroblasts (American Type Culture Collection [ATCC]). They were all maintained in DMEM based medium with 5-10% foetal calf serum and cultured in a humidified incubator with 5% CO_2 at 37°C. As all are adherent cell lines, trypsin-EDTA (Invitrogen, PL25300054, 0.5g/L Trypsin and 0.2g/L EDTA in Hanks' balanced salt solution) was required to dislodge them from the culture flasks. 293 cells, as used for adenovirus rescue, were cultured in their own media and displaced from culture flasks with 1X citrate saline rather than trypsin-EDTA.

2.2.2.2 Proliferation of Adherent Cells

Proliferation was measured by tritiated thymidine incorporation (^{3}H-TdR-Amersham Pharmacia Biotech, Amersham, UK, Cat # TRK61). Briefly, cells were cultured in 24 well plates. At a range of time-points 0.1μCi/well tritiated thymidine was added. 24 hours later, the cells were washed twice with cold PBS (D-8662), twice with 5% TCA and twice with 100% ethanol. 250μl of 0.3M sodium hydroxide was added and the plates were incubated for 15 minutes at 4°C. The samples were then added to 1ml of scintillation fluid (Packard) and read in a beta-counter (Packard Liquid Scintillation Analyzer).

Alternatively, proliferation was assessed by the CellTiter AQ_{ueous} One Solution Cell Proliferation Assay (Promega, UK), following manufacturers guidelines. Briefly, the cells were cultured 100μl of medium in flat bottomed 96 well plates, to which 20μl of One Solution Reagent (Promega, UK) was added. The plates were read 1-4 hours later by a microplate reader (Dynatech Laboratories MRX) set to a wavelength of 490nm with a reference of 630nm.

Cell counts were performed using haemocytometers and 0.4% trypan blue exclusion (Sigma).

2.2.2.3 Hoechst Staining

To assess nuclear morphology and apoptosis, cells were stained with Hoechst stain (Calbiochem H33258). Freshly made 3% paraformaldehyde solution was added to fix cells and incubated for 20 minutes at room temperature. An equal volume of 50mM NH4/Cl in D-PBS (D-8537) was added and incubated for a further 10 minutes. The cells were then washed twice in D-PBS before 0.1% Triton X-100 (in D-PBS) was added for 4 minutes. The cells were washed again and 2μg/ml of Hoechst dye (in D-PBS) was then added before a final 10 minute incubation. Following 3 final washes (in D-PBS) the cells were visualised with a fluorescent microscope (Zeiss Axiovert S100) using appropriate software (Openlab 3.0 on Apple Mac).

2.2.2.4 Cytospins

Cells were spun onto Vectabond treated microscope slides (Vector Laboratories, Peterborough, England) using a Cytospin 3 (Shandon Scientific Ltd, Runcorn, Cheshire, UK) set at 300rpm for 3 minutes. Following air-drying and methanol fixation cytospins were stained with Diffquick as per manufacturers instructions (Gamidor Ltd, Abingdon, Oxon., UK), or used for immunohistochemistry. Cytospins of purified $CD4^+$ or $CD8^+$ cells were made in the same way.

2.2.3 *IN VIVO*

2.2.3.1 Anaesthesia and Culling

Mice were anaesthetised with an intra-peritoneal injection of avertin (tribromoethanol anaesthetic) at a dose of 0.2ml per 10gm body weight. Avertin was

prewarmed to 37°C for at least 30 minutes before administration. Mice were culled with a single 0.5ml intra-peritoneal injection of phenobarbitone sodium (Sagatal, Merial Animal Health, UK).

2.2.3.2 Intra-tracheal Administration

Following anaesthesia the mice were placed in a holder in which their upper teeth were suspended from a horizontal strip of wire. The jaw was held open by a light weight suspended from the lower teeth and the pharynx was illuminated with a strong focal cold light source, thus allowing the vocal cords to be visualised. 40-50µl of the sample was instilled into the bevel of a blunted orange needle (Microlance 25G), into which a 1ml syringe barrel could be inserted without displacement. The needle (with attached syringe barrel) was then inserted into the trachea through the vocal cords and the plunger of the 1ml syringe reinserted into its barrel thus expelling the sample into the mouse lungs. Samples administered in this manner included FITC, PBS, adenovirus constructs and the SPC 'naked DNA' vectors. In all cases the volume was made up to 40-50µl with sterile PBS (D-8537).

2.2.3.3 Screening Mice

$Gli2^{+/-}$ and $Gli3^{+/-}$ mutations were screened by PCR analysis (by Ms Susan Haley) and phenotype, respectively, as described in chapter 3. Briefly, genomic DNA was isolated from mouse tail tips using a commercial kit (Promega, UK; H4131), as per manufacturer's instructions. DNA was then amplified in a 'touch-down' PCR reaction with primers specific for the neo-cassette used in the original construction of the *Gli2*$^{+/-}$ phenotype, following the recommended protocol given in The Jackson Laboratory (USA) website (www.jax.org). Products were analysed on 2% agarose gels as described below.

2.2.3.4 Bronchoalveolar Lavage (BAL)

Following culling, the mouse lungs and trachea were removed intact. A 2-3cm length of plastic tubing was inserted into the trachea and the lungs were washed with 2 volumes of sterile PBS (D-8662); though wash volumes varied between 450µl (250µl+200µl) and 1400µl (800,600) they were consistent within experiments. Typical BAL yields were between 50-80% of instilled volume. Samples were stored on ice before centrifugation at 600g for 7 minutes at 4°C. The supernatants were centrifuged at 13,000g for 5 minutes at 4°C and the supernatants from this used for cytokine analysis.

2.2.3.5 Lung Analysis

The lungs were often divided and used for immunohistochemistry (IHC), RNA and protein analysis. For IHC lungs were reinflated slowly with, and fixed in, 4% buffered formalin overnight and were then paraffin embedded. 3µm sections were stained with Hematoxylin and Eosin (Sigma) for general morphology or mounted on Vectabond treated slides (Vector Laboratories, Peterborough, England) for later IHC. For RNA extraction the lungs were initially stored at 4°C in RNAlater (Ams Biotechnology, Abingdon, UK) as per manufacturers instructions. They were then homogenised (Polytron PT3100, Kinematica, Switzerland) in volumes of 1.4-2ml of Trizol Reagent (Life Technologies); 20,000 rpm for 30 seconds with samples on ice. RNA was extracted immediately from homogenised samples as described below. For protein analysis the lung tissue was initially snap frozen in liquid nitrogen, before homogenising as for RNA but in 250µl of lysis buffer. The homogenised samples were then incubated for 30 minutes at 30°C and centrifuged at 13,000g for 20 minutes at 4°C. The supernatants were quantified and used for immunoblotting as described below.

2.2.3.6 Human Biopsy Sections

After ethical permission was obtained from Lothian Research Ethics Committee, anonymised paraffin embedded open lung biopsy material from patients with Usual Interstitial Pneumonia (UIP) was taken from the Department of Pathology archive. As with mouse blocks, 3μm sections were cut and mounted on Vectabond treated slides (Vector Laboratories, Peterborough, England) for IHC.

2.2.3.7 Assessment of lung fibrosis in the FITC model

This was based on the scoring system devised by Ashcroft *et al* in 1988, in which human biopsies were examined at x10 magnification [551]. Randomly selected fields were scored on a scale of 0 to 8 (see Table 2), dependent upon the score applicable to over 50% of the field. As proposed by Ashcroft *et al*, every effort was made to assign fields to an odd number on the scale, only using even numbers if it was difficult to decide between two odd numbers. Main airways, blood vessels and inflammatory exudates in air spaces were all excluded.

FITC and PBS treated mice lung sections were examined microscopically at x40 magnification (adjusting for difference in size between human and murine acini) by at least two observers, who agreed a consensus number for each field. To allow for differences between FITC +ve and FITC –ve areas of the lung, lung sections stained with the anti-FITC antibody were examined. A field was considered FITC +ve if >50% of the tissue within the field stained and FITC –ve if <50% stained. PBS lung sections were all FITC -ve, as would be expected. 36 FITC +ve and 36 FITC –ve fields were assessed per section, as this was in the middle of the range of field numbers proposed by Ashcroft *et al*, and also covered nearly the entirety of the section proceeding from one outside edge in non-overlapping rows. Some areas where there was poor or overinflation (usually at lobe margins) were ignored. After examining the whole section the mean score of all the fields was taken as the fibrosis score, again sub-divided into FITC +ve and FITC –ve where appropriate.

2.2.4.1 Transformation of Competent Cells

100µl of freshly thawed competent cells (*E. coli* XL1-Blue, Stratagene) and 0.9µl of β-mercaptoethanol (in kit) were incubated in a transformation tube (Falcon 352059) for 10 minutes on ice, swirling every 2 minutes. 1µl (maximum of 50ng) of DNA was added and the tube incubated for a further 30 minutes on ice, before a 45 second incubation at 42°C and a further 2 minutes on ice. 900µl of preheated (42°C) SOC medium (GibcoBrl 15544-034) was added, and the tube incubated with shaking for 60 minutes at 37°C. The transformation mixture was then plated on agar plates, with the appropriate antibiotic (eg. kanamycin, ampicillin). These were incubated overnight at 37°C and colonies picked the following day. A control plasmid, such as pUC18 (provided with competent cells), was transformed in parallel to confirm transformation efficiency.

2.2.4.2 Analysis of Transformants by DNA Miniprep

DNA minipreps were performed with a commercially available kit (Promega, UK; A1330) following manufacturer's instructions. Briefly, 5ml of LB medium (with appropriate antibiotic) was inoculated with a single bacterial colony in a 50ml Falcon tube, and incubated overnight, with shaking, at 37°C. 750µl was mixed with 750µl of 30% glycerol to make a stock, which was stored at -80°C. The remainder was centrifuged at 12,000g for 5 minutes at room temperature (RT). The pellet was resuspended in 250µl of ice cold cell resuspension solution and incubated for 5 minutes at RT. 250µl of cell lysis solution was added and the mixture incubated for a further 5 minutes. 10µl of alkaline protease solution was added, followed by a final 5 minute incubation. 350µl of neutralization solution was then added and the sample centrifuged at 13,000g for 10 minutes at RT. The cleared lysate was decanted into a spin column and centrifuged at 13,000g for 1 minute at RT, discarding flowthrough. The column was washed twice with the provided column wash (750µl and 250µl)

followed by centrifugation at 13,000g for 1 minute and 2 minutes respectively. The spin column was then transferred to a fresh tube and the DNA eluted with nuclease-free water (Sigma).

2.2.4.3 Quantification of Nucleic Acids

To determine the concentration of nucleic acids in solution, absorbance at 260 and 280 nanometers (nm) was measured, from which the concentration was calculated, in a spectrophotometer (Ultrospec 200, Pharmacia Biotech). To determine the purity of solutions of DNA and RNA, the ratio of absorbance at 260nm and 280nm ($OD_{260/280}$) was taken. This value should ideally be about 1.8 for DNA and 2.0 for RNA.

2.2.4.5 Large Scale Plasmid Preparation

Large scale DNA preparation was performed using a commercial kit (Qiagen, UK; 12263), as per the manufacturer's instructions. Briefly, 5ml of inoculated LB medium (as grown for minipreps) was used to inoculate a further 500-1000ml, which was incubated overnight, with shaking, at 37°C. The cells were harvested by centrifugation at 6000g for 15 minutes at 4°C. They were then resuspended, lysed, filtered and precipitated as per the protocol provided. The final DNA pellet was resuspended in dH_20 and quantified as above.

2.2.4.6 Agarose gel electrophoresis

Agarose gels (0.8%-2%; SeaKem LE agarose, FMC) were prepared in 1xTAE buffer (GibcoBRL UK), containing 1µl of ethidium bromide (10µg/µl, SIGMA) per 50ml of agarose. The gel was transferred to a gel tank (Biorad) containing 1xTAE buffer. In general, 10µl of the DNA sample or PCR reaction were mixed with 2µl 6x loading buffer and loaded into each well. A 50ml gel was run at 80 volts for approximately 1 hour. The UVGrab program connected to a white/ultraviolet transilluminator (UVP) was used to visualise the nucleic acid bands and capture the gel image. SIGMA's

PCR marker or Gibco's 1kb (kilobase) DNA ladder were used as molecular weight markers. The 1kb ladder included fragment sizes ranging from 75 base pairs (bp) to 12kb pairs. The brightest central band on each gel (Figure 5.3) corresponded to ~1.6kb; the bands higher than this to ~2kb, 3kb, 4kb, 5kb, 6kb, 7kb, 8kb, 9kb, 10kb, 11kb and 12kb respectively. The bands lower than the brighter 1.6kb band corresponded to ~500bp, 400bp, 350bp, 300pb, 220bp, 200bp, 150bp and 75bp, respectively. Therefore, using this ladder, the size of a fragment of DNA run on an agarose gel was estimated. In addition, the PCR ladder used (throughout the thesis) represented the following sizes from the largest molecular weight band down: 2kb, 1.5kb, 1kb, 750bp, 500bp, 300bp, 150bp and 50bp.

2.2.4.7 Restriction Enzyme Digestion

Restriction enzymes, buffers and BSA (Promega, UK) each made up 10% of the digest reaction mixture, which also included nuclease free water and the DNA sample itself. At least 1 unit of restriction enzyme was used per μg of DNA to be digested. The samples were incubated at the recommended temperature (manufacturer; generally 37°C) for 1-4 hours, followed by a 10 minute incubation at 65°C to inactivate the enzymes. For digests with two restriction enzymes an optimal common buffer was used.

2.2.4.8 Purification of DNA from agarose

To extract DNA fragments from agarose gels the sample was initially run as usual and the band of interest identified under ultraviolet light. Once visualised, the agarose containing the band was cut out and placed in a 2ml Eppendorf tube with 300μl of binding buffer (Biorad 732-6022). This was incubated at 55°C, with mixing, until the agarose had dissolved. 1ml of DNA clean-up resin (Promega, UK, Wizard DNA clean–up system A7280) was added and the mixture inserted into the barrel of a 2ml syringe, which in turn was inserted into a filter (Promega, UK, Wizard DNA clean–up system A7280). The syringe barrel was reinserted gently discarding the filtrate. 2mls of 80% isopropanol were placed in the empty syringe

and passed through the filter, which was then centrifuged at 600g for 2 minutes. To elute the DNA, 50µl of prewarmed dH_2O (65°C) was placed into the filter and incubated for 1 minute before centrifugation at 600g for 30 seconds.

2.2.4.9 Ligation of Plasmid Vector and Insert DNA

After the vector and insert DNA were prepared for ligation, by restriction enzyme digest and agarose gel extraction, they were quantified (as described) and included in a ligation reaction in 1:1, 1:3 and 3:1 ratios of vector:insert. The ligation reaction mixture also included T4 DNA ligase, ligase 10X buffer (Promega, UK) and dH_2O to a final volume of 10µl. The samples were incubated overnight at 16°C. The following day 1µl of each ligation reaction was transformed in competent cells and colonies screened by DNA minipreps.

2.2.4.10 Phenol/Chloroform Extraction

Residual salts and nucleotides were removed from DNA and RNA samples by phenol/chloroform extraction and ethanol precipitation. The DNA or RNA sample was made up to a 400µl volume with dH_2O and added to an equal volume of phenol/chloroform (Sigma P-2069). The mixture was vortexed, centrifuged at 13,000g for 5 minutes at RT, the supernatant taken and added to 1ml of 100% ethanol and 40µl of 3M sodium acetate (Sigma). The sample was incubated on dry ice for 30 minutes, centrifuged at 13,000g for 30 minutes and the pellet resuspended in 200µl of 70% ethanol. This was centrifuged at 13,000g for 15 minutes, the pellet air dried and resuspended in nuclease free dH_2O.

2.2.4.11 Polymerase Chain Reaction (PCR) and Reverse Transcription PCR (RT-PCR)

DNA sequences of interest were obtained from PubMed's DNA sequence programme (BLAST), and primers were designed using Holyrood's gcg Prime program, or

MacVector programme. They were tested for binding specificity using a DNA Strider programme.

The reverse transcription of total RNA into first strand DNA, and the synthesis of second strand complementary DNA (cDNA) and its amplification, was performed using Promega's Access RT-PCR kit (A1280), which allows the two reactions to take place in a single tube. The reaction was set up according to the manufacturer's instructions. For simple PCR reactions the AMV reverse transcriptase was omitted. Nuclease-free water was included as a negative control for each gene tested.

The thermocycler (Peltier Thermal Cycler-200 DNA engine, MJ Research) was programmed as follows:

First strand synthesis:

1 cycle	48°C for 45 minutes (Reverse Transcription)
1 cycle	94°C for 2 minutes (Reverse Transcriptase inactivation and RNA/cDNA/primer denaturation).

Second strand cDNA synthesis and PCR amplification:

35 cycles	94°C for 30 seconds (denaturation)
	primer-specific Tm for 1 minute (annealing)
	68°C for 2 minutes (extension)
1 cycle	68°C for 7 minutes (final extension)

Annealing temperatures (Tm) and number of cycles were optimised for each gene (See Table 3).

2.2.4.12 RNA Isolation

Extraction of total RNA was performed using Trizol Reagent (GibcoBrl 15596-018) as per the manufacturer's instructions. Briefly, cells or homogenised tissue was suspended in Trizol and incubated for 5 minutes at RT, chloroform (Sigma C-2432) was added (200µl per ml of Trizol), the tubes were shaken for 15 seconds and incubated for 3 minutes at RT before centrifugation at 12,000g for 15 minutes at 4°C. The aqueous phase was removed and added to isopropanol (500µl per ml of Trizol), incubated for 10 minutes at RT and centrifuged at 12,000g for 10 minutes at 4°C.

The RNA pellet was resuspended in 75% ethanol (1ml per ml of Trizol), vortexed and centrifuged at 7,500g for 5 minutes at 4°C. The pellet was air dried and resuspended in pre-warmed (55°C) nuclease free H_2O (Promega, UK).

2.2.4.13 DNase Treatment of RNA

To remove any contaminating DNA the extracted RNA was DNase treated as per manufacturers instructions (GibcoBRL DNase I, Amplification Grade). Briefly, 1μg of RNA was added to 1μl of DNase I and 1μl of 10X DNase I buffer; and DEPC treated water added to a final reaction volume of 10μl. This was incubated for 15 minutes at RT, 1μl of 25mM EDTA added and incubated for a further 10 minutes at 65°C.

2.2.4.14 Real-Time PCR

Higuchi *et al* [552] pioneered the analysis of PCR kinetics by constructing a system that detects PCR products as they accumulate in 'real time'. The reaction relies on the 5'nuclease activity of *Taq* DNA polymerase [553], which cleaves a probe that binds specifically to its target DNA sequence. Only when the PCR product is amplified is the probe cleaved, therefore the signal emitted by the probe corresponds to the amount of product amplified in real-time.

Primers and probes were designed using Primer Express® software, supplied by PE Biosystems (see Table 4). RNA samples for real-time PCR were reverse transcribed into cDNA using TaqMan MultiScribe Reverse Transcriptase kit (PE Biosystems, UK), as per the manufacturers instructions.

The thermocycler (Perkin Elmer) was programmed as follows:

1 cycle 25°C for 10 minutes. (incubation)

1 cycle 48°C for 30 minutes (reverse transcription)

1 cycle 95°C for 5 minutes (Reverse Transcriptase inactivation)

The fluorogenic probe, labelled with the fluorescent dye, 'fam' (6-carboxy-fluorescein), specifically annealed the template between the PCR primers. A

sequence detector (ABI Prism 7700, PE Biosystems, USA) measured amplification of the product, in direct proportion to the increase in fluorescence emitted by the probe. Each sample was run in duplicates in 96-well optical reaction plates (PE Biosystems). 25µl of the PCR reaction were added per well.

The thermal cycler conditions were standard for all the genes tested. These were:

40 cycles 50°C for 2 minutes
95°C for 10 minutes
95°C for 15 seconds
60°C for 1 minute

All the values obtained were normalised to 18S rRNA (labelled with the fluorescent dye, 'vic'), which was included in the Multiplex PCR reaction (more than one primer pair in the same tube) with its own set of primers and probe, as an internal endogenous control. Furthermore, each sample was compared to a relevant positive control, which was always given a value of 1. The data was plotted relative to the positive control.

2.2.4.15 Northern Blotting

Before use the gel box, casting tray and combs were cleaned with mild detergent and dH_2O. 2.89gm of agarose was added to 156ml of dH_2O (1.4% agarose when poured) and boiled until the agarose had melted, cooled to 60°C, 20ml of 20X MOPS and 34ml of 37% formaldehyde added and the gel gently poured, within a fume hood. 20µg of each RNA sample was resuspended in 5µl of TE and added to: 1µl of 20X MOPS (Sigma M-5755), 10µl of formamide (BDH 103266T), 3.5µl of 37% formaldehyde (BDH 101135B), 0.15mg of ethidium bromide and 2µl of blue juice (bromophenol blue/glycerol) dye. The samples were heat-denatured for 10-15 minutes at 60°C, loaded onto the gel next to an RNA ladder, and run at 60-70 volts for 5-7 hours. The gel was visualised, next to a ruler, using the UVGrab program connected to a white/ultraviolet transilluminator (UVP). The gel was then soaked in dH_2O for 30 minutes, in 20X SSC for 5 minutes, and transferred in 20X SSC

(GibcoBrl 15557-028) to Hybond N^+ (Amersham, UK) overnight. The Hybond N^+ was baked for 3 hours at 68°C and a further image captured before hybridization.

The specific DNA probe (linearised DNA fragment for gene of interest, normally<1kb) was then labelled with ^{32}P-dCTP (Amersham Pharmacia Biotech, UK) using the 'Ready-To-Go' DNA labelling beads (Amersham Pharmacia Biotech, UK), as per the manufacturer's protocol. Briefly, 50ng of the DNA probe was dissolved in TE to a final volume of 45µl, which was then denatured by incubation for 2-3 minutes at 95-100°C and brief centrifugation. This and 5µl (50µCi) of the ^{32}P-dCTP were added to the provided tube containing the Reaction Mix bead and gently mixed; all with appropriate radioactivity shielding. Following an incubation period of at least 30 minutes at 37°C, the unincorporated nucleotides were removed using Nick Spin Columns (Amersham Pharmacia Biotech, UK) as instructed.

Hybridization was carried out using ExpressHyb Hybridization Solution (Clontech, UK; 8015-1) following the manufacturer's protocol. Briefly, the ExpressHyb Solution was warmed to 68°C, mixed well and 5ml added to the Hybond N^+ membrane (wrapped in nylon), followed by a 30 minute incubation at 68°C with continuous rotation in a Hybaid tube. The labelled probe was denatured as above, chilled on ice and added to 5ml fresh pre-warmed (68°C) ExpressHyb Solution, which replaced the original pre-hybridization solution for a further 60 minute incubation at 68°C. This solution was then appropriately discarded, and the membrane washed three times in solution 1 (2X SSC, 0.05%SDS) at RT, and twice with solution 2 (0.1X SSC, 0.1%SDS) at 50°C; each wash lasting 40 minutes. The labelled membrane was carefully mounted on Whatmann paper (Whatmann International 1003917) and covered with plastic wrap. The membrane was finally exposed to X-ray sensitive film between two intensifying screens at -70°C. Films were processed through an X-ray developer (X-Ograph Imaging Systems, Wilts, U.K.) at various exposure time points (1 hour, 6 hours, overnight and 4-7 days).

To remove a probe from a blot (to allow reprobing), the membrane was incubated for 20 minutes (with shaking) in preheated (95-100°C) H_2O/0.5% SDS solution and air dried. Membranes were stored at -20°C between use.

2.2.4.16 Southern Blotting

Briefly, DNA samples were run on a 0.8% agarose gel at 20 volts overnight, alongside a 1kb ladder (Gibco). Similar to Northern blotting, the gel image was captured next to a ruler and the gel transferred overnight (in 0.4M sodium hydroxide) to a Hybond N^+ (Amersham, UK) membrane. The membrane was then rinsed briefly with 5X SSC, dried and UV cross-linked at 3000J (Hoefer UV cross-linker). DNA probe preparation was as described above for Northern Blotting. Hybridization was also as above apart from prehybridization and hybridisation steps taking place at 60°C rather than 68°C. Finally, the membrane was exposed to X-ray sensitive film between two intensifying screens at -70°C and the films were processed through an X-ray developer (X-Ograph Imaging Systems, Wilts, U.K.) at various exposure time points (1 hour, 6 hours, and 1-3 days).

2.2.5 PROTEIN ANALYSIS

2.2.5.1 Lysis and Fractionization

Adherent cells were removed from the culture wells with trypsin-EDTA. The cells were centrifuged at 300g for 5 minutes at 4°C and washed twice in ice cold PBS (D-8662) with further centrifugation 300g for 5 minutes at 4°C with each wash. They were then resuspended in cytoplasmic lysis buffer and incubated on ice for 10 minutes. The samples were centrifuged at 4300g for 10 minutes at 4°C and the supernatants (cytoplasmic extract) removed. The pellets were resuspended in nuclear lysis buffer and incubated on ice for a further 10 minutes. These samples were spun at 23,100g for 10 minutes at 4°C and the supernatants (nuclear protein) taken.
For subcellular fractionization (SCF), the cells were trysinized and washed as before. They were then resuspended in a physiological buffer and homogenized by 10-20 strokes of a Dounce homogenizer (Uniform), and the lysate centrifuged at 500g for 10 minutes at 4°C. Membranous and cytosolic material was obtained by centrifgation

at 500,000g (Optima TLX Ultracentrifuge) for 10 minutes at 4°C. The supernatant was designated the cytosolic fraction, and pellets, resuspended in physiological buffer (with 0.1% SDS), the membranous fraction.

2.2.5.2 Protein Quantification

The extracted protein was quantified by one of two methods. For most samples a BCA Protein Assay Kit (Pierce, USA; 23225) was used as per the manufacturer's instructions. Briefly, the provided standards and samples were aliquoted at appropriate dilutions into a 96 well plate. Following a 30 minute incubation at 37°C the plate was read by a microplate reader (Dynex Technologies MRX) set to a wavelength of 560nm.

As the physiological buffer used for SCF was incompatible with the BCA kit, protein extracts were quantified using a Bio-Rad Protein (Bradford) Assay (Bio-Rad Laboratories,UK), as per the manufacturers instructions. Briefly, 800µl of appropriately diluted standards and samples were added to 200µl of the provided dye reagent concentrate, and mixed well. Following a 10 minute incubation, the OD_{595} (against a reagent blank) was measured in a spectrophotometer (Ultrospec 200, Pharmacia Biotech).

2.2.5.3 Immunoblotting

8% or 15% mini SDS-poly acrylamide gel electrophesis (PAGE) gels were cast with 5% stacking gels. Quantified protein samples were added to 2X sample buffer (Sigma S-3401) and electrophoresed at 200 Volts, in SDS-Tris-Glycine Electrophoresis Buffer, for one hour beside pre-stained molecular weight markers (Gibco BRL, Paisley, U.K.). They were then transferred to nitrocellulose (Amersham Pharmacia Biotech, Amersham, U.K.) in Methanol Based Transfer Buffer at 400 milliAmps for 1 hour. The membranes were incubated in Ponceau S solution (Sigma P7170, 0.1% Ponceau S in 0.5% acetic acid) for 5 minutes at room temperature and rinsed briefly with distilled water to allow transferred protein to be visualized, thus confirming equal protein loading between lanes. Non-specific protein binding sites

on the nitrocellulose membrane were blocked by incubation of the membranes in 40ml of Western Blot Blocking Buffer for one hour at room temperature (RT) or overnight at 4°C. Membranes were washed 3 times in 50 ml of Western Blot Nitrocellulose Wash Buffer for 5 minutes. Appropriate primary antibodies were diluted in 20ml of the blocking buffer and incubated for one hour at RT with constant shaking. Membranes were washed 5 times with 50ml of the wash buffer at RT. For detection, horseradish peroxidase (HRP) conjugated antibodies were diluted in 20ml of the blocking buffer and incubated with the membranes for one hour at RT with gentle shaking. Membranes were washed a further 5 times with 50ml of the wash buffer before 5 minute incubation with ECL reagent (Amersham Pharmacia Biotech, Amersham, U.K.). Excess ECL reagent was removed and the membrane placed under BioMax MS-1 X-ray sensitive film. Films were processed through an X-ray developer (X-Ograph Imaging Systems, Wilts, U.K.) at various exposure time points (eg.1min, 3min, 5 min and 10 minutes). Optimally exposed films were photographed using a white trans-illuminator and gel documentation system (Ultra Violet Products, Cambridge, U.K.).

For β-catenin detection the samples were run on an 8% SDS-PAGE gel. The primary mouse IgG1 anti-mouse β-catenin monoclonal antibody (Affiniti Research Products Ltd, UK) was diluted 1:500, and the secondary HRP-Goat anti-mouse Ig antibody (Dako Corporation, Carpinteria, CA, USA) was diluted 1:2000. For Dvl1 detection the samples were run on an 8% SDS-PAGE gel. The primary rabbit anti-Dvl1 polyclonal antibody (gift from Roel Nusse, Stanford University, California, USA) was diluted 1:1000, and the secondary HRP-Donkey anti-rabbit Ig antibody (Amersham Life Science) was diluted 1:5000. For Sonic hedgehog (Shh) detection the samples were run on a 15% SDS-PAGE gel. The primary goat anti-N-Shh polyclonal antibody (Santa Cruz Biotechnology, Insight Biotechnology Ltd. Wembley, Middlesex, England) was diluted 1:200, and the secondary HRP-Rabbit anti-goat Ig antibody (Dako Corporation, Carpinteria, CA, USA) was diluted 1:2000. The β-catenin and Shh primary antibodies recognised proteins from both murine and human species.

2.2.5.4 Immunohistochemistry

Immunohistochemistry was performed on a Bio-Genex automatic staining machine (Menarini Diagnostics, Wokingham, Berkshire, UK) or using a Sequenza (Shandon). Briefly, 3μm sections of paraffin-embedded tissues were dewaxed in xylene, followed by microwave antigen retrieval using Antigen Retrieval Buffer (Vector Laboratories Ltd., Peterborough, UK) as per the manufacturers instructions. The slides were then blocked with 3% hydrogen peroxide (Sigma H-1009), followed by 20% rabbit or goat serum. Avidin/biotin blocking (Avidin/Biotin blocking kit, Vector Laboratories) was used as appropriate and slides were washed with PBS (D-8662) between steps. Slides were incubated with the primary antibody diluted in appropriate serum for 30-120 minutes at room temperature (RT) or overnight at 4°C, washed with PBS and incubated with a biotinylated secondary antibody for 30 minutes at RT. They were washed again, Vector RTU ABC (Vector Laboratories [binds to biotin]) applied and positive signal was visualised by the addition of diaminobenzidine (DAKO). Sections were counterstained with haematoxylin.

The following secondary antibodies and blocking sera were used: biotinylated rabbit anti–goat IgG (1:400 dilution, DAKO UK Ltd, Ely Cambridgeshire, UK); biotinylated goat anti-chicken Ig (1:250 dilution, Vector Laboratories, Ltd., Peterborough, UK); biotinylated goat anti-rabbit Ig (1:300 dilution, DAKO, UK); biotinylated rabbit anti–mouse IgG (1:300 dilution, DAKO UK); normal goat, rabbit, mouse and chicken serum (Scottish Antibody Production Unit, Carluke, Scotland, UK), normal human serum (Sigma-Aldrich Ltd, Poole road, Fancy, Dorset, UK). Primary antibodies to the N-terminus of Shh (goat, 1:40 dilution), the C-terminus of Ptc (goat, 1:30 dilution) [both Santa Cruz Biotechnology, Insight Biotechnology Ltd. Wembley, Middlesex, England], TGF-β1 (chicken, 1:50 dilution, R&D Systems Europe, Abingdon, UK) and β-catenin (mouse monoclonal, 1:500 dilution, Affiniti Research Products Ltd, UK) recognised murine and human proteins. Other primary antibodies included anti-Dvl1 (rabbit, 1:200 dilution, gift from Roel Nusse, Stanford University, USA), anti-Ki67 (mouse monoclonal, 1:200 dilution, Novocastra, UK) and anti-FITC (rabbit, 1:1000 dilution, DAKO, UK).

All primary antibodies were diluted in 20% normal human or mouse serum to block background reactivity on human or mouse tissue sections respectively, and blocking peptides (Santa Cruz Biotechnology, Insight Biotechnology Ltd. Wembley, Middlesex, England) were used as additional controls in conjunction with Shh and Ptc antibodies. Images were captured using a Progres 3012 camera (Kontron Elektronik) through a Zeiss Axioskop microscope.

2.2.6 T CELL EXPERIMENTS

2.2.6.1 Human PBMC isolation

Human peripheral blood mononuclear cells (PBMC) were isolated by centrifugal separation over Histopaque 1077 (Sigma H-8889). Briefly, single donor Buffy Coats, obtained from the Blood Transfusion Centre (Royal Infirmary of Edinburgh, UK) after viral screening, were made up to a volume of 200mls with D-PBS ((D-8537)), roughly equivalent to a 1:1 ratio. This was then layered in 25ml aliquots onto 15ml of Histopaque 1077 in eight 50ml falcon tubes and centrifuged at 800g for 25 minutes at room temperature. The mononuclear cell layer was gently aspirated and washed 2 times with 2 volumes of D-PBS and centrifuged at 300g for 7 minutes at room temperature. The pooled pellets were then resuspended in 50ml of PBS and counted using a haemocytometer chamber with 0.4% trypan blue exclusion (Sigma). Cells were resuspended at $1x10^8$/ml in D-PBS, to which 4ml of red blood cell lysis buffer was added per ml of PBS. The suspension was incubated on ice for 10 minutes before further centrifugation at 300g for 7 minutes at room temperature. The PBMC were resuspended in D-PBS, recounted and purified using either MACS or T cell columns as described below.

2.2.6.2 Cell Purifications

Human $CD4^+$or $CD8^+$expressing cells were separated from PBMC suspensions to generate near pure populations. This was performed either using a magnetic cell

separation method (MACS; Miltenyi Biotec, Surrey, UK) or human T cell subset negative selection affinity columns (R&D Systems, UK) both according to the manufacturer's instructions.

Briefly, for the former, single cell suspensions were generated as described above with the final resuspension in MACS buffer prior to a 15 minute incubation with antibody coated microbeads. Excess microbeads were removed by washing and labelled cells were passed through a magnetised positive selection column (Miltenyi Biotec, Germany). The selection column was washed with several volumes of MACS buffer, removing any unlabelled cells. The column was demagnetised and cells bearing the antigen of interest (i.e. CD4 or CD8) were expelled from the column with 5ml MACS buffer.

For T cell negative selection, the PBMCs were resuspended in the sterile column buffer provided to which the provided monoclonal antibody cocktail was added followed by a 15 minute incubation at room temperature. The cells were washed twice in column buffer and centrifuged at 300g for 10 minutes, then resuspended in column buffer and added to the negative selection columns. Following a further 10 minute incubation the cells of interest were eluted with 12ml of column buffer.

After either of the above selection methods, cells were washed in complete human RPMI culture media and counted using a haemocytometer with 0.4% trypan blue exclusion. Using these methods of purification typically generated ≥93% pure populations.

2.2.6.3 Polyclonal TCR stimulation using plate bound and soluble antibodies

Stimulation of purified T cell populations was performed using the combination of monoclonal antibodies against CD3ε and CD28 (Pharmingen, San Diego, CA, USA). The anti-CD3ε monoclonal antibody was immobilised onto plastic by diluting the antibody to final concentrations of 1-5μg/ml in D-PBS (D-8662) and dispensing 50μl of the diluted monoclonal per well of a flat bottomed 96 well plate. The plates were incubated for 16 hours at 4°C. Wells were washed three times with ice cold D-PBS to remove excess unbound antibody. Purified cells were plated out at $1x10^5$ per well

in complete RPMI 1640 (10^6cells/ml). Anti-CD28 monoclonal antibodies were added to the wells at a final concentration of 5μg/ml diluted in the appropriate cell culture buffer. Addition of either exogenous soluble N-Shh peptide or 5E1 antibody was performed prior to incubation at 37°C in a humidified incubator with 5% CO_2 for 72 hours. Proliferation was assessed by incorporation of tritiated methyl thymidine and assayed as described below.

2.2.6.4 Proliferation

Proliferation was assessed by addition of excess (1μCi/well) tritiated methyl thymidine (^{3}H-TdR-Amersham Pharmacia Biotech, Amersham, UK). Plates were harvested onto glass fibre filtermats (Wallac, Milton Keynes, U.K.) with an automated 96 well plate harvester (Tomtec, Harborview, USA), dried and sealed in plastic bags (Wallac, Milton Keynes, U.K.) with 10ml of scintillation fluid (Wallac, Milton Keynes, U.K.). ^{3}H-TdR incorporation was assessed using a liquid scintillation counter Betaplate 1205 (Wallac, Milton Keynes, U.K.) and associated software. Counts per minute (cpm) observed per sample were indicative of the extent of proliferation. All samples were tested in triplicate or sextuplet and each experiment repeated three times unless otherwise stated.

2.2.6.5 Apoptosis Assay (AnnexinV-FITC staining)

AnnexinV-FITC conjugate binds phospholipid phosphatidylserine (PS). PS is translocated from the inner leaflet of the plasma membrane to the outer leaflet during very early phases of apoptosis and can thus bind AnnexinV-FITC extracellularly. It can therefore be used as an early indicator of programmed cell death in flow cytometry. Propidium Iodide, used in conjunction with AnnexinV-FITC, detects membrane integrity of the cells, thus distinguishing necrotic from apoptotic cells.

AnnexinV-FITC staining of cells was performed using an apoptosis detection kit following the manufacturer's instructions (Pharmingen, BD, USA). Cells boiled for 2-3 minutes at 95°C were used as control "dead cells". Briefly, cells were washed

twice in cold PBS (D-8537) and centrifuged at 300g for 7mins at 4°C, resuspended in the supplied 1x binding buffer at 10^5 cells/100µl, and added to flexible 96 round-bottom well plates (Becton Dickinson). 5µl of AnnexinV-FITC and 2µl of PI were added per 10^5 cells and incubated for 15 minutes in the dark at room temperature. Cells were resuspended in 400µl 1x Binding Buffer and analysed by flow cytometric analysis using a Becton Dickinson FACSCalibur (BDIS, San Jose, CA, USA).

2.2.6.6 Flow Cytometry

All flow cytometry was performed on a Becton Dickinson FACSCalibur (BDIS, San Jose, CA, USA) and experiments were repeated at least three times. Phenotypic analysis of human cell surface markers was accomplished using Phycoerythrin (PE) and Fluorescein isothiocyanate (FITC) conjugated monoclonal antibodies (Pharmingen, San Diego, CA, USA) recognising the following cell surface proteins (CD3, CD4, CD8, CD25, CD69). Appropriate isotype controls were also purchased from Pharmingen. Briefly, cells of interest were washed in ice-cold D-PBS (D-8537) and resuspended in FACS staining buffer at a maximum final concentration of 10^6 cells per 100µl. 1µg of relevant monoclonal antibody was added per 10^6 cells and incubated in the dark at 4°C for 30 minutes. Samples were washed three times with ice-cold D-PBS and resuspended in ice-cold FACS fixing solution. Fixed samples were kept at 4°C and analysed as specified by Becton Dickinson within 48 hours of staining and fixing.

2.2.6.7 Enzyme Linked ImmunoSorbant Assay (ELISA)

Cytokine secretion was analysed by detecting soluble protein in aliquots of supernatants or bronchoalveolar lavage fluid as appropriate. Reagents for IL5 detection and standards were purchased from Pharmingen (San Diego, CA, USA). Briefly, the anti-IL5 capture antibody was diluted to 1µg/ml in ELISA binding buffer. 50µl of diluted capture antibody was added to the wells of enhanced protein binding ELISA plates (Corning, NY, USA). The plates were sealed and incubated

overnight at 4°C. Capture antibody was removed, 200µl of ELISA blocking buffer was added to each well and the plates incubated at 37°C for one hour. Wells were washed 3 times with ELISA wash buffer and 50µl of standards and samples were added to the wells (appropriately diluted in ELISA blocking buffer). Plates were sealed and incubated overnight at 4°C. Wells were washed 4 times with 200µl ELISA wash buffer and 50µl of 1µg/ml biotinylated IL5 detection antibody diluted in ELISA blocking buffer was added to each well. Plates were incubated for one hour at room temperature, after which wells were washed 5 times with 200µl ELISA wash buffer. 50µl of 1 in 2000 diluted (manufacturer's instructions) Streptavidin-alkaline phosphatase conjugate (Amersham Life Sciences, Amersham, U.K.) was added to the wells and incubated for 30 minutes at room temperature. Wells were washed 5 times with ELISA wash buffer to remove excess alkaline phosphatase and 100µl of substrate solution was added to wells. Plates were placed in the dark for colour change to occur and assayed at 10 minute intervals on a Microplate Reader 450 (BioRad Laboratories, Hemel Hempstead, U.K.) and associated software.

IL2, IL10, IFNγ and TGFβ1 were measured using Duoset ELISA development system kits (R&D systems, UK) following the manufacturer's protocols. As the TGFβ1 kit only measured active TGFβ1, latent TGFβ1 was activated as per the manufacturers instructions to allow total TGFβ1 to be determined. The plates were read by a microplate reader set (Dynatech Laboratories MRX) to a wavelength of 450nm with a reference of 550nm.

Grade of fibrosis	Histological Features
0	Normal lung
1	Minimal fibrous thickening of alveolar or bronchiolar walls
2	
3	Moderate thickening of walls without obvious damage to lung architecture
4	
5	Increased fibrosis with definite damage to lung structures and formation of fibrous bands or small fibrous masses
6	
7	Severe distortion of structure and large fibrous areas: 'honeycomb lung' is placed in this category
8	Total fibrous obliteration of field

Table 2: Ashcroft scoring system for lung fibrosis

Table lists scoring system used to grade fibrosis in the lungs of FITC-treated lung mice. This is taken from the original paper by Ashcroft *et al* (see text for reference)

Gene	Primer Sequence (5'-3')	PCR product (bp)	Tm (°C)
β-Actin	**For:** CCACCAACTGGGACGACATG **Rev:** GTATCAAACATGATCTGGGTCATC	151	58
Mouse Dvl1 (A)	**For:** TATGCAGTAGTGGGTGG **Rev:** AACAGAAACAGAACAGGG	894	50
Mouse Dvl1 (B)	**For:** CCAAAGCCTCACAGAAC **Rev:** ACAGAAGCAGCATTTACA	521	51
Human Ptc	**For:** CCATGTTCCAGTTAATGACTC **Rev:** ACATCATCCACACCAACA	462	58
Human Shh	**For:** CAGCGCGTGTACGTGGTGGC **Rev:** GGAGCGTCGGCAGCACCTG	335	60
Neo-Cassette	**For:** CTTGGGTGGAGAGGCTATTC **Rev:** AGGTGAGATGACAGGAGA	280	64*

Table 3: Primers used for PCR and RT-PCR

Table lists primers used for all PCR discussed in thesis, including length of products and optimal annealing temperatures (Tm). Dvl1 A+B refers to 2 different primer pairs (see Chapter 5). **For**: Forward Primer, **Rev**: Reverse Primer.

64*: Touchdown PCR reaction with Tm reducing by 0.5°C per cycle.

Gene	Primer Sequence (5'-3') and Probe
Human Ptc	**For:** CGGCAGCCGCGATAAG **Rev:** TTAATGATGCCATCTGCATCCA **Probe:** ATCGACATCAGCCAGTT GACTAAACAGCGTC
Mouse Dvl1	**For:** AGCACCTCCTCTCGGCTAGTT **Rev:** GGGACATGGTGGAGTCTGTGAT **Probe:** AAGCACAAATGCCGTCGTCGGAA
Mouse Shh	**For:** TGACCCCTTTAGCCTACAAGCA **Rev:** TTCTTGTGATCTTCCCTTCATATCTG **Probe:** TTTATTCCCAACGTAGCCGAGAAGACCC
Mouse Ptc	**For:** CTCCAAGTGTCGTCCGGTTT **Rev:** TGTACTCCGAGTCGGAGGAATC **Probe:** CGTGCCTCCTGGTCACACGAACAA

Table 4: Primers and Probes used for Real-Time PCR

Table lists primers and probes used for all Real-time PCR discussed in thesis. **For**: Forward Primer, **Rev**: Reverse Primer.

Chapter 3

The Sonic Hedgehog Pathway in Interstitial Lung Disease

3.1 Introduction

As discussed in Chapter 1 the Sonic hedgehog (Shh) signalling pathway plays an important role in lung development [55,94]. In this respect it interacts with other genes such as TGFβ and FGFs [101,102,104]. Significantly, such genes are known to be associated with the pathogenesis of interstitial lung disease (ILD) or lung fibrosis [353,358].

Upregulation of the Shh pathway results in increased proliferation of many cell types, including epithelial cells [116,117]. Indeed, as described in Chapter 4, the Shh pathway is also involved in regulation of T lymphocytes. The pathway has been reported to induce epithelial and mesenchymal hyperplasia when overexpressed *in vivo* [56], both features of ILD [292,293].

The combination of the interactions with other genes important in fibrosis and the *in vitro* and *in vivo* increased proliferation associated with overexpression of Shh prompted this investigation into whether or not the Shh pathway was induced in ILD. To address this question, a murine model of ILD [408], induced by intra-tracheal instillation of fluorescein isothiocyanate (FITC), and archival human biopsy specimens from patients with idiopathic pulmonary fibrosis (IPF) were used. Expression of components of the Shh pathway and TGFβ1 were determined by immunohistochemistry (IHC).

In this chapter the expression of these proteins is investigated, as are the effects of FITC treatment in mice deficient of downstream genes in the Shh pathway. In addition an attempt to upregulate Shh in lung epithelial cells *in vivo* using a naked DNA vector is described.

3.2 Reproducing the FITC Model

The FITC model of ILD is described in more detail in chapter 1. In the original paper the trachea was exposed surgically and 100μl of PBS or FITC resuspended in PBS instilled, a procedure which resulted in a 5-10% mortality within 24 hours [408]. An alternative non-surgical approach has been developed as described below and in chapter 2. The results presented in this chapter were verified in lung sections from mice receiving FITC by both methods.

3.2.1 INTRA-TRACHEAL INSTILLATION OF FITC

PBS or FITC was instilled intra-tracheally as detailed in chapter 2. Briefly the sample was instilled via an oral approach with no surgical intervention required. The new approach offered the advantage of a reduced mortality (<1%). However, a potential disadvantage was that the vocal cords were occasionally poorly visualised, but, with experience, the trachea could still be accurately located in such circumstances.

Mice were killed at time-points from 24hrs to 5 months following instillation. The lungs were inflated, formalin fixed and 3 μm sections cut. In the first instance sections were examined under a fluorescent microscope to ensure FITC had been deposited in the lungs. This was followed by confocal microscopy. These methods confirmed FITC deposition in a patchy distribution particularly localised around the airways (Figure 3.1A).

FITC could also be detected by IHC using a specific anti-FITC antibody (Figure 3.1 B-F). At the earlier time-points (3 days) the staining was intense. Although noted throughout the lungs it was often at its strongest within the airway epithelial cells (Figure 3.1B), as one might expect as they present one of the first points of contact for an antigen delivered by the an intra-tracheal route. Furthermore, alveolar

macrophages were also strongly positive suggestive of uptake of the free FITC and probable processing by the immune system (Figure 3.1C). The FITC could also be detected at the 5 month time-point, though generally with a more localised distribution. As before staining was notably patchy; some areas showed intense staining and others no evidence of FITC at all (Figure 3.1D). This was in keeping with the free FITC particles having been deposited in a random manner following instillation, and with appearances previously observed in the model [408]. Sites of FITC deposition corresponded to areas of scarring and fibrosis, and areas free of FITC were often histologically normal. At this later time-point the staining was predominantly peribronchial (Figure 3.1 E and F) as observed in the original paper, in which it was suggested that the FITC may be binding to elastin fibres surrounding the airways [408].

A section from every mouse was stained with the anti-FITC antibody to ensure FITC had been successfully delivered into the lungs. If the staining was negative the lung was not used for further analysis.

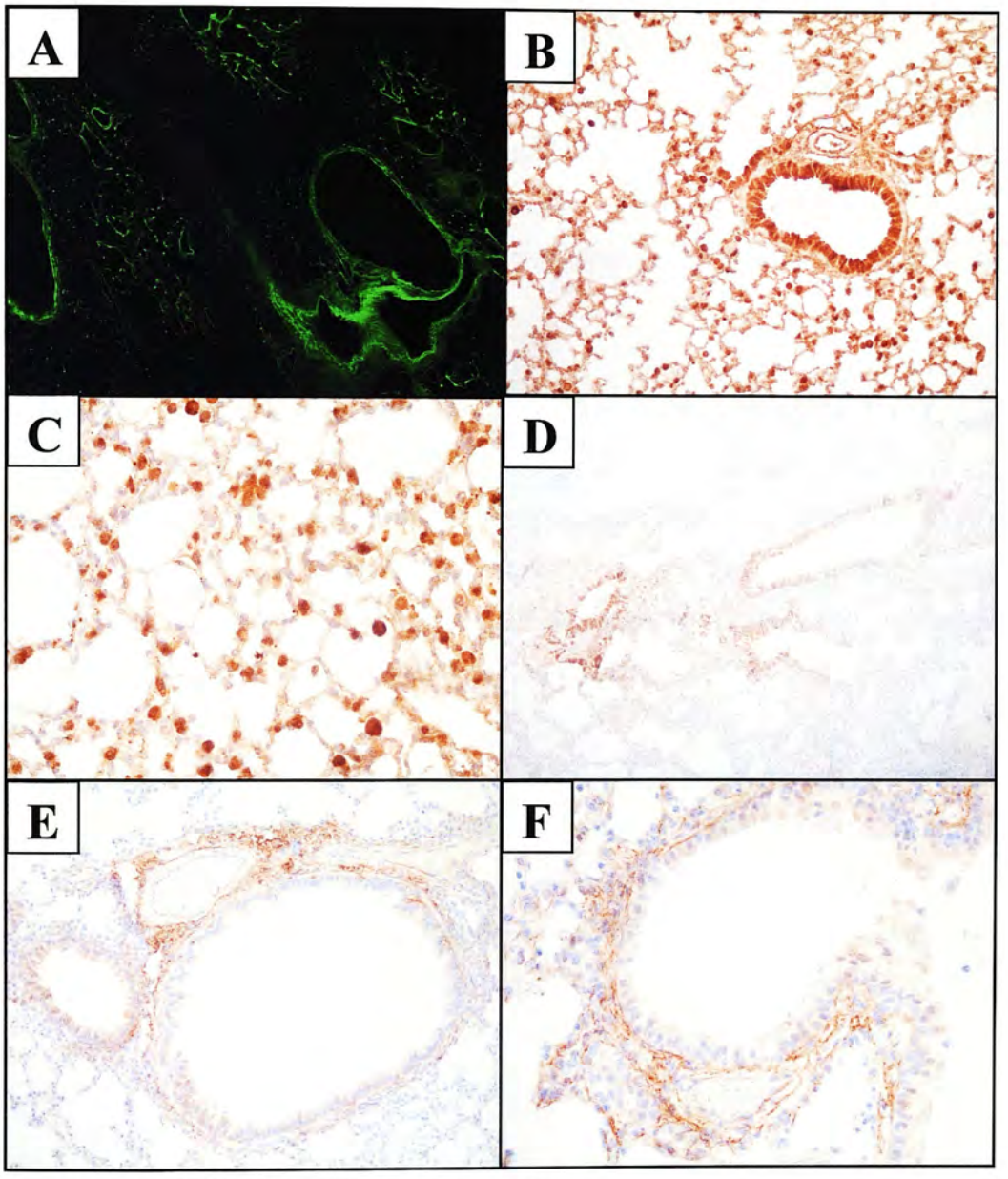

Figure 3.1: FITC deposition in mouse lungs

All sections are from FITC treated mice; magnifications are indicated in brackets

A) FITC fluorescence at day 3 post instillation as viewed by confocal microscopy (x100). Patchy FITC deposition (bright green) against background auto-fluorescence. Remaining pictures are sections stained with anti-FITC antibody. **B)** Strong epithelial cell staining 3 days after FITC (x200). **C)** Positive alveolar macrophages 3 days after FITC (x400). **D)** Patchy FITC staining 5 months after FITC (x100). **E)** Peribronchial staining 5 months after FITC (x200) and **F)** x400.

3.2.2 LUNG MORPHOLOGY FOLLOWING FITC TREATMENT

Lung sections from FITC or PBS treated mice were stained with haematoxylin and eosin to allow morphology to be assessed (Figure 3.2). PBS treated mice sections were normal with no evidence of epithelial cell damage, cellular infiltration nor fibrosis (Figure 3.2 A-C). Although only the day 7 time-point is shown appearances were similar at all time-points.

The FITC treated mice sections were altogether different. At the earlier time-points (days 3 and 7) there was a marked mononuclear cell and neutrophil infiltrate mainly surrounding the airways and, in some cases, spreading throughout the interstitium (Figure 3.2 D-F). As with FITC deposition this was often in a patchy distribution (Figure 3.2D). There was evidence of damaged airway epithelial cells, which appeared "peg-like", and of epithelial sloughing (Figure 3.2E).

By 5 months there was evidence of alveolar wall thickening and oedema (Figure 3.2G). A chronic, predominantly mononuclear inflammation was noted and areas of established largely peribronchial fibrosis often corresponding with FITC deposition. In many areas the normal lung architecture had been completely destroyed, replaced by scar and fibrous tissue (Figure 3.2 H and I).

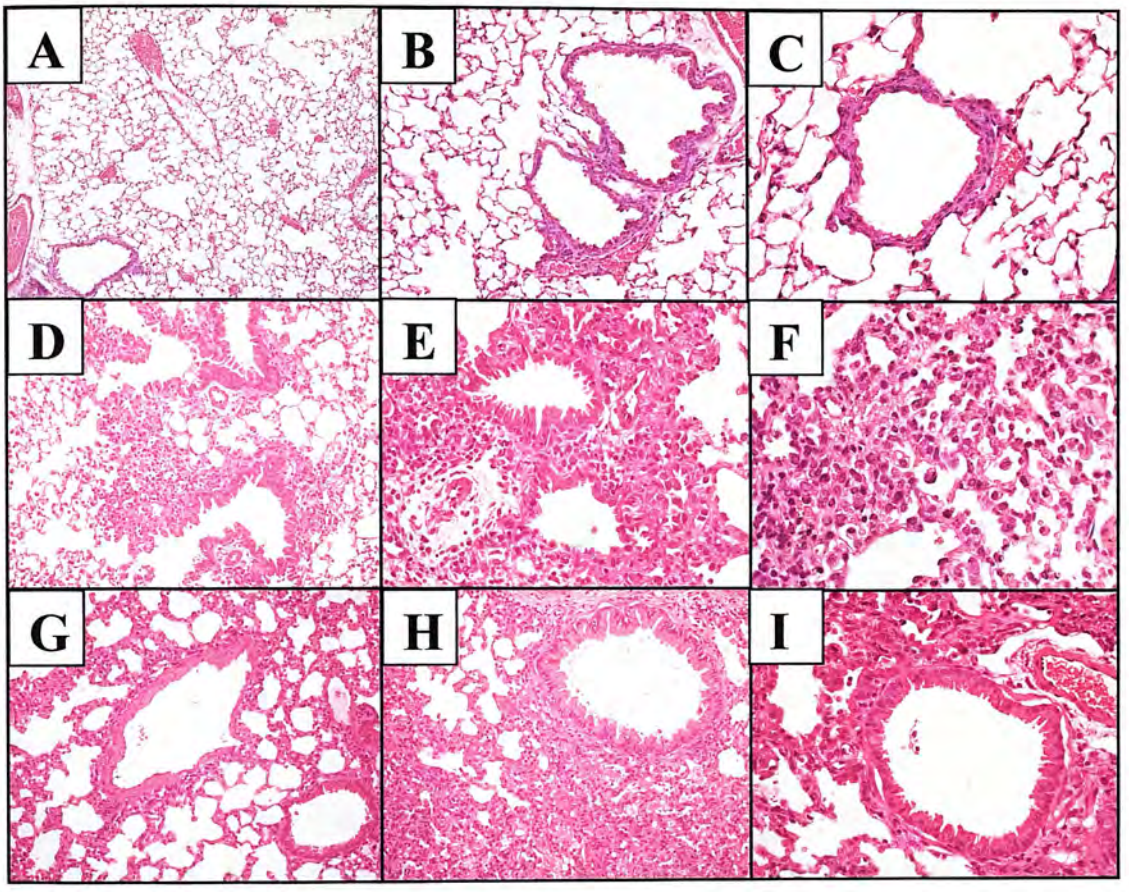

Figure 3.2: Haematoxylin and Eosin (H&E) staining of FITC and PBS treated mouse lungs

Magnifications are indicated in brackets

Normal lung architecture and morphology: **A)** 7 days after PBS (x100). **B)** 7 days after PBS (x200) **C)** 7 days after PBS (x400).

Patchy peribronchial cell infiltrate and evidence of epithelial cell damage: **D)** 3 days after FITC (x200). **E)** 3 days after FITC (x400). **F)** 7 days after FITC (x400).

Evidence of alveolar wall thickening, persisting mononuclear cell infiltrate and fibrosis: **G)** 5 months after FITC (x200). **H)** 5 months after FITC (x200). **I)** 5 months after FITC (x400)

3.2.3 SCORING FIBROSIS IN THE FITC MODEL

Lung sections from FITC and PBS treated mice were each given a fibrosis score based on a scoring system devised by Ashcroft *et al* [551], as described in Chapter 2. This was to allow comparison between different treatment groups and time-points. For each time-point sections from six FITC treated mice and two PBS mice were analysed, all treated by the new intra-tracheal approach discussed earlier. The FITC sections were further subdivided into FITC +ve and FITC -ve fields, because of the correlation noted between areas of FITC deposition and lung fibrosis in the original paper by Roberts *et al* [408]. The chosen time-points were 3 days, 1 week and 6 weeks after a single instillation or following a second instillation (FITC or PBS), administered 6 weeks after the first. Ashcroft scores for each group were averaged as shown in table 5.

Ashcroft scores from the three groups (PBS, FITC +ve and FITC -ve) were then statistically compared using the Mann-Whitney Test (Instat) as shown in table 6. FITC –ve fields did not differ significantly from PBS treated mice at any time-point. There was no significant difference between any of the groups following the first instillation. However Ashcroft scores were significantly higher in the FITC +ve fields when compared to both FITC –ve fields and PBS treated mice, following the second instillation. These results show that there was significantly more fibrosis, as assessed by Ashcroft scoring, in FITC treated mice, but only following a second treatment and only in association with FITC +ve areas (Table 6).

Each of the three groups was then analysed longitudinally. Ashcroft scores from each time-point were compared to the score at 3 days following the first instillation, within the same group (Table 7). In the FITC +ve group, all scores following the second FITC instillation were significantly higher than the 3 day time-point. There was no significant difference in the FITC -ve or PBS groups between any of the time-points, except 6 weeks following the second instillation. In both groups the score at this time-point was significantly higher than the score at 3 days. This may have been indicative of mice developing disease due to environmental exposure in

the animal house. Importantly, as described above, there was no significant difference between these two groups at this time-point, and the scores of both were significantly lower than the FITC +ve group (Table 7). Taken together, these results confirm significantly higher fibrosis scores in FITC +ve fields following a second instillation of FITC.

Ashcroft Scores	PBS	FITC +ve	FITC -ve
3 days	0.0014 ± 0.0014	0.0007 ± 0.0007	0.0006 ± 0.0006
1 week	0.0009 ± 0.0009	0.0008 ± 0.0008	0.0006 ± 0.0006
6 weeks	0.0028 ± 0.0028	0.0185 ± 0.0185	0.0056 ± 0.0056
6 weeks + 3 days	0.0009 ± 0.0009	0.9928 ± 0.06328	0.0226 ± 0.0112
6 weeks + 1 week	0.0005 ± 0.0005	1.746 ± 0.1567	0.01852 ± 0.0075
6 weeks + 6 weeks	0.337 ± 0.0465	1.595 ± 0.0749	0.3827 ± 0.0398

Table 5: Mean Ashcroft scores in the FITC fibrosis model

Table lists mean Ashcroft scores (and standard errors) in PBS treated mice, and in FITC +ve and –ve fields from FITC treated mice

p values	PBS versus -ve	PBS versus FITC+ve	FITC+ve versus -ve
3 days	ns	ns	ns
1 week	ns	ns	ns
6 weeks	ns	ns	ns
6 weeks + 3 days	ns	<0.001	<0.001
6 weeks + 1 week	ns	<0.001	<0.001
6 weeks + 6 weeks	ns	<0.001	<0.001

Table 6: Comparative Ashcroft scores in the FITC fibrosis model

Table lists statistical analysis of Ashcroft scores from table 5, comparing each of the three groups. Results show statistical significance between FITC +ve fields and both PBS and FITC –ve fields ($p<0.001$), but only at the time-points following a second treatment (6 weeks+). There was no significant (ns) difference between the other groups.

p values	3 days vs 1 week	3 days vs 6 weeks	3 days vs 6 weeks + 3 days	3 days vs 6 weeks + 1 week	3 days vs 6 weeks + 6 weeks
PBS	ns	ns	ns	ns	<0.001
FITC+ve	ns	ns	<0.001	<0.001	<0.001
FITC -ve	ns	ns	ns	ns	<0.001

Table 7: Longitudinal Ashcroft scores in the FITC fibrosis model

Table lists statistical analysis comparing Ashcroft scores from each group with the 3 day score from that group. Results show significant differences between 3 days and all of the second treatments (6 weeks+) within the FITC +ve group. There were also statistical significance in the PBS and FITC –ve groups, in relation to the final time-point, which may be related to mice developing disease due to environmental exposure in the animal disease. (ns: not significant)

3.3 Immunohistochemistry in the FITC Model

Lung sections from FITC or PBS treated mice were stained with antibodies against Shh, Patched (Ptc) and TGFβ1. IHC was performed on sections from 24hrs to 5 months, with at least six mice included for each treatment at every time-point. The results shown are representative of features noted at all time-points.

3.3.1 SONIC HEDGEHOG EXPRESSION IN THE FITC MODEL

Expression of Shh protein was analysed using the goat polyclonal anti-Shh antibody (Santa Cruz Biotechnology). The specificity of this antibody was demonstrated by Western Blotting (Figure 5.16). This antibody was raised against the amino terminus of Shh, which remains membrane bound. Shh IHC was carried out on lung sections from FITC or PBS treated mice. The observed Shh staining was specifically blocked when the associated Shh blocking peptide (Santa Cruz) was introduced (data not shown).

Shh expression was markedly upregulated in the FITC treated mice when compared with the corresponding PBS controls (Figure 3.3). This was noted at all time-points from 3 days to 5 months. The staining, though particularly strong on the bronchial and alveolar airway epithelial cells (Figure 3.3 B, D and F), was also present on infiltrating mononuclear cells (Figure 3.3F). This latter feature is consistent with findings presented in chapter 4 (Figure 4.1) where Shh expression is confirmed in human T lymphocytes.

It would, therefore, appear that Shh protein expression is upregulated in the FITC model of fibrosis.

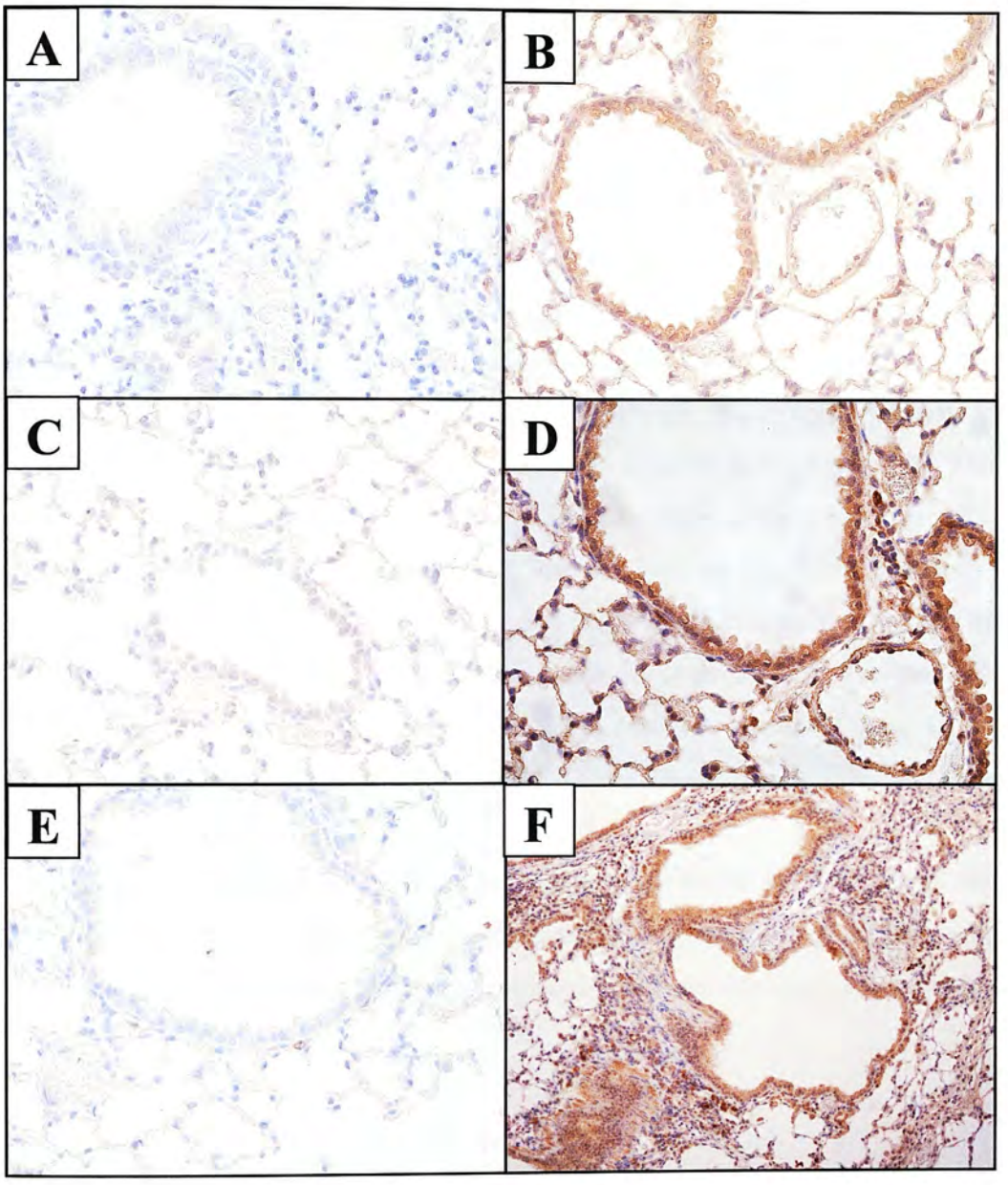

Figure 3.3: Shh expression in FITC and PBS treated mouse lungs

Magnifications are indicated in brackets

Shh IHC in mouse lungs **A)** 3 days after PBS (x400). **B)** 3 days after FITC (x400). **C)** 7 days after PBS (x400). **D)** 7 days after FITC (x400). **E)** 5 months after PBS (x400). **F)** 5 months after FITC (x400). At all time-points Shh expression is notably upregulated in the FITC treated mice, particularly in the airway epithelium

3.3.2 PATCHED EXPRESSION IN THE FITC MODEL

Ptc, the Shh receptor, expression was then assessed by IHC on the same lung sections.

Ptc was expressed in both PBS and FITC treated mice with no appreciable difference between the intensity of staining between the treatment groups (Figure 3.4). As with Shh, the bronchial and alveolar airway epithelium was strongly positive. Most notably the alveolar and interstitial macrophages were also strongly positive for Ptc throughout, as were the infiltrating mononuclear cells (Figure 3.4 D and F). This was more noticeable in the FITC treated mice as many more of these immune cells were present in the lungs. The presence of Ptc and Shh on these immune cells is in accordance with data presented in chapter 4 (Figure 4.1) in which expression of both of these proteins on human T lymphocytes is demonstrated. Ptc staining was specifically blocked when the associated Ptc blocking peptide (Santa Cruz) was introduced (data not shown).

Using IHC there is no evidence of Ptc upregulation in the FITC model of fibrosis. Unlike Shh, there appears to be constitutive Ptc expression in mouse lungs. Its presence is confirmed in both airway epithelium and mononuclear cell infiltrates.

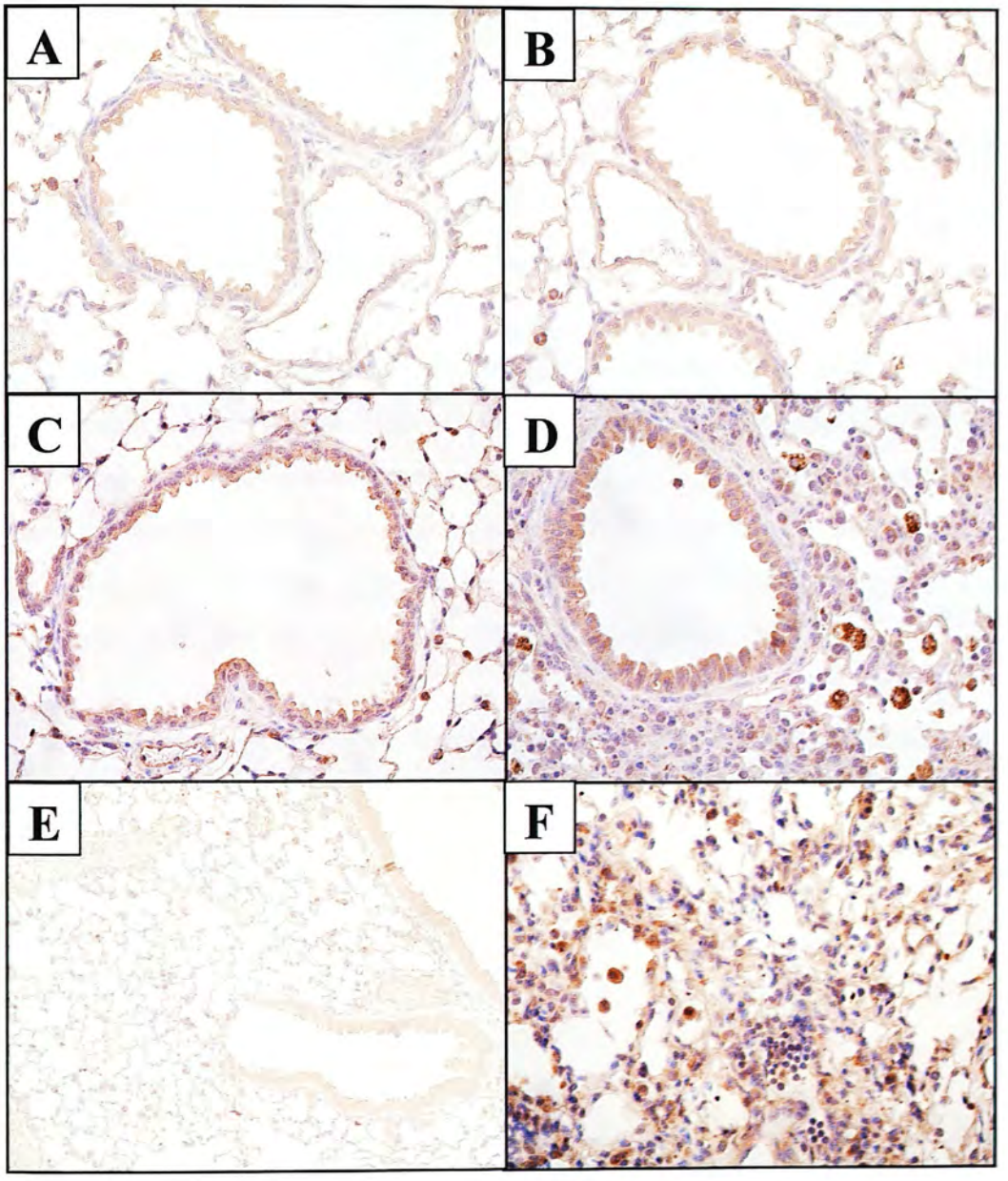

Figure 3.4: Ptc expression in FITC and PBS treated mouse lungs

Magnifications are indicated in brackets

Ptc IHC in mouse lungs **A)** 3 days after PBS (x400). **B)** 3 days after FITC (x400). **C)** 7 days after PBS (x400). **D)** 7 days after FITC (x400). **E)** 5 months after PBS (x200). **F)** 5 months after FITC (x400). Throughout the time-points Ptc expression is very similar in the airway epithelium in FITC and PBS treated sections. Notably Ptc is expressed in the alveolar macrophages and cell infiltrates

3.3.3 TRANSFORMING GROWTH FACTOR-BETA EXPRESSION IN THE FITC MODEL

TGFβ already has a proven role in the pathogenesis of ILD [358]. However its expression has not been analysed in the FITC model. TGFβ1 IHC was therefore carried out on lung sections from FITC and PBS treated mice.

TGFβ1 expression was markedly upregulated in the FITC treated mice when compared with the corresponding PBS controls (Figure 3.5). The bronchial airway epithelial cells stained particularly strongly (Figure 3.5 D and F). In addition alveolar and interstitial macrophages, and infiltrating mononuclear cells were also positive (Figure 3.5 D+F). These findings are in keeping with published work on TGFβ1 expression in other animal models and lung fibrosis in humans [353-357].

As would be expected TGFβ1 is upregulated in the FITC model of lung fibrosis.

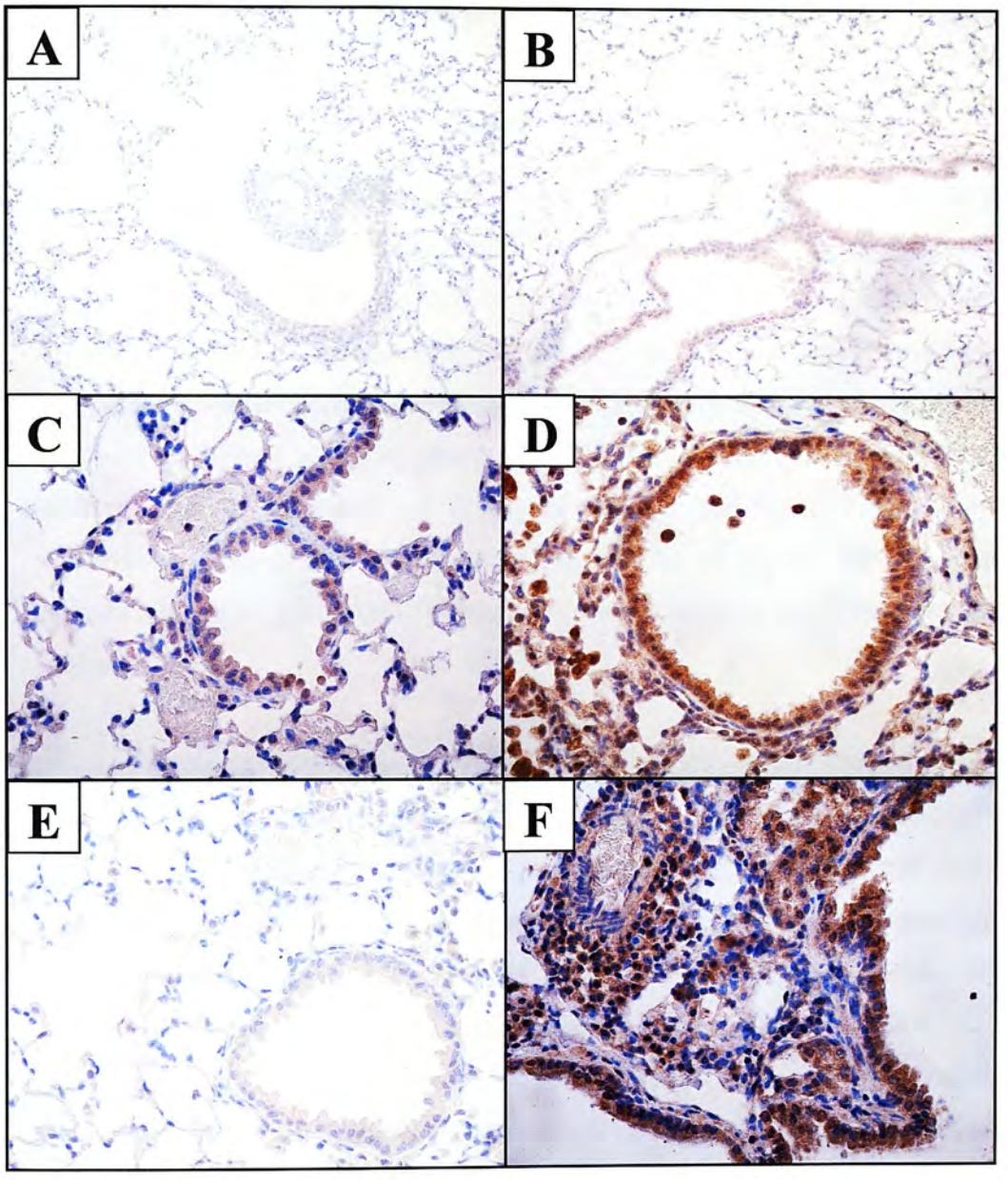

Figure 3.5: TGFβ1 expression in FITC and PBS treated mouse lungs

Magnifications are indicated in brackets

TGFβ1 IHC in mouse lungs **A)** 3 days after PBS (x200). **B)** 3 days after FITC (x200). **C)** 7 days after PBS (x400). **D)** 7 days after FITC (x400). **E)** 5 months after PBS (x400). **F)** 5 months after FITC (x400). As with Shh, TGFβ1 expression is notably upregulated in the FITC treated mice throughout the time-points, both in the airway epithelium and the cell infiltrates.

3.4 Immunohistochemistry in Idiopathic Pulmonary Fibrosis (IPF)

Having demonstrated the expression of Shh, Ptc and TGFβ1 in the FITC model of lung fibrosis the next objective was to stain for these same proteins in archival human biopsies taken from patients with IPF, also known as Cryptogenic Fibrosing Alveolitis (CFA) and more recently classified as usual interstitial pneumonia (UIP). The pathology of IPF is discussed in more detail in chapter 1. However, to reiterate, the features include a patchy distal lung fibrosis, a mononuclear interstitial cell infiltrate, type II epithelial cell hyperplasia and metaplasia, and smooth muscle proliferation. The data is representative of staining of biopsy material from six patients with IPF. Histologically normal areas from these sections were used as controls.

Shh was expressed in the remodelling type II epithelial cells and ciliated metaplastic respiratory epithelial cells at diseased sites but not in histologically normal areas (Figure 3.6 A, B, C and E). The protein was present in the cytoplasm and on the cell surface and, at higher magnifications, it was evident that Shh positive and negative cells lay in juxtaposition (Figure 3.6 C). The characteristic hypertrophic smooth muscle also stained positively for Shh (Figure 3.6 B [arrow] and D). As in the FITC model Ptc was uniformly expressed in the bronchial airway (type II) epithelial cells (Figure 3.6 G). In IPF sections expression was notable both in diseased and normal sites, consistent with significant constitutive Ptc expression (Figure 3.6 F and G). Ptc was also notably present on the mononuclear cell infiltrates and alveolar macrophages (Figure 3.6 F and H). As both the Shh and Ptc antibodies were raised in goat, normal goat serum was used as a negative control. This confirmed no background non-specific staining (Figure 3.6 L).

TGFβ1 expression was detected in both hyperplastic type II epithelial cells and metaplastic bronchial epithelial cells at sites of remodelling (Figure 3.6 J and K). It

was also present in alveolar macrophages and in the interstitial infiltrate (Figure 3.6 K). It was not, however, expressed in histologically normal alveoli (Figure 3.6 I).

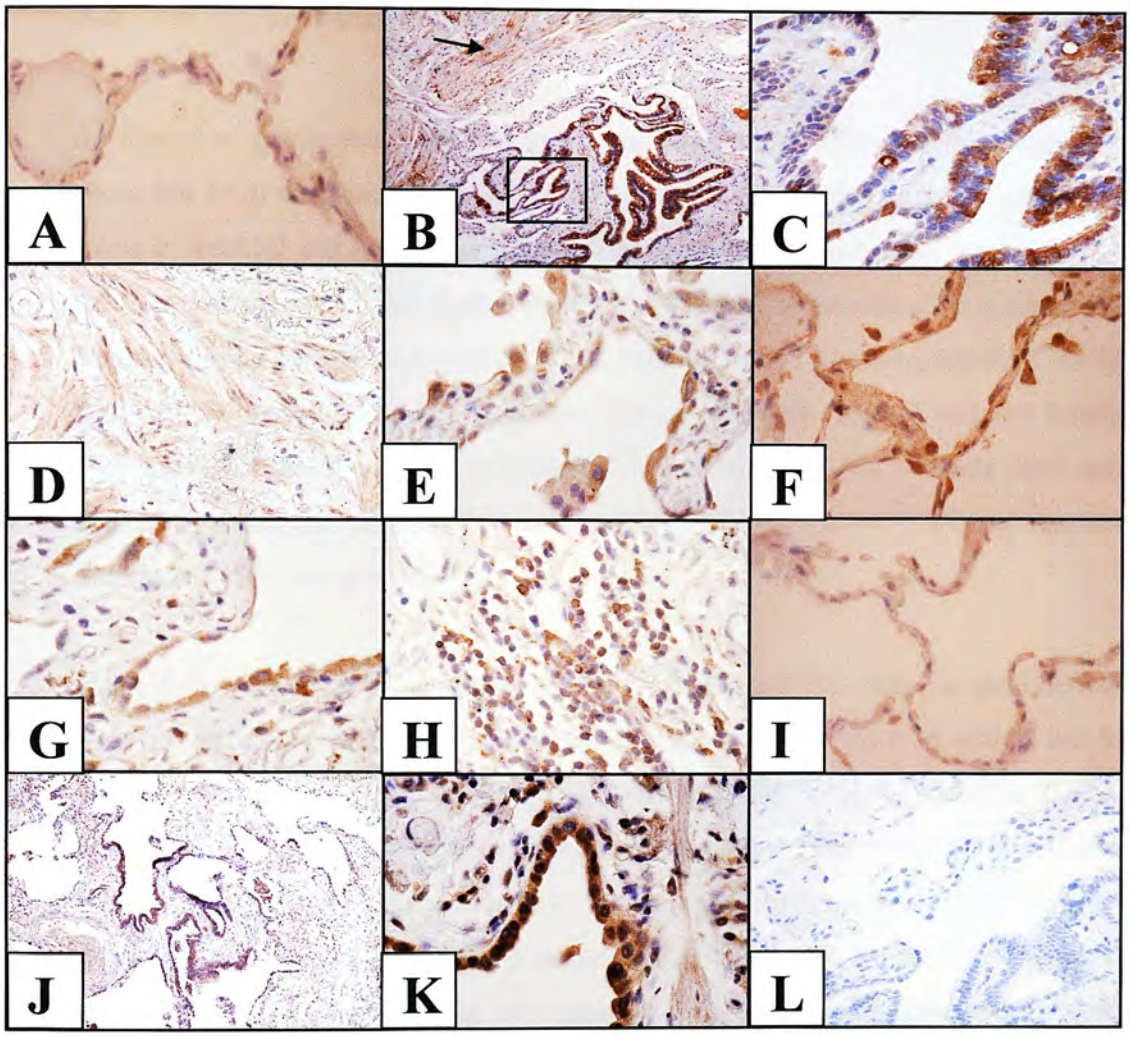

Figure 3.6: Shh, Ptc and TGFβ1 expression in Idiopathic Pulmonary Fibrosis (IPF)

All IHC in human IPF sections: comparing histologically normal areas (**A**, **F** + **I**) with fibrotic lung (remaining sections). Magnifications are indicated in brackets

A) Shh IHC (x400) Shh is not expressed in histologically normal areas **B)** Shh IHC (x100) Hypertrophic smooth muscle is arrowed and boxed area is shown in **C)** Shh IHC (x400). Staining of metaplastic epithelial cells. Shh positive and negative epithelial cells are seen in close proximity. **D)** Shh IHC (x400) Positive hypertrophic smooth muscle shown at greater magnification. **E)** Shh IHC (x600). Staining of type II epithelial cells.

F) Ptc IHC (x400) Ptc is constitutively expressed in histologically normal lung **G)** Ptc IHC (x600) Ptc expression is noted in type II epithelial cells **H)** Ptc IHC (x600). Ptc present in interstitial infiltrate.

I) TGFβ1 IHC (x400) is not expressed in histologically normal alveoli **J)** TGFβ1 IHC (x100) and **K)** TGFβ1 IHC (x600) TGFβ1 is noted in the airway type II epithelial cells and interstitial infiltrate of fibrotic lung.

L) Normal Goat Serum control (x100) Negative control showing no background staining.

3.5 The FITC Model in *Gli* gene deficient mice

As described in chapter 1 the *Gli* genes are downstream targets of Shh signalling. There are 3 *Gli*'s in mammals: *Gli1*, *Gli2* and *Gli3*. *Gli2* and *Gli3* are known to play a role in tracheal and lung development [86] in which it is thought they are required for the transduction of the Shh signal. Mice with *Gli2* null mutations display phenotypic features similar to Shh mutant mice [85,86] in keeping with a downregulation of the Shh pathway. Mice with *Gli3* null mutations have phenotypic features more in keeping with upregulation of the Shh pathway [78,83]. *Gli2/Gli3* double mutants have more marked phenotypic abnormalities than either homozygote implying common functions of the two genes [85,86].

In the following experiments the aim was to introduce FITC into *Gli* gene deficient mice to determine if the fibrotic response was altered in mice in which the Shh pathway was dysregulated. Having observed that Shh is upregulated in ILD the hypothesis was that the Shh pathway might be helping to "drive" the disease process. If this were true one might predict that the response to intra-tracheal FITC would be altered in *Gli* knockouts. It should be pointed out from the outset that lungs taken from these mice, without treatment, appeared morphologically normal, as assessed by haematoxylin and eosin staining.

3.5.1 SCREENING THE GLI GENE DEFICIENT MICE

The response to FITC was investigated in $Gli2^{+/-}$ (gift from C.C.Hui, Program in Developmental Biology, University of Toronto, Canada), $Gli3^{+/-}$ (gift from Prof A.Joyner, Skirball Institute of Biomolecular Medicine, NYU, New York) and $Gli2^{+/-}$ /$Gli3^{+/-}$ mice and compared with wild type control mice. They were all maintained in a mixed 129 and CD1 background. $Gli2^{-/-}$ and $Gli3^{-/-}$ mice could not be used as mice with these phenotypes died either before or shortly after birth [74,86].

The $Gli2^{+/-}$ mice contain a targeted deletion of the DNA-binding zinc-fingers motif of the gene [85]. They were screened by PCR analysis of DNA extracted from tail tips. Primers specific for the neo-cassette utilised in the construction of the $Gli2^{+/-}$ phenotype were used (Figure 3.7A). The $Gli3^{+/-}$ mice genotypes were screened by their characteristic limb phenotype in the form of polydactyly [90] as shown in Figure 3.7B. Both the $Gli2^{+/-}/Gli3^{+/-}$ double mutants and the wild type mice were thus discriminated by these characteristics.

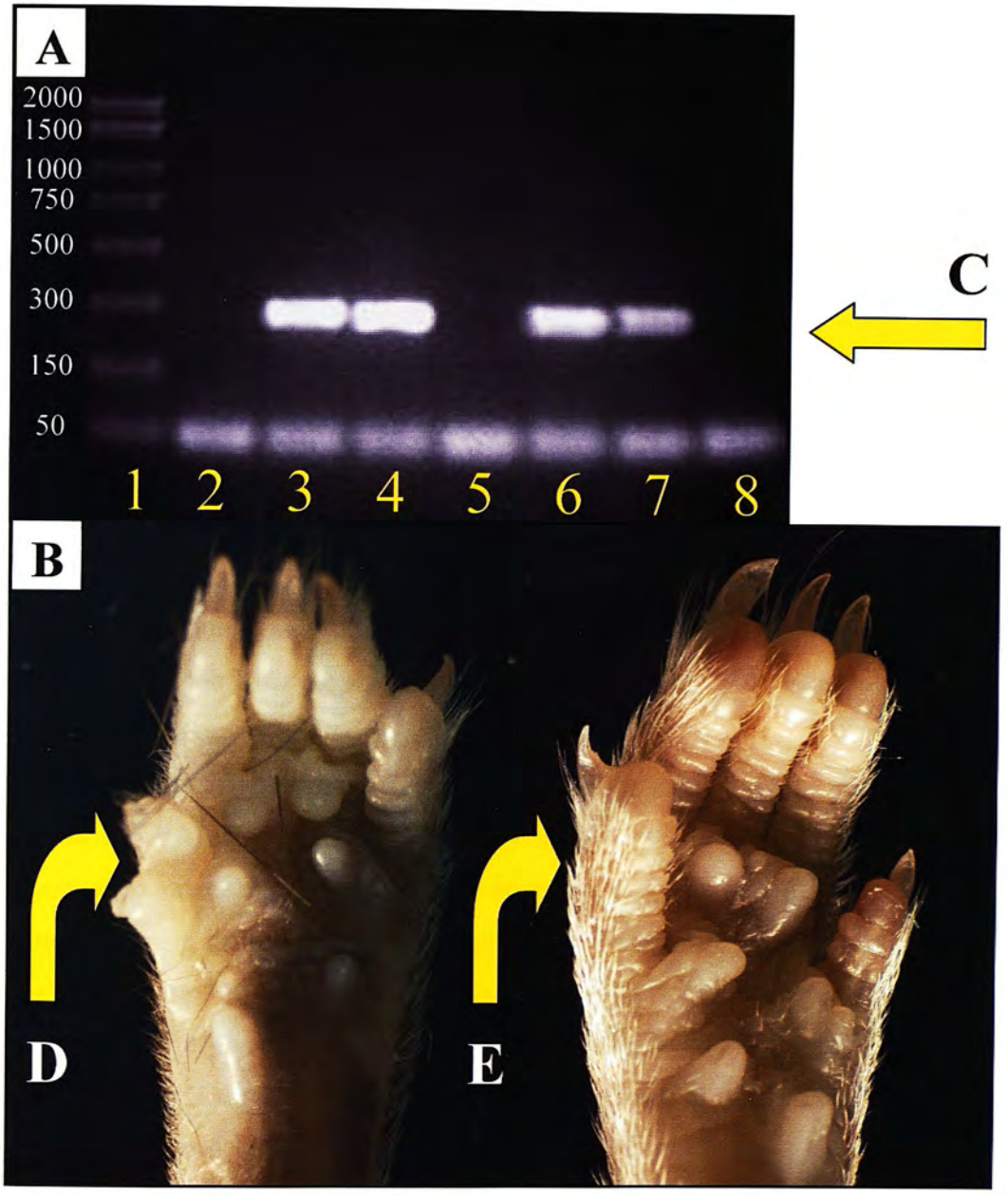

Figure 3.7: Screening the *Gli2*$^{+/-}$ and *Gli3*$^{+/-}$ mice

A) *Gli2*$^{+/-}$ screening by genotype. PCR reaction with primers specific for the neo cassette: 280 base pair (bp) product (**arrow C**). 2% agarose gel with **1**: PCR ladder with sizes (in bp) indicated in white numbering, **2+5**: mice not containing neo cassette and therefore no *Gli2* mutation, **3,4+6**: mice containing neo cassette and therefore *Gli2*$^{+/-}$, **7**: positive control from mouse known to contain neo cassette, **8**: negative (water) control for PCR reaction. **B)** *Gli3*$^{+/-}$ screening by phenotype. Pictures of wild type (left) and *Gli3*$^{+/-}$ mutant (right) paw phenotypes. Extra digit (polydactyly) indicated by **arrow E**; absent in wild type (**arrow D**)

3.5.2 LUNG MORPHOLOGY FOLLOWING FITC TREATMENT

FITC was instilled intra-tracheally as before. Initially a single dose of 100μg in 50μl of PBS was given to each mouse. However many of the mice receiving this treatment did not develop fibrosis. This may have been due to a number of factors as discussed later. Each mouse was therefore given 2 doses of FITC 6 weeks apart.

The Gli mutant (and wild type) mice were considerably larger than the BALB/c used above (up to 50g compared with weights of ~20g). Thus the 100μg dose was also adjusted. Each mouse was given 7μg per g body weight at each treatment [408]. The mice (at least 6 per treatment group per time-point) were then killed up to 6 months after the second FITC administration. The lungs were inflated and formalin fixed before sectioning and staining. As before each was stained with the anti-FITC antibody to confirm delivery before H&E staining to examine morphology.

With this modified method of FITC instillation the pathology was similar to that seen with the BALB/c mice. As always the degree of severity of fibrosis varied from mouse to mouse even within grouped animals. Most importantly there appeared to be no consistent differences between any of the *Gli* mutants and the control wild type mice (Figure 3.8). In all groups the lungs of the PBS treated mice appeared normal while those of the FITC treated bore all the hallmarks of FITC induced lung fibrosis, including cellular infiltration, alveolar wall thickening and a patchy peribronchial fibrosis (Figure 3.8).

It would therefore appear that, as assessed morphologically, the presence of these *Gli* mutations has no discernible effect on FITC induced pulmonary fibrosis.

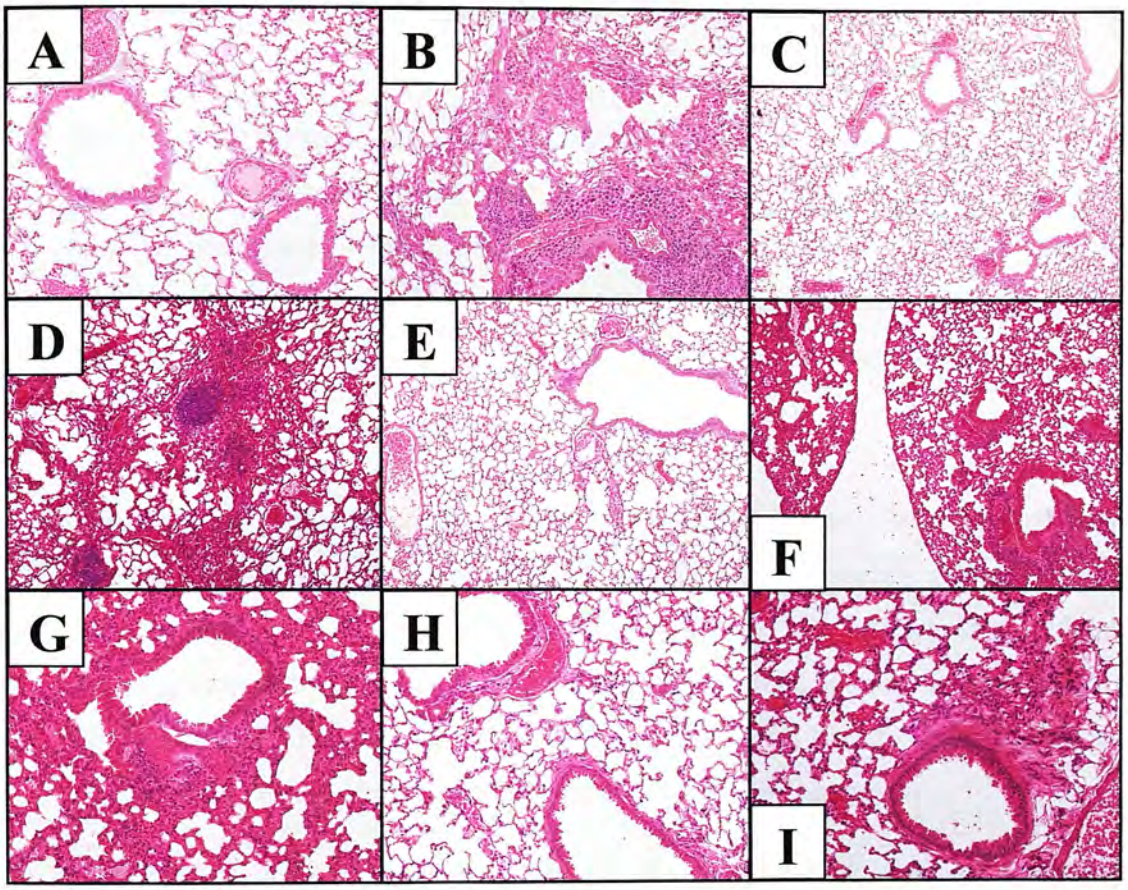

Figure 3.8: Haematoxylin and Eosin (H&E) staining of FITC and PBS treated *Gli* mutant mice lungs

Magnifications are indicated in brackets

Gli2$^{+/-}$ mice 3 months after 2nd dose of **A)** PBS (x200) **B)** FITC (x200) Note the marked perivascular cell infitrate and replacement of normal alveoli with fibrous tissue.

Gli2$^{+/-}$ *Gli3*$^{+/-}$ mice 3 months after 2nd dose of **C)** PBS (x100) **D)** FITC (x100) Note destruction of normal alveoli and central granuloma

Gli3$^{+/-}$ mice 3 months after 2nd dose of **E)** PBS (x100) **F)** FITC (x100) **G)** FITC (x200) Note the prominent peribronchial infiltrate and significant alveolar wall thickening

Wild type control mice 3 months after 2nd dose of **H)** PBS (x200) **I)** FITC (x200) Note peribronchial infiltration and scar (fibrous) tissue

3.6 The effects of intra-tracheal SPC-mouse Shh DNA

Having demonstrated that Shh is upregulated in ILD, the potential role of Shh signalling in pulmonary fibrosis was further investigated by attempting to upregulate the Shh pathway in mouse lungs. Overexpression of Shh in the lungs of mouse embryos results in epithelial and mesenchymal hyperplasia as discussed [56]. The working hypothesis was that upregulation in the adult mouse would lead to lung fibrosis.

Various ways of overexpressing Shh *in vivo* were considered. The method of choice was to rescue a replication deficient adenovirus expressing murine Shh, as successfully achieved with murine Dvl1 (Chapter 5). Unfortunately, despite numerous attempts by a colleague (Dr Susannah Lindey), an adenovirus expressing Shh was not produced. Attempts to make inducible Shh transgenic mice were also unsuccessful. The method presented below was therefore attempted.

The protocol was derived from a combination of sources. In a paper published by Meyer *et al* [554] the chloramphenicol acetyltransferase (CAT) gene, under the control of the cytomegalovirus (CMV) promoter, was successfully delivered intra-tracheally as "naked" DNA into mouse airways. CAT expression was confirmed in the lungs and trachea of treated mice; peak between 1 and 3 days and was detected up to 28 days after DNA administration. Thus, this method of gene delivery was feasible. Furthermore, Shh overexpression has been driven in mouse embryonic lung by insertion of murine Shh cDNA under the control of the surfactant protein-C (SPC) promoter, by Bellusci *et al* [56]. SPC is expressed at high levels early on in the primitive embryonic epithelium, and eventually becomes restricted to the type 2 alveolar epithelial cell lineage. This specifically allows high levels of expression in the distal respiratory epithelium. It was plausible that the SPC-mouse Shh cDNA vector, a kind gift from Dr Bellusci (Department of Cell Biology, Vanderbilt University Medical Center, Nashville, Tennessee, USA), might also be capable of driving Shh expression in the airway epithelial cells of mature mice.

Based on the above observations, the aim was to combine these two protocols, in an attempt to overexpress murine Shh in the respiratory epithelium of BALB/c mice by instilling the SPC-mouse Shh vector as naked DNA intra-tracheally. SPC alone was used as a control plasmid.

In the first instance 20μg (quantity based on the CAT expression data [554]) of either SPC-mouse Shh or SPC DNA was resuspended in 50μl of sterile PBS and inserted intra-tracheally as described in chapter 2. This was repeated 1 week later and six mice per treatment group killed at time-points from 1 week to 5 months following the second instillation. The lungs were inflated and formalin fixed for IHC. In addition, after 5 months, 6 mice from each treatment arm (SPC-mouse Shh or SPC) were each given 6 further 20μg treatments (2/week), before being killed 4 days after the final treatment.

Lung sections were made and stained as described below. The results shown are from the mice 4 days after the 6 additional doses, the rationale being that any pathology and /or expression would be most marked following such intensive treatment. Notably, histological appearances were similar throughout the time-course.

3.6.1 LUNG MORPHOLOGY AND CELL PROLIFERATION

Sections from mice treated with both SPC-Shh and SPC were stained with H&E to allow analysis of the lung morphology.

In some of the sections the epithelial cells appeared to be a little "damaged" with evidence of epithelial sloughing, denudation and "peg-like" morphology. This was evident in both treatment arms suggesting that any abnormalities were not confined to the presence of Shh, but were more likely to be due to a non-specific plasmid

effect. For the most part, however, the lungs appearances were entirely normal (Figure 3.9 A and B).

As Shh upregulation is associated with increased cell proliferation, the sections were also stained with Ki67 to assess the degree of epithelial cell proliferation. Very few, if any, airway cells were positive in any of the sections, regardless of the treatment or time-point (Figure 3.9 C and D). These appearances were similar to untreated or PBS treated mice, and differed markedly from those following adenoviral instillation (Figure 5.23).

It would appear that SPC-Shh does not affect lung morphology or epithelial cell proliferation when instilled as naked DNA into adult mouse lungs.

3.6.2 THE SHH PATHWAY AND SPC-SHH

The sections were also stained immunohistochemically for Shh and Ptc to determine whether or not the SPC-Shh DNA instillation had driven upregulation of Shh, and hence the Shh pathway, in the treated mouse lungs.

Shh expression was no different between the SPC-Shh and SPC DNA treated mice (Figure 3.10 A and B). Neither was greater than control PBS treatment. Ptc expression was also unaffected by the presence of SPC-Shh (Figure 3.10 C and D). As before Ptc expression was equivalent in the epithelial cells in both treatment groups.

As assessed by IHC, SPC-mouse Shh DNA delivered intra-tracheally as naked DNA does not increase the expression of either Shh or Ptc at protein level.

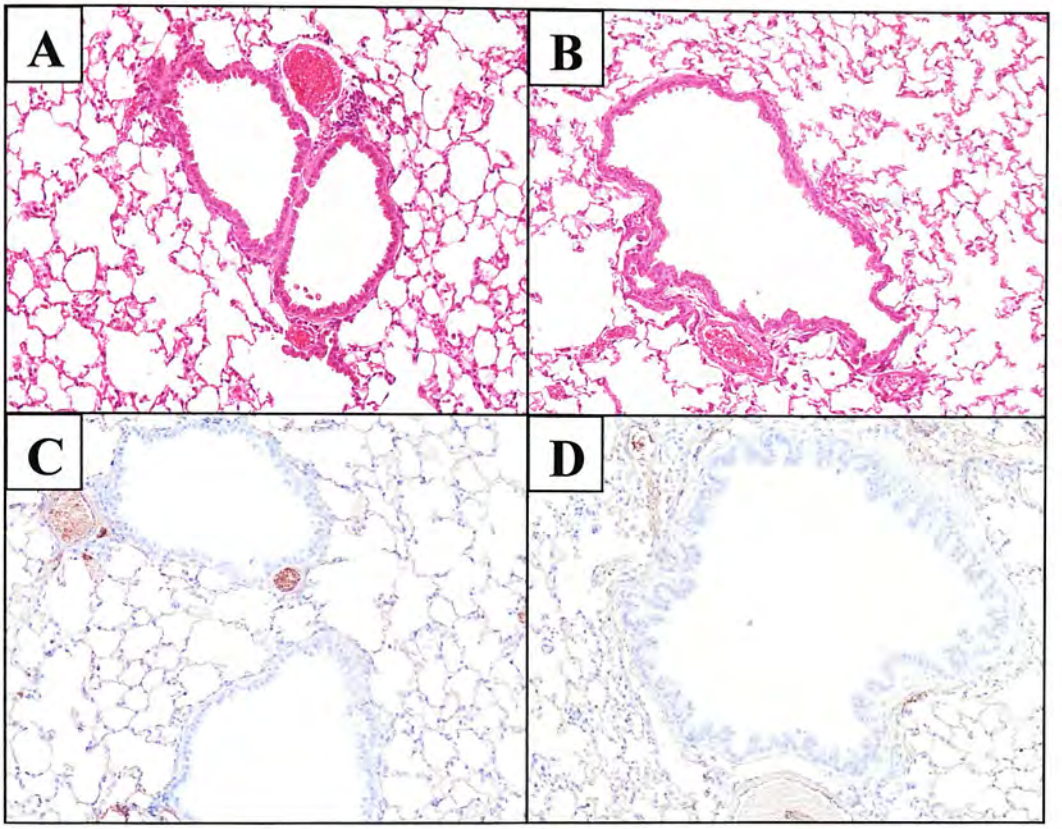

Figure 3.9: Haematoxylin and Eosin (H&E), and Ki67 staining of mouse lungs treated with SPC plasmids

Magnifications are indicated in brackets

H&E staining of **A)** SPC treated (x200) and **B)** SPC-Shh treated (x200) mice

Ki67 staining of **C)** SPC treated (x200) and **D)** SPC-Shh treated (x200) mice

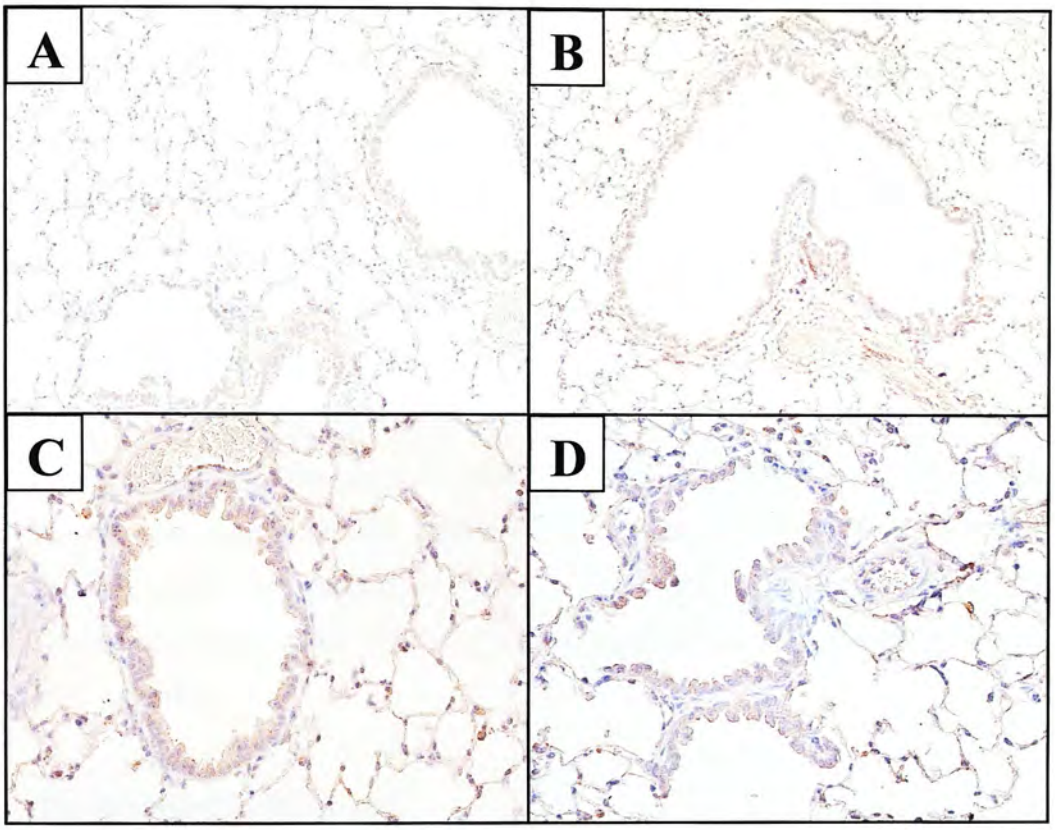

Figure 3.10: Shh and Ptc expression in mouse lungs treated with SPC plasmids

Magnifications are indicated in brackets

Shh staining of **A)** SPC treated (x200) and **B)** SPC-Shh treated (x200) mice

Ptc staining of **C)** SPC treated (x400) and **D)** SPC-Shh treated (x400) mice

3.8 Discussion

The aim of the work presented in this chapter was to determine the role of the Shh signalling pathway in ILD. To address this question, the expression of key components of the pathway were analysed both in the FITC model of ILD and in biopsy specimens from patients with IPF. Expression of the pro-fibrotic protein, TGFβ1, was also examined in similar sections.

In addition, FITC was given to mice with heterozygous mutations in *Gli 2* and *3*, downstream targets of Shh signalling, to determine if such defects in the Shh pathway would alter the pathology. Finally an attempt was made to upregulate Shh *in vivo* by instilling the Shh gene into mouse lungs as "naked" DNA under control of a SPC promoter.

The Modified FITC Model

The IHC findings presented were consistent on both archival sections from mice given FITC/PBS via the original surgical approach [408] and those receiving treatment via the modified method described, in which the trachea was accessed through the mouth. However some of the mice receiving a single dose of FITC via the oral route did not develop fibrosis. There may be several reasons for this.

Whereas in the original method of FITC instillation used there could be little doubt that all of the FITC had been delivered to the lungs, this was not always the case with the new method. Though all cases were checked with the anti-FITC antibody this information would not reveal how much of the 100μg was present. If a smaller dose were to be delivered, this may be insufficient to induce fibrosis. Importantly, in test instillations using trypan blue, the lungs were well infiltrated and there was little evidence of dye elsewhere such as in the oesophagus or stomach. In addition, the original method involved a surgical procedure as the trachea was exposed and incised. This was not the case with the new oral approach. It may be that the

associated stress on the mice during the surgical delivery in some way contributed to the development of fibrosis. For example, the immune response to FITC may be more pronounced in this context.

Regardless of the reason such inconsistency was unacceptable. In an effort to address this, the treatment (FITC or PBS) was given twice to each mouse at an interval of 6 weeks; this interval was chosen to allow the mouse to sufficiently recover from the initial dose. On each occasion a standard dose of 100μg in 50μl of PBS was given. Encouragingly the PBS mice were unaffected by this additional dose. More importantly the FITC treated mice developed significant lung fibrosis as intended.

In addition all mouse sections were stained with the anti-FITC antibody to confirm successful delivery into the lungs (Figure 3.1). Only those lungs with positive FITC staining were used for IHC.

It would therefore appear that although this new method of intra-tracheal instillation, via an oral approach has its advantages in terms of practicality and a reduced mortality, it may be less efficient at inducing fibrosis. Should this be as a result of a less reliable delivery this would obviously have implications on other *in vivo* experiments employing the same method; as in SPC mouse-Shh in this chapter and later adenoviral work.

Furthermore, lung sections from mice treated with this modified intra-tracheal instillation technique were given fibrosis scores using a system devised by Ashcroft *et al* [551]. This revealed significantly higher scores, and thus more fibrosis, in areas of lung with FITC deposition, though only following a second administration of FITC. The former finding supports the observation that fibrosis is localised to areas of FITC scarring, originally made by Roberts *et al* [408]. The fact that this was only notable following a second treatment may be due to those factors discussed above. However, mice given a second treatment were also killed at later time-points than those given a single treatment, thus allowing more time for potential lung fibrosis to develop. A

further control, assessing Ashcroft scores in mice treated only once and killed at time-points corresponding to those treated twice, would be needed to clarify this.

Immunohistochemistry in the FITC model

Shh expression was upregulated in the bronchial and alveolar epithelial cells of FITC treated mice and detected in the infiltrating immune cells (Figure 3.3). Ptc epithelial expression was appreciable even in PBS treated mice and was not clearly changed in the FITC treated lungs. It was also expressed in the infiltrating mononuclear cells (Figure 3.4).

Shh upregulation would imply that the Shh pathway was also upregulated. The pattern of Ptc expression is less clear. Normally Ptc is upregulated when the Shh pathway is induced [14,27]. Therefore one would expect Ptc and Shh expression to be increased if this were to be the case. There are several possible explanations to explain why Ptc expression is not increased.

As basal Ptc expression is already fairly high, any changes may be difficult to appreciate especially using IHC. It may well be that Ptc is upregulated in the epithelial cells but that the chosen method of analysis (IHC) is not sensitive enough to detect this. If this were true, changes in Ptc expression as analysed throughout the thesis (IHC) may also be too subtle to appreciate. As Ptc antagonises Shh signalling, by sequestering Shh [28] and inhibiting Smo, it is possible that its constitutive expression in the lung epithelial cells is a means by which they attempt to block pathway activation, possibly as a protective mechanism. It may also be that, for some reason, the observed Shh upregulation results predominantly in increases in Ptc expression elsewhere (eg. immune cells) and not in the airway epithelial cells.

Shh and Ptc were both expressed in the infiltrating immune cells, seen most clearly in the FITC mice in which more of these cells were present. This correlates with findings in T lymphocytes presented in chapter 4. Of particular relevance to ILD, it raises the possibility that the Shh signalling pathway enables communication

between the epithelial cells and the infiltrating immune cells including lymphocytes and macrophages in the disease process. The roles played by these infiltrating cells in the pathogenesis of ILD may be, at least in part, related to Shh signalling.

TGFβ1 expression was also upregulated in FITC treated lungs as assessed by IHC. As described previously [353-357], this was noted particularly in the airway epithelial cells and the infiltrating immune cells (Figure 3.5). These findings imply that, as in several other models of ILD, pulmonary fibrosis in FITC treated mice is associated with increased TGFβ1 expression.

Immunohistochemistry in IPF Patient Biopsies

The same proteins displayed similar expression patterns in archival human biopsy sections from patients with IPF.

Shh was notably expressed in remodelling type II epithelial cells, metaplastic respiratory epithelial cells and in hypertrophic smooth muscle (Figure 3.6). Interestingly Shh positive and negative cells were interspersed throughout the respiratory epithelium. It is possible that this pattern of staining is due to the dynamic nature of Shh signalling i.e. adjacent cells signalling to their neighbours and increasing Shh expression before downregulating expression themselves. It would also appear that Shh is produced by hypertrophic muscle in IPF patients, and may contribute to this hypertrophy. It is certainly associated with mesenchymal proliferation *in vivo* [56]. Significantly Shh staining was limited to diseased areas, suggestive of a specific role in the fibrotic process.

Ptc and TGFβ1 were also expressed in remodelling epithelium and in infiltrating mononuclear cells (Figure 3.6). These findings are consistent with the FITC data discussed.

The FITC model in *Gli* gene deficient mice

The Gli gene deficient mice were chosen as models of dysregulated Shh signalling. They were treated with FITC in an attempt to provide further, if indirect, evidence of the role of Shh in the pathogenesis of ILD. As described *Gli2*$^{+/-}$, *Gli3*$^{+/-}$ and *Gli2*$^{+/-}$*/Gli3*$^{+/-}$ double mutants were compared with their littermate wild type controls. There were no clear differences in morphology or degree of lung fibrosis between the Gli gene deficient mice, their littermate controls or conventional BALB/c mice in response to intra-tracheal FITC (Figures 3.2 and 3.8).

For several reasons these findings were difficult to interpret. The extent of fibrosis was assessed morphologically, but perhaps a more accurate, objective and sensitive test would have been to measure tissue hydroxyproline levels. This method has been commonly used in fibrosis models including the FITC model [409]. These sections were not formally given fibrosis (Ashcroft) scores [551] as there were clearly no consistent differences on H&E staining. In addition, the function of the different *Glis* has not been fully resolved. Though features of the *Gli2* mutants are in keeping with downregulation, and *Gli3* with upregulation of Shh signalling, these features are not absolute. They are largely based on observed phenotypic characteristics. Both are capable of either activating or repressing Shh signalling in different contexts, as discussed in detail in Chapter 1. Furthermore, there is a degree of redundancy and overlap of the different *Glis*; as observed where *Gli1* and *Gli2* compensate for each other [81,84,88], and in the phenotype of the *Gli2/3* double mutants [85,86]. Therefore even the double mutations still have preserved *Gli1* expression, which could be compensating for the other *Glis*. The extent to which Shh signalling has been altered in these mice is thus not clearly established, making any further interpretations of responses to FITC in different genotypes more difficult to dissect. Finally, as homozygous mutations of these mice result in an embryonic lethal phenotype [74,86], heterozygotes were used. Therefore absolute expression of the genes would not be lost, limiting the effect of the mutation on Shh signalling and phenotype.

Although these gene deficient animals with dysregulated Shh signalling did not provide any further evidence to implicate the pathway in ILD, they were far from ideal experimental tools. In light of the complex phenotype of the *Gli* mutant mice, it would be difficult to make any firm conclusions regarding the role of the Shh pathway in ILD based on data derived from their analysis.

Intra-tracheal SPC-mouse Shh delivery

The immunohistochemical findings discussed above prompted an attempt to overexpress Shh *in vivo* to determine if Shh upregulation *in vivo* resulted in lung fibrosis. Shh was introduced intra-tracheally as "naked" DNA in the form of SPC-mouse Shh.

In the parameters investigated there was no difference between mice receiving Shh and control mice, receiving either SPC alone or PBS. Neither a prolonged time-course nor multiple treatments resulted in any significant changes in lung morphology (Figure 3.9). Cell proliferation was also unaffected (Figure 3.9). Most significantly there was no evidence of upregulation of either Shh or Ptc in the treated lungs as assessed by IHC (Figure 3.10).

The delivery of Shh by this method would appear to have been unsuccessful. There are several possible contributing factors. The delivery of genes intra-tracheally as plasmid DNA is uncommon largely because the efficiency and level of expression are relatively poor, especially when compared with alternative methods such as adenoviruses and liposomes [555]. In addition, the SPC promoter, whilst extensively used *in utero* [56], may not be the ideal choice to allow maximal gene expression when given intra-tracheally into fully developed lungs. There is no published work in which the SPC promoter has been used for gene delivery intra-tracheally, as attempted in this thesis. Any Shh expression might be expected to be evident in the type II epithelial cells as they express SPC. In the paper quoted in the text (Meyer *et al* [554]) the pCMV (cytomegalovirus) promoter was used and not an SPC promoter. Perhaps delivery of Shh under control of the pCMV promoter would have been more

efficient. Finally, the IHC data implies that neither Shh nor Ptc were upregulated. The relatively poor sensitivity of IHC could be a contributing factor. Meyer *et al* measured CAT expression by a luciferase reporter assay of whole lung homogenate. In their discussion the authors suggest that IHC, and indeed *in situ* hybridisation, can be unrewarding in assessing naked DNA delivery. Ideally in these experiments it would have been informative to measure *Shh* and/or *Ptc* at mRNA level from whole lungs (as described in later adenovirus experiments in chapter 5). It is possible that such analysis may have shown that either or both were increased following SPC-mouse Shh instillation.

It is not clear therefore whether or not the observed effects were due to poor delivery and low Shh expression in the lungs, or because Shh upregulation has no effect on lung morphology or cell proliferation. As there is no evidence of Shh upregulation this would certainly have to be addressed in the first instance, either by repeating the plasmid DNA experiments incorporating more sensitive indicators of Shh expression or, preferably, using more reliable methods of gene delivery. This should be possible in the future, particularly as an adenovirus expressing Shh has already been rescued by Sato *et al* [120], and successfully used to drive expression of Shh in the skin.

Summary

The work detailed in this chapter provides the first report of a link between the Shh signalling pathway and ILD, in both an experimental model (FITC induced fibrosis) and in human biopsy sections from patients with IPF. The FITC model was reproduced with an alternative, non-surgical method of intra-tracheal instillation. Shh is upregulated in the remodelling airway epithelium of FITC treated mice when compared with control mice, and is also expressed in the infiltrating mononuclear cells. The Shh receptor, Ptc, is constitutively expressed in murine airway epithelium and infiltrating mononuclear cells, with particularly strong expression in the alveolar macrophages. Ptc expression does not appear to change in FITC treated mice, at least as assessed by immunohistochemistry (IHC). These features were paralleled in staining of sections from patients with IPF, in which Shh expression was increased

only in the remodelling epithelium in fibrotic areas and Ptc expression was uniform throughout, with positive infiltrates. Expression of TGFβ1 was also increased in remodelling airway epithelium and notable in cell infiltrates in both FITC treated mice and human IPF sections, by IHC.

The fibrotic response to intra-tracheal FITC was no different in mice with *Gli* (*Gli2*$^{+/-}$and/or *Gli3*$^{+/-}$) heterozygous mutations though, as discussed, this does not prove that Shh signalling has no role in the pathogenesis of ILD. An attempt to upregulate Shh *in vivo*, using intra-tracheal naked DNA, was unsuccessful in that it produced no evidence of increased Shh expression, and there were no discernible differences in either morphology or cell proliferation when compared with controls. More efficient Shh expression, as facilitated by a recombinant adenovirus, is likely to be more informative.

Therefore the Shh pathway appears to be upregulated in ILD. Whether or not Shh signalling enhances the fibrotic response or is expressed by the lungs in an attempt to control repair remains unclear. Notably, the emerging hypothesis of IPF aetiology is based on a model of abnormal wound healing/repair (Chapter 1 [292]). It may be that inappropriate Shh expression contributes to this. In addition, TGFβ is known to inhibit [112,113] and Shh to promote [94] branching morphogenesis in the developing lung, suggesting that they have antagonistic functions. Translating this to ILD, it may well be the case that, as TGFβ is profibrotic, Shh signalling is anti-fibrotic and promotes epithelial repair. These questions would be best addressed by overexpression of Shh, as intended, and Shh antagonists, such as Hedgehog-interacting protein (Hip), in both untreated mouse lungs and in models of fibrosis such as the FITC model.

Finally, although not addressed in this thesis, in collaborative work with Dr Elizabeth Jarman, Shh signalling and TGFβ1 expression were not upregulated in a murine allergic model of lung inflammation [556]. Thus implying that the observed upregulation of the Shh pathway may be specifically associated with lung fibrosis, and not with general lung inflammation as such.

Chapter 4

The Sonic Hedgehog Pathway in human $CD4^+$ T cell activation

4.1 Introduction

The Sonic Hedgehog (Shh) pathway has never previously been studied with respect to the mature human T cell. However, as discussed in Chapter 1, related work in murine thymocytes [121] and human haemotopoietic stem cells [125]has recently been published. The work described below uses similar strategies to ascertain what role the pathway plays in human $CD4^+$ T cell activation.

For all of the experiments described, human peripheral blood mononuclear cells (PBMCs) were isolated by centrifugal separation over Histopaque 1077. $CD4^+$ or $CD8^+$ T cell subsets were then obtained using either positive or negative selection techniques. Cell purity for the desired subset, as assessed by flow cytometry, was consistently at least 93% with either method. The method of isolation did not appear to affect the activity of the cells.

4.2 The Sonic Hedgehog Signalling Pathway is present in Human T Cells

4.2.1 SONIC HEDGEHOG AND PATCHED ARE EXPRESSED IN HUMAN T CELLS

These initial experiments were designed to determine if the Shh pathway was present in human T cells. To address this issue two important pathway genes were chosen: the *Shh* ligand and its receptor *Patched* (*Ptc*).

A proportion of each purified T cell subset was used to make cytospins, and RNA was extracted from a further fraction.

Immunocytochemistry for Shh and Ptc proteins was carried out using commercial primary antibodies (Santa Cruz). Cells stained with no primary antibodies were used

as negative controls. The results showed that both Shh and its receptor, Ptc, are expressed in human T cells (brown positive staining against the blue haematoxylin counterstain). Both proteins were detected on the cell surface membrane as would be expected. The cytospins illustrated are of human $CD4^+$ T cells (Figure 4.1). Similar staining was noted on $CD8^+$ cells.

RNA from purified lymphocyte populations was incorporated into reverse transcription PCR reactions, in the presence of primers specific for human *Shh* or *Ptc* mRNA (Table 2). Specific mRNAs for both were detected, thus confirming the presence of *Shh* and *Ptc* in human $CD4^+$and $CD8^+$ T cells As shown, *Ptc* was also present in human B cells, although this area was not explored further in the context of this thesis. RNA extracted from the human A549 epithelial cell line was used as a positive control in the *Shh* reaction shown (Figure 4.1).

These experiments proved that Shh and Ptc are expressed at both protein and RNA level in purified human T cells.

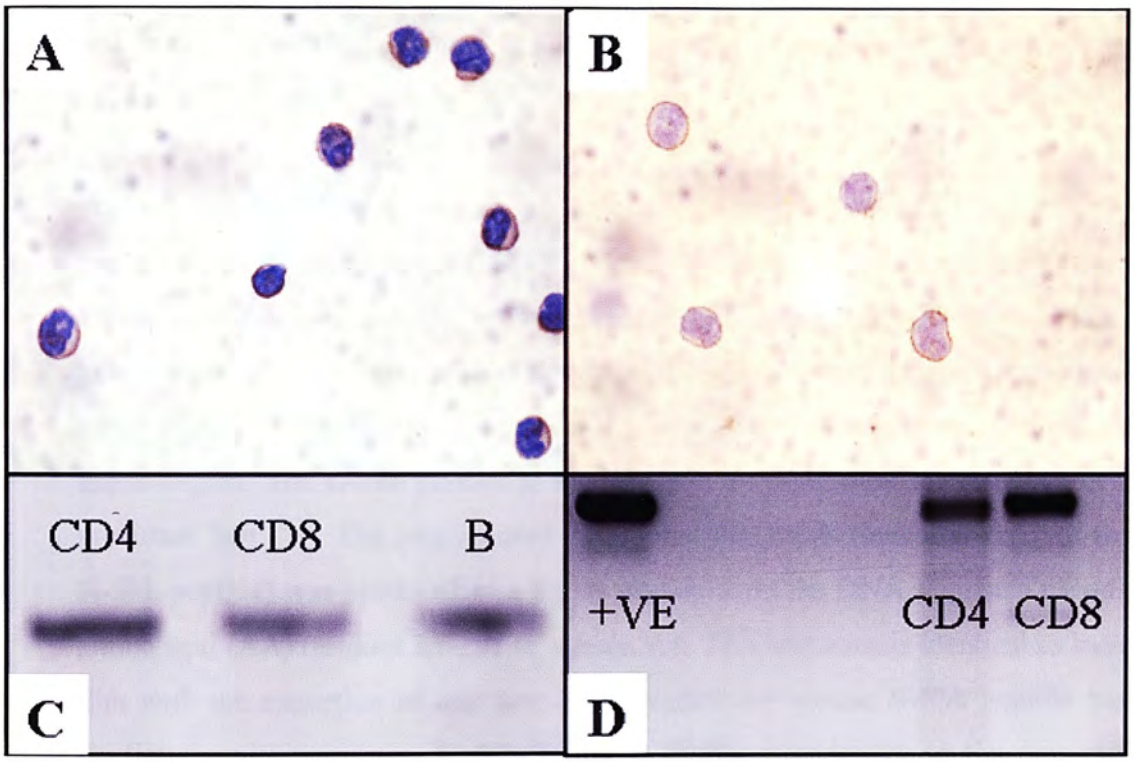

Figure 4.1: Sonic Hedgehog (Shh) and Patched (Ptc) are expressed in human T cells.

Expression of **A)** Ptc and **B)** Shh in cytospins of purified $CD4^+$ T cells (immunocytochemistry with haematoxylin counterstain)

C) *Ptc* mRNA expression in purified human $CD4^+$, $CD8^+$ and B cells; by rtPCR. Product size 462bp

D) *Shh* mRNA expression in purified human $CD4^+$ and $CD8^+$ T cells; by rtPCR. Positive control (+VE) is mRNA from human A549 cells. Product size 335bp

4.2.2 *PATCHED* EXPRESSION INCREASES UPON ADDITION OF SHH PEPTIDE TO ACTIVATED HUMAN CD4$^+$ T CELLS.

It has previously been shown that upregulation of the Shh pathway paradoxically leads to an increase in expression of its receptor Ptc [14,27,55]. It follows that an increase in Ptc expression would be indicative of an associated upregulation of the pathway. These experiments were aimed at determining the expression of *Ptc* mRNA as a marker of Shh signalling.

Purified human CD4$^+$ T cells were cultured in the presence of a commercially available murine Shh peptide (R&D Systems) at a range of concentrations. Murine Shh is produced as a precursor protein, which undergoes autoproteolysis to yield a 19 kDa amino-terminal domain (N-Shh) and a 27 kDa carboxy-terminal domain (C-Shh). The N-Shh portion remains membrane associated and is known to contain the active region. The C-Shh portion is secreted and is responsible for cleavage of the precursor Shh [10,57]. The peptide used throughout this thesis (hereafter referred to as N-Shh peptide) was produced as a fusion protein from the DNA sequence encoding amino acid (AA) residues 25–198 of mouse Shh. This sequence is identical to human Shh with the exception of one AA. The recombinant mouse N-Shh peptide has a predicted molecular mass of ~20kDa. As in similar experiments in the developing immune system, in which human and murine reagents were used interchangeably in either species, the murine peptide was used in a human system [121,123].

The N-Shh peptide was added to human CD4$^+$ cells and RNA extracted at time-points from 0–72 hours. The range of concentrations chosen were based on those previously used by others working with similar Shh peptides [117]. The T cells were either "resting" or "activated"; the former referring to cells cultured in the presence of culture medium and peptide alone, and the latter to the inclusion of anti-CD3ε (1μg/ml) and anti-CD28 (5μg/ml) antibodies.

Extracted RNA was analysed by real time PCR using a primer/probe mix specific to human *Ptc*, with an internal 18S control. Each sample was run in duplicate wells and.

and experiments were repeated with consistent results (n=3). Values were expressed as a ratio of the concentration of *Ptc* mRNA relative to T cells cultured in the absence of the N-Shh peptide, which were given a value of 1.

Peak expression of *Ptc* mRNA was found to be maximal after 24 hours in culture in both resting and activated cells.

In "resting" (non-activated) human $CD4^+$ T cells (Figure 4.2A) *Ptc* expression was greater upon the addition of N-Shh peptide with a peak expression at 100ng/ml; 1.7-fold > control expression. The 48 hour time-point has been included to illustrate that:
a) Expression of *Ptc* was less than at 24 hours. All values were compared to *Ptc* expression in the untreated (0ng/ml) cells at 24 hrs to allow this comparison to be made.
b) *Ptc* expression at 48 hours also peaked at the 100ng/ml concentration of N-Shh peptide.

In "activated" human $CD4^+$ T cells (Figure 4.2B) *Ptc* expression was again greater upon the addition of N-Shh peptide with a peak expression, as before, at 100ng/ml. The difference was greater in activated than resting T cells with a 4.7-fold greater *Ptc* expression at 100ng/ml than the 0ng/ml control.

These experiments show that *Ptc* mRNA is upregulated in the human $CD4^+$ T cells in the presence of N-Shh peptide. The biological relevance of these differences is less clear. In similar work comparing RNA expression in the context of gene microarrays only differences of >2-fold were considered significant [557,558]. Applying these same principles, only the differences in *Ptc* expression in the "activated" T cells were significant. Therefore, at least in activated human $CD4^+$ T cells, the N-Shh peptide appears to trigger Shh signalling, as assessed by *Ptc* mRNA expression.

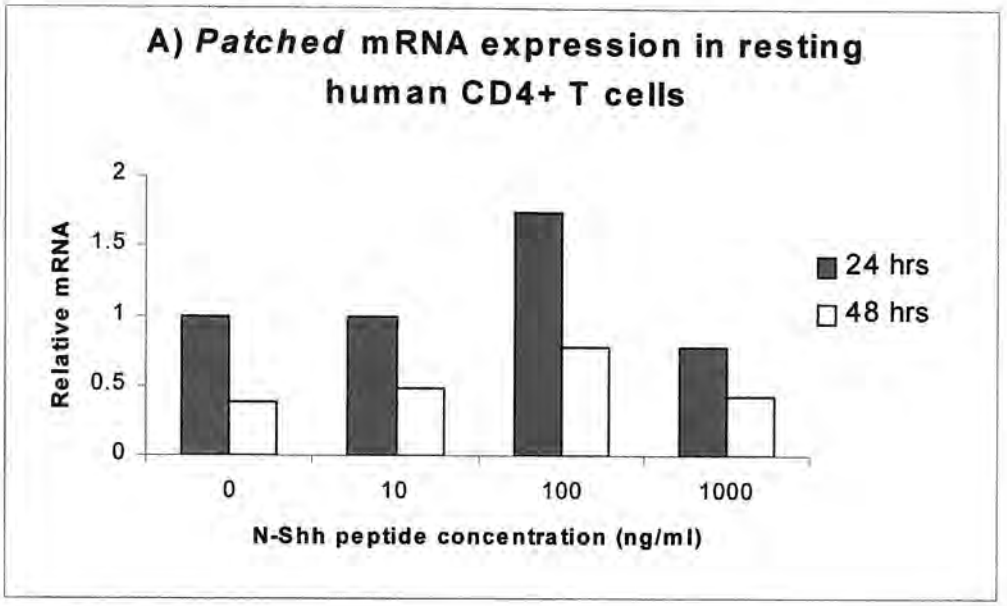

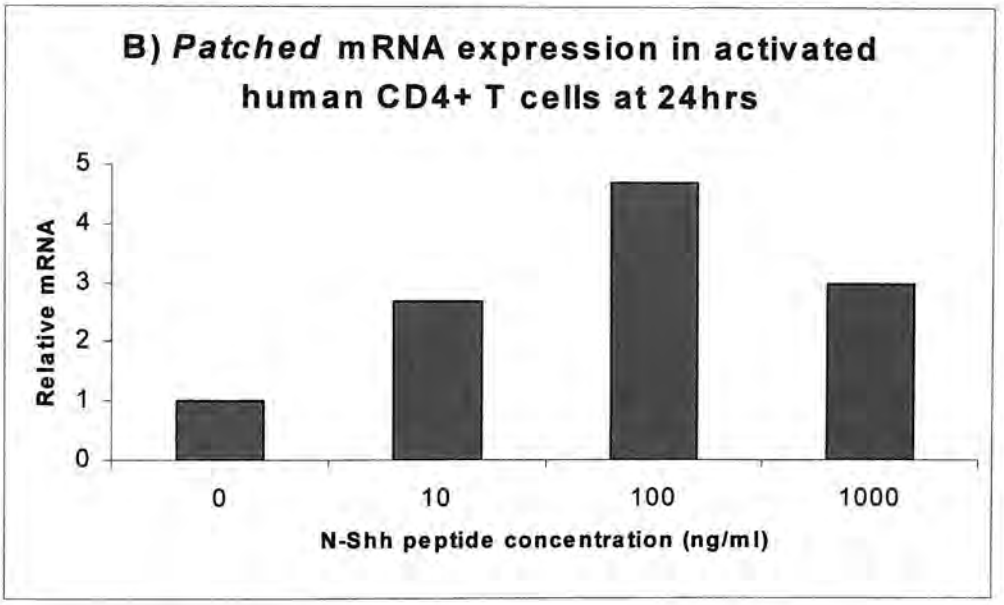

Figure 4.2: *Patched* mRNA expression increases upon addition of N-Shh peptide to human CD4$^+$ T cells.

Graphs are representative of mRNA concentrations as calculated following real time PCR reactions specific for human *Ptc* compared with an 18S control. In both graphs values are compared with the baseline *Ptc* expression seen in the untreated (0ng/ml) cells at 24hrs, which has been given a value of 1. Results are representative of triplicate experiments. **(A)** Relative *Ptc* mRNA expression in purified resting (not activated) human CD4$^+$ T cells after 24 and 48 hrs in culture. **(B)** Relative *Ptc* mRNA expression in purified activated human CD4$^+$ T cells after 24hrs in culture, in which cells were activated with a combination of plate-bound anti-CD3 (1μg/ml) and soluble anti-CD28 (5μg/ml) antibodies.

4.3 Sonic Hedgehog Signalling amplifies T cell receptor mediated activation in human T cells

In the following series of experiments the recombinant murine N-Shh peptide was added to purified human $CD4^+$ T cells. In all cases the T cells were activated using plate-bound anti-CD3ε (1μg/ml) and soluble anti-CD28 (5μg/ml) antibodies. Preliminary proliferation experiments omitting the anti-CD28 antibody were also carried out with similar results to below (data not shown).

4.3.1 N-SHH PEPTIDE AUGMENTS HUMAN T CELL PROLIFERATION

The N-Shh peptide was added at a range of concentrations to purified, activated human $CD4^+$ and $CD8^+$ T cell sub-populations. Following 72 hrs in culture sample wells were pulsed with tritiated thymidine and read 16-24 hrs later.

In the illustrated experiment, $CD4^+$ proliferation increased in a dose dependent manner with a peak in the range of 1 –100ng/ml ($p< 0.001$) of N-Shh peptide (Figure 4.3A). In subsequent experiments 100ng/ml was identified as the optimal concentration giving maximal proliferation, the same concentration that induced maximal *Ptc* mRNA expression. At higher concentrations of peptide, such as 500ng/ml, $CD4^+$ proliferation fell towards control levels again. The control ('resting') wells contained T cells cultured in medium alone.

$CD8^+$ cell proliferation also increased with N-Shh peptide concentration. Proliferation was optimal at a concentration of 100ng/ml ($p< 0.001$) and, as with the $CD4^+$ cells, began to tail off with higher doses such as 500ng/ml (Figure 4.3B).

Activated samples with peptide were statistically compared with activated samples without i.e 0ng/ml. The raw data was analysed using the ANOVA method in the "Instat software" package:

* $p < 0.05$

** $p < 0.01$

*** $p < 0.001$

These experiments demonstrated that N-Shh peptide augments proliferation of both $CD4^+$ and $CD8^+$ T cells in a dose dependent manner (Figure 4.3). The $CD8^+$ experiments were discussed at this point to illustrate that N-Shh peptide is capable of enhancing proliferation of both T cell subsets. However, the remaining work presented throughout this chapter is focussed on human $CD4^+$ cell activation.

It should be stressed at this point that not all donor $CD4^+$ T cells responded in the same manner to the addition of the N-Shh peptide. From the many donors tested (n>20), increased proliferation was observed in approximately 50%. These are hereafter referred to as 'responders'.

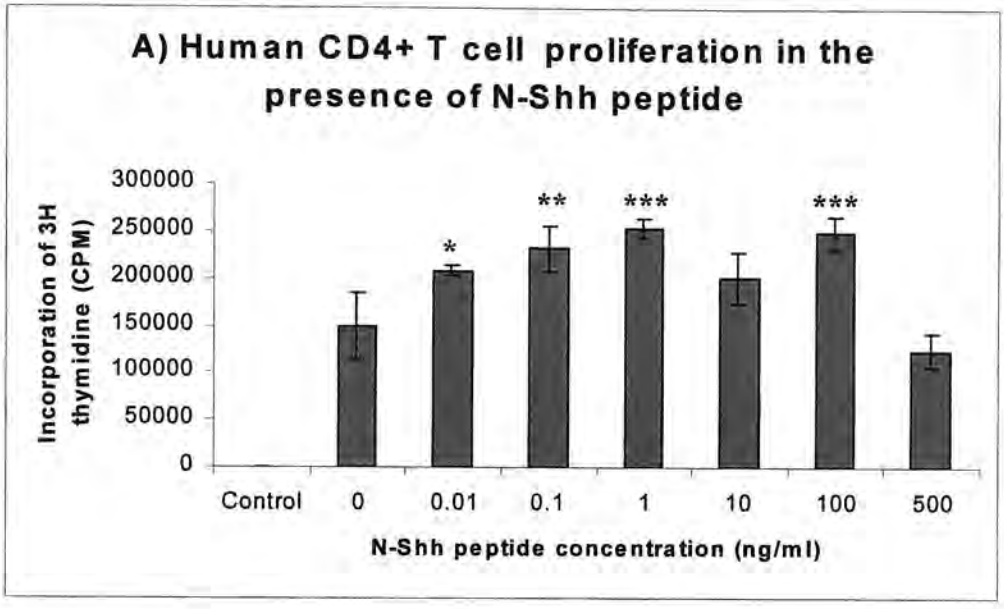

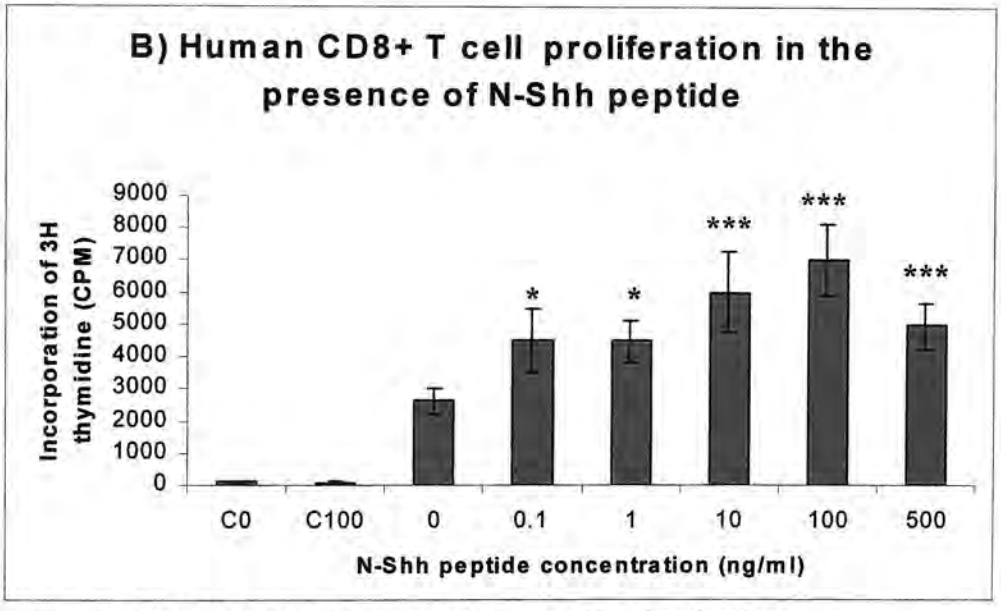

Figure 4.3: N-Shh peptide augments human T cell activation.

Graphs are representative of proliferation (samples in at least triplicate) of T cells activated in the presence of plate-bound anti-CD3 (1μg/ml) and soluble anti-CD28 (5μg/ml) antibodies. Each well was pulsed with tritiated thymidine after 72hrs in culture and read 16-24hrs later. Results are representative of at least 3 experiments, showing means and standard deviations. Statistically all activated samples are compared with those wells containing no peptide: 0ng/ml. Control cells (also represented by "C") were cultured in the absence of anti-CD3 and anti-CD28. Proliferation of purified **(A)** human $CD4^+$ and **(B)** human $CD8^+$ T cells in the presence of N-Shh peptide.

*** $p < 0.05$; ** $p < 0.01$; *** $p < 0.001$**

4.3.2 N-SHH PEPTIDE ENHANCES CYTOKINE RELEASE FROM ACTIVATED HUMAN $CD4^+$ T CELLS

Supernatants from the 'responder' donors, in whom N-Shh had enhanced $CD4^+$ proliferation, were taken at 24, 48 and 72 hrs. Levels of the human cytokines interleukin (IL) 2, 5 and 10, and interferon gamma (IFNγ) were then measured.

IL2 was detectable from 24hrs in most cases and the concentration progressively increased up to the 72 hr time-point. IL2 levels were elevated by the addition of N-Shh peptide in a dose dependent manner (Figure 4.4A), suggesting that IL2 production may be one method by which the peptide increases proliferation. Of note, the levels of the cytokine continue to rise with higher concentrations of the peptide such as 1000ng/ml ($p< 0.001$). This contrasted with the proliferation data in which such concentrations resulted in a fall in counts towards control levels (Figure 4.3).

IFNγ was optimally detected from 48 hrs onward. As with IL2 levels of IFNγ increased with N-Shh peptide dose and were highest at peptide concentrations of 1000ng/ml ($p< 0.001$)(Figure 4.4B).

IL10 was optimally detected from 48hrs. Rises in IL10 followed the same pattern as that observed with IL2 and IFNγ ($p< 0.001$)(Figure 4.5A).

IL5 was difficult to detect in many experiments, even when other cytokines were detectable at high concentrations. This may have been in part due to a difference in sensitivity between the different cytokine analysis kits, as IL5 was measured using a different method to the others (see methods). When detectable, there was no appreciable difference in IL-5 levels in the presence of N-Shh peptide at a range of concentrations (Figure 4.5B).

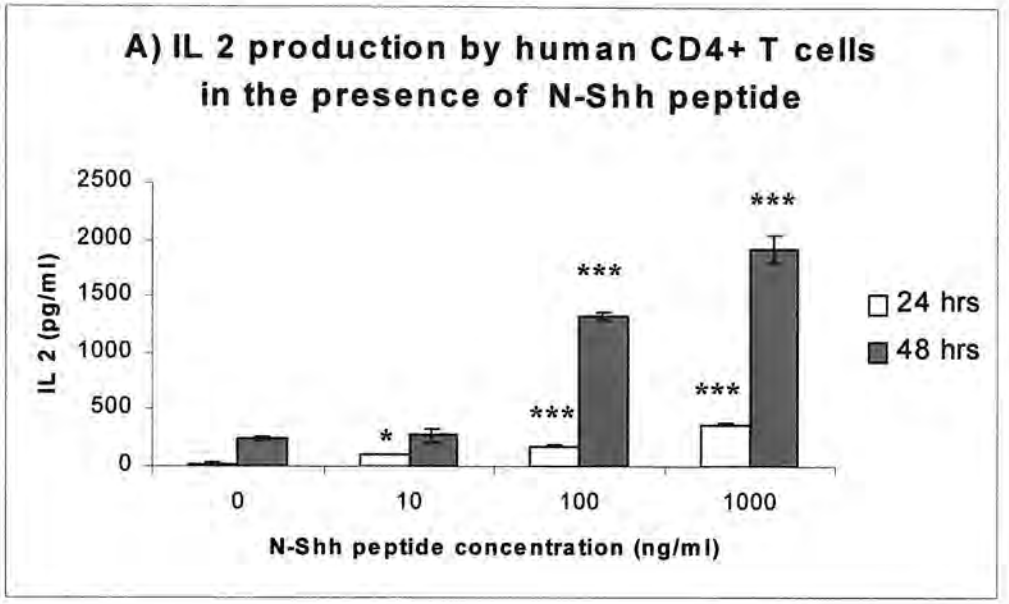

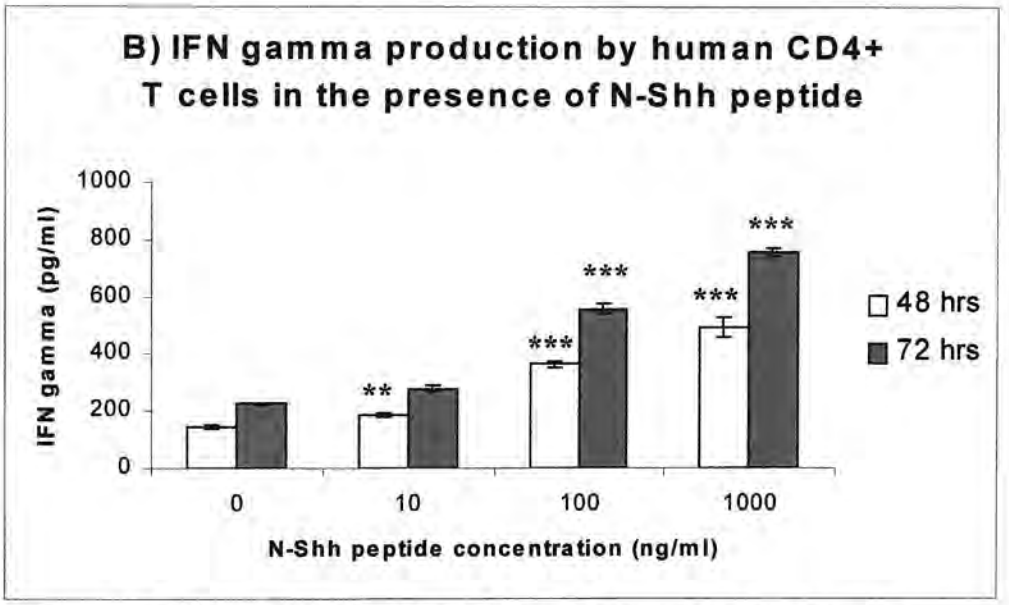

Figure 4.4: N-Shh peptide increases IL2 and IFNγ release from human $CD4^+$ T cells.

Graphs are representative of cytokine levels, as measured by ELISA, in supernatants (triplicate wells) taken from $CD4^+$ T cells activated in the presence of plate-bound anti-CD3 (1μg/ml) and soluble anti-CD28 (5μg/ml) antibodies. Statistically samples are compared with those wells containing no peptide at the equivalent time-point. **(A)** IL2 levels measured at 24 and 48hrs. **(B)** IFNγ levels measured at 48 and 72hrs. Results are representative of at least 3 experiments, showing means and standard deviations.

*** $p < 0.05$; ** $p < 0.01$; *** $p < 0.001$**

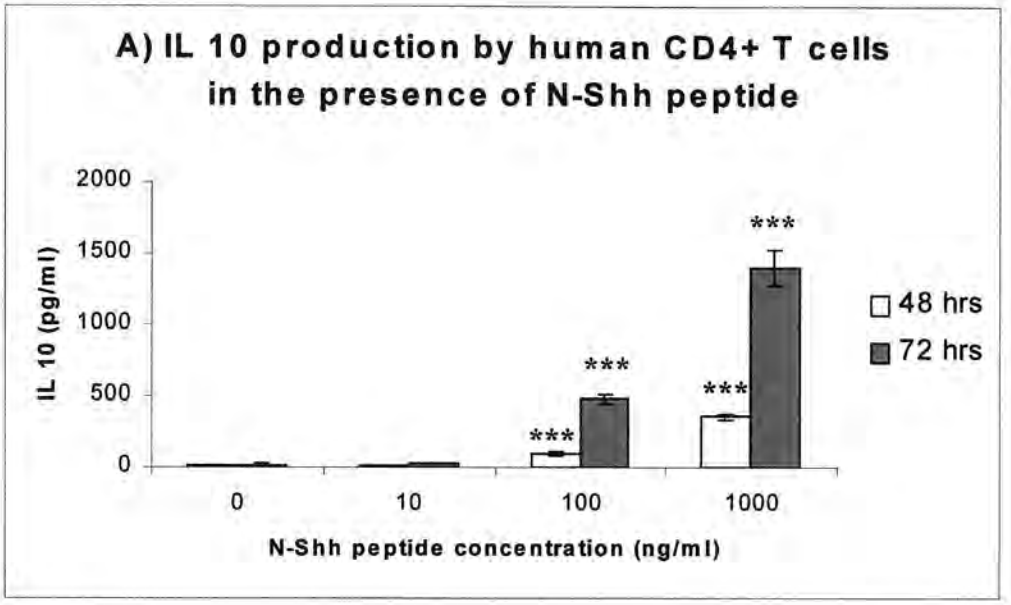

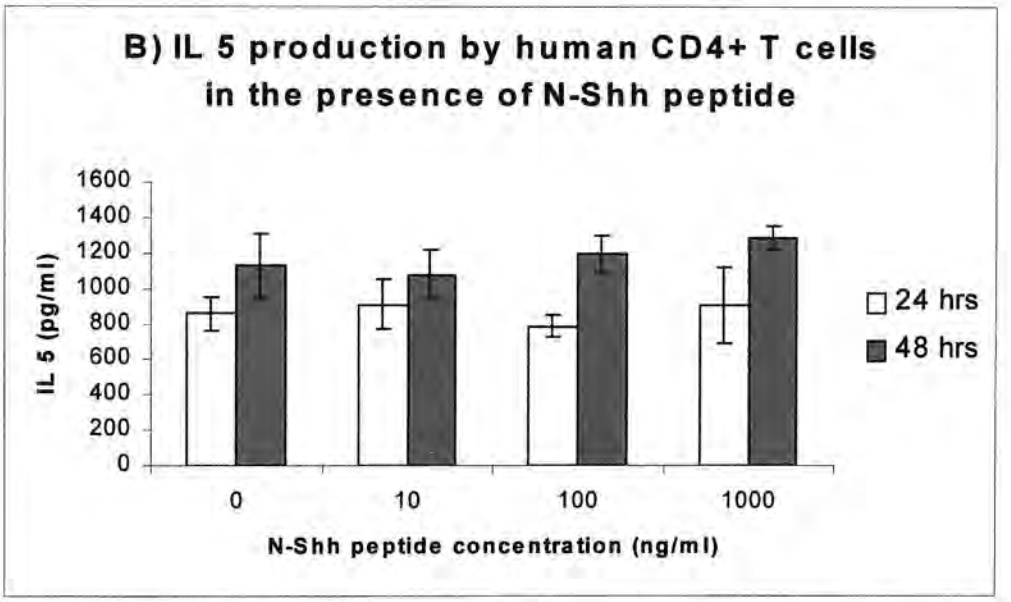

Figure 4.5: N-Shh peptide increases IL10 but not IL5 release from human CD4$^+$ T cells.

Graphs are representative of cytokine levels, as measured by ELISA, in supernatants (triplicate wells) taken from CD4$^+$ T cells activated in the presence of plate-bound anti-CD3 (1μg/ml) and soluble anti-CD28 (5μg/ml) antibodies. Statistically samples are compared with those wells containing no peptide at the equivalent time-point. **(A)** IL10 levels measured at 48 and 72hrs. **(B)** IL5 levels measured at 24 and 48hrs. Results are representative of at least 3 experiments, showing means and standard deviations.

*** $p < 0.05$; ** $p < 0.01$; *** $p < 0.001$**

4.3.3 N-SHH PEPTIDE INCREASES THE EXPRESSION OF CD25 AND CD69 IN ACTIVATED HUMAN $CD4^+$ T CELLS

As in experiments to date, the N-Shh peptide was added at a range of concentrations to purified, activated human $CD4^+$ T cells. Cells from responder donors were stained for the presence of CD25 and CD69 after 24, 48 and 72hrs in culture and analysed by flow cytometry. Both of these proteins are upregulated on the surface of human $CD4^+$ T cells upon activation through the T cell receptor (TCR) [498,499,517,518]. In each case the cells were also stained with appropriate isotype-matched control antibodies. In general CD25 expression was low at 24hrs (not shown), higher at 48hrs and maximal at the 72hr time-point. CD69 expression was detectable from 24hrs (not shown), maximal at 48 hrs and beginning to drop at 72 hrs. The data shown represents expression of both CD25 (Figures 4.6 and 4.7) and CD69 (Figures 4.8 and 4.9) at 48 and 72hrs. Data shown is representative of at least three repeated experiments.

The T cells were gated on viable cell populations shown as either R1 or R2 (Figures 4.6A, 4.7A, 4.8A and 4.9A). Expression of the relevant markers was examined in the gated sub-populations. The isotype-matched controls were used to allow discrimination between positive and negative staining, with the region of positive staining (CD25 or CD69) labelled as M1 (Figures 4.6B, 4.7B, 4.8B and 4.9B).

In the representative experiment shown, the percentage of CD25 positive cells at 48hrs was greater in those cells cultured in the presence of the N-Shh peptide (1000ng/ml) than in control activated cells: 61% (Figure 4.6D) against 22% (Figure 4.6C), as listed in the corresponding tables. The CD25 mean fluorescent intensity was also greater in the presence of the peptide (74 against 53). At 72 hrs the same pattern was observed (Figure 4.7), with both the percentage of CD25 +ve cells and their mean fluorescent intensity increasing in a dose dependant manner, maximal at the 1000ng/ml concentration of N-Shh peptide (Figure 4.7C-F). This correlates with the cytokine data, which of course included IL2.

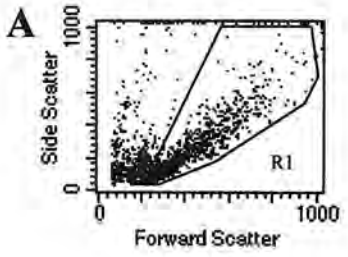

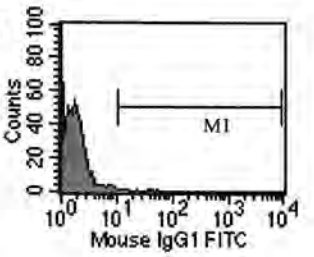

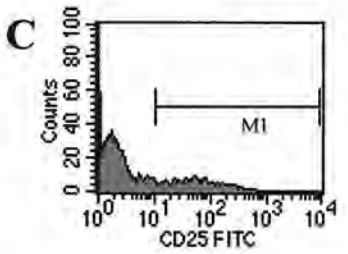

Marker	% Gated	Geo Mean
All	100.00	4.21
M1	22.04	52.52

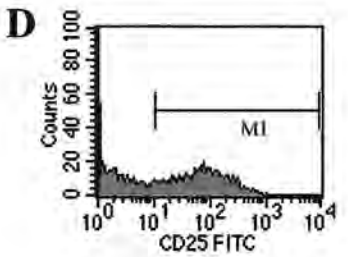

Marker	% Gated	Geo Mean
All	100.00	19.53
M1	61.12	73.81

Figure 4.6: N-Shh peptide increases CD25 expression in human CD4$^+$ T cells at 48hrs.

(A) Dot plot representing all T cells after **48hrs** in culture. Further histograms are of the gated R1 population. **(B)** Isotype control histogram. Positive population gated as M1 based on this control. Remaining histograms represent CD25 expression in cells cultured in the presence of **(C)** no peptide (0ng/ml) and **(D)** N-Shh peptide at a concentration of 1000ng/ml. Corresponding tables represent the percentage cells (% Gated) staining for CD25 and their mean fluorescent intensity (Geo Mean).

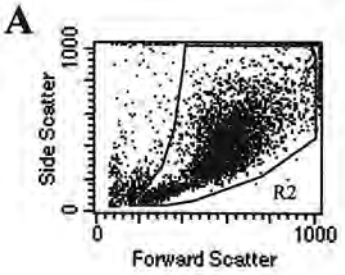

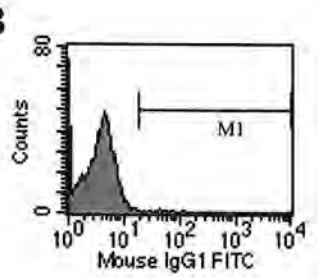

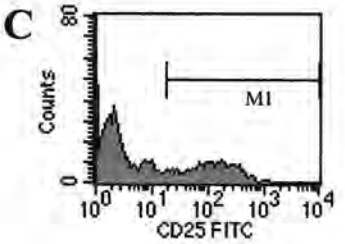

Marker	% Gated	Geo Mean
All	100.00	8.08
M1	31.36	110.84

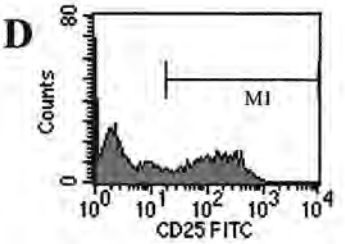

Marker	% Gated	Geo Mean
All	100.00	15.17
M1	44.23	126.97

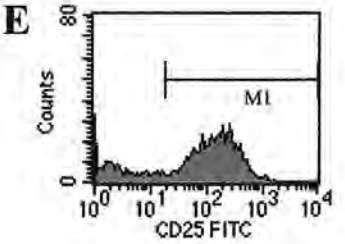

Marker	% Gated	Geo Mean
All	100.00	67.08
M1	80.11	142.25

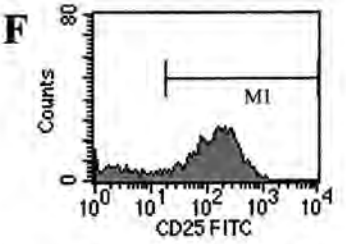

Marker	% Gated	Geo Mean
All	100.00	82.91
M1	84.06	148.59

Figure 4.7: N-Shh peptide increases CD25 expression in human CD4$^+$ T cells at 72hrs.

(A) Dot plot of CD4$^+$ T cells after **72hrs** in culture. Further histograms are gated on the R2 population. **(B)** Isotype control histogram. Remaining histograms show cells cultured with **(C)** 0ng/ml **(D)** 10ng/ml **(E)** 100ng/ml and **(F)** 1000ng/ml of N-Shh peptide. CD25 positive cells fall within the M1 region.

In the representative experiment shown, the percentage of CD69 positive cells at 48hrs was also greater in those cells cultured in the presence of the N-Shh peptide than in activated control cells (Figure 4.8C-F), with the CD69 mean fluorescent intensities essentially following suit (Figure 4.8D). CD69 expression was greatest at the 100ng/ml, and 1000ng/ml peptide concentrations (Figure 4.8E). At 72hrs the same pattern was observed (Figure 4.9), with peak expression at the 100ng/ml peptide concentration. In contrast to CD25, CD69 levels were less at 72hrs than at 48hrs.

Therefore, addition of the N-Shh peptide increases expression of both CD25 and CD69 in activated $CD4^+$ T cells, in a dose-dependent manner. These increases are significant, as determined by a paired T test using a one-tailed p value, in repeated experiments. The presence of N-Shh at a concentration of 1000ng/ml increased the number of CD25 positive cells significantly at both 48hrs ($p=0.026$, $n=6$) and 72hrs ($p=0.32$, $n=7$). CD69 expression followed suit: 48hrs ($p=0.048$, $n=7$) and 72hrs ($p=0.028$, $n=5$).

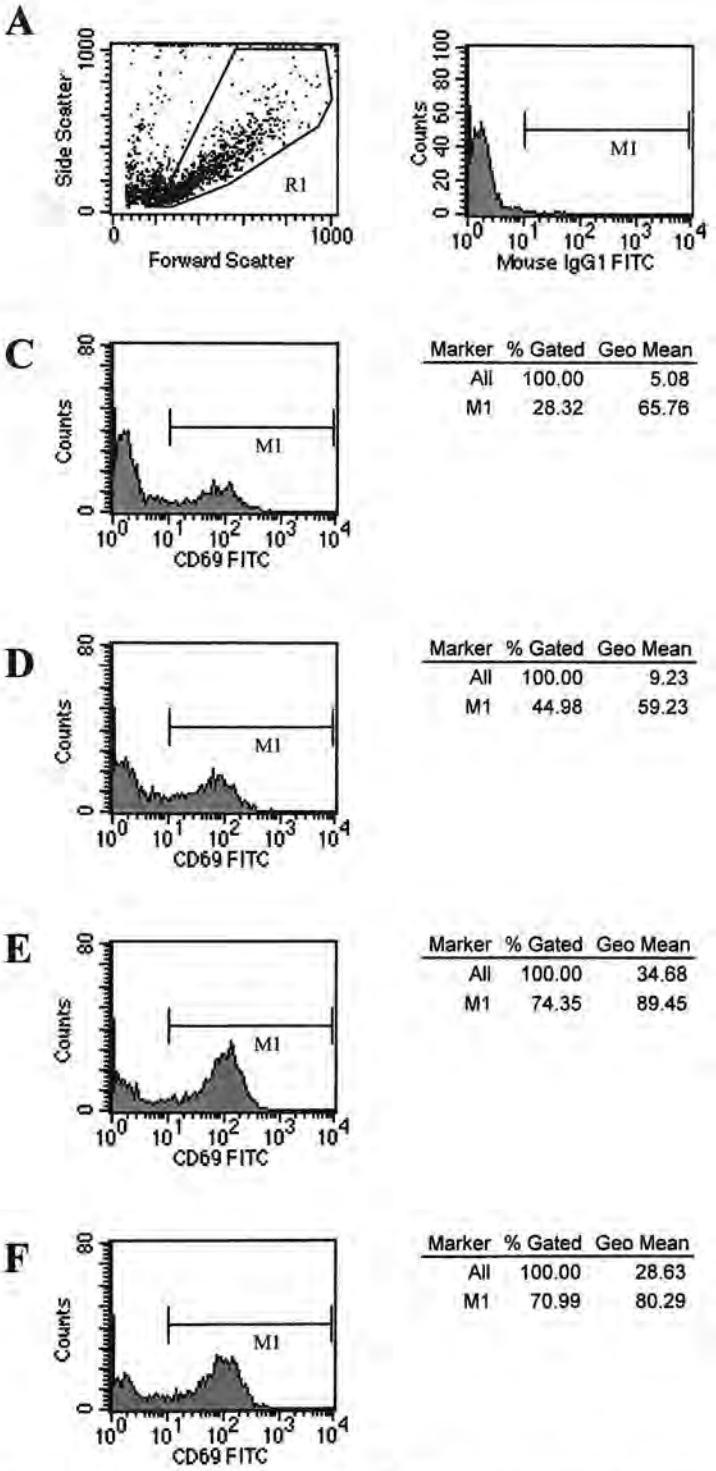

Figure 4.8: N-Shh peptide increases CD69 expression in human CD4$^+$ T cells at 48hrs.

(A) Dot plot of CD4$^+$ T cells after **48hrs** in culture. Further histograms are gated on the R1 population. **(B)** Isotype control histogram. Remaining histograms show cells cultured with **(C)** 0ng/ml **(D)** 10ng/ml **(E)** 100ng/ml and **(F)** 1000ng/ml of N-Shh peptide. CD69 positive cells fall within the M1 region.

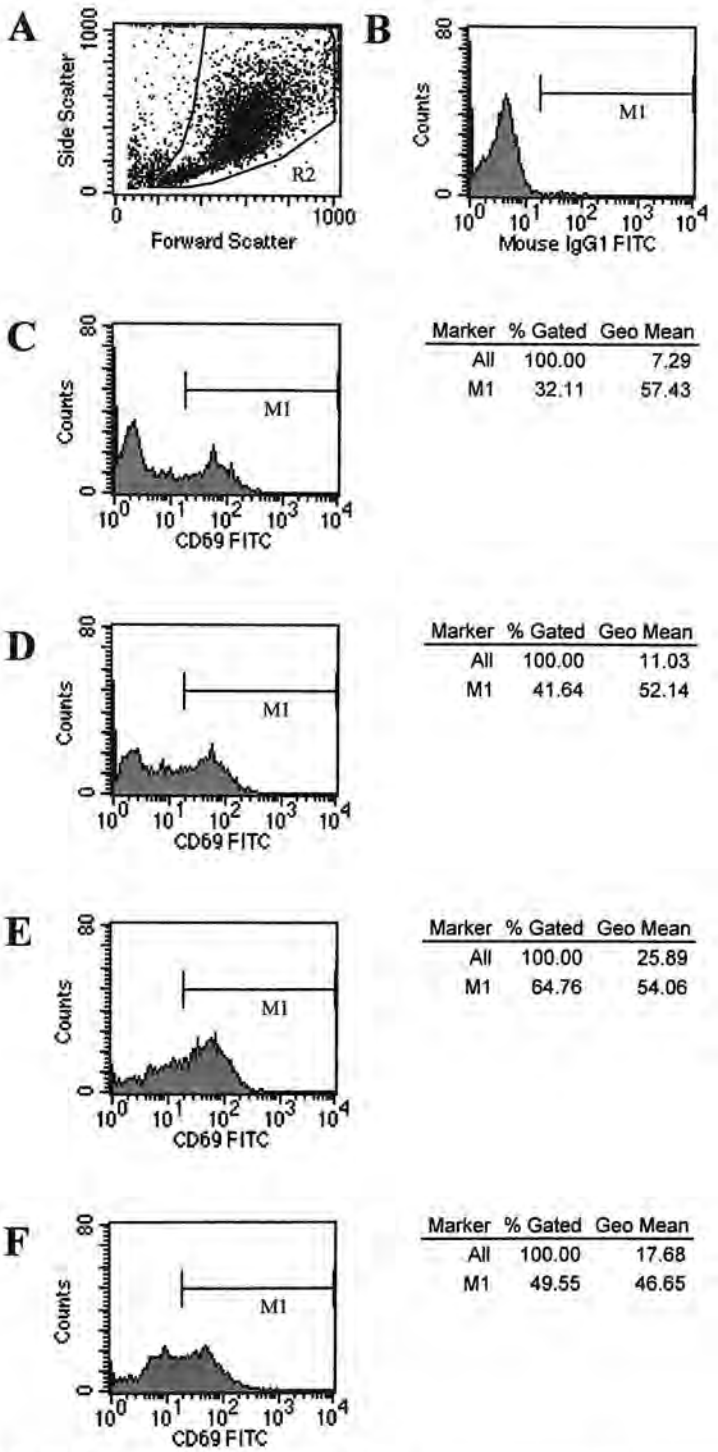

Figure 4.9: N-Shh peptide increases CD69 expression in human CD4$^+$ T cells at 72hrs.

(A) Dot plot of CD4$^+$ T cells after **72hrs** in culture. Further histograms are gated on the R2 population. **(B)** Isotype control histogram. Remaining histograms show cells cultured with **(C)** 0ng/ml **(D)** 10ng/ml **(E)** 100ng/ml and **(F)** 1000ng/ml of N-Shh peptide. CD69 positive cells fall within the M1 region.

4.3.4 N-SHH PEPTIDE DOES NOT AFFECT CELL SURVIVAL IN ACTIVATED HUMAN $CD4^+$ T CELLS

Shh is known to have anti-apoptotic properties in organogenesis [559,560] and to induce expression of the anti-apoptotic factor, bcl-2 [561]. Therefore, as the N-Shh peptide enhances T cell proliferation, it was important to determine if this was related to increased cell survival. In order to assess the effect of the N-Shh peptide on cellular apoptosis and/or survival the peptide was added at the usual range of concentrations to activated human $CD4^+$ T cells. After 24hrs, 48hrs and 72hrs in culture the cells were stained with AnnexinV and Propidium Iodide (PI). In each experiment the cells were analysed without gating. The individual quadrants were set with unstained control cells, cells stained with AnnexinV-FITC alone and cells stained with PI alone (Figure 4.10 and 4.11 B-D). Experimental samples were stained with both AnnexinV-FITC and PI. Data shown is representative of at least three repeated experiments.

In the presented data, cells in the lower left (LL) quadrant do not stain for either AnnexinV or PI and are, therefore, considered to be viable cells. Cells in the lower right (LR) quadrant stain positively for AnnexinV-FITC indicating the cell membrane has lost symmetry and PS has translocated to the outer leaflet of the plasma membrane. These cells are actively undergoing early apoptosis. The upper right quadrant (UR) cells are at advanced stages of apoptosis, since these cells stain positively for AnnexinV and are also Propidium Iodide (PI) positive due to increased plasma membrane permeability. Events acquired in the upper left quandrants (UL) indicate necrotic cells which stain positively for PI, but not for AnnexinV-FITC as the membranes are no longer capable of binding AnnexinV (Figure 4.10 and 4.11).

In the representative experiments shown the percentage of T cells, at each time-point, in each quadrant remained the same regardless of the concentration of N-Shh peptide in the system (Figure 4.10 and 4.11 F-I). Therefore, there was no increase in cell survival associated with the addition of the peptide at either the 24hr or 72hr time-

points, thus implying that the measured increases in proliferation shown before were not related to an improved T cell survival.

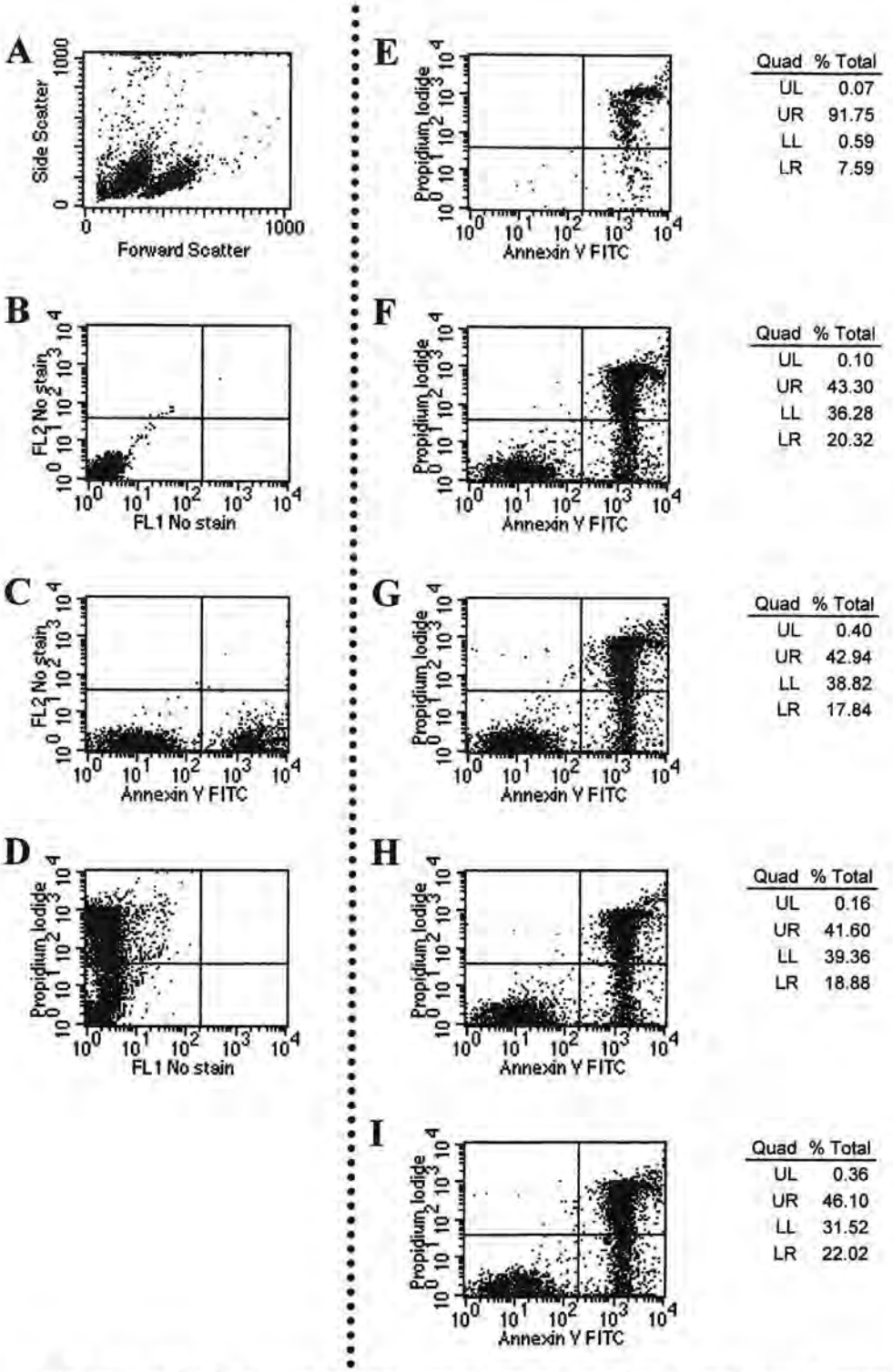

Figure 4.10: N-Shh peptide does not affect cell survival in activated human CD4$^+$ T cells at 24hrs.

Control samples: **(A)** All cells (FSC/SSC) **(B)** Cells unstained **(C)** AnnexinV single stain **(D)** PI single and **(E)** "Dead cells" control. Thereafter, activated cells cultured in the presence of **(F)** 0ng/ml **(G)** 10ng/ml **(H)** 100ng/ml and **(I)** 1000ng/ml of N-Shh peptide for 24hrs and stained for AnnexinV and PI.

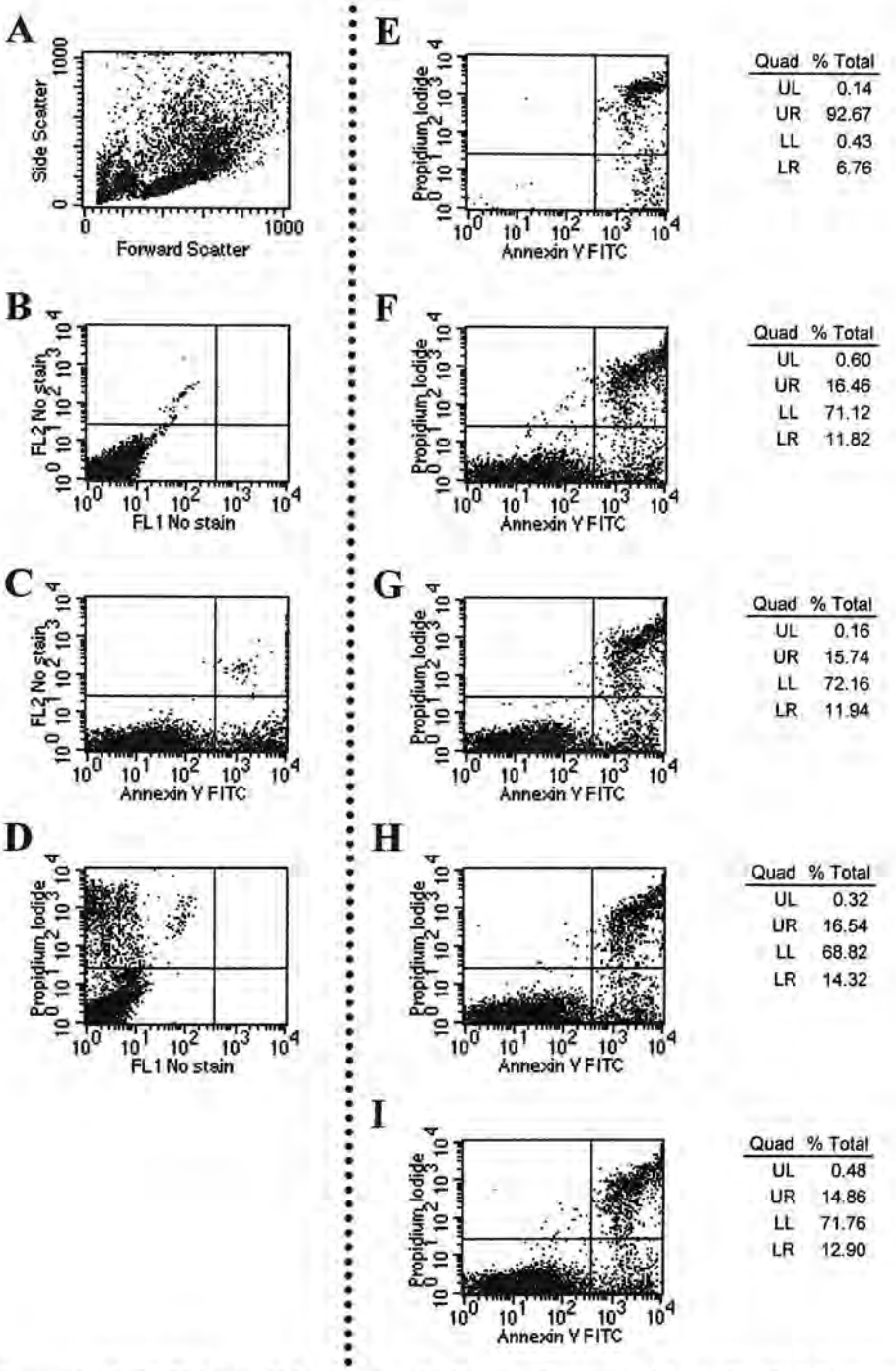

Figure 4.11: N-Shh peptide does not affect cell survival in activated human CD4$^+$ T cells at 72hrs.

Control samples: **(A)** All cells (FSC/SSC) **(B)** Cells unstained **(C)** AnnexinV single stain **(D)** PI single and **(E)** "Dead cells" control. Thereafter, activated cells cultured in the presence of **(F)** 0ng/ml **(G)** 10ng/ml **(H)** 100ng/ml and **(I)** 1000ng/ml of N-Shh peptide for 72hrs and stained for AnnexinV and PI.

4.4 Blocking Sonic Hedgehog Signalling inhibits T cell receptor mediated activation in human CD4$^+$ T cells

In the following series of experiments a neutralizing anti-Shh antibody (Developmental Studies Hybridoma bank: 5E1) was added to purified human CD4$^+$ T lymphocytes. This antibody has been shown to inhibit the function of Shh and thus Shh signalling [121,125]. In all cases the T cells were activated using plate-bound anti-CD3 (1μg/ml) and soluble anti-CD28 (5μg/ml) antibodies, and the 5E1 concentrations used were in the same range as those used previously by other groups [121,125]. Results are of representative experiments, which were repeated at least three times.

4.4.1 ANTI-SHH NEUTRALIZING ANTIBODY INHIBITS HUMAN CD4$^+$ T CELL PROLIFERATION

The 5E1 antibody was added at a range of concentrations to purified, activated human CD4$^+$ T cells. The same time course was used as in the N-Shh peptide proliferation experiments. Following 72 hrs in culture, sample wells were pulsed with tritiated thymidine and read 16-24 hrs later.

The 5E1 antibody inhibited proliferation of the activated human CD4$^+$ T cells when used at concentrations of 20μg/ml and above (Figure 4.12). Unactivated ("resting") T cells were included as a further negative control (Figure 4.12B). Significantly, as discussed in the recently published paper [556], an isotype control antibody for 5E1 used at equivalent concentrations had no inhibitory effects on T cell activation (work completed by Dr Sonia Wakelin).

As noted in the parallel N-Shh peptide experiments, the 5E1 antibody had no effect on proliferation in approximately 50% of donor CD4$^+$ T cells. The remaining analysis presented is focussed on the 'responder' donors.

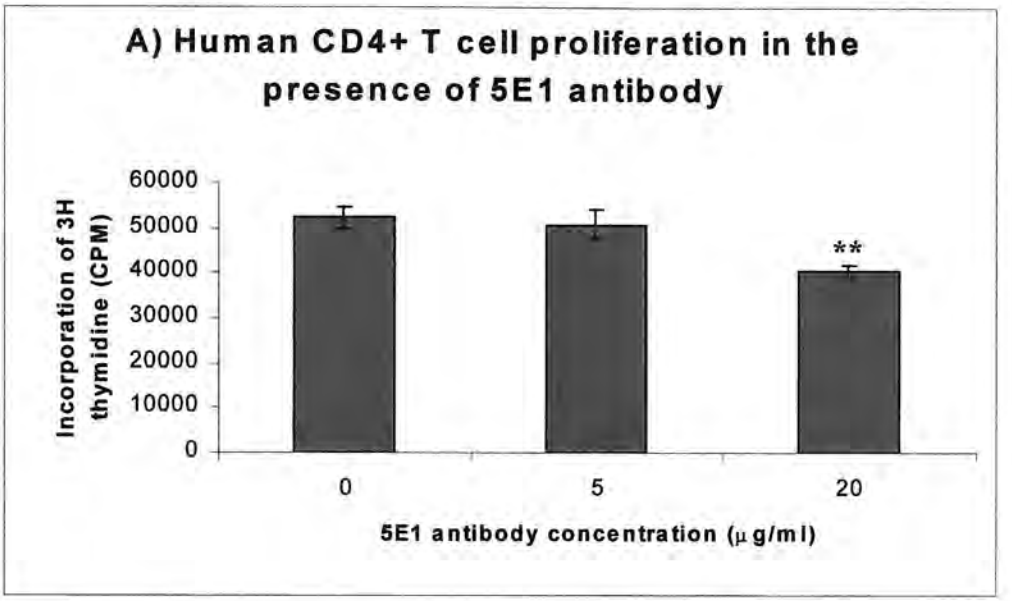

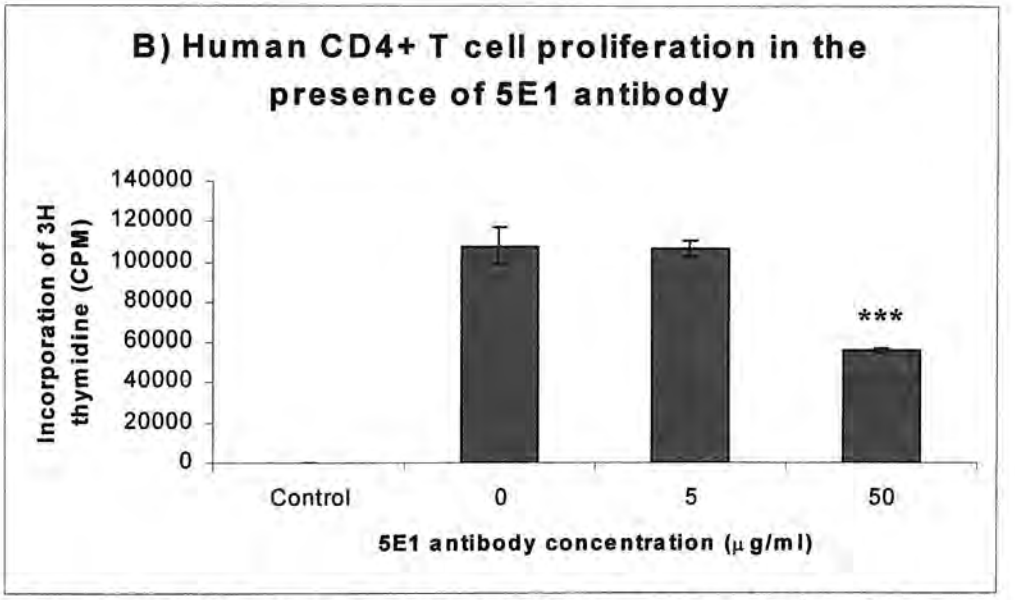

Figure 4.12: 5E1 antibody inhibits proliferation of human CD4$^+$ T cells.

Graphs are representative of proliferation (samples in triplicate at least) of T cells activated in the presence of plate-bound anti-CD3 (1μg/ml) and soluble anti-CD28 (5μg/ml) antibodies. Each well was pulsed with tritiated thymidine after 72hrs in culture and read 16-24hrs later. Statistically all activated samples are compared with those wells containing no antibody (0μg/ml). Control cells were cultured in the absence of anti-CD3 and anti-CD28. The graphs show proliferation of purified human CD4$^+$ T cells (means and standard deviations) in the presence 5E1 antibody in concentrations up to **(A)** 20μg/ml and **(B)** 50μg/ml.

*** $p < 0.05$; ** $p < 0.01$; *** $p < 0.001$**

4.4.2 ANTI-SHH NEUTRALIZING ANTIBODY REDUCES CYTOKINE RELEASE FROM ACTIVATED HUMAN $CD4^+$ T CELLS

Supernatants from responder donors, in whom the 5E1 antibody inhibited $CD4^+$ T cells proliferation, were taken from 24 to 72 hrs. Levels of interleukin (IL) 2, 5 and 10, and interferon gamma (IFNγ) were then measured.

IL2 was detectable from 24hrs onwards, increasing up to 72hrs. The addition of the 5E1 antibody resulted in a reduction in IL2 levels in a dose dependant manner with maximum effect at a concentration of 20μg/ml ($p< 0.001$)(Figure 4.13A).

IFNγ was optimally detected from 48 hrs onward. As with IL2, IFNγ levels were reduced in the presence of the 5E1 antibody at concentrations of 10μg/ml and 20μg/ml ($p< 0.001$)(Figure 4.13B).

IL10 and IL5 were most easily detected at 72hrs. However, as before IL5 was often difficult to detect in many experiments. In addition, there was consistently no appreciable difference in either IL10 or IL5 levels in the presence of the 5E1 antibody (Figure 4.14).

Therefore, addition of the neutralizing anti-Shh antibody (5E1) to activated T cells reduces the release of IL2 and IFNγ in a dose dependent manner, but does not affect IL10 or IL5. An isotype control antibody for 5E1, used at equivalent concentrations, had no inhibitory effect on cytokine secretion [556].

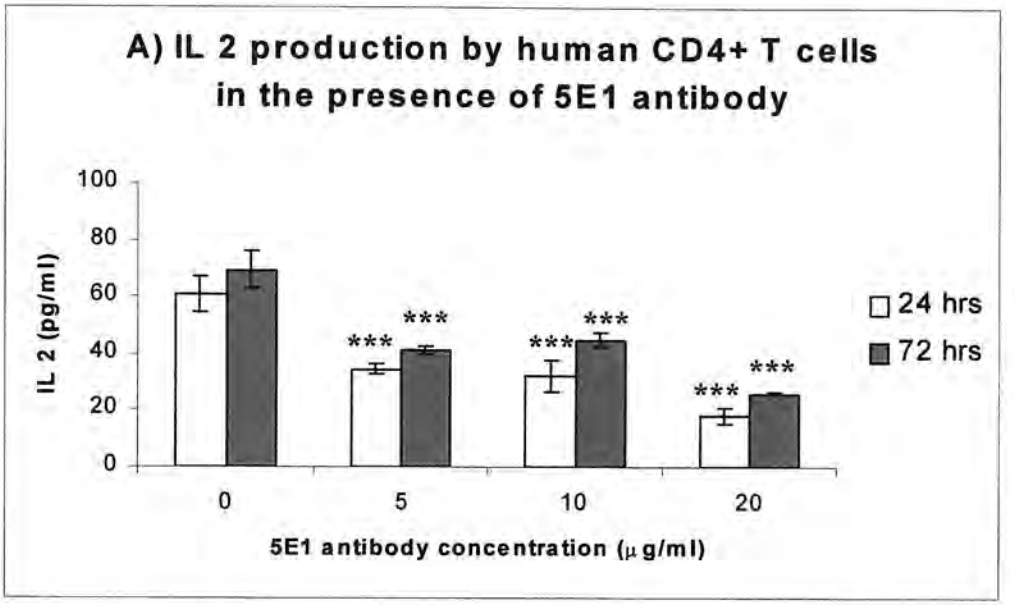

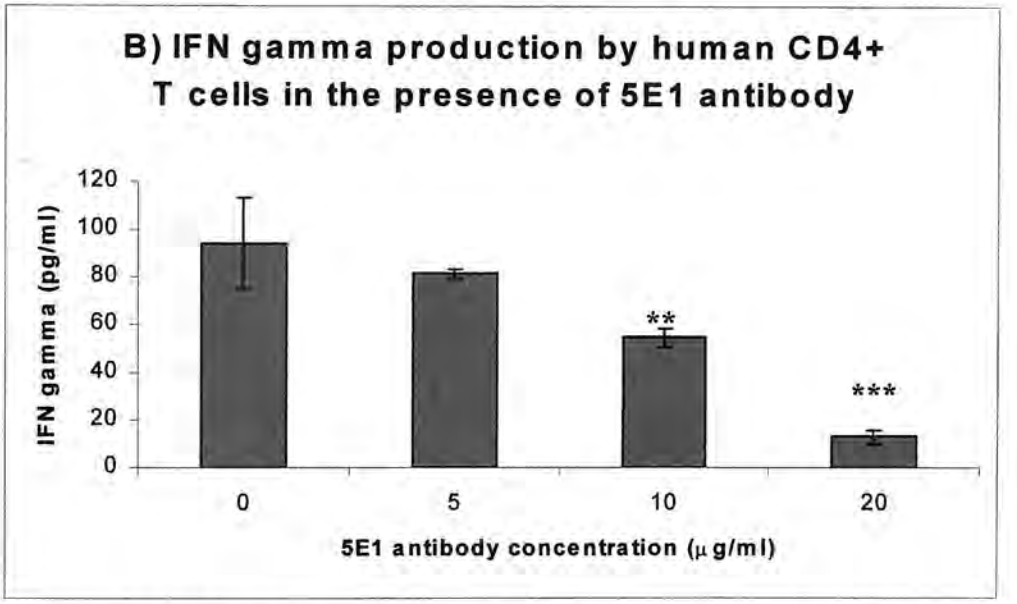

Figure 4.13: 5E1 antibody decreases IL2 and IFNγ release from human $CD4^+$ T cells.

Graphs are representative of cytokine measurements of supernatants (triplicate wells) taken from $CD4^+$ T cells activated in the presence of plate-bound anti-CD3 (1μg/ml) and soluble anti-CD28 (5μg/ml) antibodies, showing means and standard deviations. Statistically samples are compared with those wells containing no antibody (0μg/ml) at the equivalent time-point. **(A)** IL2 levels measured at 24 and 72hrs. **(B)** IFNγ levels measured at 72hrs.

*** $p < 0.05$; ** $p < 0.01$; *** $p < 0.001$**

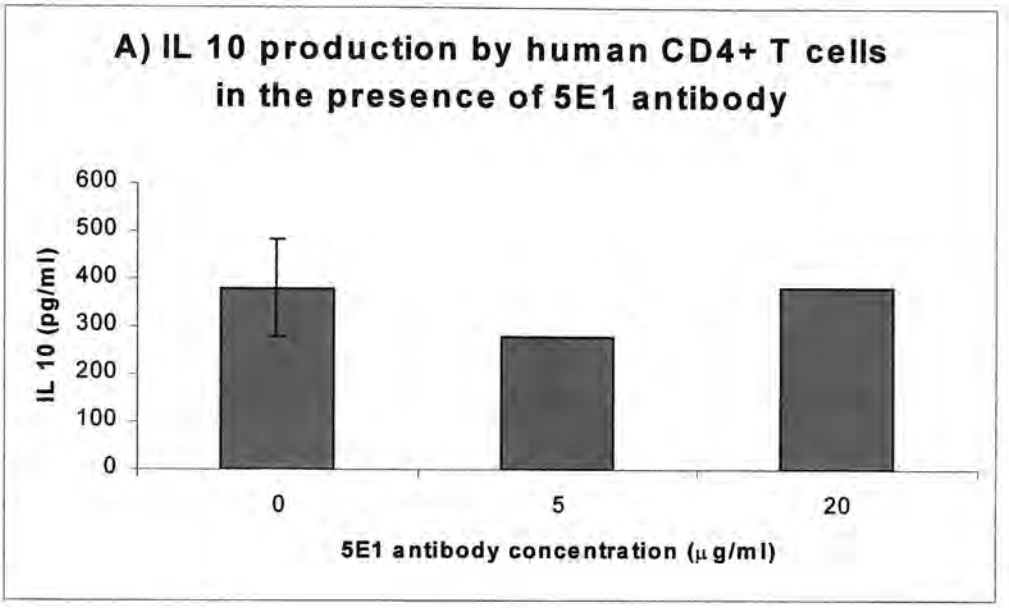

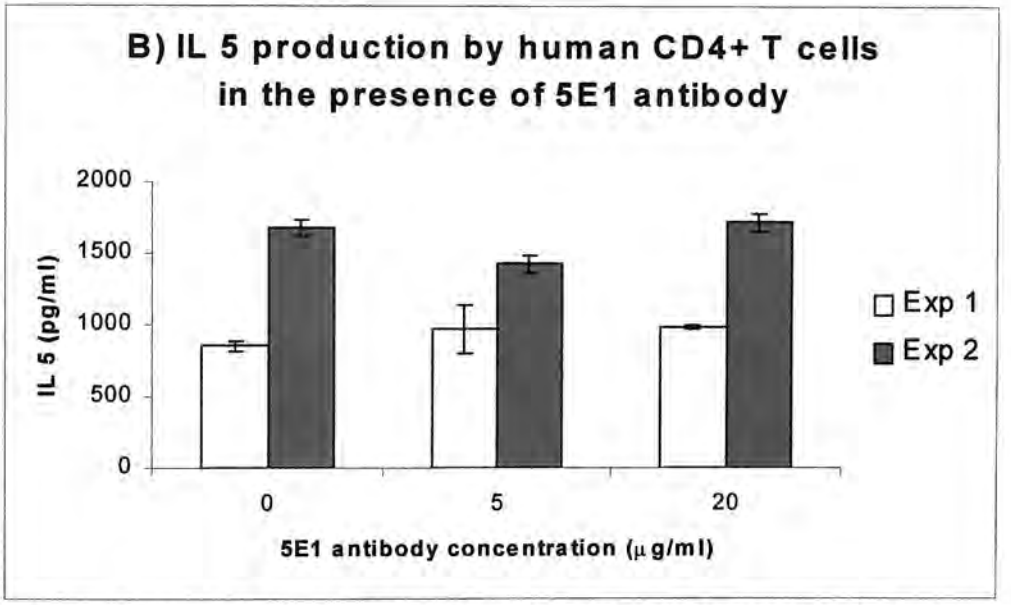

Figure 4.14: 5E1 antibody does not alter IL10 or IL5 release from human CD4$^+$ T cells.

Graphs are representative of cytokine measurements of supernatants (triplicate wells) taken from CD4$^+$ T cells activated in the presence of plate-bound anti-CD3 (1μg/ml) and soluble anti-CD28 (5μg/ml) antibodies, showing means and standard deviations. Statistically samples are compared with those wells containing no antibody (0μg/ml) at the equivalent time-point. **(A)** IL10 levels measured at 72hrs. Error bars at the 5μg/ml and 20μg/ml concentrations are included, but are too narrow to appreciate **(B)** IL5 levels measured at 72hrs in 2 separate experiments (Exp 1 and 2).

*** $p < 0.05$; ** $p < 0.01$; *** $p < 0.001$**

4.4.3 ANTI-SHH NEUTRALIZING ANTIBODY REDUCES THE EXPRESSION OF CD25 AND CD69 IN ACTIVATED HUMAN $CD4^+$ T CELLS

The 5E1 antibody was added at a range of concentrations to purified, activated human $CD4^+$ T cells and the expression of the activation markers CD25 and CD69, in responder donors, measured by flow cytometry. As with the parallel experiments using the N-Shh peptide, the viable cell populations gated as R1 or R2 were analysed. Suitable isotype matched antibody controls were again used to allow discrimination between positive (M1) and negative staining (Figures 4.15 and 4.16 B). The optimal time-points for peak CD25 (72hrs) and CD69 (48hrs) expression, as discussed earlier, are shown (Figures 4.15 and 4.16).

In the representative experiment shown, the percentage of CD25 +ve cells was marginally reduced from 56% (without) to 53% in the presence of the 5E1 (20μg/ml) antibody. In the same experiment, the associated reduction in mean fluorescent intensity was more notable falling from 347 to 278 (Figure 4.15 C-D; Experiment 1). The final two histograms (Figure 4.15 E-F; Experiment 2) were from a separate experiment, with a different isotype control (not shown) and hence M1 region, in which a dose of 50μg/ml of 5E1 antibody was used. They show a more pronounced reduction in both the percentage +ve cells (from 51% to 35%) and mean fluorescent intensity (from 154 to 114), with this higher concentration. Even at the 20μg/ml dose the percentage of CD25 positive cells, in a series of donor experiments, was significantly reduced at both 48hrs ($p=0.014$, $n=4$) and 72hrs ($p=0.033$, $n=4$). These findings correlate with the proliferation data (Figure 4.12).

The expression of CD69, as measured by the percentage of +ve cells (from 36% to 18%) and their mean fluorescent intensity (from 151 to 127), was also reduced in the presence of the 5E1 neutralizing antibody (Figure 4.16). As with CD25 expression, the effect was most notable at the 50μg/ml concentration (Figure 4.16F). Unfortunately there was insufficient data for group statistics to be performed, but the trend remained consistent.

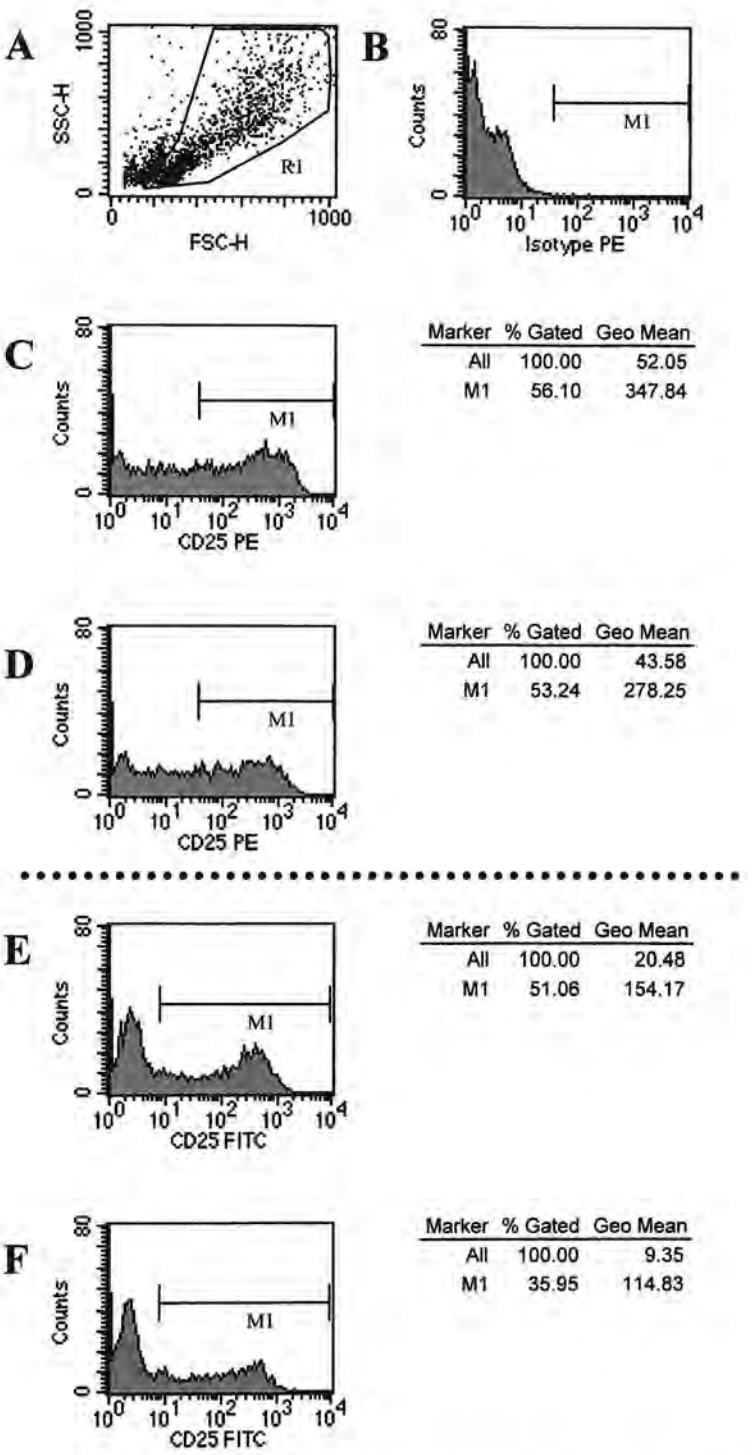

Figure 4.15: 5E1 antibody reduces CD25 expression in human CD4$^+$ T cells at 72hrs.

Experiment 1:(A) Dot plot of CD4$^+$ T cells after **72hrs** in culture. Further histograms gated on the R1 population. **(B)** Isotype control histogram. Remaining histograms show cells cultured with **(C)** 0μg/ml and **(D)** 20μg/ml **Experiment 2:**CD4$^+$ T cells after **72hrs** in culture with **(E)** 0μg/ml and **(F)** 50μg/ml of 5E1 antibody. CD25 positive cells: M1 region.

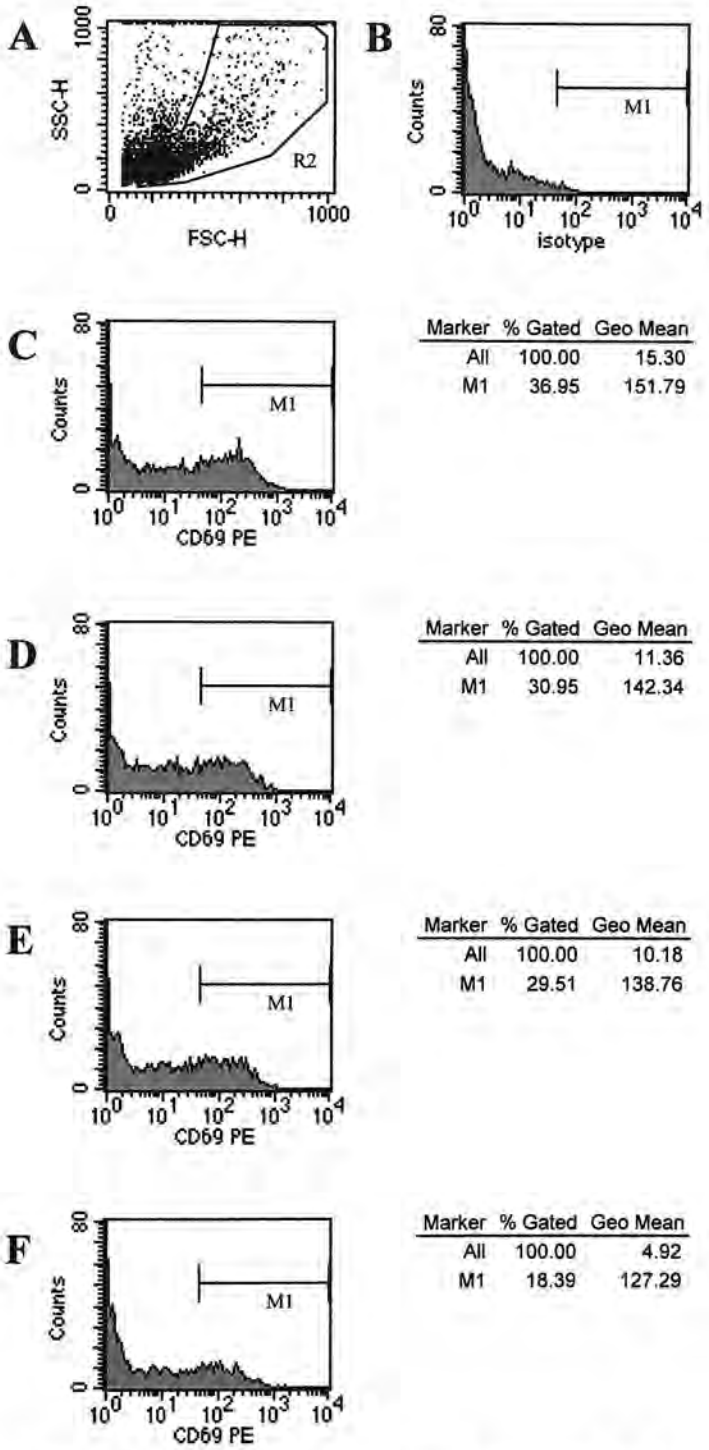

Marker	% Gated	Geo Mean
All	100.00	15.30
M1	36.95	151.79

Marker	% Gated	Geo Mean
All	100.00	11.36
M1	30.95	142.34

Marker	% Gated	Geo Mean
All	100.00	10.18
M1	29.51	138.76

Marker	% Gated	Geo Mean
All	100.00	4.92
M1	18.39	127.29

Figure 4.16: 5E1 antibody reduces CD69 expression in human CD4$^+$ T cells at 48hrs.

(A) Dot plot of CD4$^+$ T cells after **48hrs** in culture. Further histograms gated on the R2 population. **(B)** Isotype control histogram. Remaining histograms show cells cultured with **(C)** 0μg/ml **(D)** 5μg/ml **(E)** 20μg/ml and **(F)** 50μg/ml of 5E1 antibody. CD69 positive cells fall within the M1 region.

4.4.4 ANTI-SHH NEUTRALIZING ANTIBODY DOES NOT AFFECT CELL SURVIVAL IN ACTIVATED HUMAN $CD4^+$ T CELLS

As the 5E1 neutralizing antibody inhibits T cell proliferation, it was important to determine if this was related to reduced cell survival, particularly in view of the links between Shh signalling and apoptosis [559-561]. To assess the effect of 5E1 on cellular apoptosis and/or survival, the antibody was added to purified, activated human $CD4^+$ T cells, as before. As in the peptide experiments the cells were stained with AnnexinV-FITC and Propidium Iodide (PI) at 24hrs and 72 hrs, before flow cytometry analysis (see Section 4.3.4). Data shown is representative of at least repeated experiments.

In the experiments shown, there was no detectable difference in cell survival/apoptosis between T cells cultured in the presence or absence of the 5E1 antibody, at either time-point (Figures 4.17 and 4.18). This would imply that reductions in proliferation seen with this antibody were not due to any toxic or pro-apoptotic effects.

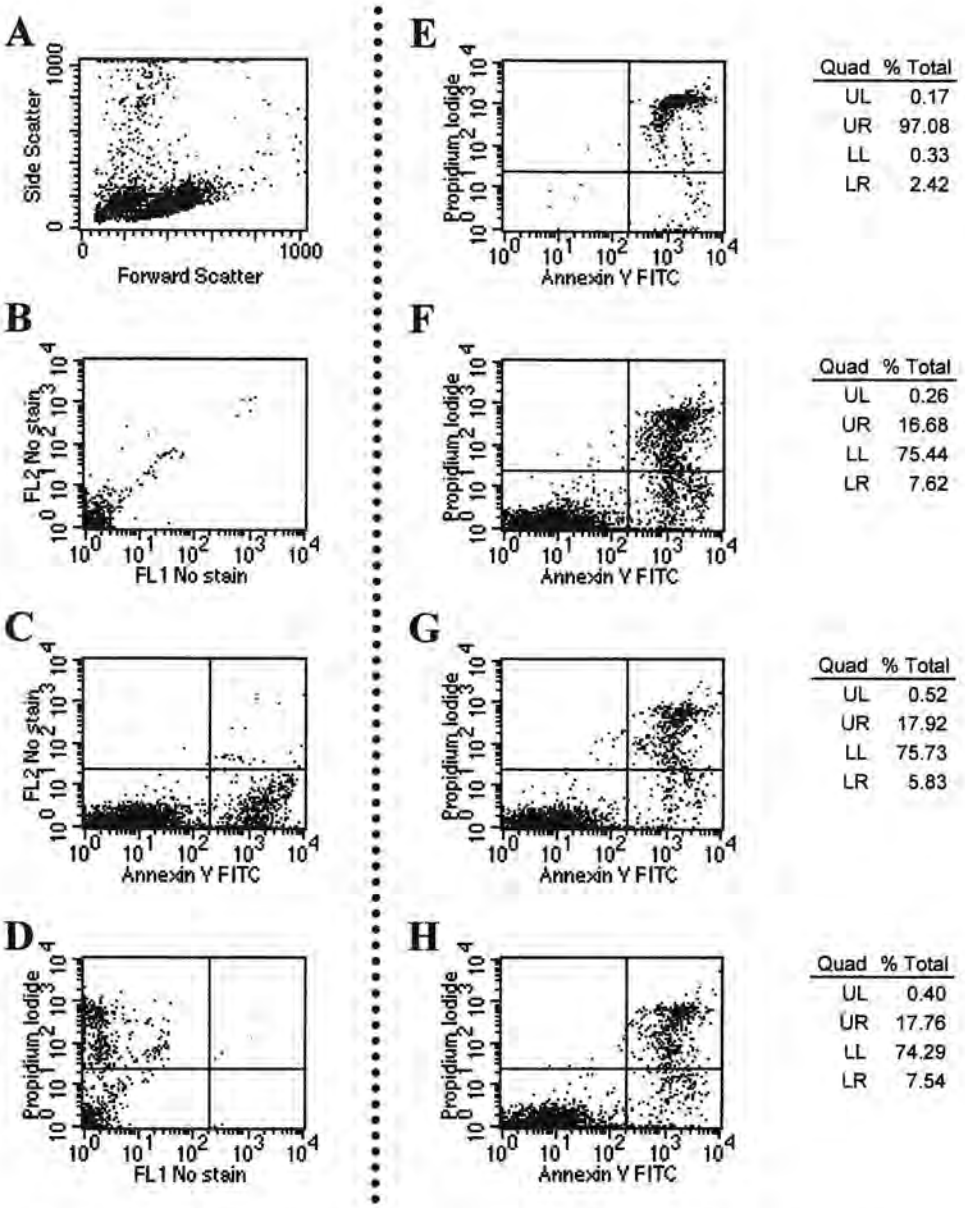

Figure 4.17: 5E1 antibody does not affect cell survival in activated human CD4$^+$ T cells at 24hrs.

Control samples: **(A)** All cells (FSC/SSC) **(B)** cells unstained **(C)** AnnexinV single stain **(D)** PI single stain and **(E)** "Dead cells" control. Thereafter, activated cells cultured in the presence of **(F)** 0μg/ml **(G)** 10μg/ml **(H)** 20μg/ml of 5E1 antibody for 24hrs and stained for AnnexinV and PI.

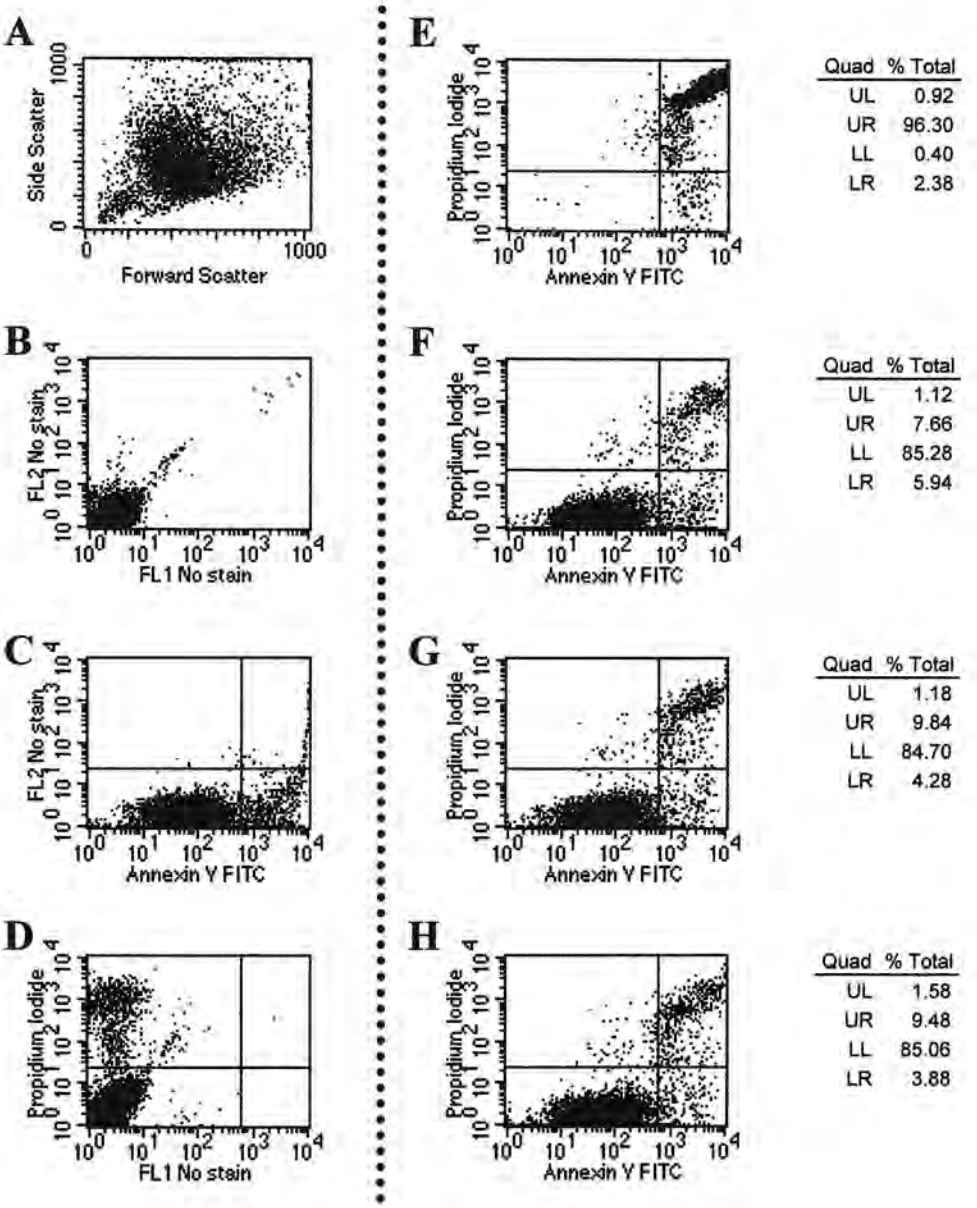

Figure 4.18: 5E1 antibody does not affect cell survival in activated human CD4$^+$ T cells at 72hrs.

Control samples: **(A)** All cells (FSC/SSC) **(B)** cells unstained **(C)** AnnexinV single stain **(D)** PI single stain and **(E)** "Dead cells" control. Thereafter, activated cells cultured in the presence of **(F)** 0μg/ml **(G)** 10μg/ml **(H)** 20μg/ml of 5E1 antibody for 72hrs and stained for AnnexinV and PI.

4.5 Sonic Hedgehog signalling does not induce proliferation of non-activated ('resting') human $CD4^+$ T cells

The experiments outlined above have concentrated almost exclusively on purified human $CD4^+$ T cells activated using anti-CD3 and anti-CD28 antibodies. It was of interest to determine whether Shh had any effect on unstimulated cells. Thus, similar experiments using non-activated ('resting') T cells were carried out, using both the N-Shh peptide and 5E1 antibody.

4.5.1 SONIC HEDGEHOG SIGNALLING DOES NOT INFLUENCE PROLIFERATION OF RESTING T CELLS

Purified human $CD4^+$ T cells were cultured in the presence of either the N-Shh peptide (Figure 4.19A) or the 5E1 anti-Shh blocking antibody (Figure 4.19B). These resting T cells were cultured for 72hrs before pulsing with tritiated thymidine. As before readings were taken 16-24 hrs later.

The counts were generally very low, as would be expected in the absence of activation. In addition, neither the N-Shh peptide nor the 5E1 antibody altered cell proliferation, from any of the donors, when used at concentrations equivalent to those proven to affect activated T cells. Notably, 'activated' and resting $CD4^+$ cells from the same donor were often analysed simultaneously. Even in 'responder' donors, the resting T cells appeared to be unaffected by either the peptide or the antibody. Similar results were seen with resting human $CD8^+$ T cells as shown earlier (Figure 4.3B).

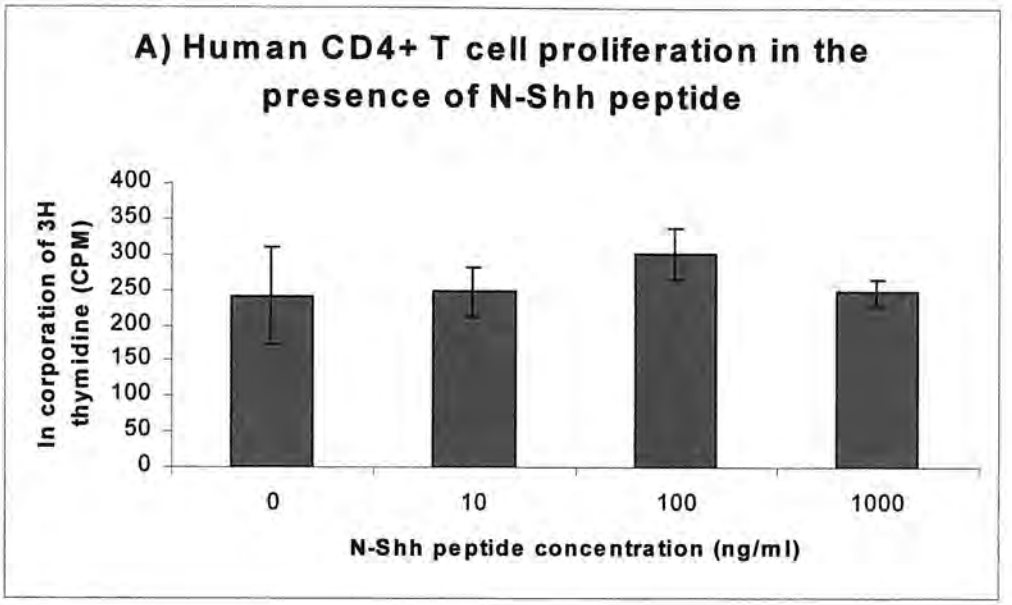

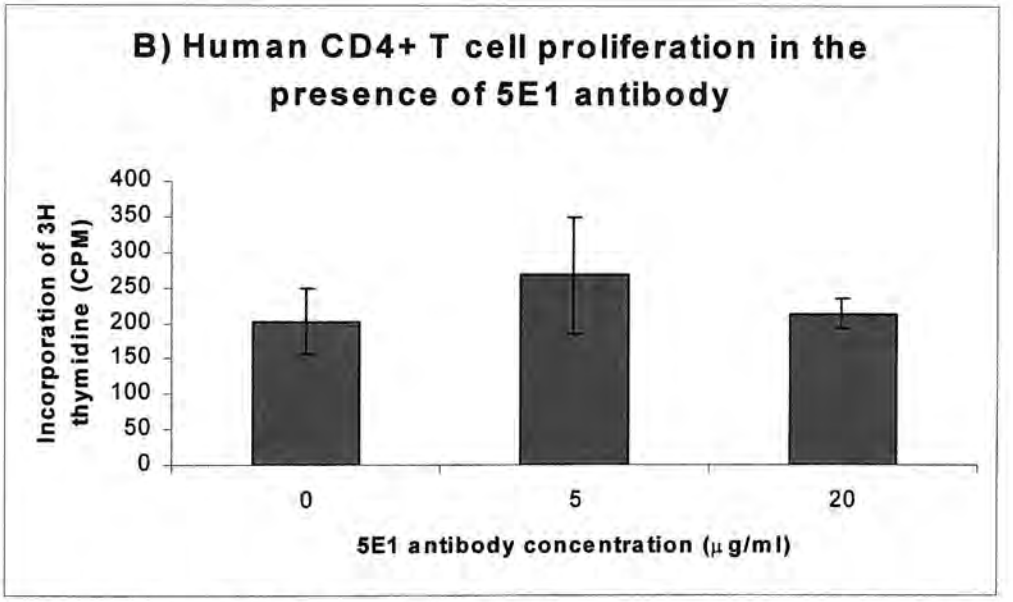

Figure 4.19: Neither the N-Shh peptide nor the 5E1 antibody affect proliferation of resting $CD4^+$ T cells.

Graphs are representative of proliferation (samples in triplicate at least) of T cells cultured without activation. Each well was pulsed with tritiated thymidine after 72hrs in culture and read 16-24hrs later. Proliferation of purified human $CD4^+$ T cells (showing means and standard deviations) in the presence of **(A)** N-Shh peptide and **(B)** 5E1 antibody. Results are representative of at least 3 experiments.

4.5.2 SONIC HEDGEHOG SIGNALLING DOES NOT AFFECT RESTING T CELL SURVIVAL

Purified human $CD4^+$ T cells were cultured in the presence of either the N-Shh peptide or the 5E1 anti-Shh blocking antibody without activation. To assess whether or not either of these compounds affected survival and/or apoptosis in a "resting" population, the T cells were stained, for AnnexinV-FITC and PI and analysed by flow cytometry.

Neither the N-Shh peptide nor the 5E1 antibody affected resting $CD4^+$ T cell survival or apoptosis (Figures 4.20,4.21 and 4.22). These findings correlate with the parallel survival experiments in activated T cells.

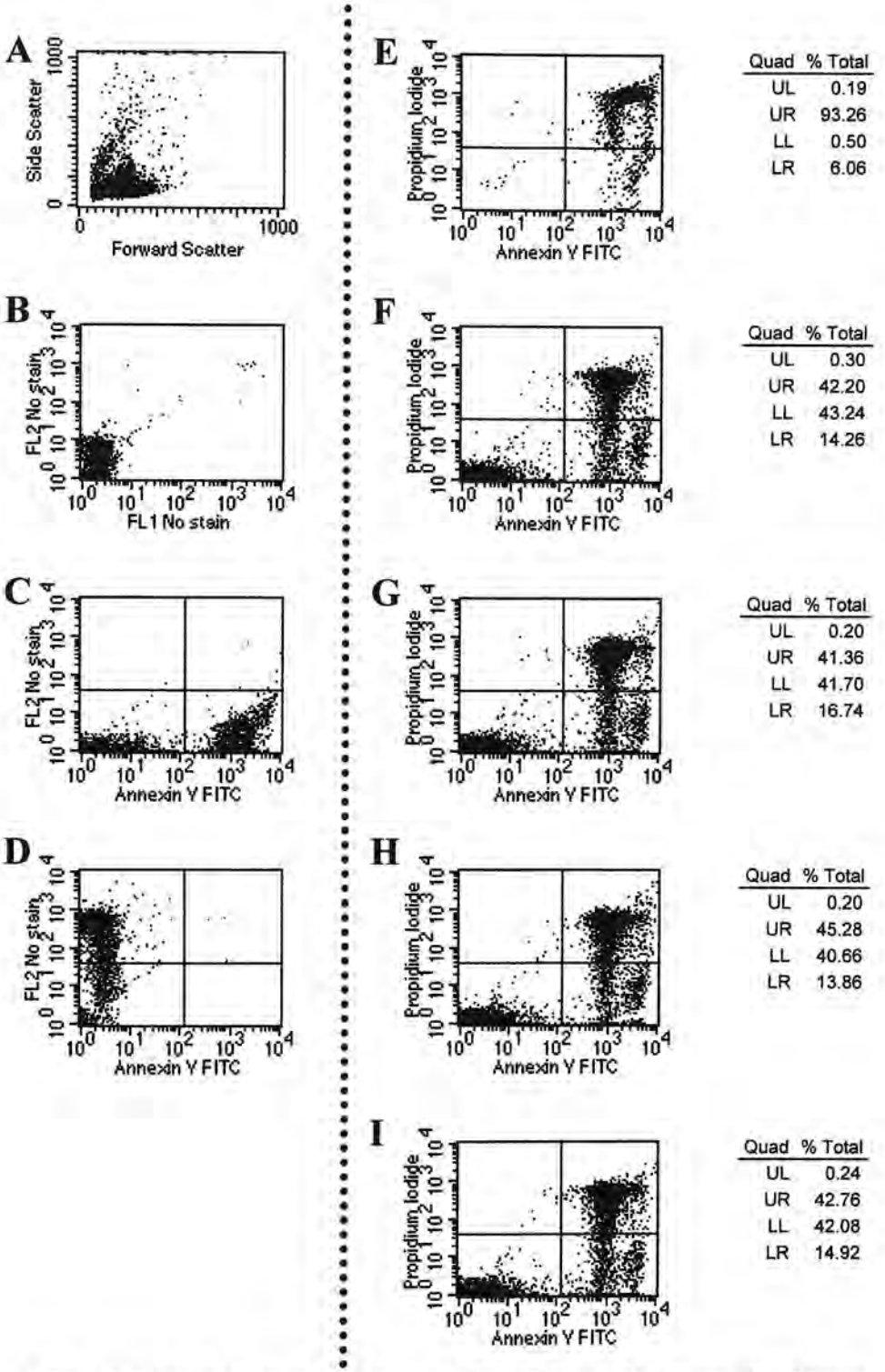

Figure 4.20: N-Shh peptide does not affect cell survival in resting human CD4$^+$ T cells at 24hrs.

Control samples: **(A)** All cells (FSC/SSC) **(B)** cells unstained **(C)** AnnexinV single stain **(D)** PI single and **(E)** "Dead cells" control. Thereafter, resting cells cultured in the presence of **(F)** 0ng/ml **(G)** 10ng/ml **(H)** 100ng/ml and **(I)** 1000ng/ml of N-Shh peptide for 24hrs and stained for AnnexinV and PI.

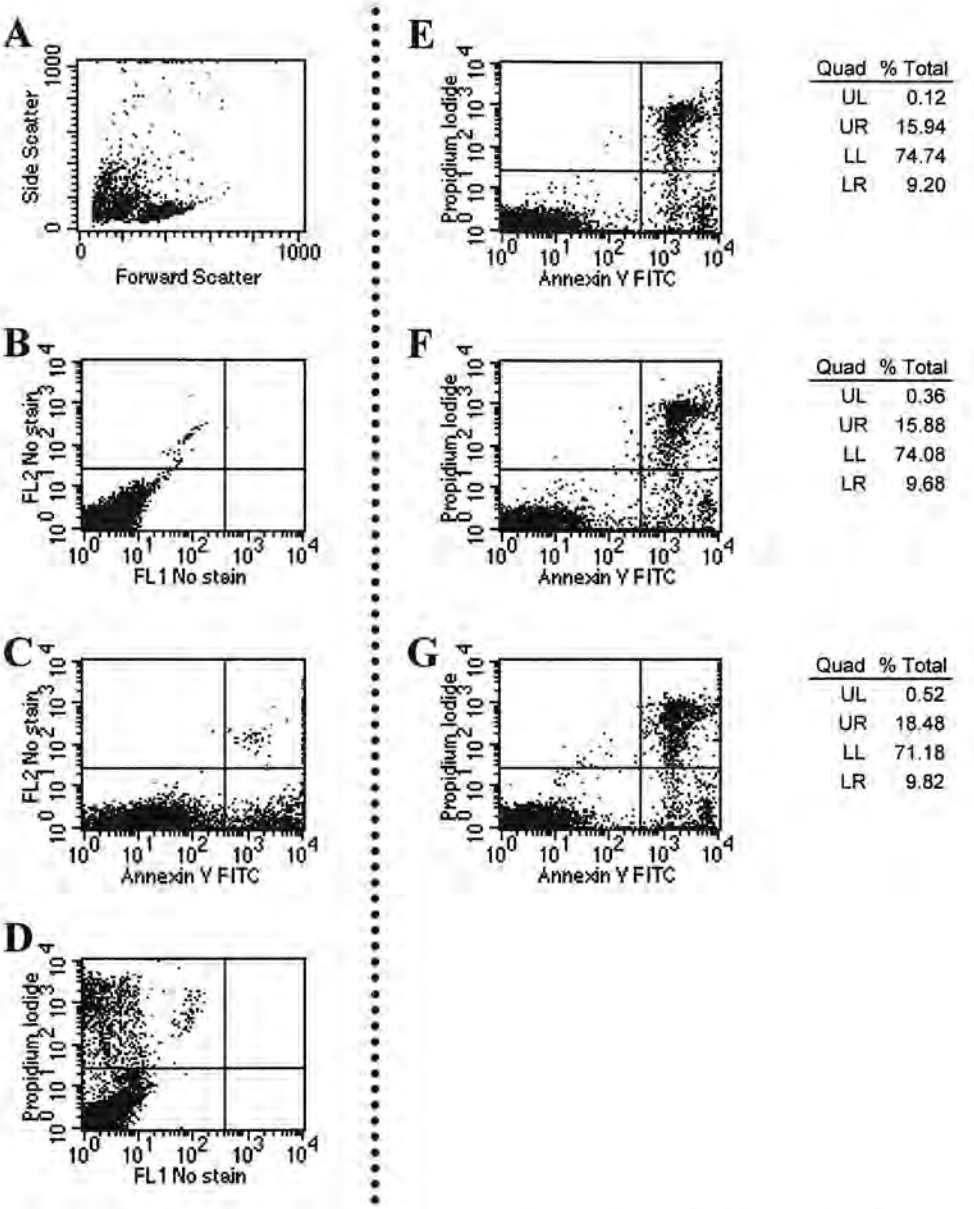

Figure 4.21: N-Shh peptide does not affect cell survival in resting human CD4$^+$ T cells at 72hrs.

Control samples: **(A)** All cells (FSC/SSC) **(B)** cells unstained **(C)** AnnexinV single stain and **(D)** PI single. "Dead cells" control was as for Figure 4.11 (not shown here). Thereafter, activated cells cultured in the presence of **(E)** 0ng/ml **(F)** 100ng/ml and **(G)** 1000ng/ml of N-Shh peptide for 72hrs and stained for AnnexinV and PI.

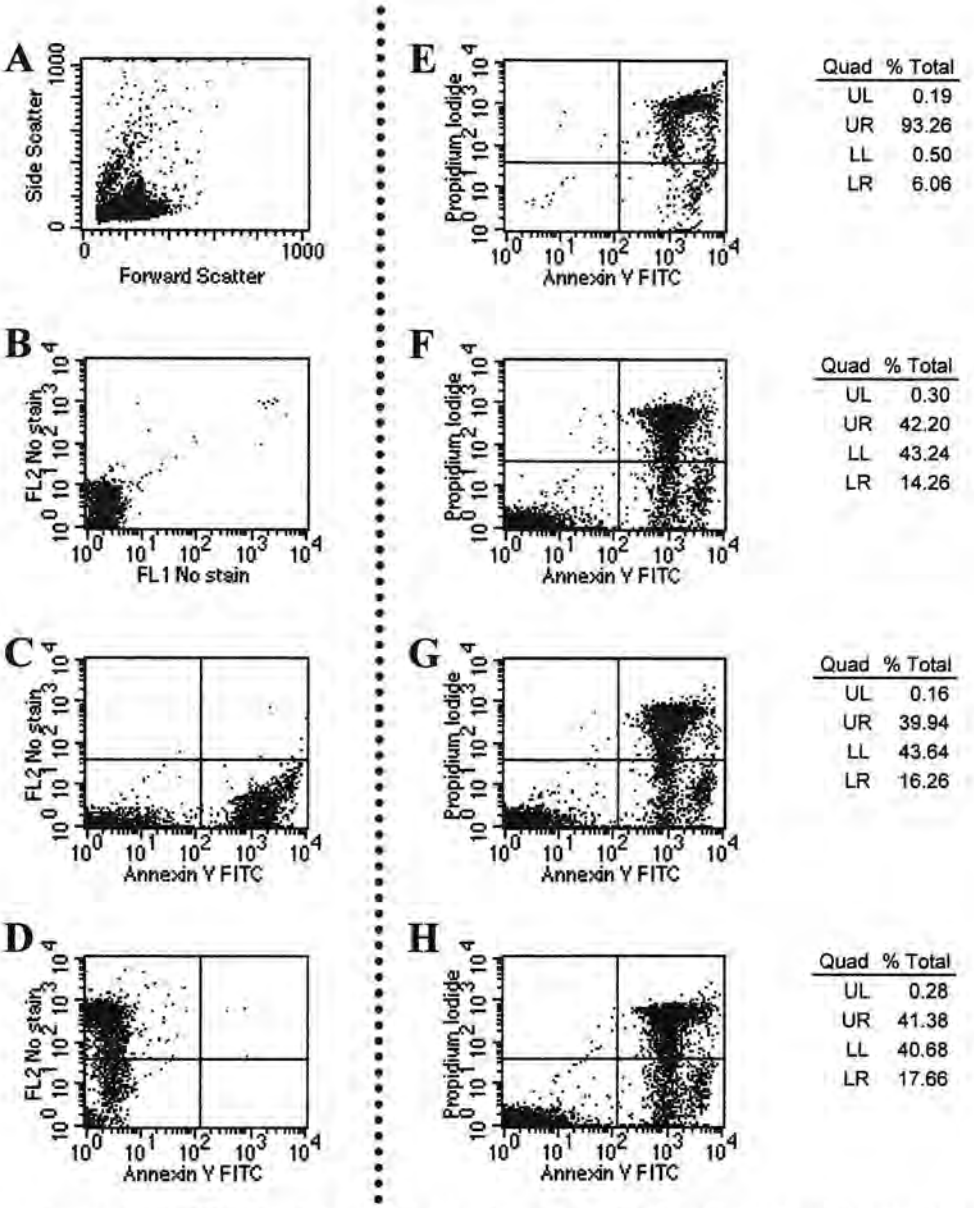

Figure 4.22: 5E1 blocking antibody does not affect cell survival in resting human CD4$^+$ T cells.

Control samples: **(A)** All cells (FSC/SSC) **(B)** cells unstained **(C)** AnnexinV single stain **(D)** PI single and **(E)** "Dead cells" control. Thereafter, activated cells cultured in the presence of **(F)** 0μg/ml **(G)** 5μg/ml and **(H)** 20μg/ml of 5E1 antibody for 24hrs and stained for AnnexinV and PI.

4.6 Discussion

As mentioned in the introduction to this chapter the Shh signalling pathway has never previously been studied with respect to the mature immune system, and indeed has only very recently identified in the developing immune system of humans and mice [121,125].

Sonic Hedgehog Pathway expression in Human T cells

The findings reported here importantly confirm the presence of the ligand (*Shh*) and the receptor (*Ptc*) of the Shh pathway, at both RNA and protein level, in human T cells. The presence of *Ptc* is interesting in that it implies that human T cells could respond to a Shh signal from other cell types, such as epithelial cells, *in vivo*. The presence of *Shh* in these T cells suggests a potential for this pathway to play a role in T cell autocrine signalling, and to allow T cells to send signals to other cells. As described in chapter 3, both Shh and Ptc are also present in macrophages. Shh signalling may also play a role in their function and activation, and possibly in T cell-macrophage interactions.

Upregulation of the Shh pathway leads to a paradoxical increase in *Ptc* expression itself. Therefore, an increase in *Ptc* expression has been used as an indicator of Shh signalling [14,27,55]. The data presented showed that *Ptc* mRNA expression is indeed increased in both resting and activated human $CD4^+$ T cells upon addition of the N-Shh peptide. From this, one can postulate that the Shh pathway is functional in human $CD4^+$ T cells and that the N-Shh peptide is a suitable ligand. However, these results were obtained using real time PCR analysis, as discussed in chapter 2. Briefly, this is a relatively new technique in which the levels of the gene of interest are compared to an internal positive control such as 18S, thereby allowing expression of a particular gene to be quantitatively compared between samples. A potential problem in data interpretation is determining what constitutes a significant relative difference in RNA expression between two samples. In published work, comparing

RNA expression in the context of gene microarrays [557,558], it was concluded that a 2-fold difference (or greater) in RNA expression could be considered significant. Therefore, the 4.7-fold increase in *Ptc* in activated T cells would be considered significant, but the 1.7-fold difference in 'resting' T cells would not (Figure 4.2). In addition, the relevance of any increase in mRNA alone could also be questioned. Increased RNA expression does not necessarily equate with increased expression of the associated protein, as other factors may be required for protein translation, or indeed post-translational modification. However, in these experiments, Ptc protein upregulation was difficult to evaluate, because the Ptc antibody proved incompatible with either Western blotting or flow cytometry, and appreciation of increased Ptc expression by immunocytochemistry against strong basal staining in untreated cells (Figure 4.1) was not possible. Therefore relative *Ptc* expression could only be assessed at the RNA level in this system.

Shh signalling and T cell receptor (TCR) mediated T cell activation

Addition of the N-Shh peptide to human T cells activated by anti-CD3/CD28 antibody treatment resulted in a dose dependant increase in proliferation, with peak levels noted at a concentration of 100ng/ml. As the N-Shh peptide has been shown to upregulate the Shh pathway, these findings imply that Shh signalling results in augmentation of T cell receptor mediated activation. Shh signalling, as induced by similar Shh peptides, has already been shown to increase proliferation in a range of cell types [116,117,120], including haematopoietic stem cells [125]. It would appear that the pathway behaves in a similar manner in human T lymphocytes. The optimal concentration for peak proliferation (100ng/ml) was the same at which peak *Ptc* mRNA expression was noted in previous experiments. Thus maximal *Ptc* expression, suggestive of optimal Shh pathway activity, is associated with the greatest proliferation.

Notably, as described, the proliferation of approximately 50% of donor $CD4^+$ T cells was unaffected by the addition of exogenous Shh. The reason for such 'responders' and 'non-responders' is not clear. Bearing in mind that mutations in *Ptc* and *Smo* are

known to result in constitutive Shh signalling activation [68,132,133], it is possible that there may be also polymorphisms which bring about the loss or modulation of function of the pathway. Thus such polymorphisms may have rendered the donors unresponsive to the N-Shh peptide.

Analysis of cytokine production followed similar trends to proliferation. Of most significance, secretion of 3 of the 4 cytokines (IL2, IFNγ and IL10 but not IL5) measured was increased in the presence of the N-Shh peptide, in a dose dependent manner. The observed increase in IL2 secretion was in accordance with the increase in T cell proliferation, since IL2 release is proportional to the amount of activation of $CD4^+$ T cells [562]. It is possible that the IL5 results may have been affected by the sensitivity of the assay used for this cytokine; a different system to the other measured ELISAs. Indeed IL5 was often difficult to detect even in the presence of high levels of the other cytokines. As discussed in Chapter 1, IL2 and IFNγ are associated with Th1 T cells, and IL5 and to a lesser extent IL10 with Th2 [461,462]. As the pattern of cytokine secretion observed in the presence of the N-Shh peptide does not appear to conform to either phenotype, it would therefore appear that Shh signalling results in a polyclonal increase in cytokine secretion.

Furthermore, the highest levels of IL2, IFNγ and IL10 were associated N-Shh peptide concentrations of 1000ng/ml. This differed slightly from the mRNA and proliferation experiments in which 100ng/ml was found to be the peak concentration, above which levels of *Ptc* transcript and proliferation diminished.

The presence of N-Shh also increased the proportion of cells staining positively for both CD25 (IL2 receptor α chain) and CD69 (Activation Inducer Molecule or AIM), in a dose dependent manner. These cell surface markers are themselves upregulated upon activation of T lymphocytes. CD25 expression is maintained on the surface of T lymphocytes by activated STAT5 (A and B) although initial expression of CD25 is regulated by T cell receptor (TCR) activation [516]. Maintenance of CD25 expression on T cells works in a cyclic pattern whereby ligation of IL2 to the IL2 receptor (IL2R) initiates STAT5 activation, which in turn induces expression of IL2R.

Expression of CD69, however, is regulated by activated Ras [507], which plays an integral role in TCR mediated signalling [508,563]. It may be that Shh signalling modifies STAT5 and Ras activation, thus leading to upregulation of CD25 and CD69.

CD25 expression increased in a dose dependant manner with maximal expression in the presence of the higher 1000ng/ml concentration of the N-Shh peptide. It is encouraging to note that this matches the pattern observed in IL2 secretion. CD69 expression was most marked at the intermediate dose of 100ng/ml. This correlates more closely with the proliferation and real time data and less so with cytokine secretion. Therefore, it would appear that optimal N-Shh peptide concentrations vary with different aspects of T cell function, including proliferation, cytokine secretion and surface activation marker expression. Of course, there is a large body of evidence, which demonstrates that proliferation can be dissociated from other T cell effector functions, such as cytotoxic activity and cytokine production [564].

As described, Shh signalling has been previously linked with apoptosis [559-561]. To determine whether the observed increases in T cell proliferation with the N-Shh peptide were influenced by improved cell survival, flow cytometric analysis, using AnnexinV-FITC and PI, was carried out. Neither AnnexinV binding nor PI staining was altered in the presence of N-Shh, demonstrating that enhanced proliferation was not due to increased cellular survival. Therefore, Shh signalling augments TCR mediated T cell activation without affecting cell survival or apoptosis. These observations bear similarities to those presented by Outram *et al* [121] who showed that, whilst Shh signalling affects thymocyte differentiation and proliferation, it does not affect thymocyte survival.

The effects of blocking endogenous Shh signalling on (TCR) mediated T cell activation

5E1 has been established as an anti-Shh neutralizing antibody in several systems [121,125]. In effect, it has been used to inhibit Shh signalling by preventing binding of

endogenous Shh protein to the Ptc receptor. As both Shh and Ptc are present in human T cells it would be logical to assume that autocrine signalling may take place.

As one might predict, 5E1 inhibited proliferation of human $CD4^+$ T cells, at concentrations of 20μg/ml and above, in keeping with observed affects in human haematopoietic stem cells at similar concentrations [125]. Therefore, it would appear that endogenous Shh maintains proliferation in the $CD4^+$ T cell culture, and blocking of this endogenous Shh thus decreases proliferation. As with the N-Shh peptide, the 5E1 antibody had no effect on the $CD4^+$ proliferation in approximately 50% of donors, presumably for the same reason.

The presence of the 5E1 antibody resulted in a reduction in both IL2 and IFNγ secretion from activated human $CD4^+$ T cells, but did not affect either IL5 or IL10 production. Their reduction was in accordance with the decrease in proliferation; as were increases with the N-Shh peptide with enhanced proliferation. IL5 appears to be unaffected by either enhancing or inhibiting Shh signalling. However, as discussed earlier, these findings may be related to the sensitivity of the IL5 ELISA. In addition, it is not clear why exogenous Shh (N-Shh) increases IL10 secretion, whilst blocking endogenous Shh does not reduce it. It may be that IL10 production can be regulated by TCR signalling independently of Shh activation.

It is also notable that the concentrations of 5E1 as low as 5μg/ml significantly lowered cytokine production, whereas only levels of 20μg/ml and above affected proliferation. As in the peptide experiments, different concentrations of 5E1 affect T cell proliferation and cytokine production.

Consistent with these findings, expression of the surface activation markers CD25 and CD69 was also reduced in the presence of the 5E1 neutralizing antibody. This effect was most pronounced at the highest 50μg/ml dose. Considering these observations, and the effects of the antibody on proliferation and IL2 secretion, it is plausible that the induction of Shh signalling is a physiological component of T cell activation following the ligation of TCR and co-stimulatory receptors.

As with N-Shh, AnnexinV and PI analysis was performed to determine if the decrease in T cell proliferation seen with 5E1 was in any way due to cellular apoptosis or necrosis. The staining of both was unchanged confirming that these processes were not responsible and that 5E1 was not affecting T cell survival.

Shh signalling in unstimulated ('resting') T Cells

Similar experiments using both the N-Shh peptide and the 5E1 antibody were carried out in "resting" T cells i.e. purified human $CD4^+$ T cells cultured in the absence of the anti-CD3 and anti-CD28 antibodies. The aim was to see if the observed effects described could occur in the absence of T cell activation.

As already discussed, relative *Ptc* mRNA expression in 'resting' T cells, in the presence of the N-Shh peptide, was only 1.7-fold greater than with no peptide, compared with up to 4.7-fold in activated cells. Accepting 2-fold differences as the cut-off for biological significance [557,558], exogenous Shh does not appear to stimulate Shh signalling in 'resting' T cells populations.

Neither the N-Shh peptide nor the 5E1 antibody altered proliferation in resting T cells, even from donors in whom these agents significantly affected activated T cell proliferation. AnnexinV/PI analysis confirmed that neither the peptide nor the antibody affected cellular apoptosis or necrosis in resting T cells. Cytokine secretion was measured in resting T cells but, as would be expected, levels were invariably undetectable. The same was true for surface activation marker (CD25 and CD69) expression (data not shown).

Therefore, it would appear that the Shh pathway is not functional in resting T cells. This correlates with published work, in which Shh was unable to recruit quiescent neuronal precursor cells into cell cycle but could sustain cell cycle progression once initiated [565].

Summary

The work detailed in this chapter confirms that the Shh pathway is present and functional in purified human $CD4^+$ T cells. Increased pathway activity, by addition of exogenous Shh, enhances T cell receptor mediated T cell activation as demonstrated by proliferation, cytokine secretion and surface marker expression. Blocking the endogenous Shh pathway inhibits activation as determined by the same assays. Taken together these features suggest that the induction of Shh signalling is a physiological component of peripheral $CD4^+$ T cell responses. However, the pathway does not appear to have any affect on T cell survival, nor does it induce proliferation in non-activated ('resting') T cells. This latter feature suggests that Shh may act as a cofactor, which potentiates TCR mediated signalling and amplifies clonal expansion.

Although not shown in this thesis, similar experiments carried out using purified murine $CD4^+$ T cells (collaborative work with Dr Jacqueline Lowry) suggest that the pathway functions in a similar manner in mice. As the Shh (and hedgehog) pathway is highly conserved throughout species, so may be the biological effects demonstrated in the human system reported here and in this related mouse work.

Chapter 5

The construction and use of an adenovirus expressing murine Dvl1

5.1 Introduction

The Wnt Signalling Pathway, like the Shh Pathway, is highly conserved throughout species (see Chapter 1), and the two pathways are known to interact with one another [3,238,239]. As discussed in chapter 1, dysregulated Wnt signalling has been implicated in several diseases in mature mammals, and particularly in tumourigenesis. Upregulation of the Wnt pathway can result in an increase in epithelial cell proliferation [248-250]. Furthermore, it has been recently reported that Wnt signalling is associated with increased fibronectin expression and with TGFβ signalling [203,240,241,566], both of which have close associations with fibrosis. These features together prompted the proposed hypothesis that the Wnt pathway may play a role in the pathogenesis of Interstitial Lung Disease (ILD). More specifically, the aim of the work presented in this chapter was to upregulate Wnt signalling in mouse lungs to determine whether or not this lead to lung fibrosis.

It has been shown that overexpression of dishevelled (dsh) upregulates Wnt signalling [187-189]. The main objective, therefore, was to overexpress the mammalian homolog, Dvl1, *in vitro* and *in vivo* in mammalian systems in an attempt to induce Wnt signalling. This was to be achieved by constructing a replication deficient adenovirus expressing *Dvl1*. The particular advantages of adenovirus vectors are discussed in Chapter 1.

The work in this chapter addresses the expression of Wnt pathway members in ILD, and the construction of a Dvl1 adenovirus with its use *in vitro* and *in vivo*. It is important to point out that the experiments were not all carried out in the order in which they have been discussed in this chapter. In particular, due largely to a paucity of available reagents, much of the initial immunohistochemistry (IHC) presented (Section 5.2) was not performed until later in the project. Hence, the adenoviral experiments were not biased by these negative IHC findings.

5.2 The Wnt Signalling Pathway in the FITC Model of ILD

The FITC model was used as a tool to investigate the Wnt pathway in the context of lung fibrosis. Lungs sections taken from both PBS and FITC treated mice were stained by IHC for two components (Dvl1 and β-catenin) of the pathway. Results are representative of at least six mice per treatment per time-point.

5.2.1 DVL1 EXPRESSION IS UNALTERED IN THE FITC MODEL OF ILD

Several Dvl1 antibodies, obtained commercially or as gifts, were tested and found to have no specificity for Dvl1 protein. A polyclonal antibody kindly provided by Dr Roel Nusse [567] was found to be particularly useful for Western blotting. However this antibody also recognises Dvl2; its cross-reactivity on Dvl3 is not known (personal correspondence with Dr Karl Willert, Howard Hughes Medical Institute, Stanford University School of Medicine). The antibody had not been previously used for IHC.

To establish if Dvl1 expression varied in lung fibrosis, lung sections from BALB/c mice treated intra-tracheally with either FITC or PBS were stained with the polyclonal anti-Dvl1 antibody. The airway epithelial cells were strongly positive (brown staining) and the alveolar epithelium less so, whilst the remaining lung tissue - including endothelium and cell infiltrates - was negative (Figure 5.1). The same pattern and intensity of staining was noted in both PBS and FITC treated mice at all time-points from 24hrs to 5 months (Figure 5.1). Therefore, based on the results of stains with this antibody, expression of Dvl1 did not appear to change in the FITC model of lung fibrosis.

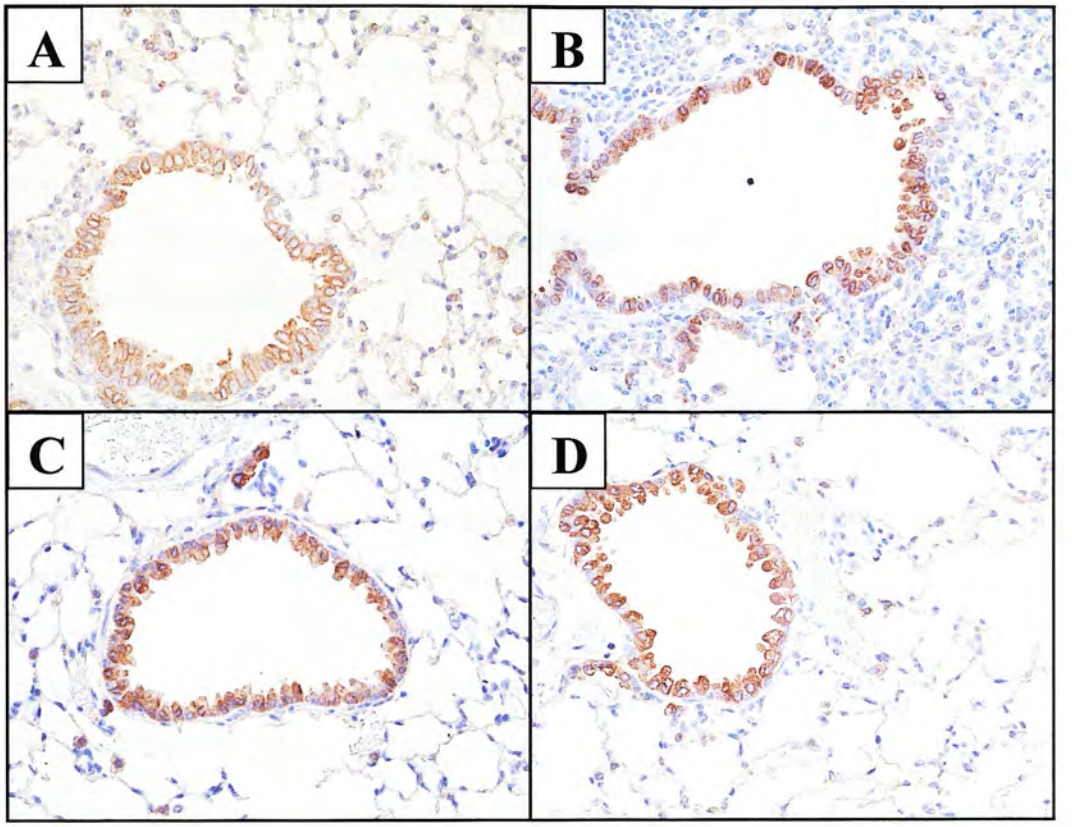

Figure 5.1: Dvl1 expression in the FITC model of lung fibrosis

Dvl1 expression by immunohistochemistry in BALB/c mouse lungs

A) Day 7 after PBS instillation (x 400 magnification)

B) Day 7 after FITC instillation (x 400 magnification)

C) 5 months after PBS instillation (x 400 magnification)

D) 5 months after FITC instillation (x 400 magnification)

5.2.2 BETA-CATENIN EXPRESSION, AS ANALYSED BY IHC, IS UNALTERED IN THE FITC MODEL OF ILD

Further lung sections from FITC and PBS treated mice where stained for the presence of β-Catenin. Samples from time-points from 24hrs to 5 months post instillation were analysed.

There was no discernible difference in β-Catenin expression between the treatment groups at any of the time-points (Figure 5.2). Predominantly membrane staining was observed, which was most apparent on the airway epithelial cells and less so on the alveoli (Figure 5.2). Since β-Catenin is predominantly localised to the cell membrane, where it interacts with cadherins in cellular adhesion, this distribution is as would be expected. Interestingly, the staining was largely confined to areas of the cell membrane in contact with adjacent cells as seen most clearly in Figure 5.2 C and D.

It has been shown that upregulation of the Wnt pathway results in increased cytosolic β-Catenin levels. There was no evidence of increased cytoplasmic staining in sections either from the FITC or PBS treated mice (Figure 5.2).

Therefore, as assessed by IHC, β-Catenin expression in mouse lungs is unaffected by FITC treatment. Most importantly, there is no evidence from the data presented that the Wnt pathway is upregulated in ILD.

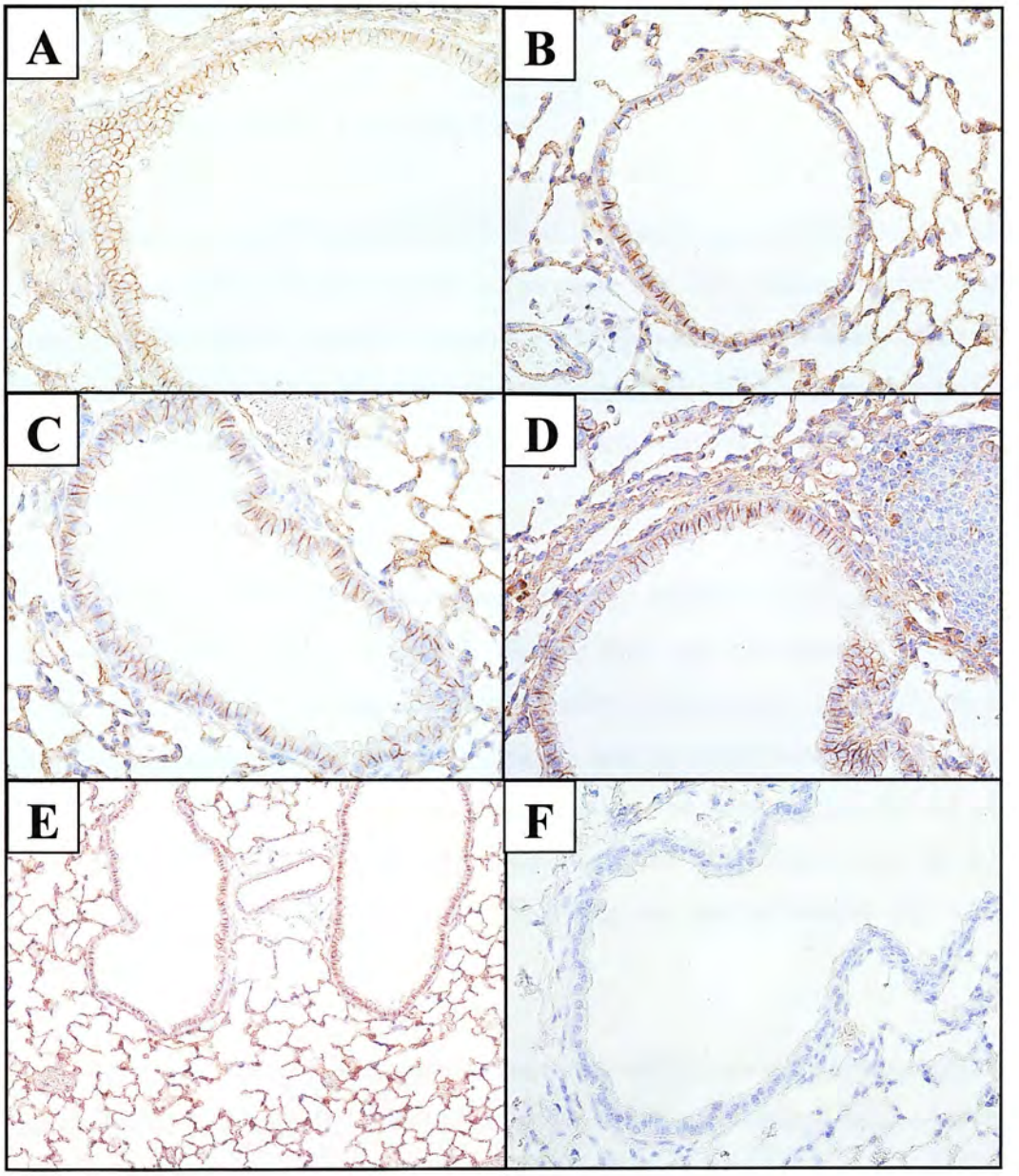

Figure 5.2: β-Catenin expression in the FITC model of lung fibrosis

β-Catenin expression by immunohistochemistry in BALB/c mouse lungs

A) Day 3 after PBS instillation (x 400 magnification)

B) Day 3 after FITC instillation (x 400 magnification)

C) 5 months after PBS instillation (x 400 magnification)

D) 5 months after FITC instillation (x 400 magnification)

E) Day 3 after FITC instillation (x 200 magnification)

F) Negative control: Day 3 after FITC instillation (x 400 magnification)

5.3 Adenovirus Construction

5.3.1 CLONING OF DVL1 INTO PDK6

The murine Dvl1 cDNA was a kind gift from Dr Daniel Sussman, provided as pSK^+-Dvl1 (Figure 5.3D). The initial aim was to clone this into a shuttle vector (pDK6), containing the MCMV (murine cytomegalovirus) promoter, a polyadenylation signal and essentially the "left side" of the adenovirus genome: Ad-5 sequences from 0 to 1 and 9.8 to 15.8 map units (mu), with the E1 region, which is essential for adenovirus replication, deleted.

The pSK^+-Dvl1 and pDK6 cDNAs were initially amplified using a commercially available kit as detailed in chapter 2. 10μg of each was then digested overnight at 37^0C. The pSK^+-Dvl1 was initially digested with the restriction enzymes EcoR I and Xho I in the presence of Buffer H (Promega), and the pDK6 with EcoR I and Sal I with Buffer D. The cut Dvl1 fragment would later be inserted into the cut pDK6 using these sites. This was possible because digests with Xho I and Sal I have compatible ends; therefore an EcoR I/Xho I fragment can be inserted into an EcoR I/Sal I site.

Following these initial digests samples were analysed by agarose gel electrophoresis. As described in chapter 2, with the 1kb ladder, the brighter central band on each gel (Figure 5.3) corresponds to ~1.6kb; the bands higher than this to ~2kb, 3kb, 4kb, 5kb, 6kb, 7kb, 8kb, 9kb, 10kb, 11kb and 12kb respectively, and the lower bands to ~500bp, 400bp, 350bp, 300pb, 220bp, 200bp, 150bp and 75bp, respectively. The PCR ladder used represents: 2kb, 1.5kb, 1kb, 750bp, 500bp, 300bp, 150bp and 50bp, from the largest molecular weight band down. Cutting pSK^+-Dvl1 with EcoR I/Xho I resulted in 2 fragments: Dvl1 (3.29kb) and pSK^+ (2.96kb). This is not obvious in the gel shown, as they are so similar in size (Figure 5.3A). However 2 bands were consistently observed when the gel was run for longer allowing greater band separation (not shown). The EcoR I/Sal I cut was within the multiple cloning site of

the pDK6, and resulted in a large (~7.9kb) fragment and a very small fragment consisting of < 50bp. Only the former was visible on the agarose gel (Figure 5.3A). The pDK6 was cut in 10 separate, identical restriction enzyme digests, and the final digests pooled before purification.

The cut pSK^+-Dvl1 and pDK6 (pooled) were then purified by phenol/chloroform extraction and ethanol precipitation. Because of the closeness in size of the Dvl1 and pSK^+ bands, the latter was cut into 2 smaller fragments using Pvu I in the presence of Buffer D (Promega). Importantly this enzyme does not cut Dvl1. A check gel confirmed an intact Dvl1 fragment (3.29kb) and 2 smaller fragments of pSK^+ (Figure 5.3B). The upper (Dvl1) band was excised, and the extracted DNA was run on a further gel confirming a single Dvl1 band of the correct size (Figure5.3C)

The cut and purified pDK6 was also run on a fresh gel and the large single band excised. As with Dvl1 the DNA was extracted and a final check gel confirmed a single pure band of pDK6 of the correct size (Figure 5.3C). These Dvl1 and pDK6 fragments were then ready for ligation.

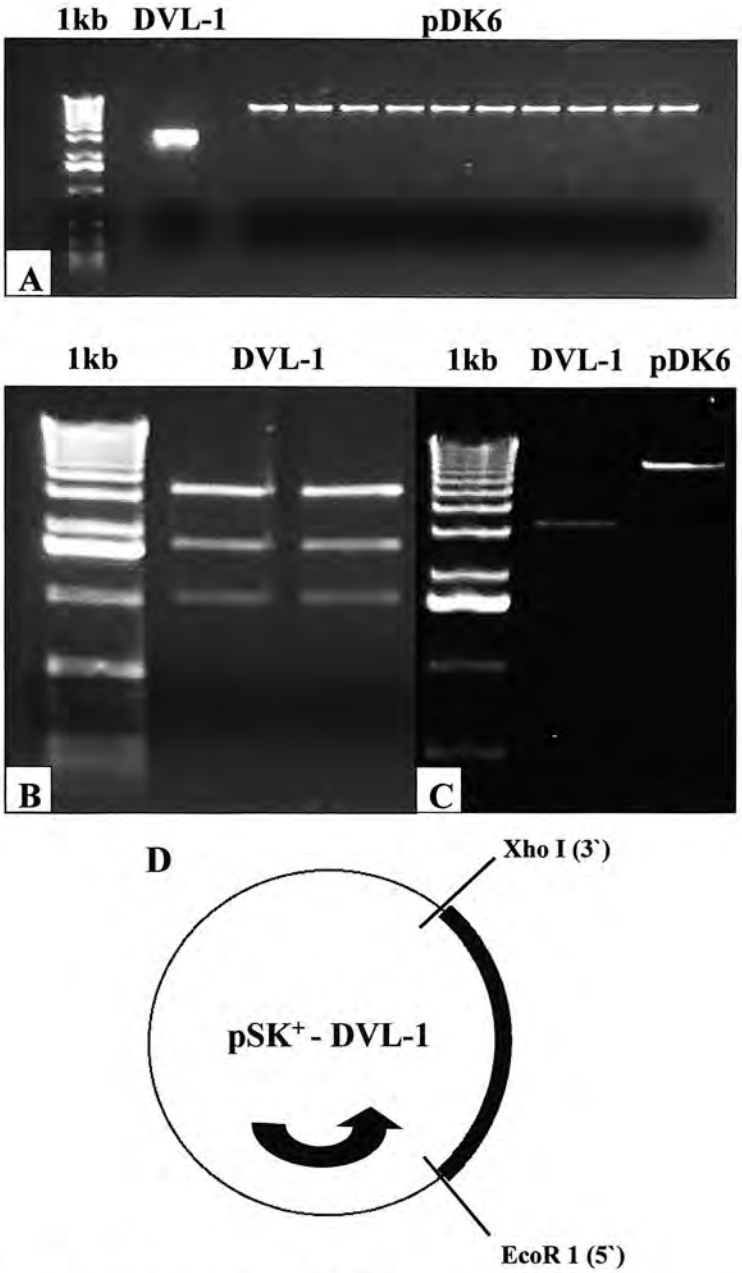

Figure 5.3: Cloning of Dvl1 into pDK6

A) 1% agarose gel with samples of pSK$^+$-Dvl1 (EcoR I and Xho I) and pDK6 (EcoR I and Sal I) following initial digests; Dvl1 being 3.29kb,pSK$^+$ 2.96kb and pDK6 7.9kb.The two Dvl1 and pSK$^+$ bands appear as one on this gel. **B)** 1% agarose gel showing Dvl1 following additional digest with Pvu I This has cut the pSK$^+$ into 2 smaller fragments (lower 2 bands) whilst leaving the 3.29Kb Dvl1 intact (top bands). **C)** 1% agarose gel with the gel extracted Dvl1 and pDK6 fragments; ready for ligation. **D)** Plasmid map of pSK$^+$-Dvl1 showing the Dvl1 fragment (thicker segment) between the chosen restriction enzyme sites

5.3.2 THE PDK6-DVL1 LIGATION

It was necessary to confirm the ligation of Dvl1 into pDK6. As already mentioned the former was cut using EcoR I/Xho I and the latter using EcoR I/Sal I. The ligation was possible because Xho I and Sal I leave compatible ends. However this restriction site would be destroyed in a successful ligation reaction. There were few other available compatible enzymes that would allow the insert to be cleanly cut, without also cutting either the insert or plasmid (pDK6) in other regions. Therefore successful ligations could not be simply verified by cutting out the (Dvl1) insert. This problem was dealt with in two ways.

The ligation product was cut with only the EcoR I enzyme. This only cut in one site and effectively "linearised" the DNA. Both pDK6 alone and the candidate pDK6-Dvl1 ligations were cut with EcoR I. Linearised pDK6 was ~7.9kb in size and pDK6-Dvl1 ~11.2kb (7.9+3.29kb) as shown in Figure 5.4A. As this was a rather crude estimate further evidence was required. To confirm this finding 2 sets of primer pairs (A and B) were designed specifically for murine Dvl1 cDNA. DNA from the pDK6-Dvl1ligation and control Dvl1 DNA were incorporated in PCRs with these primer pairs. Dvl1 cDNA was used as a positive control. The PCR products, run on a 1% agarose gel, were of the correct predicted size, confirming successful pDK6- Dvl1 ligation (Figure 5.4A).

5.3.3 DVL1 IS PRESENT WITHIN THE ADENOVIRUS PLAQUES

Following the pDK6-Dvl1ligation, the next stage was to co-transfect this product with the remainder of the adenovirus genome. The co-transfection was carried out with the plasmid pBHG10 (which contains the entire adenovirus genome apart from 0.5-3.7 mu and 78-85.6 mu) in the presence of 293 cells (human embryonic, kidney epithelial cells). Homologous recombination gave rise to an E1-deleted (replication deficient) adenovirus containing murine Dvl1 cDNA under the control of the MCMV promoter (Ad5-MCMV-Dvl1).

The 293 cells provided the E1 region *in trans* allowing replication and amplification of the adenovirus to be facilitated. The rescue of a replicating recombinant adenovirus resulted in the development of slowly expanding areas of dying cells seen beneath an agarose overlay, referred to as "plaques". Details of adenovirus construction are discussed in greater detail in Chapter 2.

Following a number of co-transfection attempts, 2 plaques developed simultaneously in one of the culture plates (plaques 1 and 2). DNA originating from these plaques was then analysed for Dvl1 expression.

As with the pDK6-Dvl1 ligation PCR reactions were carried out using both sets of Dvl1 primer pairs (A and B). These confirmed the presence of Dvl1 cDNA in both plaques (Figure 5.4B), demonstrating that Ad-5-MCMV-Dvl1 had been successfully rescued.

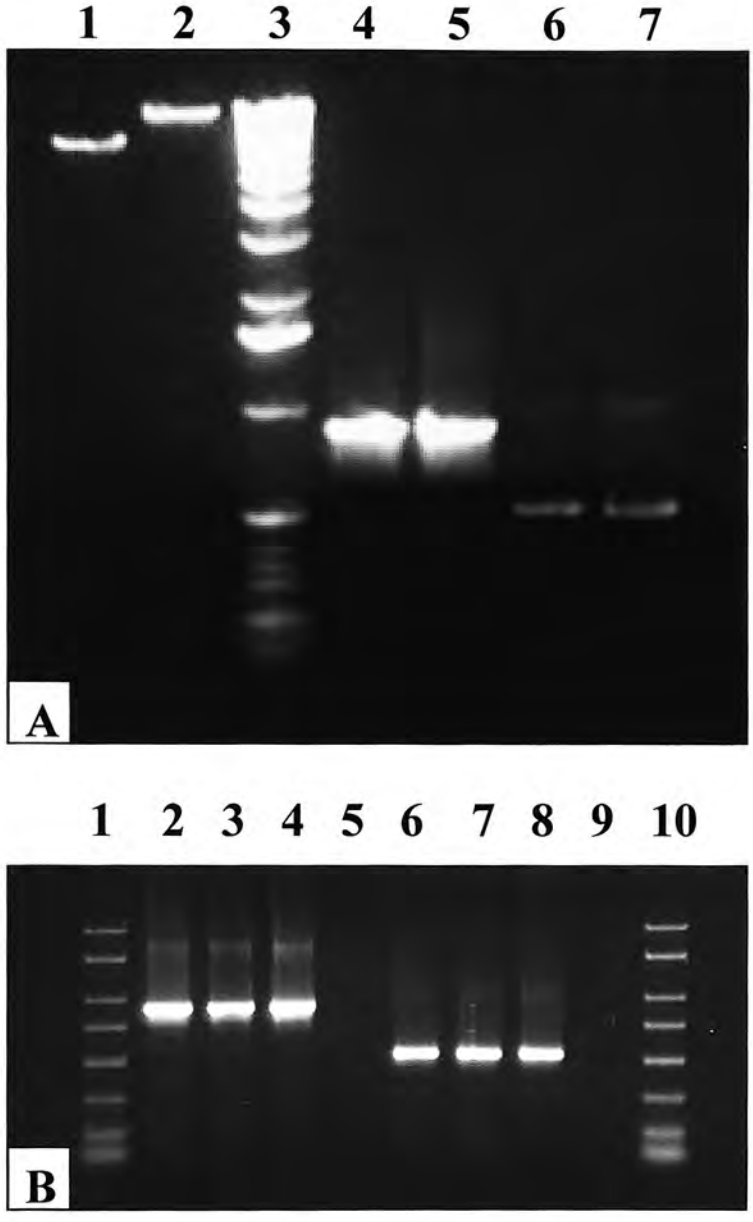

Figure 5.4: Confirming Dvl1 DNA expression

A) 1% agarose gel. EcoR1 digests of **1,** pDK6, and **2,** pDK6-Dvl1. **3** 1kb ladder. PCR using Dvl1 primer set A (**4**+**5**) and B (**6**+**7**); former giving a PCR product of 894bp and latter of 521bp. **4** and **6** represent products of PCR reactions using Dvl1 as a positive control. **5** and **7** are of PCR reactions containing ligation products**. B)** Further PCR reactions analysing DNA extracted from adenovirus plaques; **2-5** primer set A and **6-9** primer set B. **1** and **10** PCR ladders. Within each reaction: **2**+**6** DNA from plaque 1, **3**+**7** from plaque 2, **4**+**8** using pSK^{+}-Dvl1 as a positive control and **5**+**9** using water only in the PCR reactions as a negative control.

To confirm Dvl1 expression in these plaques, the extracted DNA was also used in Southern Blots. Initially the DNA was digested with the restriction enzyme Hind III in the presence of Buffer E (Promega). Both 5µl and 10µl of each plaque digest were loaded onto the gel (Figure 5.5 lanes 4 to 7). The plasmid pBHG10 was digested in the same manner and run on the same agarose gel (Figure5.5 lane 3). Finally linearised (Xho I single digest) pSK^+-Dvl1was added as a positive control (lane 2).

Hind III is known to cut pBHG10 into 10 fragments of sizes: 8010bp, 5324bp, 4597bp, 3790bp, 3437bp, 3012bp, 2937bp, 2081bp, 1539bp and 75bp. These are visible in lane 3 (Figure 5.5). All are visible except the smallest 75bp band, and the 3012bp and 2937bp bands are probably seen merged as the brighter band just below arrow **A**. Once homologous recombination has taken place, and the shuttle vector has become integrated into the pBHG10 backbone, a number of the Hind III sites are moved or lost. This leads to an altered restriction digest pattern. In the case of pDK6-Dvl1 one would predict the 3790bp, 3437bp and 1539bp bands would be lost with an additional band at ~8kb. This was indeed observed. Arrow **A** indicates the presence of the 3790bp and 3437bp bands in the pBHG10 digest (Figure 5.5 lane 3) and their absence in the plaque digests (lanes 4-7). In addition, the 1539bp band (lowest seen in lane 3) was absent in the plaque DNA lanes. Any additional ~8kb band would be difficult to distinguish from the preserved 8010bp band. These digests were consistent with a successful homologous recombination leading to the formation of the observed adenoviral plaques (The streaking observed in the plaque DNA lanes is due to the presence of genomic DNA).

Following blotting the membrane, containing the transferred DNA, was hybridised with a ^{32}P-labelled probe specific to murine Dvl1. The probe was made by digesting DVL-1 with Kpn I: producing a 574bp Dvl1 cDNA probe (not shown). This fragment was gel excised before labelling and hybridisation. In Figure 5.5, the bottom panel shows a radiograph of the same blot as the top gel picture. The probe recognised the linearised +ve control (pSK^+-Dvl1) at the expected size of 6.2kb (+ve)[Arrow **C**]. Additionally it did not cross-react with the digested pBHG10, which should not contain Dvl1, therefore acting as a suitable –ve control. Most

importantly the probe recognised ~8kb bands within all of the plaque DNA lanes [Arrow **B**]. From the predicted Hind III digest the additional ~8kb band would be expected to contain the Dvl1 cDNA, and therefore bind to the Dvl1 probe. In lanes 4 to 7, the 10μl samples are outer (4+7) and the 5μl innermost (5+6) for plaques 1 and 2, which correlates with the strength of signal observed in each lane.

The Southern Blot and digest therefore confirmed that the recombinant adenovirus present in plaques 1 and 2 did indeed express Dvl1 cDNA. Ad5-MCMV-Dvl1 had been successfully rescued.

Further details of large scale preparation and purification to produce the banded Ad5-MCMV-Dvl1 (for experimental use) are described in Chapter 2. Control adenoviruses used included a Lac Z expressing virus (gift from Dr Jean-Michel Sallenave) and dl70-3 (gift from Prof Jack Gauldie). The dl70-3 adenovirus contains no insert eg. pDK6 co-transfected with no Dvl1. Both of these control viruses were produced in a similar manner to Ad5-MCMV-Dvl1.

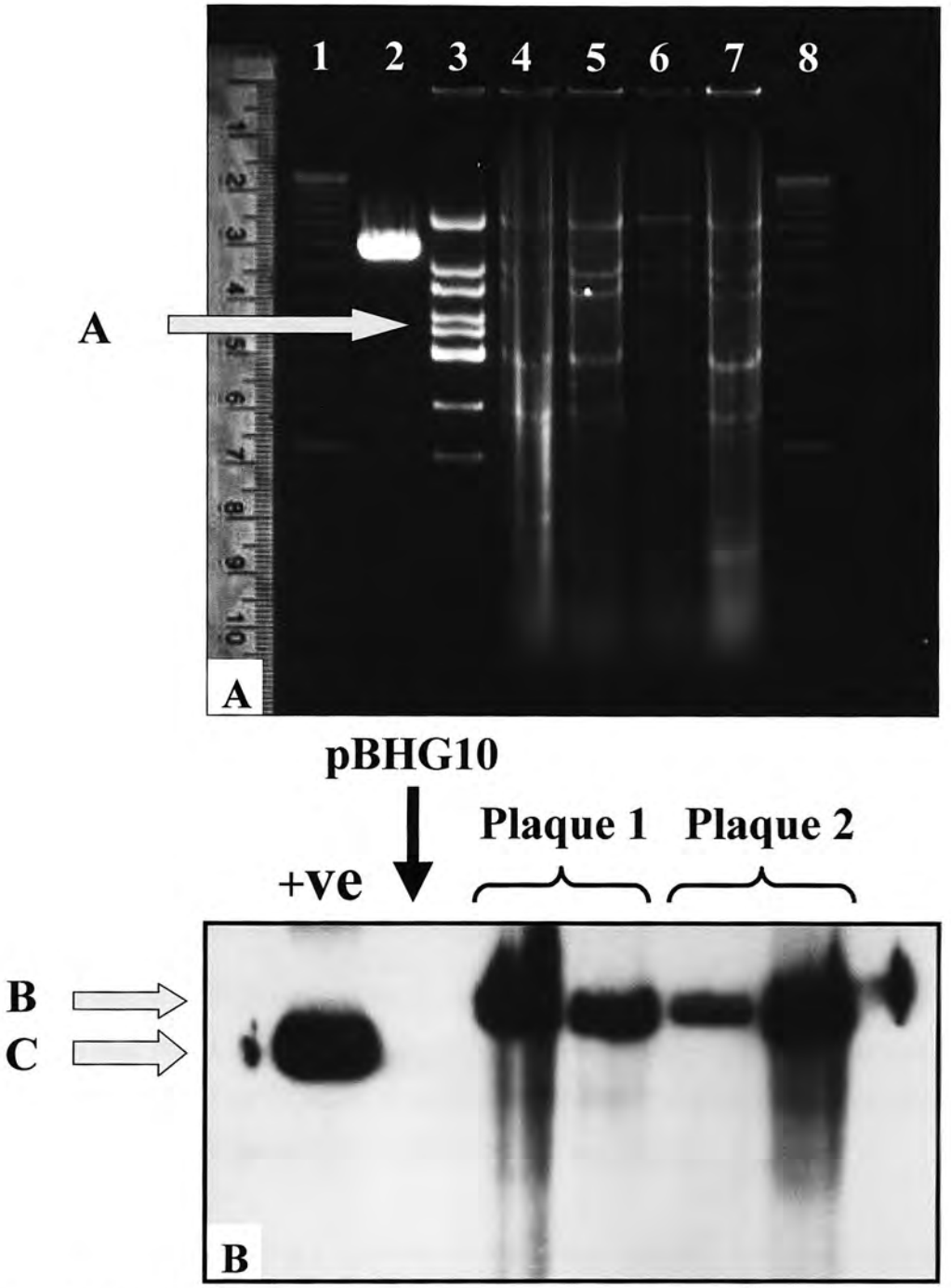

Figure 5.5: Southern Blot of Ad5-MCMV-Dvl1

The upper panel illustrates the 0.8% agarose gel with **1** and **8** being 1kb ladder, **2** the +ve control (linearised pSK^+-Dvl1), **3** digested pBHG10 control, and **4**+**5** (plaque 1) and **6**+**7** (plaque 2) digests of plaque DNA. Arrow **A** indicates where bands present in the pBHG10 digest are lost in the plaque DNA digests.

The lower panel is a radiograph of the same blot following hybridisation with a ^{32}P labelled probe specific to murine Dvl1. Arrow **B** indicates the +ve bands noted within the plaque DNA samples: ~8kb. Arrow **C** indicates the +ve control band (linearised pSK^+-Dvl1): ~6.2kb

5.4 Effects of the Dvl1 Adenovirus *in vitro*

In the following series of experiments the purified, banded Ad5-MCMV-Dvl1 was added to different cell types and a variety of effects analysed. The Lac Z and dl70-3 adenoviruses were used as controls in each transfection. In order to ensure equivalent concentrations of these different viruses were used the titre of each was calculated, as described in chapter 2. Each titre was expressed as plaque forming units per ml (pfu/ml). The titre of the Dvl1 adenovirus was $1.6x10^{10}$pfu/ml, Lac Z was $1.8x10^{10}$pfu/ml and dl70-3 was $2.7x10^{10}$pfu/ml.

Knowing the titre, the amount of virus added to each culture dish or well can be calculated. The quantity of virus added *in vitro* is expressed as a multiplicity of infection (moi), which is the ratio of pfu's of virus to the number of cells within the well (eg. moi of 10 signifies that 10 pfu's of adenovirus are added per cell).

5.4.1 AD5-MCMV-DVL1 RAISES *DVL1* RNA EXPRESSION *IN VITRO*

The Ad5-MCMV-Dvl1 was added to A549 cells (human epithelial lung carcinoma cell line) and Rat 1 fibroblasts at a range of moi's. These cells were harvested at time-points from 24 to 72 hrs post-transfection. RNA was extracted, quantified and run on formaldehyde gels (Figure 5.7A) for Northern Blotting.

The radiographs in Figure 5.6 show the expression of *Dvl1* and *GAPDH* mRNA following adenoviral transfection. The top radiograph is representative of the blot following hybridisation with a ^{32}P labelled probe specific to murine *Dvl1*. This was the same probe as that used for the Southern Blot described (Figure 5.5). In the A549 cells *Dvl1* expression was negligible in untreated cells (moi 0). *Dvl1* levels rose with increasing moi of Ad5-MCMV-Dvl1; from moi 1 to 100. This was evident at both 48hrs and 72hrs post-transfection. In the case of the Rat 1 fibroblasts *Dvl1* was detectable even in untreated cells and increased with increasing moi; though not to

the same extent as in A549 cells. In both cell types the Dvl1 signal was present as a doublet at ~4kb. This was slightly larger than Dvl1 cDNA (3286bp). This larger size was most likely as a result of the additional poly-A tail associated with mRNA and not cDNA. The reason for the doublet was less clear. It is possible that the probe also picked up a spliced variant of Dvl1, though time constraints meant this was not investigated further during this thesis.

The lower radiograph in Figure 5.5 shows the same blot following stripping of the *Dvl1* probe and hybridisation with a second ^{32}P labelled probe specific to *GAPDH* (~500bp). This "house-keeping gene" was used to assess whether or not the same amount of RNA had been loaded in each lane, thereby validating the data presented above. The observed increases in *Dvl1* were therefore real. Although less than A549 cells, the level of *GAPDH* expression was equal between the Rat 1 fibroblast lanes, confirming that the observed increases in *Dvl1* in these cells were also genuine

As mentioned, *Dvl1* expression appeared to increase to a greater extent in A549 than Rat 1 cells with equivalent moi's of Ad5-MCMV-Dvl1. This may have been as a result of a relatively more efficient transfection of the A549 cells and/or related to the baseline expression of *Dvl1* in the two cell types. Notably, neither cell is of mouse origin (inserting murine *Dvl1*); though the strong homology of the Wnt pathway between species is established.

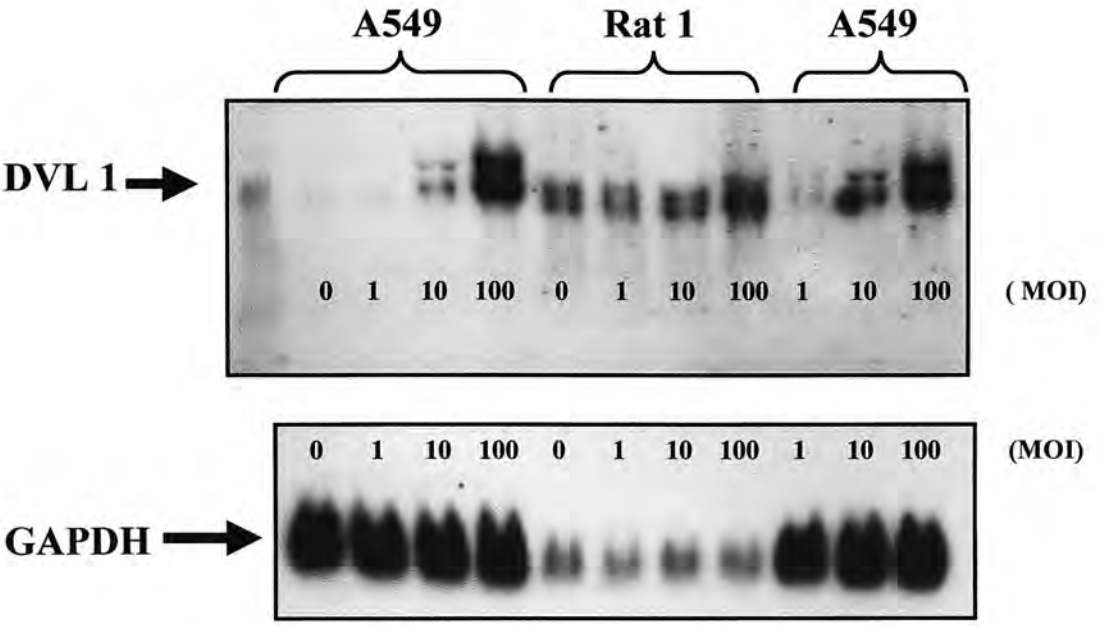

Figure 5.6: Northern 1 of Ad5-MCMV-Dvl1 *in vitro*

The samples in both radiographs are human A549 cells and Rat 1 fibroblasts treated with different concentrations of Ad5-MCMV-Dvl1. The numbering indicates the concentration, referred to as the multiplicity of infection (MOI) of adenovirus; ranging from 0 (no virus added) to 100. The first bracketed A549 cells were harvested (for RNA extraction) at 72hrs, as were the Rat 1 fibroblasts. The final three A549 lanes contained cells harvested at 48hrs.

The top caption is a radiograph following hybridisation with a ^{32}P labelled probe specific to murine *Dvl1*.The faint band in the marker lane immediately adjacent to the Dvl1 arrow (extreme left) is ~4kb.

The lower radiograph is of the same blot following stripping of the *Dvl1* probe and hybridisation with a second ^{32}P labelled probe specific to *GAPDH*.

Northern blot data confirmed that *Dvl1* mRNA is upregulated *in vitro* upon transfection with Ad5-MCMV-Dvl1. Since a control adenovirus had not been included in these preliminary experiments, it was necessary to repeat the transfections incorporating matched controls.

As before, the Ad5-MCMV-Dvl1was added at a range of moi's to A549 cells and Rat 1 fibroblasts. The extracted RNA (48hr time-point) was run on a formaldehyde gel (Figure 5.7A). This was then blotted overnight onto nitrocellulose membrane (Figure 5.7B) before hybridisation.

In Figure 5.8 (as in Figure 5.6) the two radiographs are of the same blot; the upper probed with murine *Dvl1* and the lower with *GAPDH*. As before *Dvl1* expression increased with the moi of Ad5-MCMV-Dvl1. Additionally adding the control adenovirus (Lac Z) at equivalent moi's to Ad5-MCMV-Dvl1 did not increase *Dvl1* levels. The effect therefore was specific to the Dvl1 virus. The GAPDH radiograph again confirmed equal RNA loading of both the A549 cells and Rat 1 fibroblasts; validating the Dvl1 data.

A sample of mouse brain RNA was also included in this northern blot (Figure 5.8) as a positive control; *Dvl1* is highly expressed in neural tissue. The *Dvl1* expression in this control was similar to that in the *in vitro* transfections. Significantly, a doublet was also noted with brain RNA. This finding was therefore not specific to adenovirally transfected cells.

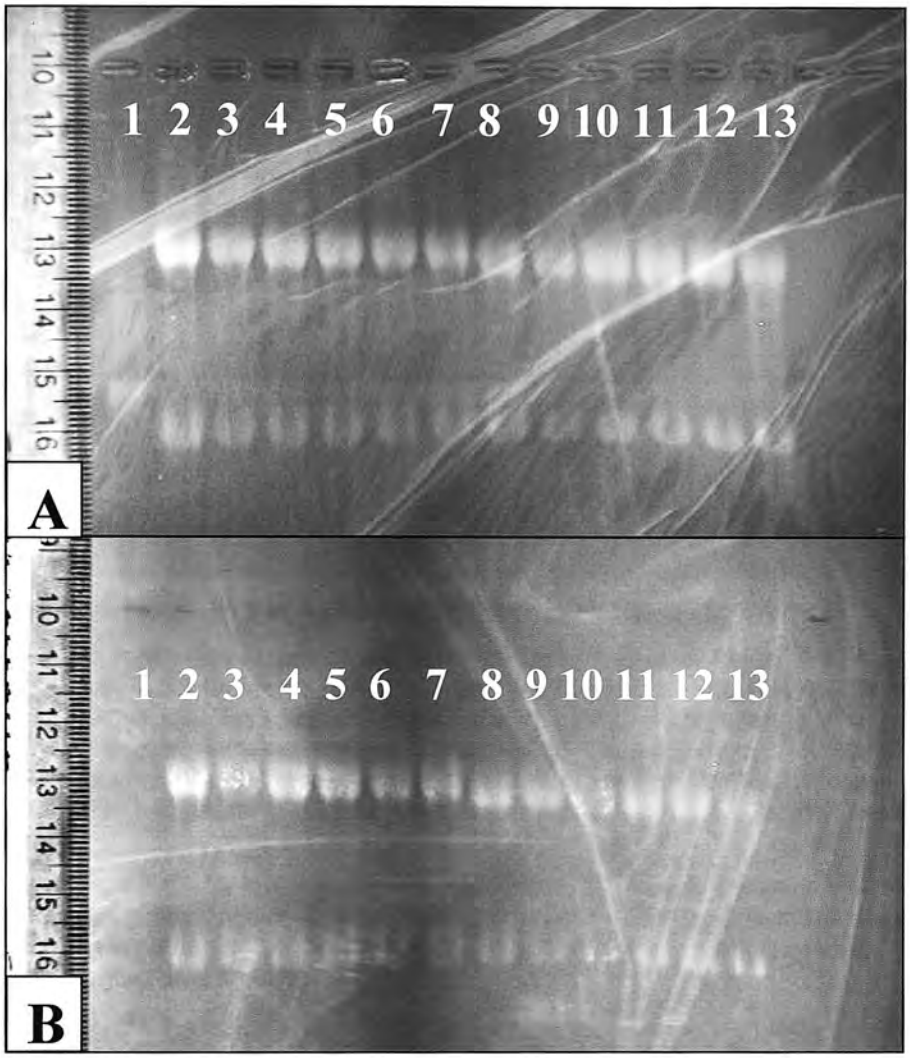

Figure 5.7: Northern 2 of Ad5-MCMV-Dvl1 *in vitro*: gel and membrane

A) Formaldehyde gel of RNA from A549 cells and Rat 1 fibroblasts treated with either Ad5-MCMV-Dvl1 or a control adenovirus expressing Lac Z. All cells were harvested at 48hrs. In lanes **2-13** the upper bands are 28S (4718bp) and the lower 18S (1874bp). Lane **1**: RNA ladder. Lanes **2-7**: A549 cells. Lanes **8-12**: Rat 1 fibroblasts. Lane **13**: RNA from mouse brain as a +ve control. (The lines across the gel are due to the cling film it was wrapped in for protection from any RNases)

B) Nitrocellulose membrane containing the same RNA samples as above, following blotting. This membrane was later hybridised with the specific probes before exposure to film (Figure 5.8).

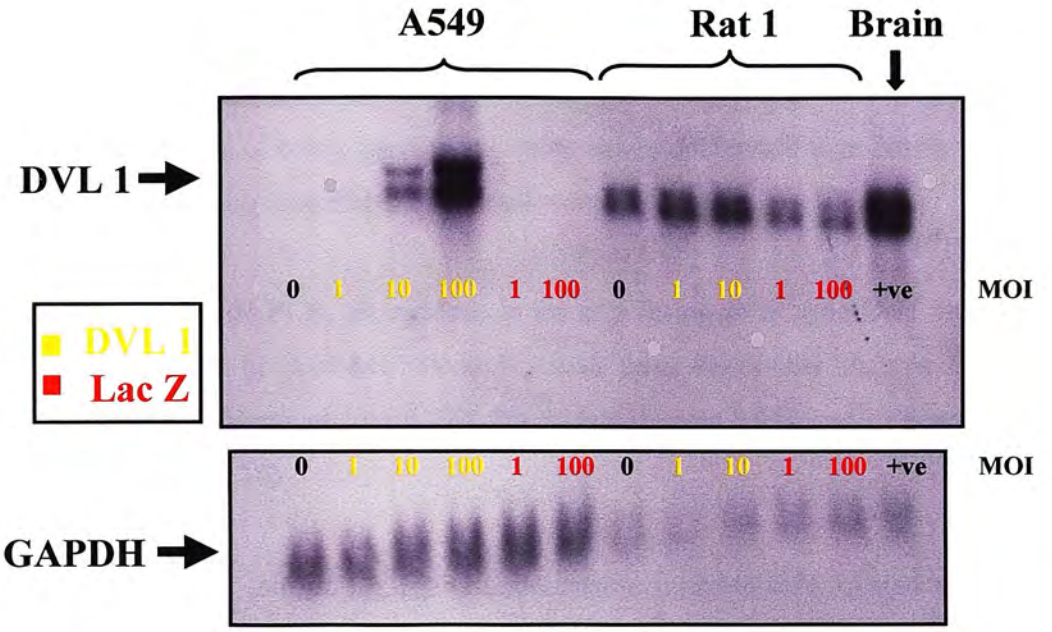

Figure 5.8: Northern 2 of Ad5-MCMV-Dvl1 *in vitro*: radiographs

The radiographs above are of the same samples shown in Figure 5.7. As in Figure 5.6 the numbering refers to the multiplicity of infection (MOI) of adenovirus used. These are also colour coded. The black numbering refers to cells not treated with adenovirus (0 moi) or to the positive control sample (mouse brain RNA). As in the key the yellow numbering refers to cells treated with the Dvl1 expressing adenovirus and the red to the Lac Z (control virus) virus.

As in Figure 5.6, the top caption is a radiograph following hybridisation with a ^{32}P labelled probe specific to murine *Dvl1*. The lower radiograph is of the same blot following stripping of the *Dvl1* probe and hybridisation with a second ^{32}P labelled probe specific to *GAPDH*.

Dvl1 mRNA expression was thus confirmed by Northern blotting. For comparison, samples transfected with adenovirus were also analysed by real time PCR. This has the advantage of being quicker and more easily performed than Northern blotting, as well as yielding immediate quantitative data.

Using real time PCR, an increase in the expression of murine *Dvl1* was observed in the presence of Ad5-MCMV-Dvl1, in a dose dependant manner in A549 cells (Figure 5.9A), mouse Swiss 3T3 fibroblasts (Figure 5.9B) and in a mouse Clara cell line (Figure 5.10).

In A549 cells murine Dvl1 was undetectable in those cells treated with the control adenovirus (dl70-3) and in untreated cells. As they are human cells this is not unexpected, though one would not have been surprised should the primers have picked up endogenous human *Dvl1* (full sequence unknown). With the addition of Ad5-MCMV-Dvl1 the levels of *Dvl1* rose steadily (Figure 5.9A).

In the mouse Swiss 3T3 fibroblasts a baseline level of *Dvl1* was detectable. This rose proportionally in response to the Dvl1 adenovirus with peak levels (moi 100 at 72hrs) at almost 40 fold greater than baseline (Figure 5.9B).

When Ad5-MCMV-Dvl1was added to a mouse Clara cell line (Figure 5.10) the level of *Dvl1* expression greatly increased with the higher moi's (100). As with the Swiss 3T3 fibroblasts *Dvl1* was detectable in untreated cells (this is not clear in Figure 5.10 due to the graph scale). The relative *Dvl1* mRNA level rose to ~ 240 fold at 24hrs and ~1300 fold at 48hrs, compared to expression in untreated cells.

The real time PCR and northern blot data therefore concur. It is clear that Ad5-MCMV-Dvl1 increases murine *Dvl1* mRNA levels *in vitro* in several cell lines.

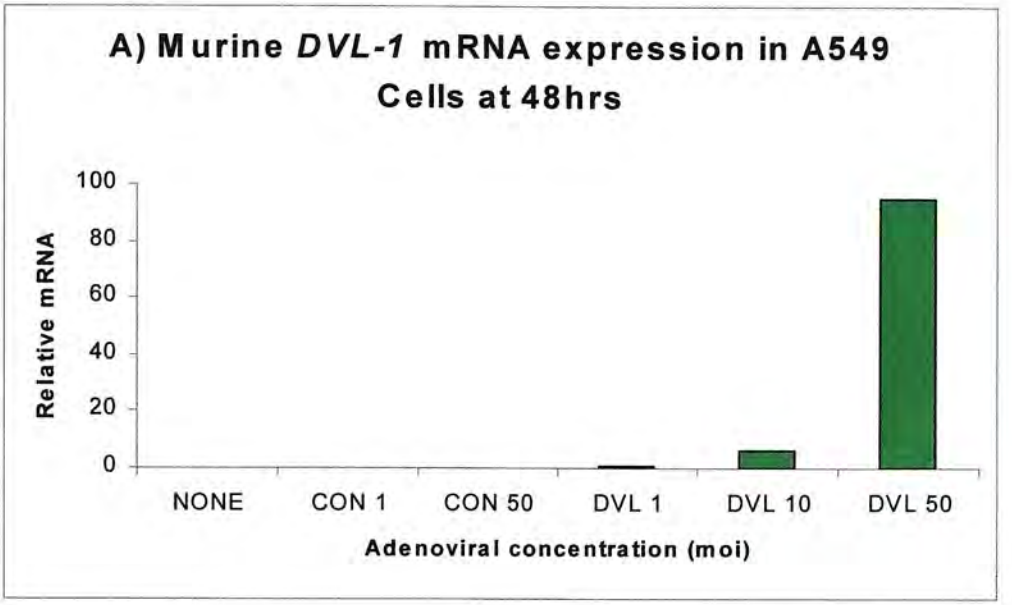

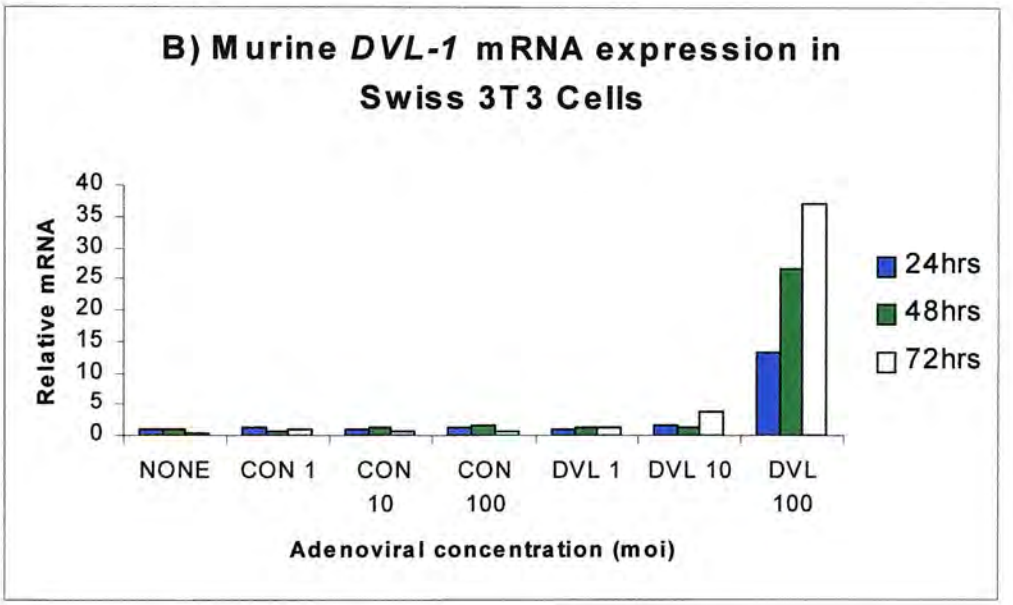

Figure 5.9: Ad5-MCMV-Dvl1 increases *Dvl1* mRNA expression *in vitro* as assessed by real time PCR

A) Relative *Dvl1* mRNA expression in A549 cells 48hrs after treatment with either Ad5-MCMV-Dvl1 or a control adenovirus (dl70-3). Each point is representative of an average of 2 identically treated samples. As murine *Dvl1* was undetectable in both the untreated (NONE) and control virus (CON) groups, remaining results are expressed relative to the expression in the DVL moi 1 (Dvl1) samples, which were given a value of 1(n=3) **B)** Relative *Dvl1* mRNA expression in mouse Swiss 3T3 fibroblasts after treatment with either Ad5-MCMV-Dvl1 or a control adenovirus (dl70-3). All values are expressed relative to the baseline expression in untreated (NONE) cells at 24hrs: given a value of 1. RNA levels are shown at 24hrs, 48hrs and 72hrs (n=3)

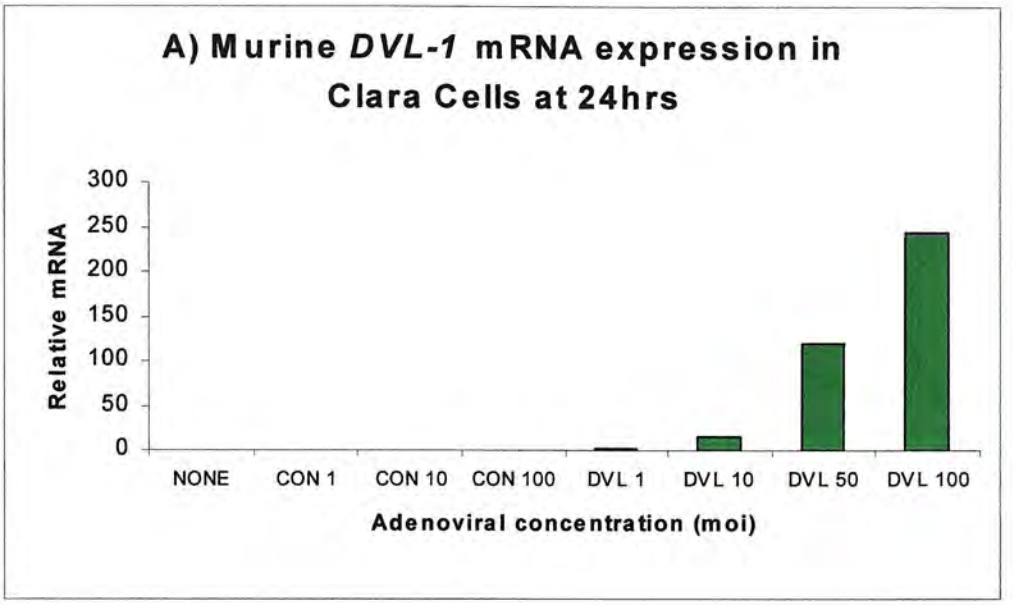

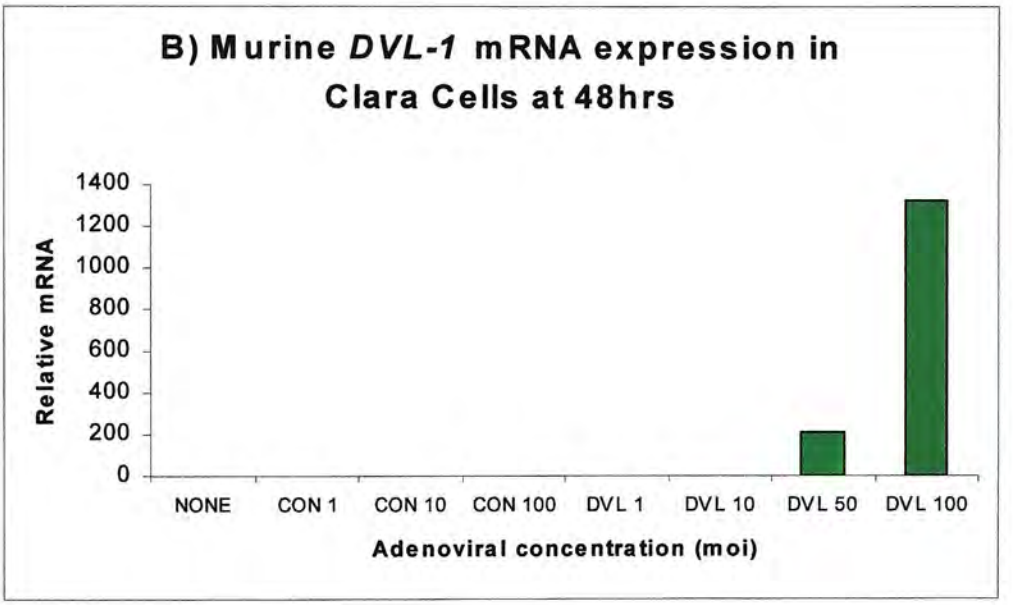

Figure 5.10: Ad5-MCMV-Dvl1 increases *Dvl1* mRNA expression in murine Clara Cells

Relative murine *Dvl1* mRNA expression in mouse Clara cells after treatment with either Ad5-MCMV-Dvl1 or a control adenovirus (dl70-3). At each time-point all values are expressed relative to the baseline expression in untreated (NONE) cells: given a value of 1. **A)** 24hrs and **B)** 48hrs (n=3)

5.4.2 AD5-MCMV-DVL1 RAISES DVL1 PROTEIN EXPRESSION *IN VITRO*

The data presented above demonstrates that Ad5-MCMV-Dvl1 induces *Dvl1* mRNA production *in vitro*. However it is possible for an adenovirus to produce mRNA without protein translation (Prof Gauldie, personal communication). It was therefore important to confirm whether or not Ad5-MCMV-Dvl1 also induces Dvl1 at protein level.

To address this A549 and murine Clara cells were transfected with Ad5-MCMV-Dvl1 or control adenovirus (dl70-3) at a range of moi's. At time-points from 6hrs to 72hrs cells were harvested and the cytoplasmic lysate separated, which also contained a large proportion of the membranous proteins. Following quantification equal amounts of each sample were loaded onto SDS-Page gels for Western blotting. The blots were then incubated with the anti-Dvl1 polyclonal antibody (Roel Nusse) before ECL development.

The addition of Ad5-MCMV-Dvl1 to both A549 and Clara cells lead to a dose-dependant rise in Dvl1 protein (Figure 5.11). Dvl1 was barely detectable in either untreated cells or in those treated with the control adenovirus. The Dvl1 antibody recognised several bands at ~80kDa, as had previously reported by others [567]. As already mentioned the antibody is known to cross-react with Dvl2, and it is not known if it recognises Dvl3.

Cytospins made from Clara cells transfected with Ad5-MCMV-Dvl1 or dl70-3, at moi's of 100, were stained immunocytochemically using the same anti-Dvl1 antibody. These clearly showed positive membrane staining in cells treated with the Dvl1 adenovirus but not in the control cells (Figure 5.11 A and B). This is a significant observation in that it is known that Dvl1 migrates to the cell membrane upon upregulation [186].

Therefore Ad5-MCMV-Dvl1 induces Dvl1 protein synthesis *in vitro*.

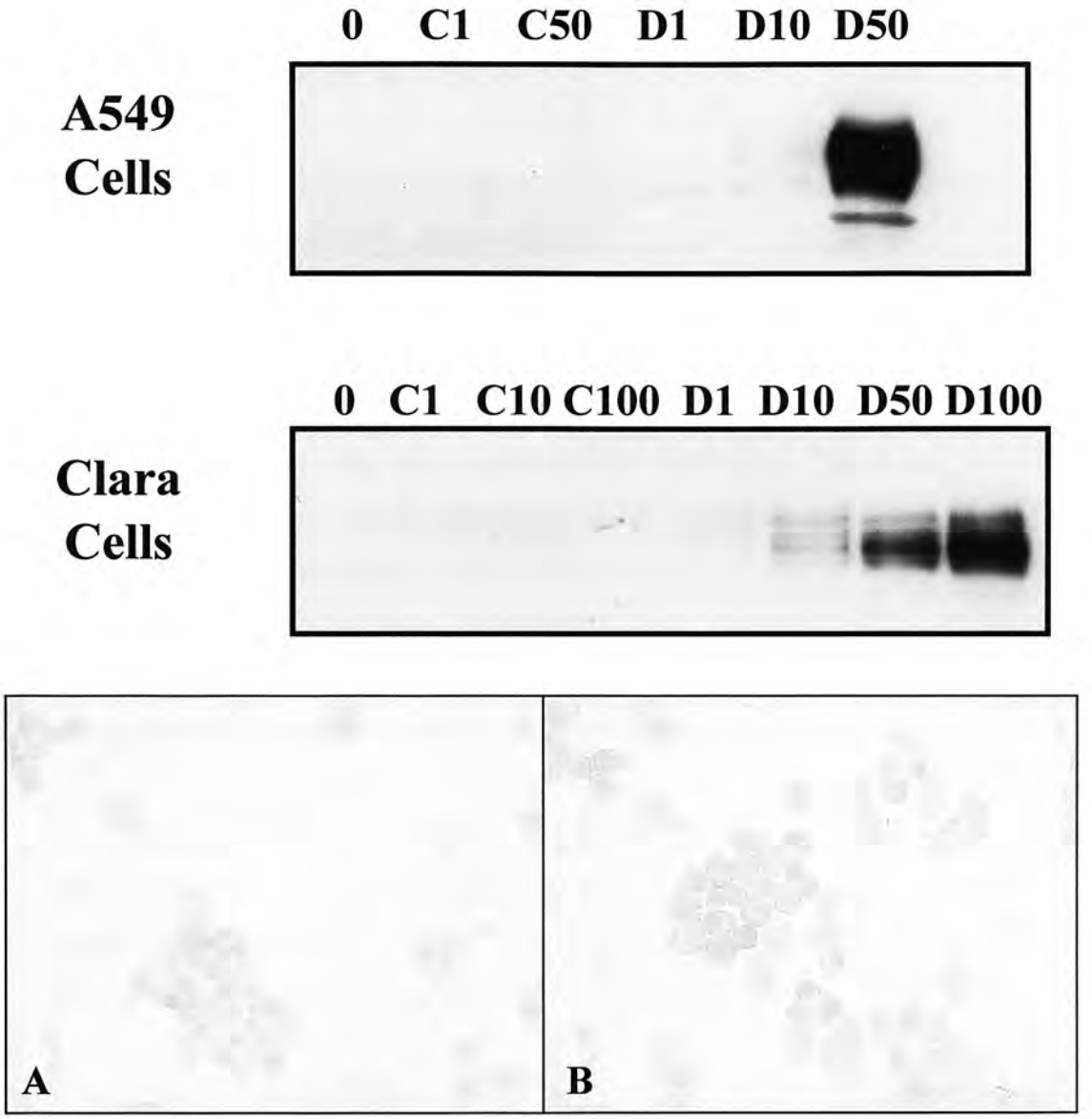

Figure 5.11: Ad5-MCMV-Dvl1 increases Dvl1 protein expression in A549 and Clara Cells

In each of the radiographs **C** represents control adenovirus (dl70-3) and **D**, Ad5-MCMV-Dvl1. The numbering is indicative of the moi of virus used. **0** indicates untransfected cells.

The top radiograph is a western blot of transfected A549 cells and the lower of transfected Clara cells incubated with the anti-Dvl1 antibody. In both cases the visible bands are ~80kDa; correct size for Dvl1 (n=3)

The images **A** and **B** are cytospins of transfected Clara cells stained immunocytochemically with the anti-Dvl1 antibody. Positive staining is brown against a haemotoxylin (blue) counterstain. **A)** Cells transfected with control adenovirus (dl70-3) at a moi of 100. **B)** Cells transfected with Ad5-MCMV-Dvl1 moi 100 (n=3)

5.4.3 DVL1-AD RAISES CYTOSOLIC BETA-CATENIN LEVELS IN A549 CELLS BUT NOT IN CLARA CELLS

As described in more detail in chapter 1, β-Catenin levels are known to rise in the presence of Wnt signalling, probably through protection from ubiquitination [170]. As a result, increases in β-Catenin are regarded as indicative of active Wnt signalling, and dishevelled (Dvl) upregulation. However the baseline expression of β-Catenin in the cell membrane far exceeds that in the cytosol, and it is mainly cytosolic β-catenin which is seen to rise with upregulation of the Wnt pathway. Therefore, looking at cellular β-Catenin levels as a whole, any increase in the cytosolic component may well be masked by the large stable membranous pool. To address this issue other groups have separated the membranous and cytosolic pools (subcellular fractionization) to allow β-Catenin to be analysed in separately [251]. These fractions were separated in a similar manner to that described in chapter 2.

No difference in either membranous or cytosolic β-Catenin was seen between Clara cells transfected with Ad5-MCMV-Dvl1, control adenovirus (dl70-3) or untransfected cells (Figure 5.12A). It would, therefore, appear that upregulation of Dvl1 in murine Clara cells does not result in increased β-catenin stabilization.

However this was not the case in A549 cells. Membranous β-Catenin levels were greater in cells treated with Ad5-MCMV-Dvl1 than in control samples (control virus or untransfected) (Figure 5.12B). In the figure shown, expression appears to be greater in control treated cells than in untransfected. This was not a consistent finding. More significantly the cytosolic β-catenin levels were greater in Ad5-MCMV-Dvl1 transfected cells (Figure 5.12B; upper bands). This would imply that, unlike in Clara cells, Dvl1 upregulation increases β-catenin stabilization in A549 cells. The nuclear β-Catenin levels in A549 cells were unaffected by Dvl1 upregulation (Figure 5.12C). The slightly weaker band seen in the untransfected sample (**0**) was due to less protein loading as confirmed by Ponceau S staining.

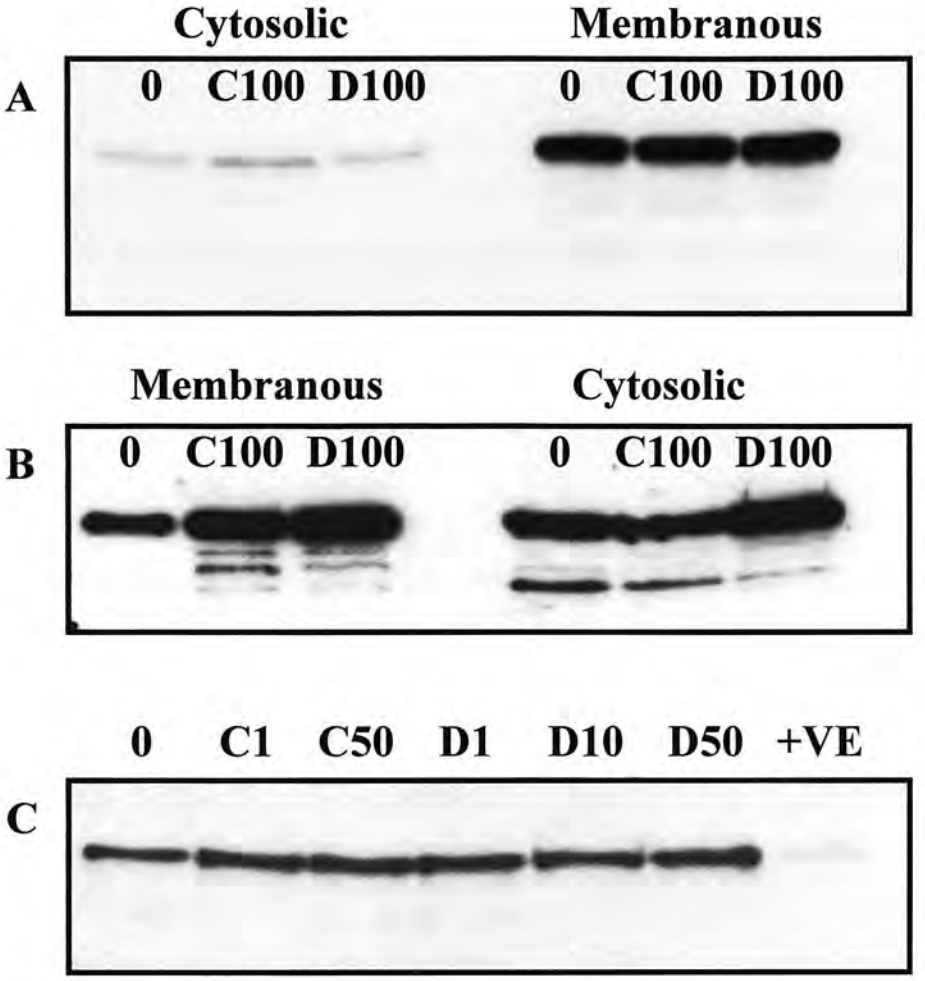

Figure 5.12: Ad5-MCMV-Dvl1 and β-catenin levels

In each of the radiographs **C** represents control adenovirus (dl70-3) and **D**, Ad5-MCMV-Dvl1. The numbering is indicative of the moi of virus used. Membranous and cytosolic fractions are labelled accordingly. **0** indicates untransfected cells. The positive β-catenin bands were consistently found to be at the correct predicted size of ~92kDa (n=3)

A) β-catenin western blot of membranous and cytosolic fractions of transfected Clara cells.

B) β-catenin western blot of membranous and cytosolic fractions of transfected A549 cells.

C) β-catenin western blot of nuclear fractions of transfected A549 cells. **+ve** indicates positive control lysate; Hela cell extract provided with the antibody

5.4.4 DVL1-AD AND CELL PROLIFERATION

The aim of producing an adenovirus expressing Dvl1 was to upregulate the Wnt signalling pathway. As increased Wnt signalling is normally associated with greater cell proliferation it was important to assess the effect of Ad5-MCMV-Dvl1 on proliferation. This was particularly relevant in view of recently published data suggesting Dvl1 overexpression results in increased cellular apoptosis, not proliferation [262].

The appearance of murine Clara cells transfected with Ad5-MCMV-Dvl1 differed from control wells in that, from 24hrs post-transfection, there were consistently more "rounded up" and loosely adherent cells in the presence of Dvl1 (Figure 5.13 A+B). These cells were distinct from the main adherent monolayer and were easily displaced. Unfortunately, possibly because of their fragility, it was not possible to make cytospins of these cells to look at their morphology more closely. Many were lost even during *in situ* Hoechst staining (Figure 5.13D).

In Figure 5.13 (C and D) a few of these loosely adherent cells are shown as they appeared under light microscopy and following staining with Hoechst. These cells appeared to be apoptotic under light microscopy, with evidence of cyoplasmic shrinkage and blebbing of membranes. With Hoechst staining, the nuclei were condensed and intensely stained in keeping with apoptosis. However, as already mentioned, very few of these cells remained following staining which made general observations about the rate of apoptosis very difficult. In addition, particularly when 2 such cells were adjacent as in Figure 5.13 (arrow), it was difficult to discriminate between apoptotic and post-mitotic cells. Thus there was no conclusive evidence that the observed loosely adherent cells were apoptotic, and therefore that Dvl1 increased the percentage of apoptotic cells. It was also possible that the loosely adherent cells were due to Dvl1 overexpression driving increased proliferation with subsequent cell detachment from a confluent cell monolayer.

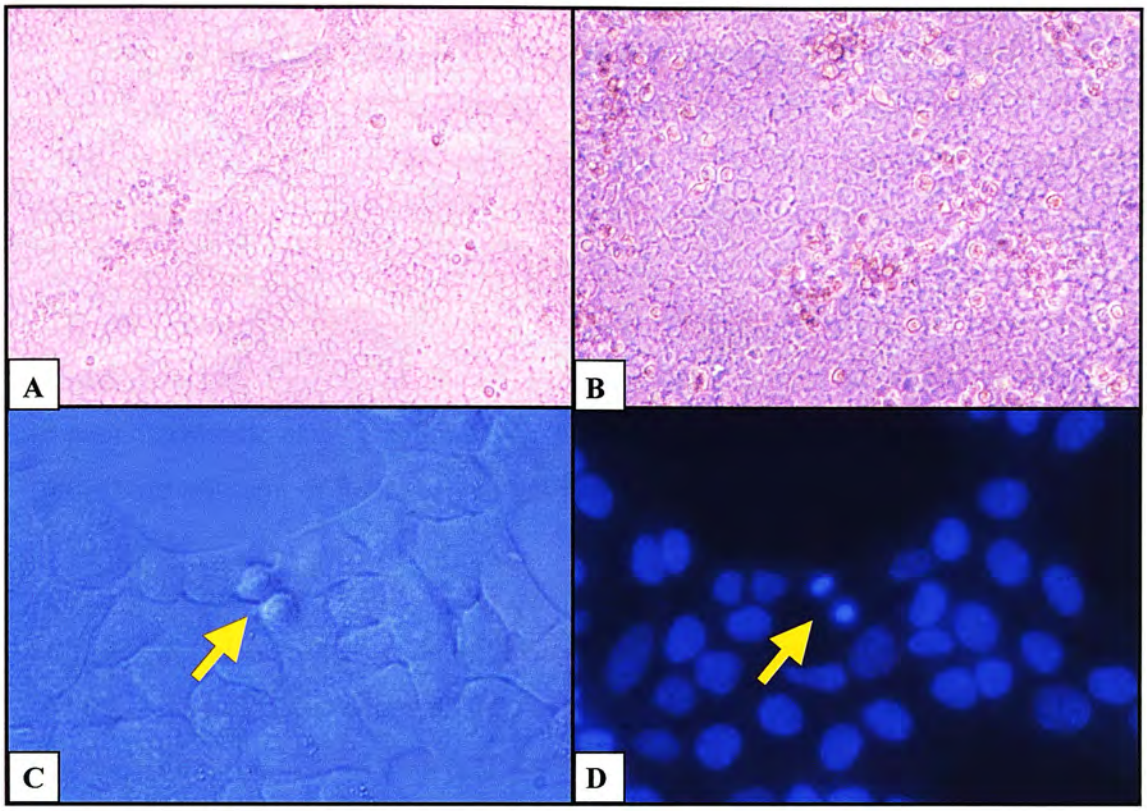

Figure 5.13: Ad5-MCMV-Dvl1 and Clara cell morphology

A) Clara cells transfected with control (dl 70-3) adenovirus; moi 100

B) Clara cells transfected with Ad5-MCMV-Dvl1; moi 100

C) Clara cells transfected with Ad5-MCMV-Dvl1; moi 100

D) Clara cells transfected with Ad5-MCMV-Dvl1; moi 100; Hoechst stain

(n=3)

To investigate the effects of Dvl1 expression on cell proliferation/survival more quantitatively a number of methods were employed. These included cell counting following trypan blue exclusion, tritiated thymidine incorporation and the colorimetric One Solution Cell Proliferation Assay (Promega).

There appeared to be no difference in Clara cell proliferation between transfections with Ad5-MCMV-Dvl1 or dl70-3, as assayed by both thymidine incorporation and the colorimetric assay (Figure 5.14). These results were unaffected by variations in the concentration of foetal calf serum in the post-transfection culture medium, from 0% to 5%.

There was also no detectable difference in A549 proliferation between transfections with Ad5-MCMV-Dvl1 or dl70-3, as assessed by cell counts and the colorimetric assay (Figure 5.15). No variation was noted at time-points from 8hrs to 72hrs. Data shown is representative of the pattern seen at all time-points for both cell types.

These observations were consistent regardless of the cell confluency at transfection, which was varied between 50-80%, thus controlling for growth arrest through contact inhibition.

Therefore, as measured by the chosen assays, Dvl1 adenoviral expression did not alter Clara or A549 cell proliferation.

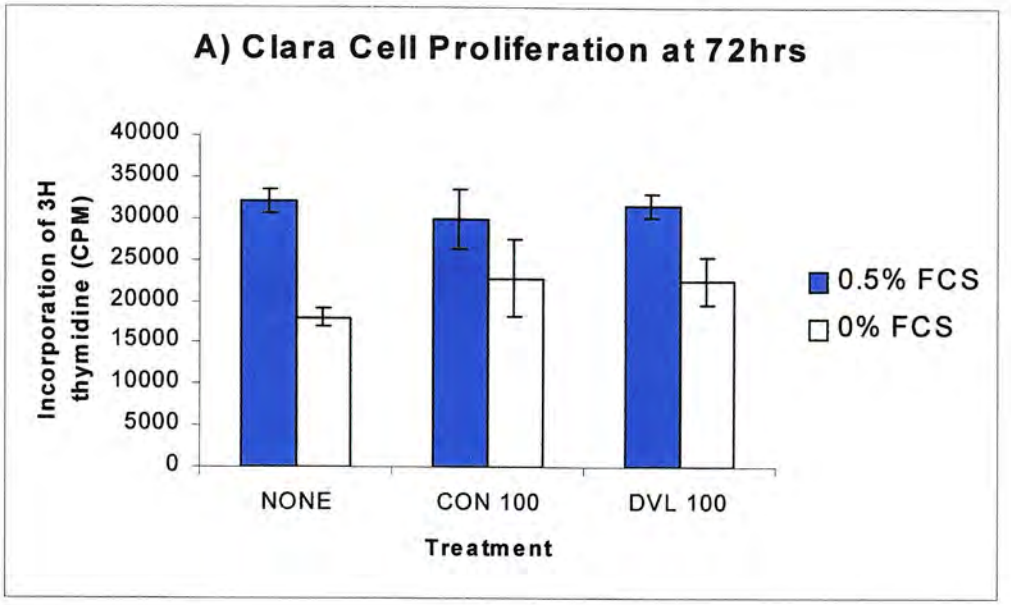

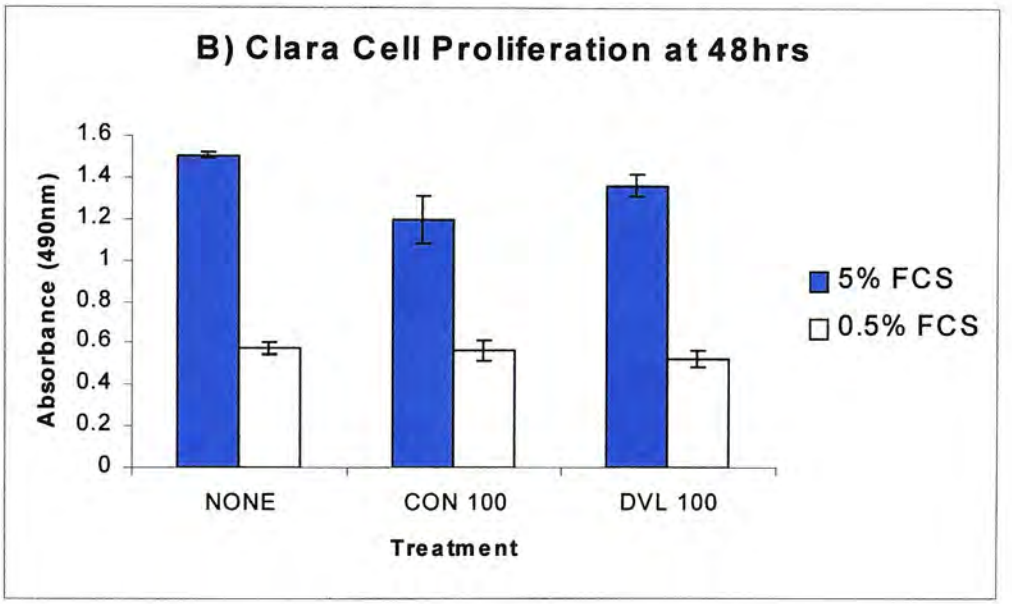

Figure 5.14: Ad5-MCMV-Dvl1 and Clara cell proliferation

In each of the above cells were transfected with dl 70-3 (CON), Ad5-MCMV-Dvl1 (DVL) or not transfected (NONE). Each virus was used at a moi of 100.

A) Clara cell proliferation as measured by tritiated thymidine incorporation at 72hrs post-transfection. The cells were cultured in media containing either 0.5% or 0% foetal calf serum (FCS) following transfection. Each point is the mean of triplicate wells. **B)** Clara cell proliferation as measured by One Solution Cell Proliferation Assay (Promega) at 48hrs post-transfection. The cells were cultured in media containing either 5% or 0.5% FCS following transfection. Each point is the mean of triplicate wells (n=3)

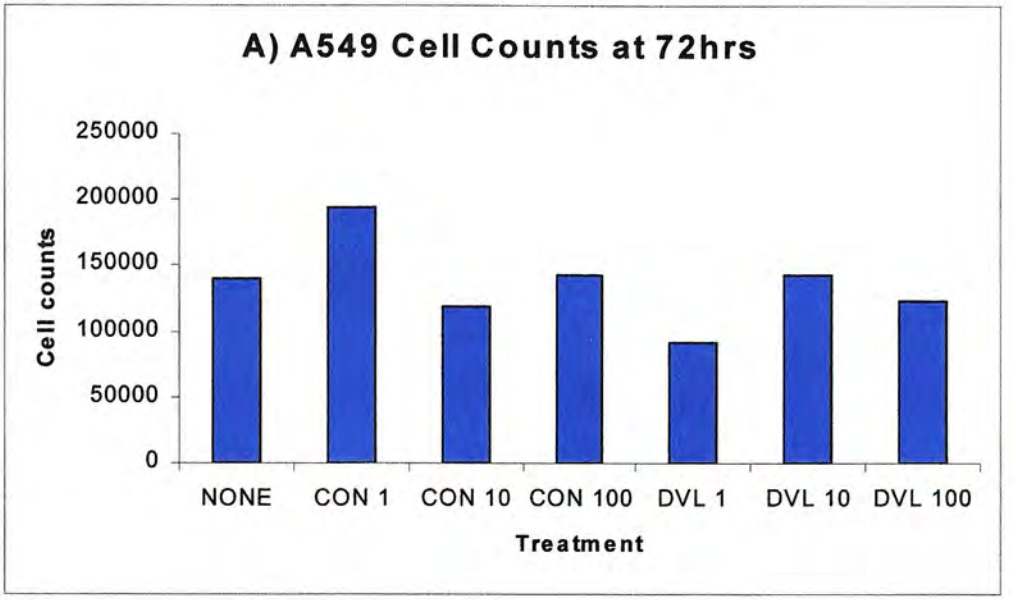

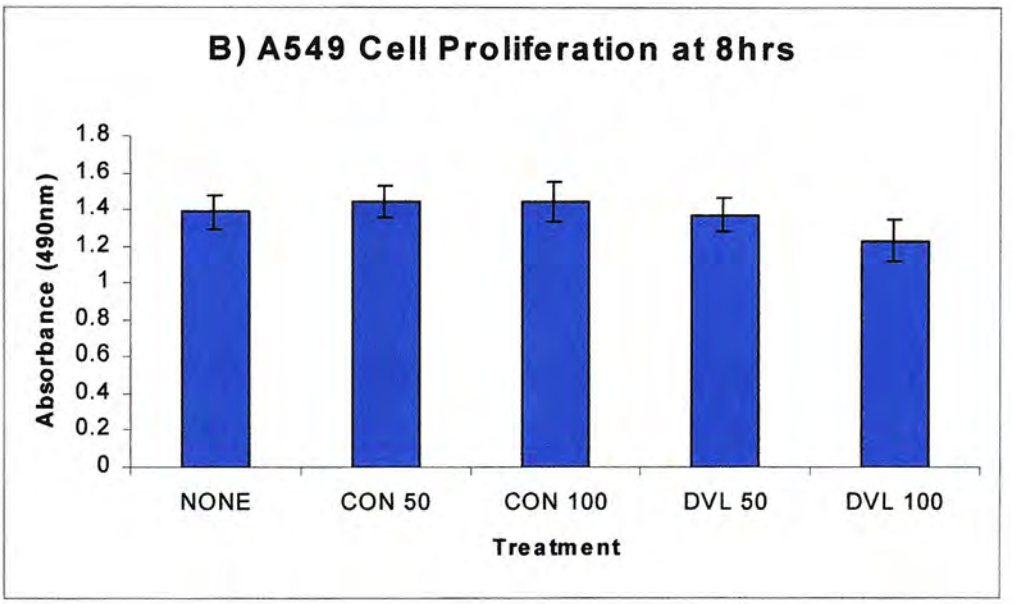

Figure 5.15: Ad5-MCMV-Dvl1 and A549 cell proliferation

In each of the above cells were transfected with dl 70-3 (CON), Ad5-MCMV-Dvl1 (DVL) or not transfected (NONE). Moi's varied from 1-100 as stated eg. CON 50 represents dl 70-3 at a moi of 50.

A) A549 cell counts (duplicates) by trypan blue exclusion at 72hrs post-transfection.

B) A549 cell proliferation as measured by One Solution Cell Proliferation Assay (Promega) at 8hrs post-transfection. Each point is the mean of triplicate wells.

(n=3)

5.4.5 DVL1-AD AND THE SHH SIGNALLING PATHWAY

Wnt signalling is a direct target of Shh signalling [3]. It has also been suggested, largely based studies using *Drosophila*, that Wnt signalling itself leads to an increase in Shh signalling [238,239], probably in a paracrine or autocrine manner. Assuming that Dvl1 upregulation mimics Wnt signalling, these experiments were designed to determine if increased Dvl1 expression would lead to upregulation of the Shh pathway.

Shh protein was not detectable either in A549 or Clara cells whether they were untransfected, treated with Ad5-MCMV-Dvl1 or control adenovirus, dl70-3 (Figure 5.16). The positive control sample (mouse brain) did contain detectable Shh confirming that the anti-Shh antibody worked. This was reinforced in a further Western blot in which the same antibody recognised the recombinant amino-terminus Shh peptide (Figure 5.16), used in chapter 4. In this case the stronger band was ~19kDa (arrow **B**) in keeping with N-Shh, and a weaker band was noted at ~45kDa (arrow **A**) consistent with full length Shh.

In Clara cells mouse *Shh* mRNA was detectable even in the untreated cells. Expression did not alter in the presence of either adenovirus (data not shown). This could not be verified in A549 cells, as suitable human *Shh* real time PCR primers were unavailable.

Expression of mouse *Ptc* mRNA was not significantly changed by transfection with either Ad5-MCMV-Dvl1 or dl 70-3 (Figure 5.17), based on the assumption that only differences >2 fold are significant in real time PCR analysis [557,558] as discussed further in Chapter 4. This was evident in (**A**) Clara cells and (**B**) Swiss 3T3 fibroblasts throughout time-points from 24 to 72hrs. Likewise, human *Ptc* mRNA expression was unaltered in A549 cells (not shown). There was therefore no evidence that Ad5-MCMV-Dvl1 upregulates Shh signalling.

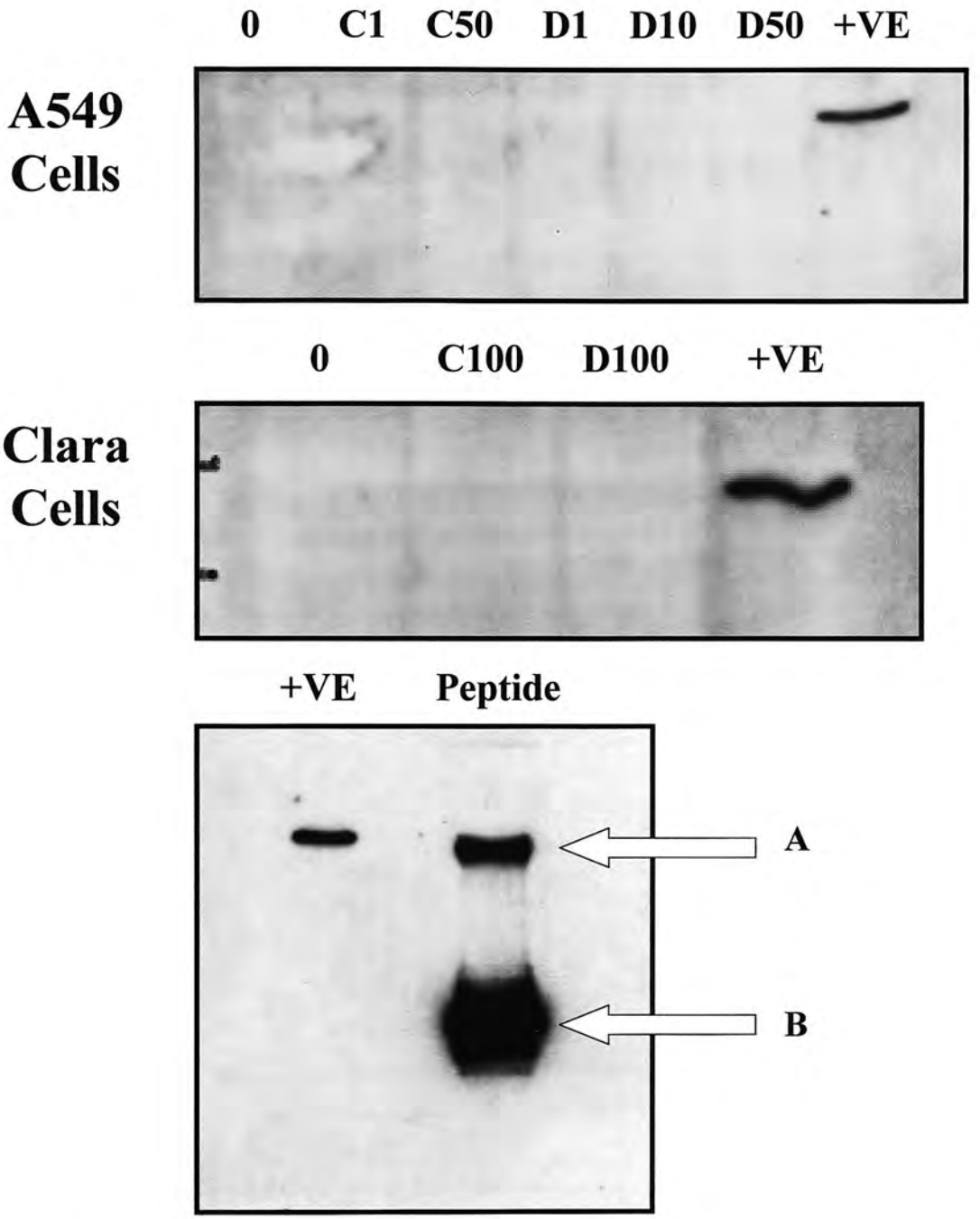

Figure 5.16: Ad5-MCMV-Dvl1 and Shh protein expression

In each of the radiographs **C** represents control adenovirus (dl70-3) and **D**, Ad5-MCMV-Dvl1. The numbering is indicative of the moi of virus used. The +ve control used was mouse brain lysate; Dvl1 is highly expressed in neural tissue. The top 2 radiographs show expression of Shh in A549 and clara cells transfected with adenovirus; 48hrs post-transfection. The bottom radiograph shows the recombinant Mouse Shh amino-terminal peptide (N-Shh) as used in chapter 4. Arrow **A** is ~45kDa, the size of full length Shh. Arrow **B** is ~19kDa, the size of the active amino-terminal Shh peptide (n=3)

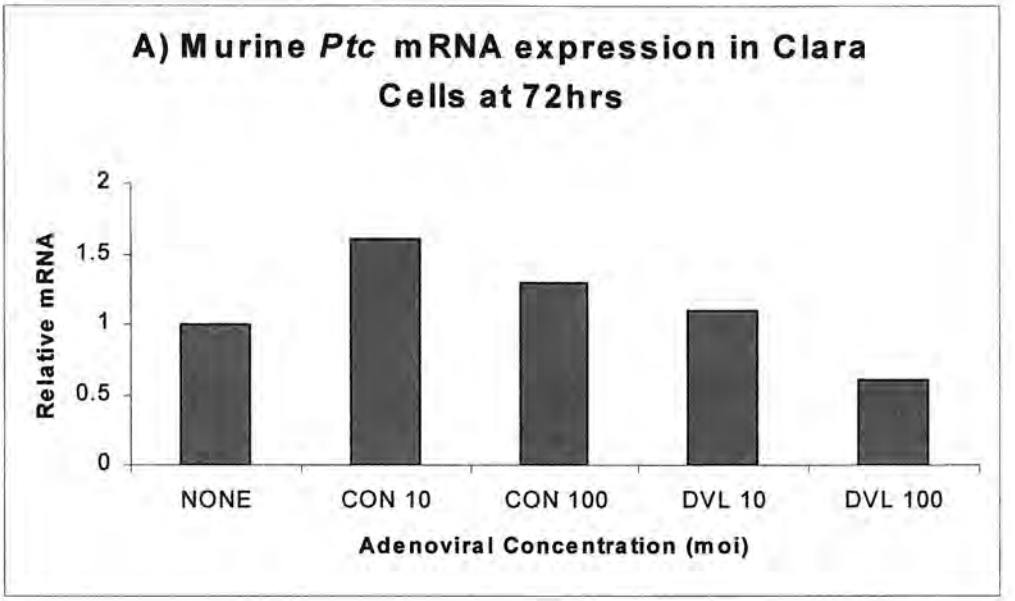

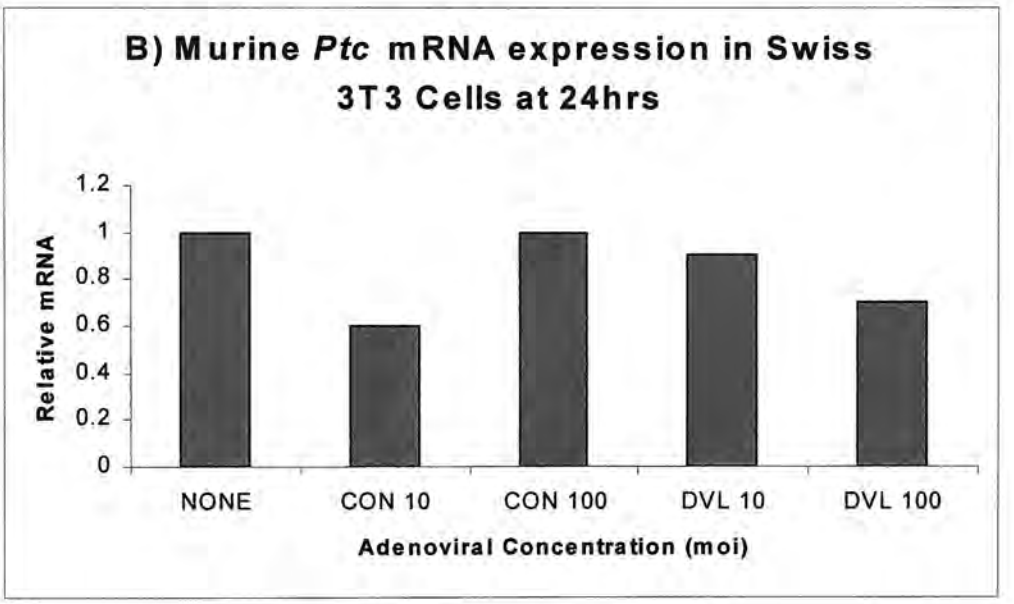

Figure 5.17: Ad5-MCMV-Dvl1 and *Ptc* mRNA expression

In the above graphs each point is an average of duplicate wells; hence no error bars. NONE indicates untransfected cells, CON: cells transfected with the control adenovirus (dl 70-3) and DVL: cells transfected with Ad5-MCMV-Dvl1. The numbering is indicative of moi used. In each graph expression is relative to that in untreated cells (NONE), which is given a value of 1 (n=3)

A) Relative murine *Ptc* mRNA expression in Clara cells at 72hrs as assessed by real time PCR.

B) Relative murine *Ptc* mRNA expression in Swiss 3T3 cells at 24hrs as assessed by real time PCR.

5.5 Effects of the Dvl1 Adenovirus *in vivo*

The Ad5-MCMV-Dvl1 was made to allow both *in vitro* and *in vivo* expression of Dvl1. As the hypothesis was centred on the Wnt pathway playing a role in ILD, overexpression of Dvl1 in mouse lungs was a major objective.

Unlike *in vitro* work the number of "target cells" for an adenovirus cannot be controlled when performing *in vivo* experiments. The treatments are therefore not expressed as multiplicities of infection (moi); rather as plaque forming units (pfu). The titres of adenovirus used for *in vivo* mouse lung work vary between different groups and different adenovirus constructs. The doses chosen in these experiments were based on preliminary experiments trying a range of doses from $3x10^7$ to $8x10^8$ pfu.

5.5.1 THE DVL1 ADENOVIRUS RAISES *DVL1* RNA EXPRESSION *IN VIVO*

As the *in vitro* adenovirus work demonstrated, Northern blot data and real time PCR analysis correlate well for *Dvl1* expression. Therefore real time PCR was used to assess *Dvl1* mRNA expression *in vivo*.

A single intra-tracheal instillation of sterile phosphate buffered saline (PBS), control dl70-3 adenovirus or Ad5-MCMV-Dvl1 was given in a final volume of 40µl. The mice were killed, and lungs removed for RNA extraction, at time-points ranging from 1 to 7 days. The data shown illustrates relative mRNA expression in these mouse lungs. In Figure 5.18 and 5.19A the viral dose given was $3x10^8$ pfu.

The administration of Ad5-MCMV-Dvl1 resulted in greater *Dvl1* mRNA expression than either control (dl 70-30) adenovirus or PBS alone (Figure 5.18). This was more notable at (**A**) 24hrs than (**B**) 72hrs post-instillation. However, the level of expression varied greatly between different animals receiving the same treatment.

This may have been due to a number of factors including the general well-being of the individual mouse, its response to the adenovirus and, more directly, the division of the lungs from each treated mouse for RNA extraction, protein extraction and immunohistochemistry. As a result, the data obtained from lung tissue may vary depending on the portion of lung chosen, and the distribution of the instilled virus.

Even with this experimental variation the *Dvl1* expression in individual mice was consistently higher in the Ad5-MCMV-Dvl1 treated group (Figure 5.18). Averaging the data from each treatment group revealed a trend toward greater *Dvl1* expression in the Ad5-MCMV-Dvl1 group (Figure 5.19A). However, it must be stressed that error bars were not included in this averaged data because of the wide variation, particularly in the Ad5-MCMV-Dvl1 group.

Comparing the lung *Dvl1* expression in Ad5-MCMV-Dvl1 ($8x10^8$ pfu) treated mice alone, *Dvl1* mRNA levels tended to be greater at 3 days post-instillation than 7 days (Figure 5.19B). This is consistent with reported expression made using a similar adenoviral construct [568]. Again there was a great deal of variation between animals. The group averages were calculated to reveal the trend (Figure 5.19B). Significantly, the relative *Dvl1* mRNA expression (compared with PBS controls) at this higher dose of Ad5-MCMV-Dvl1 ($8x10^8$ pfu) was much greater than seen with the lower dose ($3x10^8$ pfu) (Figure 5.18), up to in excess of 100 fold with the former against little more than 10 fold with the latter.

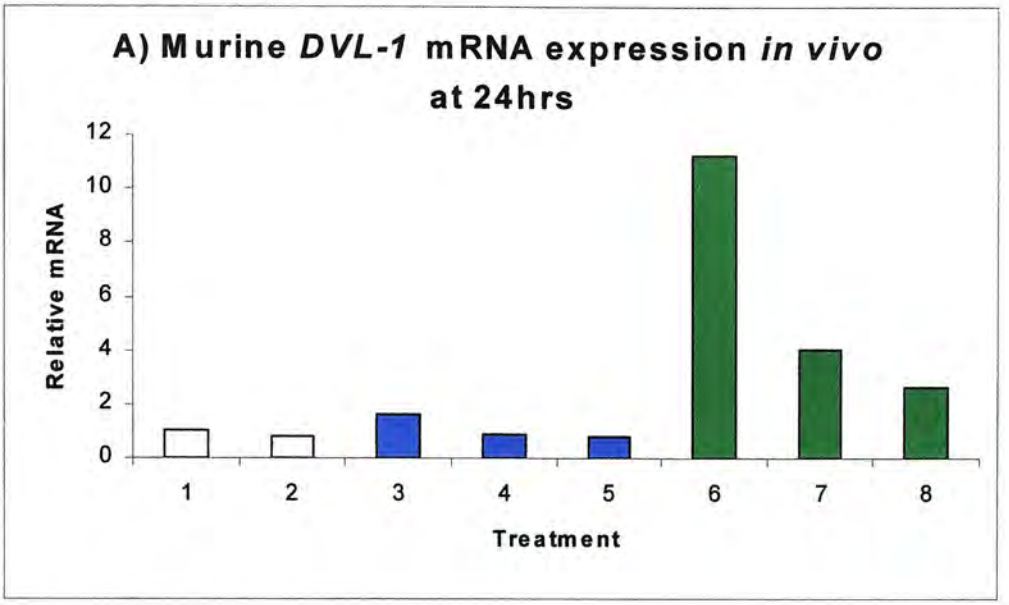

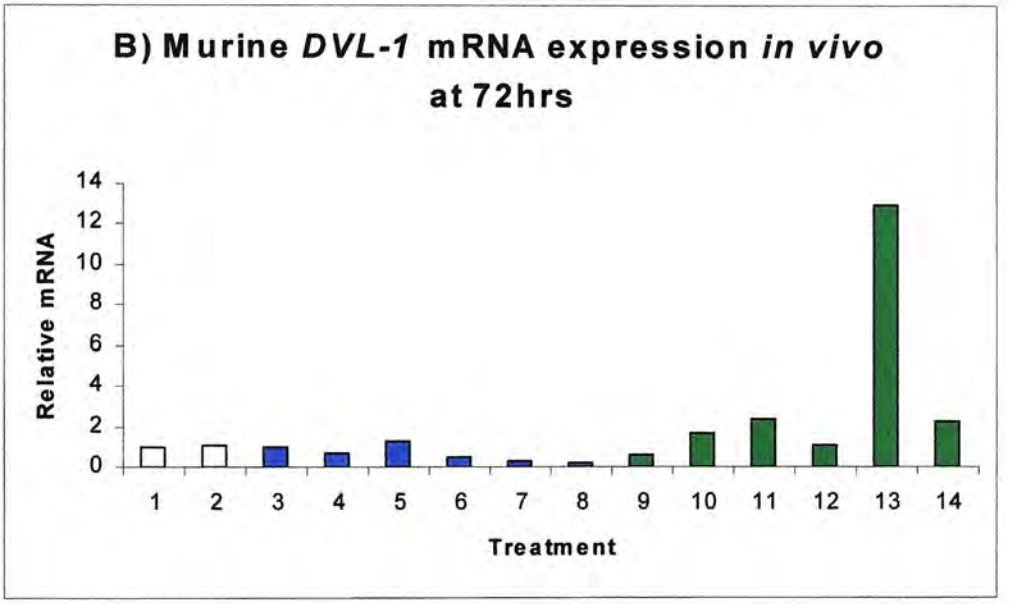

Figure 5.18: Ad5-MCMV-Dvl1 increases *Dvl1* mRNA expression *in vivo* as assessed by real time PCR

Relative *Dvl1* mRNA expression in BALB/c mouse lungs following intra-tracheal instillation of PBS (white bars), control dl 70-3 adenovirus (blue bars) or Ad5-MCMV-Dvl1 (green bars). Both viruses were given at a dose of $3x10^8$ pfu. Each bar represents an individual mouse. All RNA levels are expressed relative to mouse 1 (for each time-point), which is itself given a value of 1. Each point is an average of duplicate wells.

A) Relative *Dvl1* expression at 24hrs post-instillation

B) Relative *Dvl1* expression at 72hrs post-instillation

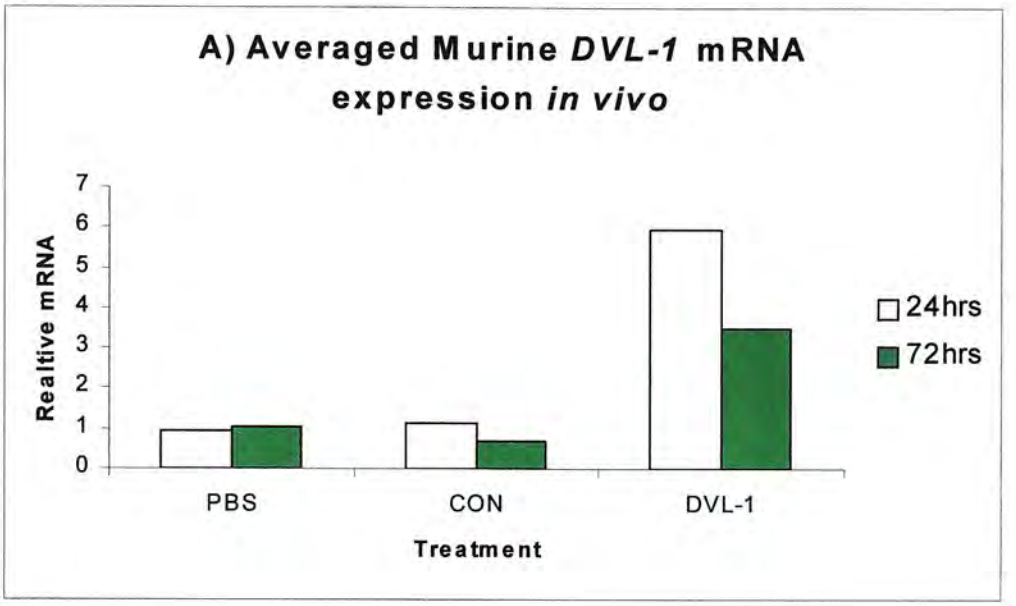

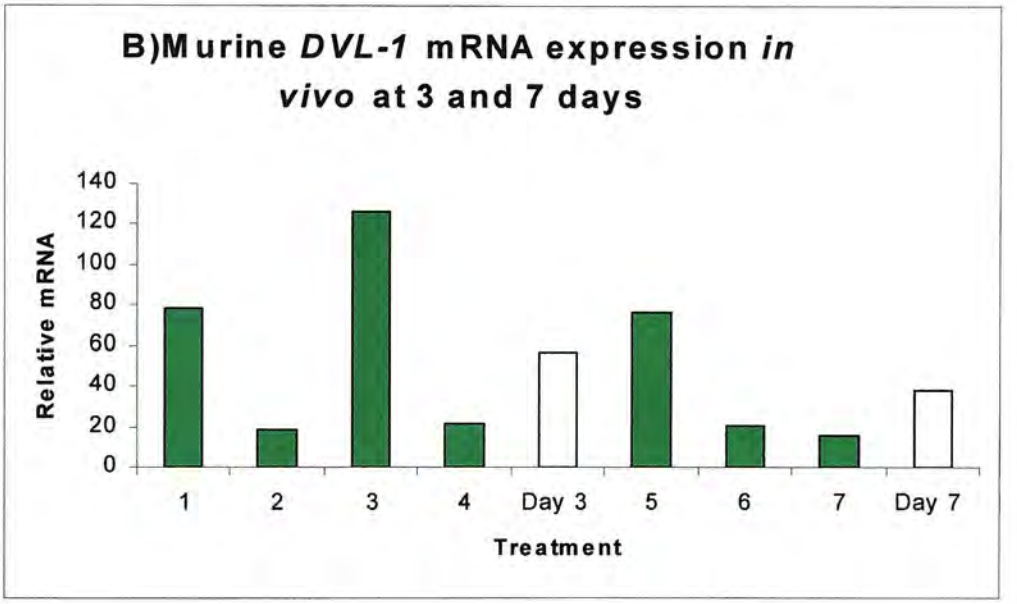

Figure 5.19: Ad5-MCMV-Dvl1 increases *Dvl1* mRNA expression *in vivo* as assessed by real time PCR

A) Averaged *Dvl1* mRNA expression 24hrs and 72hrs post-instillation of PBS, dl70-3 (CON) or Ad5-MCMV-Dvl1 (DVL). Data is averaged individual BALB/c mouse lung data for each treatment; summary of data in Figure 5.18

B) Relative *Dvl1* mRNA expression in BALB/c mouse lungs following intra-tracheal instillation of Ad5-MCMV-Dvl1at a dose of $8x10^8$ pfu. Green bars represent individual mice at 3 days (**1-4**) and 7 days (**5-7**) post-instillation. Each is an average of duplicate wells and all values are relative to *Dvl1* expression 3 days following PBS treatment: given a value of 1 (not included in graph shown). White bars represent averaged individual mouse expression at each time-point i.e green bar data averaged.

5.5.2 THE DVL1 ADENOVIRUS RAISES DVL1 PROTEIN EXPRESSION *IN VIVO*

It was important to show that Ad5-MCMV-Dvl1 increased Dvl1 expression at protein as well as mRNA level *in vivo*. In order to address this PBS, Ad5-MCMV-Dvl1 or control adenovirus (dl 70-3) were instilled intra-tracheally into BALB/c mice. Portions of lungs from the same mouse were often divided for RNA, protein and immunohistochemistry. In the data shown 30μg of each sample was loaded onto the original SDS gel for Western blotting.

At 3 days DVL-1 protein was detected at the highest dose of Ad5-MCMV-Dvl1 ($8x10^8$ pfu) but not at a lower dose ($3x10^8$ pfu), (Figure 5.20A). Importantly, it was not detectable at equivalent doses of the control virus. It was also evident that Dvl1 protein levels were higher at 3 days than at 7 days post-instillation; again with the highest dose of Ad5-MCMV-Dvl1 ($8x10^8$ pfu), (Figure 5.20B). This peak expression correlates with previous work [568], and indeed with the RNA expression data (Figure 5.19B). In terms of the doses required it would appear that the lower $3x10^8$ pfu dose of Ad5-MCMV-Dvl1 is sufficient to increase *Dvl1* mRNA, but does not cause detectable changes in protein expression; at least as assessed by Western blotting.

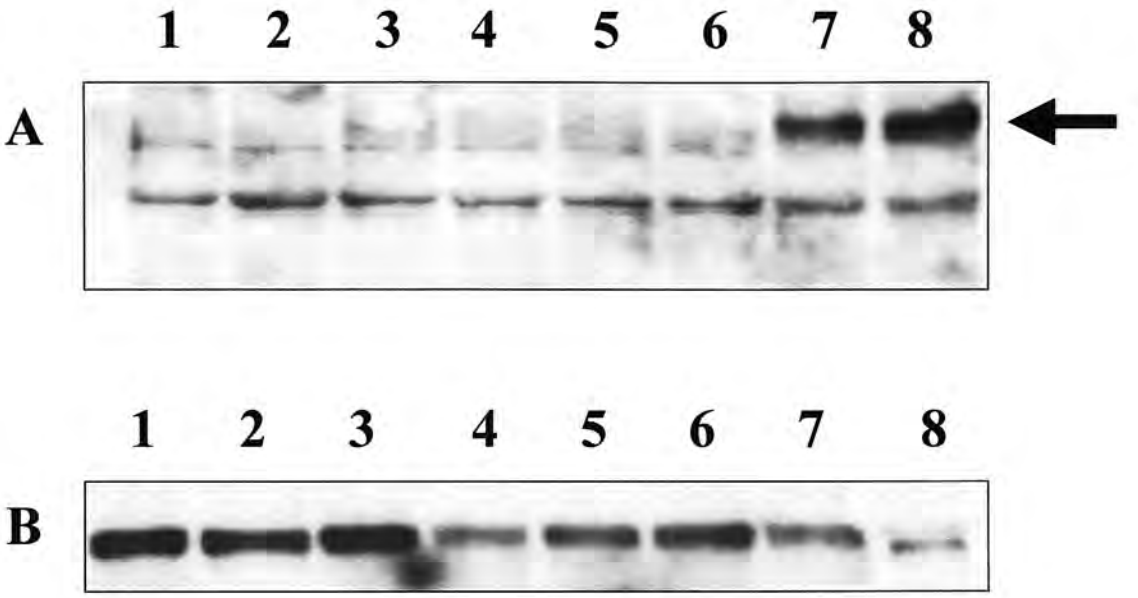

Figure 5.20: Ad5-MCMV-Dvl1 increases Dvl1 protein expression *in vivo*

Western blots showing Dvl1 expression in BALB/c mouse lungs following intra-tracheal instillation of Ad5-MCMV-Dvl1 or control (dl 70-3) virus. Dvl1 bands detected at ~80kDa as expected.

A) Radiograph of Dvl1 expression 3 days following instillation of virus. **1+2**: dl70-3 ($3x10^8$ pfu). **3+4**: Ad5-MCMV-Dvl1 ($3x10^8$ pfu). **5+6**: dl 70-3 ($8x10^8$ pfu). **7+8**: Ad5-MCMV-Dvl1 ($8x10^8$ pfu). Dvl1 band is indicated by arrow.

B) Radiograph of Dvl1 expression 3 and 7 days following instillation of Ad5-MCMV-Dvl1 at a dose of $8x10^8$ pfu.**1-3**: 3 days. **4-7**: 7 days. **8**: positive control (mouse brain lysate).

5.5.3 DVL1-ADENOVIRUS AND DVL1 IHC IN MOUSE LUNGS

As with the FITC model (Figure 5.1) tissue sections of BALB/c mice receiving PBS, control adenovirus (dl70-3) or Ad5-MCMV-Dvl1 were stained by IHC for Dvl1; using the anti-Dvl1 polyclonal antibody. Doses of virus ranged from 10^8 to $8x10^8$ pfu; the latter having been shown to increase Dvl1 expression by Western blotting (Figure 5.20).

The specific and intense staining of bronchial airway epithelial cells noted previously in both PBS and FITC treated mice (Figure 5.1) was also seen in mice receiving both control and Dvl1 adenovirus (Figure 5.21). This strong baseline staining made any further interpretation of possible changes in Dvl1 expression impossible. As discussed later this feature may have been due to antibody characteristics or related to Dvl protein expression in mouse lungs. In any case Dvl1 IHC was generally unhelpful.

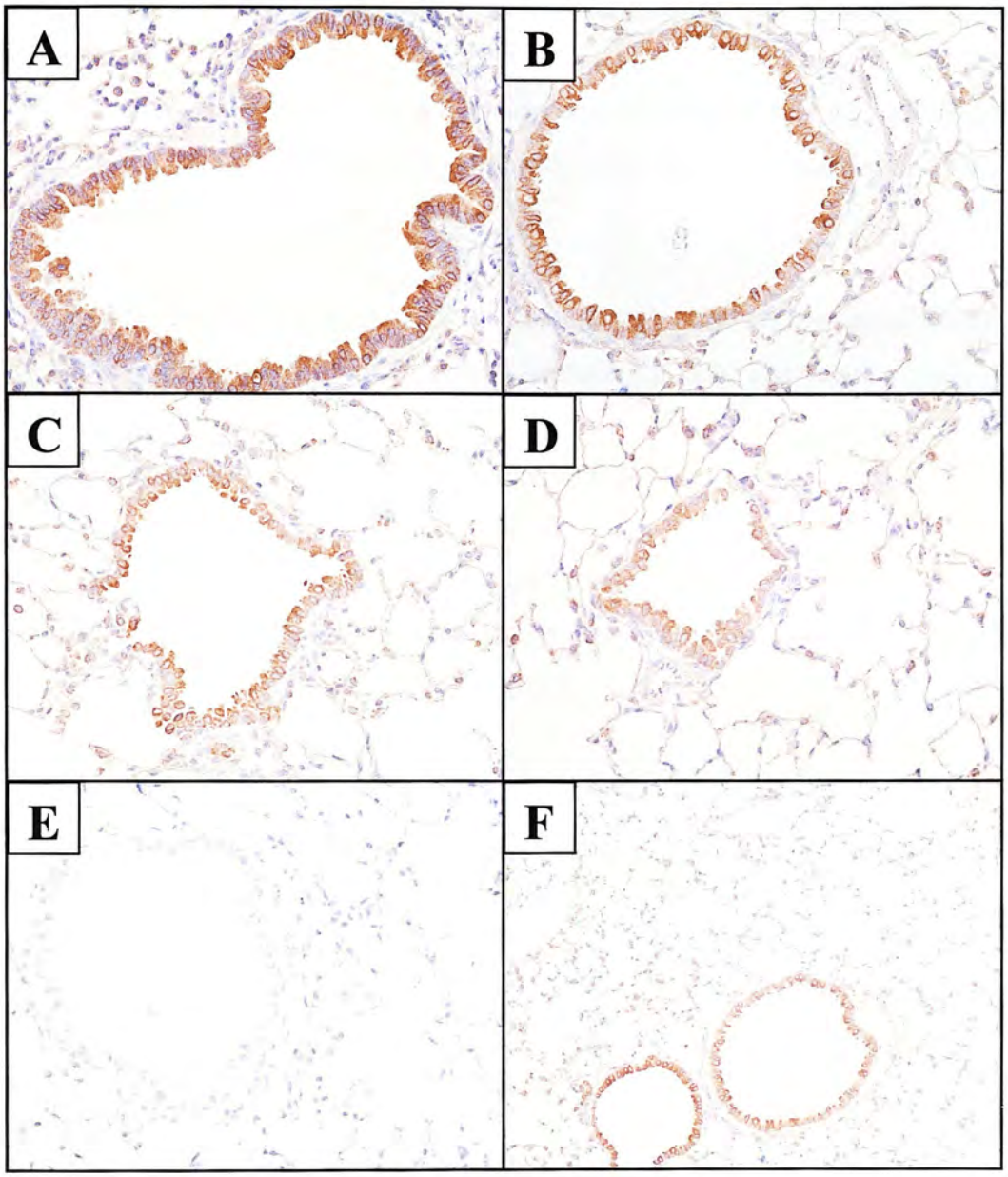

Figure 5.21: Dvl1 expression in mouse lungs following adenoviral instillation

Dvl1 expression by immunohistochemistry in BALB/c mouse lungs (n=6)

A) 7 days after dl70-3 (10^8 pfu); (x400 magnification)

B) 7 days after Ad5-MCMV-Dvl1 (10^8 pfu); (x400)

C) 7 days after Ad5-MCMV-Dvl1 ($8x10^8$ pfu); (x400)

D) 3 days after Ad5-MCMV-Dvl1 ($8x10^8$ pfu); (x400)

E) 7 days after Ad5-MCMV-Dvl1 (10^8 pfu); -ve IHC control (x400)

F) 7 days after Ad5-MCMV-Dvl1 (10^8 pfu); (x200)

5.5.4 DVL1 DOES NOT AFFECT LUNG MORPHOLOGY *IN VIVO*

Sections of mouse lung following treatment with either dl 70-3 or Ad5-MCMV-Dvl1 were also stained with haematoxylin and eosin to allow examination of lung morphology.

At day 3 following intra-tracheal instillation there was no apparent difference between control and Ad5-MCMV-Dvl1 sections, the only abnormality being slight disruption (some denudation and "peg-like" cells) of the bronchial airway epithelium, suggestive of damage (Figure 5.22 A and B).

By day 7 the most notable additional feature was the presence of marked peribronchial and perivascular predominantly mononuclear cell infiltrates (Figure 5.22 C and D). Again both viruses appeared to have similar effects.

By 8 weeks the lungs in both groups were essentially normal with no evidence of fibrosis in either. In some cases patches of cellular infiltrates, similar to those noted at day 7, persisted (Figure 5.22 E and F).

Both dl 70-3 and Ad5-MCMV-Dvl1 had similar effects when instilled intra-tracheally into BALB/c mouse lungs. These features were similar at viral doses of up to $8x10^8$ pfu ($3x10^8$ pfu shown). Parallel experiments in which the viruses were instilled intra-nasally (not shown) produced comparable results.

It has been suggested that different strains of mice have different potentials to develop lung fibrosis. In particular, C57 BL6 mice have been shown to be more susceptible to bleomycin-induced fibrosis [569]. With this in mind dl70-3 and Ad5-MCMV-Dvl1 were given intra-tracheally to a group of C57 BL6 mice. The features were similar to those observed with the BALB/c mice; again with no difference between treatment arms.

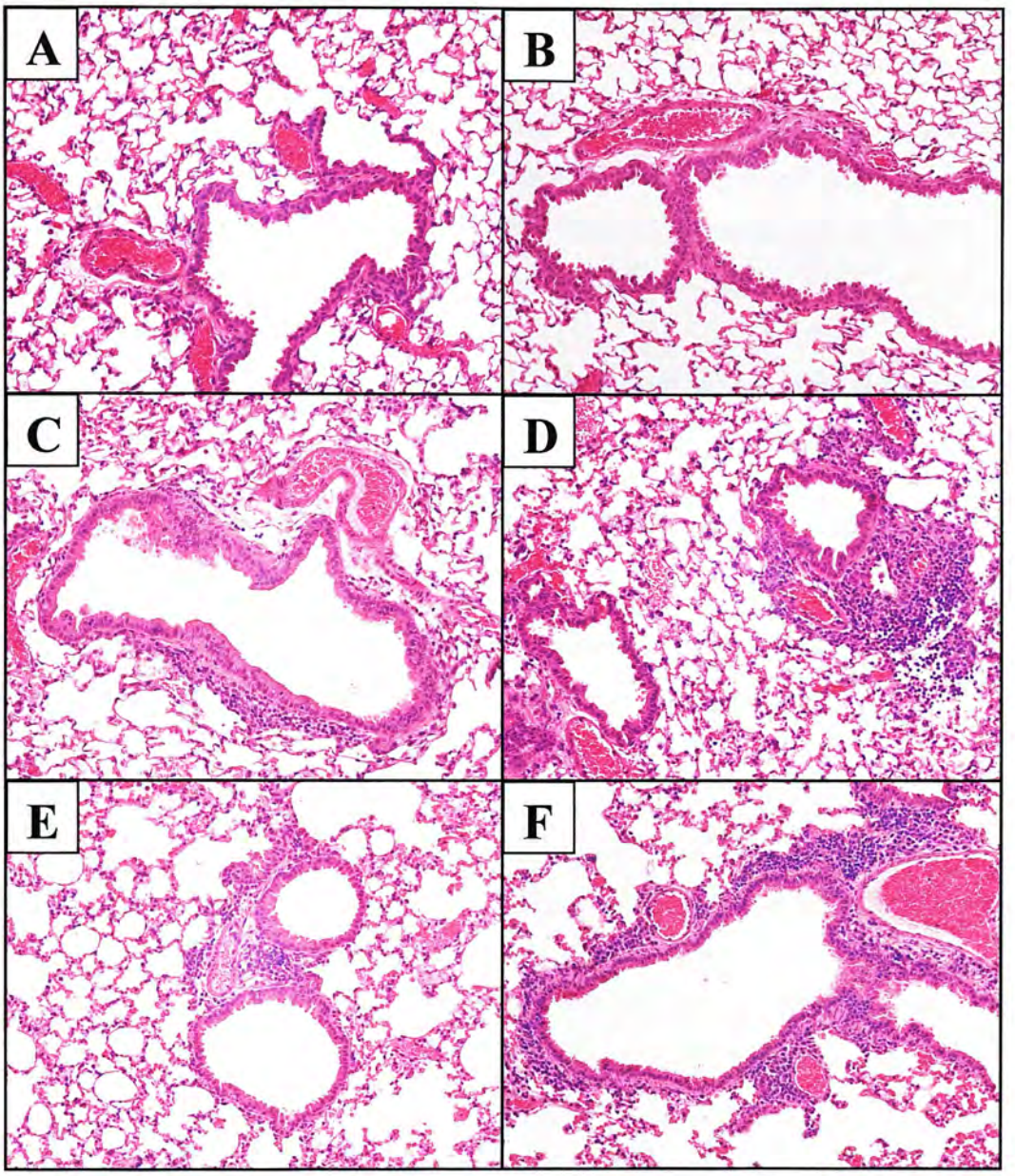

Figure 5.22: Mouse lung morphology following adenoviral instillation

BALB/c mouse lung sections stained with haematoxylin and eosin. All x200 magnification

A) 3 days after dl 70-3 ($3x10^8$ pfu)

B) 3 days after Ad5-MCMV-Dvl1 ($3x10^8$ pfu)

C) 7 days after dl 70-3 ($3x10^8$ pfu)

D) 7 days after Ad5-MCMV-Dvl1 ($3x10^8$ pfu)

E) 8 weeks after dl 70-3 ($3x10^8$ pfu)

F) 8 weeks after Ad5-MCMV-Dvl1 ($3x10^8$ pfu)

5.5.5 DVL1 DOES NOT AFFECT CELL PROLIFERATION *IN VIVO*

Dvl1 did not appear to affect proliferation of either A549 or Clara cells (Figures 5.15 and 5.16). It was also important to determine if Dvl1 expressed *in vivo* altered cell proliferation. To address this lung sections from mice treated with dl 70-3 or Ad5-MCMV-Dvl1 were stained with the nuclear proliferation marker Ki67.

3 days following instillation many of the bronchial airway epithelial cells were positive for Ki67 indicating they were undergoing proliferation (Figure 5.23 A and B). This was true following both dl 70-3 and Ad5-MCMV-Dvl1 treatments.

By day 7 the bronchial airway epithelial cells were predominantly negative. At this time there was a marked cellular infiltrate as noted before (Figure 5.22). Many of these cells stained positively for Ki67 (Figure 5.23 C and D). Again there was little difference between treatment groups.

There was therefore no evidence that Dvl1 expression has any effect on cell proliferation *in vivo* as assessed by Ki67 staining. As the observed effects were also seen with the control virus, it would seem likely that they were a response to the presence of adenovirus itself rather than Dvl1 expression. The increased airway epithelial proliferation may be a response to adenovirally induced epithelial damage similar to that observed in the FITC model of ILD [408].

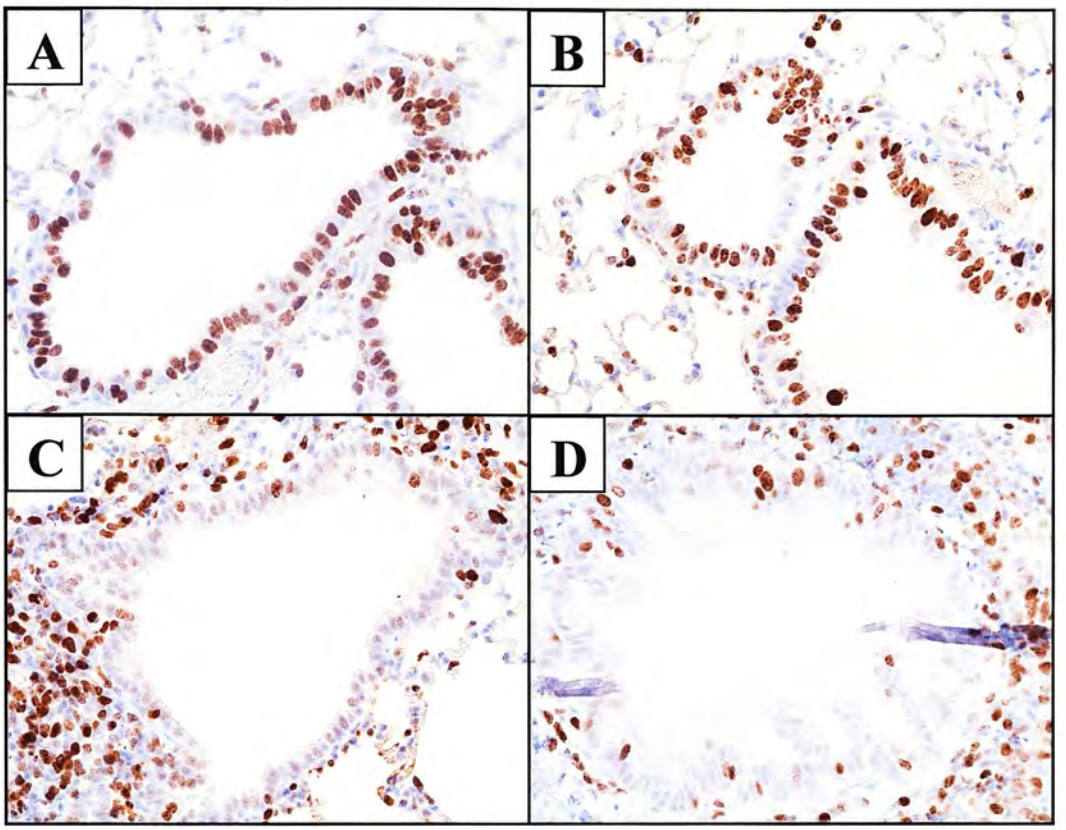

Figure 5.23: Ki67 expression in mouse lungs following adenoviral instillation

BALB/c mouse lung sections stained with Ki67 antibody. All x400 magnification

A) 3 days after dl 70-3 ($3x10^8$ pfu)

B) 3 days after Ad5-MCMV-Dvl1 ($3x10^8$ pfu)

C) 7 days after dl 70-3 ($3x10^8$ pfu)

D) 7 days after Ad5-MCMV-Dvl1 ($3x10^8$ pfu)

5.5.6 AD5-MCMV-DVL1 AND THE EXPRESSION OF SHH AND TGF-BETA *IN VIVO*

Dvl1 does not appear to upregulate Shh expression *in vitro*. This question was also addressed *in vivo* by IHC. Lung tissue sections from BALB/c mice post-adenovirus instillation were stained with a Shh antibody; as used in Chapter 3.

As illustrated 7 days after instillation, Shh expression was unaffected by treatment with either the control adenovirus (dl70-3) or Ad5-MCMV-Dvl1 (Figure 5.24 A-C). This was consistent all time-points. It would therefore appear that Shh expression is not increased either *in vitro* or *in vivo* by Ad5-MCMV-Dvl1.

As discussed, the Wnt pathway and TGFβ are known to be associated. Therefore it was important to determine whether or not Ad5-MCMV-Dvl1 altered TGFβ expression in vivo. This was particularly relevant in view of the strong links between TGFβ and pulmonary fibrosis [351,352,358].

TGFβ1 expression was unaffected by treatment with either the control adenovirus (dl70-3) or Ad5-MCMV-Dvl1 (Figure 5.24 D-F). As with Shh this was the case at all time-points. In addition, ELISAs of bronchoalveolar lavage (BAL) fluid revealed no significant active or latent levels of TGFβ1 in mice treated with dl70-3, Ad5-MCMV-Dvl1or PBS (data not shown).

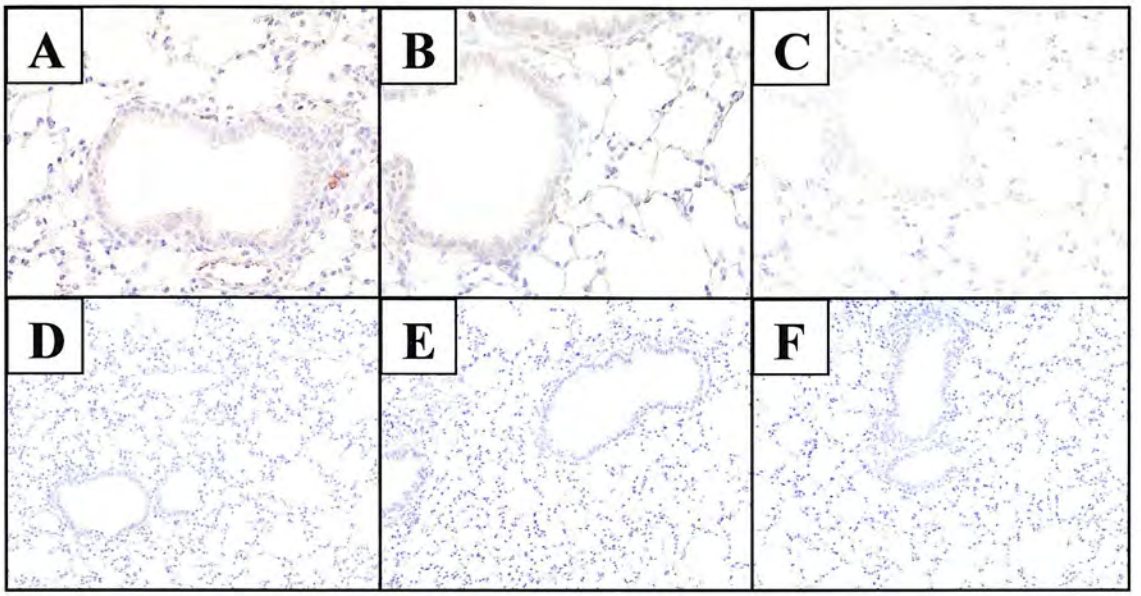

Figure 5.24: Shh and TGFβ1 expression in mouse lungs following adenoviral instillation

BALB/c mouse lung sections stained with anti-Shh antibody. All x400 magnification

A) 7 days after dl 70-3 (10^8 pfu)

B) 7 days after Ad5-MCMV-Dvl1 (10^8 pfu)

C) 7 days after Ad5-MCMV-Dvl1 ($8x10^8$ pfu)

BALB/c mouse lung sections stained with anti-TGFβ1 antibody. All x200 magnification

D) 7 days after dl 70-3 (10^8 pfu)

E) 7 days after Ad5-MCMV-Dvl1 (10^8 pfu)

F) 7 days after Ad5-MCMV-Dvl1 ($8x10^8$ pfu)

(n=6)

5.6 Discussion

As described in the introduction, the main aim of the work presented in this chapter was to upregulate the Wnt pathway by constructing a virus expressing murine Dvl1. However, at the time of planning the project much of the work on the mammalian Wnt pathway was in its infancy. Since that time a great deal of progress has been made in this field. With particular relevance to this body of work, Dvl1 has been associated with more than just the Wnt pathway. It has also been shown to interact with the JNK (c-Jun kinase) and Notch pathways [188,217,218]. In addition, whereas it was initially thought that Dvl1 overexpression lead to increased cell proliferation, recent work has shown that it can actually result in increased cell death by apoptosis [262].

It would, therefore, appear that the effects of Dvl1 overexpression are more complex. Regardless, the experiments in this chapter were designed to determine if an adenovirus expressing Dvl1 affected cell proliferation and Shh pathway activity, and if it would induce lung fibrosis.

Dvl1 Immunohistochemistry (IHC) in the FITC lung fibrosis model and with Ad5-MCMV-Dvl1

Though presented at the beginning of the chapter the Dvl1 IHC was not carried out until late in the project, due to the lack of a suitable anti-Dvl1 antibody. Notably, the antibody used is also known to recognise Dvl2; it is possible that it may also recognise Dvl3 (not known). It had been previously used for immunoblotting but not for IHC.

IHC for Dvl1 proved unhelpful. Even in PBS treated mice there was strong and specific staining of the bronchiolar airway epithelial cells (Figure 5.1). This staining pattern remained unchanged with FITC treatment and with adenoviral instillation, including Ad5-MCMV-Dvl1 (Figures 5.1 and 5.21). This may have been due to the

basal expression of Dvl1 in airway epithelium, the characteristics of the anti-Dvl1 antibody or a combination of the two.

It may well be that Dvl1 is already expressed at high levels in normal mice. The staining was certainly appeared to be very specific. Against this assumption, the Western data following adenoviral instillation *in vivo* (Figure 5.20) suggested that the level of Dvl1 was low unless the highest dose of $8x10^8$ pfu of Ad5-MCMV-Dvl1 was given.

It is also possible that the anti-Dvl1 antibody recognises another protein by IHC. It cross-reacts with Dvl2, which may be present in the airway epithelium. The antibody may therefore be binding to this making interpretation of any changes in Dvl1 expression impossible. The antibody may even be recognising another protein altogether, whose expression is unrelated to Dvl1. Against this, the antibody was raised specifically to the C-terminal 46 amino acids of Dvl1 and has been proven to recognise Dvl1 in Western blotting [567], though it did recognise several bands of similar size both in previous work and this project (Figure 5.10). It is possible, though difficult to prove without available Dvl proteins, that these bands include Dvl2 amongst others. However, it is reassuring that specific upregulation of Dvl1 was detected by this antibody after induction with the Dvl1 expressing adenovirus and not with control virus.

β-Catenin Immunohistochemistry (IHC) in the FITC lung fibrosis model

β-Catenin IHC staining was the same in both FITC and PBS treatment arms (Figure 5.2). There was no evidence of cytoplasmic staining as would be expected if the Wnt Signalling pathway was upregulated in the FITC treated mice. Therefore there is no evidence from the presented data, that the Wnt pathway is upregulated in ILD. At least not via β-Catenin stabilization, which of course does not exclude Wnt interacting with other pathways/genes involved in lung fibrosis.

Construction of DVL-1 Adenovirus (Ad5-MCMV-Dvl1)

The construction of the Dvl1 expressing adenovirus is described both in this chapter and in chapter 2. The murine cytomegalovirus promoter (MCMV) was chosen as this promoter had been demonstrated to be particularly efficient in published work [550]. The work shown here summarises the important cloning and expression experiments involved in the rescue of the crude, unbanded Ad5-MCMV-Dvl1.

Ad5-MCMV-Dvl1 *in vitro*

At the outset the main objective was to determine whether or not Ad5-MCMV-Dvl1 transfections resulted in Dvl1 expression at both RNA and protein level. As shown by Northern blotting, the Dvl1 adenovirus specifically upregulates *Dvl1* at RNA level, in both A549 cells and Rat-2 fibroblasts (Figures 5.6, 5.7 and 5.8). The reason for the double bands noted in both Northern blots remains unclear. It may well be that the Dvl1 probe binds to spliced variants of *Dvl1*, though none have been identified to date. Importantly the same doublet was also noted in the positive control (mouse brain RNA, Figure 5.8). It would therefore be reasonable to assume that the binding is real and is not to any non-specific adenoviral effect.

The Northern blot data was further supported by real time PCR analysis, confirming upregulation of *Dvl1* mRNA in A549 cells, mouse Clara cells and Swiss 3T3 fibroblasts (Figure 5.9 and 5.10). This latter technique also allowed direct quantification of the relative increases in mRNA, of which the highest was up to 1300 fold in Clara cells 48hrs post-transfection. Additionally relative *Dvl1* mRNA rose to different degrees in each of the cell types transfected. This may have been due to different efficiencies of adenoviral transfection [550] and/or characteristics of the Wnt pathway itself, in the chosen cell types.

Ad5-MCMV-Dvl1 transfections also lead to an increase in Dvl1 at protein level in both A549 and Clara cells (Figure 5.11). Interestingly, the Dvl1 antibody proved to be discriminatory when used in immunocytochemistry when it had been of little use

in IHC sections. Only Clara cells transfected with Ad5-MCMV-Dvl1 stained positively for Dvl1 (Figure 5.11). When used in IHC the Dvl1 antibody recognised the airway epithelial cells even in control (PBS treated) mice. Many of these cells are Clara cells in mice [570] and the cell line illustrated was derived from mouse Clara cells. The reason for this difference is unclear. It may be a feature of using a transformed cell line as such. If this were the case one might expect primary murine Clara cells to stain positively with this antibody without transfection. Alternatively, the discrepancy may be related to the different *in vitro* and *in vivo* environments in which the cells were transfected [570].

The ICC staining was specifically localised to the cell membrane. This correlates with previous findings implying that Dsh (*Drosophila* dishevelled) is recruited to the cell membrane compartment upon overexpression [185].

Having confirmed Dvl1 overexpression in response to Ad5-MCMV-Dvl1, the next priority was to determine if this in turn lead to upregulation of the Wnt pathway. As described this has often been confirmed by a specific increase in cytosolic β-Catenin levels. The findings suggested that Ad5-MCMV-Dvl1 causes an increase in β-Catenin in A549 cells but not in Clara cells (Figure 5.12). This may be a feature of the different cell types, as A549 cells are phenotypically type II pneumocytes. It may be that Dvl1, and the Wnt pathway, function differently in each cell type. These are both derived cell lines in which the Wnt pathway may behave differently than in primary cells and, of course, A549 cells are of human origin and the Clara cells are derived from mice. On this final point one might have expected murine Dvl1 (as expressed in Ad5-MCMV-Dvl1) to prove more effective in a mouse than a cell line, and not the opposite as observed.

As β-Catenin translocates to the nucleus upon Wnt signalling [194] the levels of nuclear β-Catenin following adenovirus transfection of A549 cells were also determined (Figure 5.12). They did not appear to be increased with the Ad5-MCMV-Dvl1 compared with dl70-3. The reason for this is unclear.

The effects of Ad5-MCMV-Dvl1 on cell proliferation were minimal. The original hypothesis had been that Dvl1 upregulation would lead to increased cell proliferation. This was later countered by published data implying that it may result in cellular apoptosis [262]. Morphologically there appeared to be differences between Clara cells transfected with Ad5-MCMV-Dvl1, dl70-3 and untransfected cells. Consistently, only in Ad5-MCMV-Dvl1 treated wells, many loosely adherent, friable cells were noted (Figure 5.13). Morphologically these cells appeared to be apoptotic though too few remained adherent during Hoechst staining to make any firm conclusions. Notably there was no clear morphological difference in A549 cells between treatment groups (not shown). More objective measures of cell proliferation by trypan blue cell counts, thymidine incorporation and a colorimetric assay were also employed. By these methods there was no consistent difference in proliferation between untransfected and adenovirally (both Dvl1 and control) transfected A549 or Clara cells (Figures 5.14 and 5.15).

These findings would suggest that Dvl1 expression does not affect cell proliferation. This of course could be influenced by several factors. The observed morphological changes associated with Ad5-MCMV-Dvl1 could not be translated into objective data, largely because the cells of interest were too fragile and loosely adherent to be satisfactorily isolated and analysed. However these cells were still accounted for in the colorimetric assay in which no difference in treatment groups was noted. It may be that the basal high level of proliferation of the chosen cell lines masked any changes exerted by the presence of Dvl1. When the percentage of foetal calf serum was reduced in an attempt to limit baseline proliferation rates, similar results were obtained. As both were adherent cell lines measuring proliferation at all was technically difficult. Finally, it is also possible that Dvl1 overexpression affects each cell type differently; neither A549 nor the Clara cell line were used by other groups investigating the effects of Dvl1 on apoptosis. It may be that proliferation/survival is not affected in the same way in these cell lines as in those previously used [262].

Based on the assumption that increased Wnt signalling may upregulate the Shh pathway, the expression of Shh and Ptc were analysed in response to Ad5-MCMV-Dvl1. Of course, the evidence suggesting that the Wnt pathway is itself upregulated by Ad5-MCMV-Dvl1 is conflicting as determined by β-Catenin expression (Figure 5.12). Regardless, the possibility of an interaction between Dvl1 overexpression and the Shh pathway was assessed. Neither Shh or *Ptc* expression was significantly altered by treatment, of A549 or Clara cells, with Ad5-MCMV-Dvl1 (Figures 5.16 and 5.17). *Ptc* expression in Swiss 3T3 cells was also unaffected. Therefore, it would appear that, in the chosen cell lines, Dvl1 overexpression does not affect Shh signalling.

Ad5-MCMV-Dvl1 *in vivo*

As in the *in vitro* experiments the starting point for the *in vivo* work was to determine if Ad5-MCMV-Dvl1 caused an increase in Dvl1 at both RNA and protein level. By real time PCR *Dvl1* mRNA expression was increased in the lungs of mice treated with Ad5-MCMV-Dvl1 from 24hrs (first time-point chosen) onwards (Figures 5.18 and 5.19) at doses as low as $3x10^8$ pfu. In addition expression at 3 days was greater than at 7 days (Figure 5.19), as demonstrated by others with similar constructs [568].

In vivo Dvl1 protein expression was also confirmed, by Western blotting, in BALB/c mouse lungs following Ad5-MCMV-Dvl1 instillation (Figure 5.20). Unlike RNA expression Dvl1 protein was only detectable at the highest $8x10^8$ pfu dose of virus used. This may have been in some part due to the sensitivity of the Western blot. Dvl1 IHC, as with staining of FITC fibrosis sections, was uninformative.

The lungs of mice receiving Ad5-MCMV-Dvl1 or dl70-3 intra-tracheally were morphologically very similar (Figure 5.22). There was a non-specific viral effect in both, in the form of sloughed and reactive airway epithelial cells at day 3 and significant mononuclear cell infiltrates from day 7. By the later 8-week time-point, other than some residual infiltrates, the lungs were essentially normal with no

evidence of fibrosis. Similar observations were made using the intranasal route of adenovirus administration, and in C57 BL6 mice treated intra-tracheally.

Cell proliferation was analysed in the mouse lungs by staining with Ki67 (Figure 5.23). In lung sections of mice following adenoviral instillation many of the "reactive" airway epithelial cells were positive, indicating a high rate of proliferation; possibly compensatory hyperplasia following viral damage. This contrasts with the largely negative epithelial staining of lung sections from mice treated with the SPC plasmids shown in chapter 3 (Figure 3.9), which equates with the appearance of normal, untreated mouse lungs. As proliferation was equally marked in both the Dvl1 and the control adenovirus it was likely to be a virus related effect. Indeed, it would be difficult to appreciate any additive effects due to Dvl1 expression against this viral response. By day 7 the airway epithelium was largely negative again as in untreated lungs. Not surprisingly many of the infiltrating mononuclear cells were positive at this later time-point; predominantly lymphocytes as one would expect in response to an adenovirus.

Essentially Dvl1 expression itself does not appear to have any effect on either lung morphology or cell proliferation. Although not shown, preliminary IHC on lungs from mice treated with Ad5-MCMV-Dvl1 showed no evidence of increased cytoplasmic β-catenin staining, again consistent with a failure to augment Wnt signalling, at least via the Wnt/β-catenin pathway. Several possible explanations exist. Dvl1 protein was only detected at the highest dose of Ad5-MCMV-Dvl1 ($8x10^8$ pfu) used. This was the highest dose that could be given as a single 50μl intra-tracheal treatment, and repeat adenoviral administration is inadvisable due to the associated immune response as discussed in Chapter 1. It may be that a higher dose may have resulted in more significant *in vivo* effects in terms of Wnt signalling and lung morphology, though it should be stressed that the dose given was appreciable. It is also possible that the observed Dvl1 overexpression was driving alternative pathways such as the c-Jun N-terminal kinase/stress-activated protein kinase (JNK/SAPK) cascade [217,218]. Due to time constraints, this issue was not addressed in this thesis.

Finally, further lung sections stained with specific antibodies confirmed that Ad5-MCMV-Dvl1 does not upregulate either Shh or TGFβ1 (Figure 5.24). Shh expression *in vivo* would have been particularly relevant in view of the findings presented in chapter 3. The TGFβ1 IHC data was supported by TGFβ1 ELISA analysis of the BAL fluid in similarly treated mice, in which no significant active or latent TGFβ1 was detected (not shown). As the evidence presented suggests, Dvl1 overexpression may not increase expression of these two proteins, but this does not necessarily mean that Wnt upregulation does not.

Summary

The work presented in this chapter details the successful rescue of a replication deficient adenovirus expressing murine DVL-1 (Ad5-MCMV-Dvl1). This virus allows upregulation of Dvl1 at both mRNA and protein level *in vitro* and *in vivo*. The evidence presented does not prove that overexpression of Dvl1 in this manner mimics Wnt signalling, as was the original prediction. In addition, the adenovirus does not cause significant, objective changes in cell proliferation when used in cell culture or instilled into mouse lungs. Neither the Shh signalling pathway nor TGFβ1 are stimulated by Ad5-MCMV-Dvl1. Finally, when used *in vivo*, any observed effects were consistent with a non-specific adenoviral reaction, and the treated mice did not develop any features of pulmonary fibrosis. Using available tools there was no evidence of Dvl1 upregulation (IHC), or of cytosolic β-Catenin stabilisation, in the mouse model of ILD.

It would appear that, based on the work presented, that Ad5-MCMV-Dvl1 neither upregulates Wnt/β-catenin signalling in all lung epithelial cell types, nor influences cell proliferation. There is certainly no evidence that it causes lung fibrosis. Additionally the Wnt pathway itself does not appear to be upregulated in ILD. Whether or not Wnt signalling upregulation by another route would cause lung fibrosis isn't known, but at present would seem unlikely. Of course, this does not

exclude the possibility that upregulation of the Wnt pathway has an anti-fibrotic effect, as is possible for Shh signalling, and as implied by preliminary experiments looking at β-catenin expression in models of ILD and airway epithelial repair [275,276].

Essentially, although the desired genetic tool has been created, its application to date has produced largely negative data. It may well be that Ad5-MCMV-Dvl1 can be used to determine the effects of Dvl1 upregulation in other systems and/or cell types.

Conclusions

In the work described in this thesis the role of the Shh pathway in ILD and human $CD4^+$ T cell activation was investigated. In addition, the potential involvement of the Wnt pathway in the pathogenesis of ILD was studied, and an attempt made to upregulate this pathway using a recombinant adenoviral vector expressing Dvl1.

In chapter 3, the expression of Shh and its receptor, Ptc, was assessed both in a murine model of pulmonary fibrosis, induced by FITC instillation, and in archival biopsy sections taken from patients with IPF. It was demonstrated that Shh expression was increased in the remodelling airway epithelium of FITC treated mice and in IPF sections suggesting that the Shh pathway is upregulated in ILD. Curiously, Ptc was constitutively expressed in the airway epithelium with no evidence of increased expression in fibrotic lung. Expression of both Shh and Ptc was noted in the infiltrating mononuclear cells in mouse and human sections. Furthermore, the FITC model was reproduced in mice containing heterozygous mutations of *Gli2* and *3* to determine if dysregulated Shh signalling altered the fibrotic response. There was no demonstrable difference in the severity of fibrosis between the wild type and mutant mice, though the latter were far from ideal research tools, as described. An attempt to increase Shh expression, and hence pathway activity, *in vivo* was also made. However, as assessed by IHC and morphology this was unsuccessful, possibly as a result of inefficient gene transfer and/or a sub-optimal promoter. Finally, increased TGFβ1 expression was noted in the remodelling airway epithelial cells in mouse and human sections, in keeping with established correlations between TGFβ and the fibrotic process.

The expression of Shh and Ptc in mononuclear cells demonstrated in fibrotic tissue sections in chapter 3 was paralleled by their observed expression in human T cells, described in chapter 4. Having confirmed that the pathway was present in these cells, a N-Shh peptide and an anti-Shh neutralizing antibody (5E1) were used to upregulate and inhibit Shh signalling respectively, in purified human $CD4^+$ T cells, activated with anti-CD3 and anti-CD28 antibodies. It was thus demonstrated that increased Shh signalling enhances TCR mediated T cell activation as evidenced by proliferation, cytokine secretion and expression of the surface activation markers,

CD25 and CD69. Conversely, reduced Shh signalling inhibits activation as assessed by these same assays. However, such manipulation of the Shh pathway did not affect T cell survival, nor did it have any influence on non-activated T cells. Of those tested, only T cells from approximately 50% of donors were affected by altered Shh signalling. This may have been due to a Ptc or Smo polymorphism rendering the pathway inactive in these 'non-responding' donors.

As discussed, Shh signalling promotes, whereas the profibrotic cytokine, TGFβ, inhibits branching morphogenesis of the developing lung. It may therefore be the case that the observed upregulation of the Shh pathway in ILD is more indicative of an attempted repair process by the lungs, thus antagonising TGFβ. Further experiments, in particular aimed at upregulating the Shh pathway *in vivo*, would be necessary to determine this. However, it should be stressed that the observed upregulation of Shh in ILD is not in itself proof that the pathway is specifically linked to the fibrotic process. Indeed the *in vivo Gli* mutant and intra-tracheal SPC-Shh cDNA experiments, accepting their weaknesses, if anything suggested that Shh signalling does not influence fibrosis in murine lungs. It certainly would have been worthwhile expanding the *in vitro* Shh experiments to structural cells such as fibroblasts in order to provide more proof of such a link. For example, as already described, TGFβ is known to stimulate *in vitro* expression of ECM proteins, such as collagen and fibronectin, and to induce the myofibroblast phenotype from classical fibroblasts [351,352]. Similar experiments designed to look at the production of such ECM proteins and myofibroblast differentiation, characterized by α smooth muscle actin expression, in the context of Shh signalling could have been performed. As in the T cell work described, the pathway could be stimulated or inhibited by the addition of the N-Shh peptide or the anti-Shh neutralizing antibody (5E1), respectively. Although some preliminary experiments of this nature were carried out they were not sufficient to warrant inclusion in this thesis.

The presence of the Shh pathway in infiltrating mononuclear cells, and its effects on TCR mediated T cell activation, suggest that Shh signalling may be involved in

communication between T cells, macrophages and indeed epithelial cells. Furthermore, such communication may play a role in the pathogenesis of ILD, or alternatively in the body's attempt to attenuate the fibrotic response. In essence, it would be fascinating to link the two main positive findings from this thesis: the observed increase in Shh expression in ILD and the presence and function of the pathway in mature T cells. As outlined in the introductory chapter, lymphocytes and their cytokines have been closely associated with ILD. It may be that any influence Shh signalling exerts on the fibrotic process is dependent on the manipulation of T cell activation. If so, the discrimination between "responder" and "non-responder" T cell donors (to altered Shh signalling) may define whether or not individuals are likely to develop ILD.

The Wnt pathway also plays a role in embryonic lung branching morphogenesis, and has recently been associated with TGFβ signalling. In chapter 5, it was shown that neither β-catenin nor Dvl1 expression was altered in the FITC model of ILD. A replication deficient adenovirus expressing murine Dvl1 (Ad5-MCMV-Dvl1) was successfully rescued. This drove increased Dvl1 expression *in vitro* and *in vivo*, but did not induce upregulation of Wnt or Shh signalling, nor did it result in objective changes in cell proliferation. Finally, increased Dvl1 expression, in the lungs of BALB/c and C57 Bl6 mice, did not cause pulmonary fibrosis. Therefore, from the data presented in this chapter there is no evidence of a correlation between the Wnt pathway and ILD. As Shh and Wnt signalling have been shown to drive each other, this would suggest that any link between Shh and ILD is independent of Wnt signalling. It may be related to other targets of the Shh pathway, such as the Bmp's, which are afterall members of the TGFβ superfamily.

Future work could be addressed at upregulating the Shh pathway in the lungs of mature mice using either a gene vector, such as an adenovirus, or an inducible Shh transgenic mouse. This, in addition to the potential *in vitro* experiments discussed above, may answer the question of whether or not Shh signalling contributes to the development of fibrosis. Such experiments could be combined with a fibrosis model, such as the FITC model, in which either Shh or a Shh antagonist (eg. Hip) could be

overexpressed during the fibrotic response. It would be interesting to determine if Shh expression is also increased in fibrosis of other organs such as the liver and gut. It would also be informative to analyse the mechanism of action of the Shh pathway in $CD4^+$ T cells and to determine how this is linked to existing mechanisms of T cell signalling. Furthermore, one could analyse the activity of Shh signalling in T cells isolated from mice with lung fibrosis and compare this with normal controls. Similar studies could be carried out comparing T cells from patients with ILD with matched controls. The role of the Shh pathway in macrophage function is also yet to be determined; a project that is now ongoing within the group. Finally, although much of the data produced using Ad5-MCMV-Dvl1 has been negative to date, it did successfully drive Dvl1 expression. It could therefore be used to establish the effects of Dvl1 upregulation in other systems and cell types.

References

1. Nusslein-Volhard,C. & Wieschaus,E. Mutations affecting segment number and polarity in Drosophila. *Nature* **287**, 795-801 (1980).

2. Mohler,J. Requirements for hedgehog, a segmental polarity gene, in patterning larval and adult cuticle of Drosophila. *Genetics* **120**, 1061-1072 (1988).

3. Ingham,P.W. & Hidalgo,A. Regulation of wingless transcription in the Drosophila embryo. *Development* **117**, 283-291 (1993).

4. Basler,K. & Struhl,G. Compartment boundaries and the control of Drosophila limb pattern by hedgehog protein. *Nature* **368**, 208-214 (1994).

5. Kingsley,D.M. The TGF-beta superfamily: new members, new receptors, and new genetic tests of function in different organisms. *Genes Dev.* **8**, 133-146 (1994).

6. Nellen,D., Burke,R., Struhl,G. & Basler,K. Direct and long-range action of a DPP morphogen gradient. *Cell* **85**, 357-368 (1996).

7. Zecca,M., Basler,K. & Struhl,G. Direct and long-range action of a wingless morphogen gradient. *Cell* **87**, 833-844 (1996).

8. Struhl,G., Barbash,D.A. & Lawrence,P.A. Hedgehog acts by distinct gradient and signal relay mechanisms to organise cell type and cell polarity in the Drosophila abdomen. *Development* **124**, 2155-2165 (1997).

9. Struhl,G., Barbash,D.A. & Lawrence,P.A. Hedgehog organises the pattern and polarity of epidermal cells in the Drosophila abdomen. *Development* **124**, 2143-2154 (1997).

10. Lee,J.J. *et al.* Autoproteolysis in hedgehog protein biogenesis. *Science* **266**, 1528-1537 (1994).

11. Porter,J.A. *et al.* The product of hedgehog autoproteolytic cleavage active in local and long-range signalling. *Nature* **374**, 363-366 (1995).

12. Fietz,M.J., Jacinto,A., Taylor,A.M., Alexandre,C. & Ingham,P.W. Secretion of the amino-terminal fragment of the hedgehog protein is necessary and sufficient for hedgehog signalling in Drosophila. *Curr. Biol.* **5**, 643-650 (1995).

13. Porter,J.A., Young,K.E. & Beachy,P.A. Cholesterol modification of hedgehog signaling proteins in animal development. *Science* **274**, 255-259 (1996).

14. Porter,J.A. *et al.* Hedgehog patterning activity: role of a lipophilic modification mediated by the carboxy-terminal autoprocessing domain. *Cell* **86**, 21-34 (1996).

15. McMahon,A.P. More surprises in the Hedgehog signaling pathway. *Cell* **100**, 185-188 (2000).

16. Ramirez-Weber,F.A. & Kornberg,T.B. Cytonemes: cellular processes that project to the principal signaling center in Drosophila imaginal discs. *Cell* **97**, 599-607 (1999).

17. Pepinsky,R.B. *et al.* Identification of a palmitic acid-modified form of human Sonic hedgehog. *J. Biol. Chem.* **273**, 14037-14045 (1998).

18. Stone,D.M. *et al.* The tumour-suppressor gene patched encodes a candidate receptor for Sonic hedgehog. *Nature* **384**, 129-134 (1996).

19. Hooper,J.E. & Scott,M.P. The Drosophila patched gene encodes a putative membrane protein required for segmental patterning. *Cell* **59**, 751-765 (1989).

20. Nakano,Y. *et al.* A protein with several possible membrane-spanning domains encoded by the Drosophila segment polarity gene patched. *Nature* **341**, 508-513 (1989).

21. Marigo,V., Davey,R.A., Zuo,Y., Cunningham,J.M. & Tabin,C.J. Biochemical evidence that patched is the Hedgehog receptor. *Nature* **384**, 176-179 (1996).

22. Alcedo,J., Ayzenzon,M., Von Ohlen,T., Noll,M. & Hooper,J.E. The Drosophila smoothened gene encodes a seven-pass membrane protein, a putative receptor for the hedgehog signal. *Cell* **86**, 221-232 (1996).

23. Ingham,P.W., Taylor,A.M. & Nakano,Y. Role of the Drosophila patched gene in positional signalling. *Nature* **353**, 184-187 (1991).

24. Hooper,J.E. Distinct pathways for autocrine and paracrine Wingless signalling in Drosophila embryos. *Nature* **372**, 461-464 (1994).

25. Ingham,P.W. *et al.* Patched represses the Hedgehog signalling pathway by promoting modification of the Smoothened protein. *Curr. Biol.* **10**, 1315-1318 (2000).

26. Murone,M., Rosenthal,A. & de Sauvage,F.J. Sonic hedgehog signaling by the patched-smoothened receptor complex. *Curr. Biol.* **9**, 76-84 (1999).

27. Li,W., Ohlmeyer,J.T., Lane,M.E. & Kalderon,D. Function of protein kinase A in hedgehog signal transduction and Drosophila imaginal disc development. *Cell* **80**, 553-562 (1995).

28. Chen,Y. & Struhl,G. Dual roles for patched in sequestering and transducing Hedgehog. *Cell* **87**, 553-563 (1996).

29. Orenic,T.V., Slusarski,D.C., Kroll,K.L. & Holmgren,R.A. Cloning and characterization of the segment polarity gene cubitus interruptus Dominant of Drosophila. *Genes Dev.* **4**, 1053-1067 (1990).

30. Marigo,V., Johnson,R.L., Vortkamp,A. & Tabin,C.J. Sonic hedgehog differentially regulates expression of GLI and GLI3 during limb development. *Dev. Biol.* **180**, 273-283 (1996).

31. Slusarski,D.C., Motzny,C.K. & Holmgren,R. Mutations that alter the timing and pattern of cubitus interruptus gene expression in Drosophila melanogaster. *Genetics* **139**, 229-240 (1995).

32. Aza-Blanc,P., Ramirez-Weber,F.A., Laget,M.P., Schwartz,C. & Kornberg,T.B. Proteolysis that is inhibited by hedgehog targets Cubitus interruptus protein to the nucleus and converts it to a repressor. *Cell* **89**, 1043-1053 (1997).

33. Dominguez,M., Brunner,M., Hafen,E. & Basler,K. Sending and receiving the hedgehog signal: control by the Drosophila Gli protein Cubitus interruptus. *Science* **272**, 1621-1625 (1996).

34. Alexandre,C., Jacinto,A. & Ingham,P.W. Transcriptional activation of hedgehog target genes in Drosophila is mediated directly by the cubitus interruptus protein, a member of the GLI family of zinc finger DNA-binding proteins. *Genes Dev.* **10**, 2003-2013 (1996).

35. Hepker,J., Wang,Q.T., Motzny,C.K., Holmgren,R. & Orenic,T.V. Drosophila cubitus interruptus forms a negative feedback loop with patched and regulates expression of Hedgehog target genes. *Development* **124**, 549-558 (1997).

36. Methot,N. & Basler,K. Hedgehog controls limb development by regulating the activities of distinct transcriptional activator and repressor forms of Cubitus interruptus. *Cell* **96**, 819-831 (1999).

37. Chen,C.H. *et al.* Nuclear trafficking of Cubitus interruptus in the transcriptional regulation of Hedgehog target gene expression. *Cell* **98**, 305-316 (1999).

38. Akimaru,H., Hou,D.X. & Ishii,S. Drosophila CBP is required for dorsal-dependent twist gene expression. *Nat. Genet.* **17**, 211-214 (1997).

39. Ingham,P.W. Transducing Hedgehog: the story so far. *EMBO J.* **17**, 3505-3511 (1998).

40. Jiang,J. & Struhl,G. Regulation of the Hedgehog and Wingless signalling pathways by the F-box/WD40-repeat protein Slimb. *Nature* **391**, 493-496 (1998).

41. Chen,Y., Gallaher,N., Goodman,R.H. & Smolik,S.M. Protein kinase A directly regulates the activity and proteolysis of cubitus interruptus. *Proc. Natl. Acad. Sci. U. S. A* **95**, 2349-2354 (1998).

42. Ohlmeyer,J.T. & Kalderon,D. Hedgehog stimulates maturation of Cubitus interruptus into a labile transcriptional activator. *Nature* **396**, 749-753 (1998).

43. Grau,Y. & Simpson,P. The segment polarity gene costal-2 in Drosophila. I. The organization of both primary and secondary embryonic fields may be affected. *Dev. Biol.* **122**, 186-200 (1987).

44. Robbins,D.J. *et al.* Hedgehog elicits signal transduction by means of a large complex containing the kinesin-related protein costal2. *Cell* **90**, 225-234 (1997).

45. Preat,T. *et al.* Segmental polarity in Drosophila melanogaster: genetic dissection of fused in a Suppressor of fused background reveals interaction with costal-2. *Genetics* **135**, 1047-1062 (1993).

46. Preat,T. Characterization of Suppressor of fused, a complete suppressor of the fused segment polarity gene of Drosophila melanogaster. *Genetics* **132**, 725-736 (1992).

47. Vortkamp,A. *et al.* Regulation of rate of cartilage differentiation by Indian hedgehog and PTH-related protein. *Science* **273**, 613-622 (1996).

48. Bitgood,M.J. & McMahon,A.P. Hedgehog and Bmp genes are coexpressed at many diverse sites of cell- cell interaction in the mouse embryo. *Dev. Biol.* **172**, 126-138 (1995).

49. Bitgood,M.J., Shen,L. & McMahon,A.P. Sertoli cell signaling by Desert hedgehog regulates the male germline. *Curr. Biol.* **6**, 298-304 (1996).

50. Echelard,Y. *et al.* Sonic hedgehog, a member of a family of putative signaling molecules, is implicated in the regulation of CNS polarity. *Cell* **75**, 1417-1430 (1993).

51. Krauss,S., Concordet,J.P. & Ingham,P.W. A functionally conserved homolog of the Drosophila segment polarity gene hh is expressed in tissues with polarizing activity in zebrafish embryos. *Cell* **75**, 1431-1444 (1993).

52. Riddle,R.D., Johnson,R.L., Laufer,E. & Tabin,C. Sonic hedgehog mediates the polarizing activity of the ZPA. *Cell* **75**, 1401-1416 (1993).

53. Chang,D.T. *et al.* Products, genetic linkage and limb patterning activity of a murine hedgehog gene. *Development* **120**, 3339-3353 (1994).

54. Roelink,H. *et al.* Floor plate and motor neuron induction by vhh-1, a vertebrate homolog of hedgehog expressed by the notochord. *Cell* **76**, 761-775 (1994).

55. Litingtung,Y., Lei,L., Westphal,H. & Chiang,C. Sonic hedgehog is essential to foregut development. *Nat. Genet.* **20**, 58-61 (1998).

56. Bellusci,S. *et al.* Involvement of Sonic hedgehog (Shh) in mouse embryonic lung growth and morphogenesis. *Development* **124**, 53-63 (1997).

57. Williams,K.P. *et al.* Functional antagonists of sonic hedgehog reveal the importance of the N terminus for activity. *J. Cell Sci.* **112 (Pt 23)**, 4405-4414 (1999).

58. Takabatake,T. *et al.* Hedgehog and patched gene expression in adult ocular tissues. *FEBS Lett.* **410**, 485-489 (1997).

59. Motoyama,J., Takabatake,T., Takeshima,K. & Hui,C. Ptch2, a second mouse Patched gene is co-expressed with Sonic hedgehog. *Nat. Genet.* **18**, 104-106 (1998).

60. Goodrich,L.V., Johnson,R.L., Milenkovic,L., McMahon,J.A. & Scott,M.P. Conservation of the hedgehog/patched signaling pathway from flies to mice: induction of a mouse patched gene by Hedgehog. *Genes Dev.* **10**, 301-312 (1996).

61. Epstein,D.J., Marti,E., Scott,M.P. & McMahon,A.P. Antagonizing cAMP-dependent protein kinase A in the dorsal CNS activates a conserved Sonic hedgehog signaling pathway. *Development* **122**, 2885-2894 (1996).

62. Delattre,M., Briand,S., Paces-Fessy,M. & Blanchet-Tournier,M.F. The Suppressor of fused gene, involved in Hedgehog signal transduction in Drosophila, is conserved in mammals. *Dev. Genes Evol.* **209**, 294-300 (1999).

63. Kogerman,P. *et al.* Mammalian suppressor-of-fused modulates nuclear-cytoplasmic shuttling of Gli-1. *Nat. Cell Biol.* **1**, 312-319 (1999).

64. Ding,Q. *et al.* Mouse suppressor of fused is a negative regulator of sonic hedgehog signaling and alters the subcellular distribution of Gli1. *Curr. Biol.* **9**, 1119-1122 (1999).

65. Stone,D.M. *et al.* Characterization of the human suppressor of fused, a negative regulator of the zinc-finger transcription factor Gli. *J. Cell Sci.* **112 (Pt 23)**, 4437-4448 (1999).

66. Hammerschmidt,M., Brook,A. & McMahon,A.P. The world according to hedgehog. *Trends Genet.* **13**, 14-21 (1997).

67. Ingham,P.W. The patched gene in development and cancer. *Curr. Opin. Genet. Dev.* **8**, 88-94 (1998).

68. Goodrich,L.V. & Scott,M.P. Hedgehog and patched in neural development and disease. *Neuron* **21**, 1243-1257 (1998).

69. Marigo,V., Scott,M.P., Johnson,R.L., Goodrich,L.V. & Tabin,C.J. Conservation in hedgehog signaling: induction of a chicken patched homolog by Sonic hedgehog in the developing limb. *Development* **122**, 1225-1233 (1996).

70. Concordet,J.P. *et al.* Spatial regulation of a zebrafish patched homologue reflects the roles of sonic hedgehog and protein kinase A in neural tube and somite patterning. *Development* **122**, 2835-2846 (1996).

71. Hui,C.C., Slusarski,D., Platt,K.A., Holmgren,R. & Joyner,A.L. Expression of three mouse homologs of the Drosophila segment polarity gene cubitus interruptus, Gli, Gli-2, and Gli-3, in ecto. *Dev. Biol.* **162**, 402-413 (1994).

72. Ruppert,J.M., Vogelstein,B., Arheden,K. & Kinzler,K.W. GLI3 encodes a 190-kilodalton protein with multiple regions of GLI similarity. *Mol. Cell Biol.* **10**, 5408-5415 (1990).

73. Matise,M.P. & Joyner,A.L. Gli genes in development and cancer. *Oncogene* **18**, 7852-7859 (1999).

74. Grindley,J.C., Bellusci,S., Perkins,D. & Hogan,B.L. Evidence for the involvement of the Gli gene family in embryonic mouse lung development. *Dev. Biol.* **188**, 337-348 (1997).

75. Hynes,M. *et al.* Induction of midbrain dopaminergic neurons by Sonic hedgehog. *Neuron* **15**, 35-44 (1995).

76. Lee,J., Platt,K.A., Censullo,P. & Altaba,A. Gli1 is a target of Sonic hedgehog that induces ventral neural tube development. *Development* **124**, 2537-2552 (1997).

77. Platt,K.A., Michaud,J. & Joyner,A.L. Expression of the mouse Gli and Ptc genes is adjacent to embryonic sources of hedgehog signals suggesting a conservation of pathways between flies and mice. *Mech. Dev.* **62**, 121-135 (1997).

78. Altaba,A. Combinatorial Gli gene function in floor plate and neuronal inductions by Sonic hedgehog. *Development* **125**, 2203-2212 (1998).

79. Dai,P. *et al.* Sonic Hedgehog-induced activation of the Gli1 promoter is mediated by GLI3. *J. Biol. Chem.* **274**, 8143-8152 (1999).

80. Sasaki,H., Nishizaki,Y., Hui,C., Nakafuku,M. & Kondoh,H. Regulation of Gli2 and Gli3 activities by an amino-terminal repression domain: implication of Gli2 and Gli3 as primary mediators of Shh signaling. *Development* **126**, 3915-3924 (1999).

81. Aza-Blanc,P., Lin,H.Y., Altaba,A. & Kornberg,T.B. Expression of the vertebrate Gli proteins in Drosophila reveals a distribution of activator and repressor activities. *Development* **127**, 4293-4301 (2000).

82. Brewster,R., Lee,J. & Altaba,A. Gli/Zic factors pattern the neural plate by defining domains of cell differentiation. *Nature* **393**, 579-583 (1998).

83. Buscher,D., Bosse,B., Heymer,J. & Ruther,U. Evidence for genetic control of Sonic hedgehog by Gli3 in mouse limb development. *Mech. Dev.* **62**, 175-182 (1997).

84. Park,H.L. *et al.* Mouse Gli1 mutants are viable but have defects in SHH signaling in combination with a Gli2 mutation. *Development* **127**, 1593-1605 (2000).

85. Mo,R. *et al.* Specific and redundant functions of Gli2 and Gli3 zinc finger genes in skeletal patterning and development. *Development* **124**, 113-123 (1997).

86. Motoyama,J. *et al.* Essential function of Gli2 and Gli3 in the formation of lung, trachea and oesophagus. *Nat. Genet.* **20**, 54-57 (1998).

87. Ding,Q. *et al.* Diminished Sonic hedgehog signaling and lack of floor plate differentiation in Gli2 mutant mice. *Development* **125**, 2533-2543 (1998).

88. Bai,C.B. & Joyner,A.L. Gli1 can rescue the in vivo function of Gli2. *Development* **128**, 5161-5172 (2001).

89. Franz,T. Extra-toes (Xt) homozygous mutant mice demonstrate a role for the Gli-3 gene in the development of the forebrain. *Acta Anat. (Basel)* **150**, 38-44 (1994).

90. Hui,C.C. & Joyner,A.L. A mouse model of greig cephalopolysyndactyly syndrome: the extra-toesJ mutation contains an intragenic deletion of the Gli3 gene. *Nat. Genet.* **3**, 241-246 (1993).

91. Chuang,P.T. & McMahon,A.P. Vertebrate Hedgehog signalling modulated by induction of a Hedgehog- binding protein. *Nature* **397**, 617-621 (1999).

92. Bellusci,S., Henderson,R., Winnier,G., Oikawa,T. & Hogan,B.L. Evidence from normal expression and targeted misexpression that bone morphogenetic protein (Bmp-4) plays a role in mouse embryonic lung morphogenesis. *Development* **122**, 1693-1702 (1996).

93. Urase,K. *et al.* Spatial expression of Sonic hedgehog in the lung epithelium during branching morphogenesis. *Biochem. Biophys. Res. Commun.* **225**, 161-166 (1996).

94. Pepicelli,C.V., Lewis,P.M. & McMahon,A.P. Sonic hedgehog regulates branching morphogenesis in the mammalian lung. *Curr. Biol.* **8**, 1083-1086 (1998).

95. Tsukui,T. *et al.* Multiple left-right asymmetry defects in Shh(-/-) mutant mice unveil a convergence of the shh and retinoic acid pathways in the control of Lefty-1. *Proc. Natl. Acad. Sci. U. S. A* **96**, 11376-11381 (1999).

96. Meyers,E.N. & Martin,G.R. Differences in left-right axis pathways in mouse and chick: functions of FGF8 and SHH. *Science* **285**, 403-406 (1999).

97. Goodrich,L.V., Milenkovic,L., Higgins,K.M. & Scott,M.P. Altered neural cell fates and medulloblastoma in mouse patched mutants. *Science* **277**, 1109-1113 (1997).

98. Theil,T., Kaesler,S., Grotewold,L., Bose,J. & Ruther,U. Gli genes and limb development. *Cell Tissue Res.* **296**, 75-83 (1999).

99. Winnier,G., Blessing,M., Labosky,P.A. & Hogan,B.L. Bone morphogenetic protein-4 is required for mesoderm formation and patterning in the mouse. *Genes Dev.* **9**, 2105-2116 (1995).

100. Weaver,M., Yingling,J.M., Dunn,N.R., Bellusci,S. & Hogan,B.L. Bmp signaling regulates proximal-distal differentiation of endoderm in mouse lung development. *Development* **126**, 4005-4015 (1999).

101. Sekine,K. *et al.* Fgf10 is essential for limb and lung formation. *Nat. Genet.* **21**, 138-141 (1999).

102. Min,H. *et al.* Fgf-10 is required for both limb and lung development and exhibits striking functional similarity to Drosophila branchless. *Genes Dev.* **12**, 3156-3161 (1998).

103. Arman,E., Haffner-Krausz,R., Gorivodsky,M. & Lonai,P. Fgfr2 is required for limb outgrowth and lung-branching morphogenesis. *Proc. Natl. Acad. Sci. U. S. A* **96**, 11895-11899 (1999).

104. Lebeche,D., Malpel,S. & Cardoso,W.V. Fibroblast growth factor interactions in the developing lung. *Mech. Dev.* **86**, 125-136 (1999).

105. Bellusci,S., Grindley,J., Emoto,H., Itoh,N. & Hogan,B.L. Fibroblast growth factor 10 (FGF10) and branching morphogenesis in the embryonic mouse lung. *Development* **124**, 4867-4878 (1997).

106. van Tuyl,M. & Post,M. From fruitflies to mammals: mechanisms of signalling via the Sonic hedgehog pathway in lung development. *Respir. Res.* **1**, 30-35 (2000).

107. Post,M. *et al.* Keratinocyte growth factor and its receptor are involved in regulating early lung branching. *Development* **122**, 3107-3115 (1996).

108. Guo,L., Degenstein,L. & Fuchs,E. Keratinocyte growth factor is required for hair development but not for wound healing. *Genes Dev.* **10**, 165-175 (1996).

109. Park,W.Y., Miranda,B., Lebeche,D., Hashimoto,G. & Cardoso,W.V. FGF-10 is a chemotactic factor for distal epithelial buds during lung development. *Dev. Biol.* **201**, 125-134 (1998).

110. Pelton,R.W., Dickinson,M.E., Moses,H.L. & Hogan,B.L. In situ hybridization analysis of TGF beta 3 RNA expression during mouse development: comparative studies with TGF beta 1 and beta 2. *Development* **110**, 609-620 (1990).

111. Zhao,Y. & Young,S.L. Expression of transforming growth factor-beta type II receptor in rat lung is regulated during development. *Am. J. Physiol* **269**, L419-L426 (1995).

112. Zhao,J. *et al.* Abrogation of transforming growth factor-beta type II receptor stimulates embryonic mouse lung branching morphogenesis in culture. *Dev. Biol.* **180**, 242-257 (1996).

113. Serra,R., Pelton,R.W. & Moses,H.L. TGF beta 1 inhibits branching morphogenesis and N-myc expression in lung bud organ cultures. *Development* **120**, 2153-2161 (1994).

114. Kaartinen,V. *et al.* Abnormal lung development and cleft palate in mice lacking TGF-beta 3 indicates defects of epithelial-mesenchymal interaction. *Nat. Genet.* **11**, 415-421 (1995).

115. Zhou,L., Dey,C.R., Wert,S.E. & Whitsett,J.A. Arrested lung morphogenesis in transgenic mice bearing an SP-C-TGF-beta 1 chimeric gene. *Dev. Biol.* **175**, 227-238 (1996).

116. Parisi,M.J. & Lin,H. The role of the hedgehog/patched signaling pathway in epithelial stem cell proliferation: from fly to human. *Cell Res.* **8**, 15-21 (1998).

117. Fujita,E. *et al.* Involvement of Sonic hedgehog in the cell growth of LK-2 cells, human lung squamous carcinoma cells. *Biochem. Biophys. Res. Commun.* **238**, 658-664 (1997).

118. Fan,H. & Khavari,P.A. Sonic hedgehog opposes epithelial cell cycle arrest. *J. Cell Biol.* **147**, 71-76 (1999).

119. Cobourne,M.T., Hardcastle,Z. & Sharpe,P.T. Sonic hedgehog regulates epithelial proliferation and cell survival in the developing tooth germ. *J. Dent. Res.* **80**, 1974-1979 (2001).

120. Sato,N., Leopold,P.L. & Crystal,R.G. Induction of the hair growth phase in postnatal mice by localized transient expression of Sonic hedgehog. *J. Clin. Invest* **104**, 855-864 (1999).

121. Outram,S.V., Varas,A., Pepicelli,C.V. & Crompton,T. Hedgehog signaling regulates differentiation from double-negative to double-positive thymocyte. *Immunity.* **13**, 187-197 (2000).

122. Ericson,J., Morton,S., Kawakami,A., Roelink,H. & Jessell,T.M. Two critical periods of Sonic Hedgehog signaling required for the specification of motor neuron identity. *Cell* **87**, 661-673 (1996).

123. Detmer,K., Walker,A.N., Jenkins,T.M., Steele,T.A. & Dannawi,H. Erythroid differentiation in vitro is blocked by cyclopamine, an inhibitor of hedgehog signaling. *Blood Cells Mol. Dis.* **26**, 360-372 (2000).

124. Incardona,J.P., Gaffield,W., Kapur,R.P. & Roelink,H. The teratogenic Veratrum alkaloid cyclopamine inhibits sonic hedgehog signal transduction. *Development* **125**, 3553-3562 (1998).

125. Bhardwaj,G. *et al.* Sonic hedgehog induces the proliferation of primitive human hematopoietic cells via BMP regulation. *Nat. Immunol.* **2**, 172-180 (2001).

126. Maeno,M. *et al.* The role of BMP-4 and GATA-2 in the induction and differentiation of hematopoietic mesoderm in Xenopus laevis. *Blood* **88**, 1965-1972 (1996).

127. Bhatia,M. *et al.* Bone morphogenetic proteins regulate the developmental program of human hematopoietic stem cells. *J. Exp. Med.* **189**, 1139-1148 (1999).

128. Dieterlen-Lievre,F., Godin,I. & Pardanaud,L. Where do hematopoietic stem cells come from? *Int. Arch. Allergy Immunol.* **112**, 3-8 (1997).

129. Roessler,E. *et al.* Mutations in the human Sonic Hedgehog gene cause holoprosencephaly. *Nat. Genet.* **14**, 357-360 (1996).

130. Chiang,C. *et al.* Cyclopia and defective axial patterning in mice lacking Sonic hedgehog gene function. *Nature* **383**, 407-413 (1996).

131. Kelley,R.L. *et al.* Holoprosencephaly in RSH/Smith-Lemli-Opitz syndrome: does abnormal cholesterol metabolism affect the function of Sonic Hedgehog? *Am. J. Med. Genet.* **66**, 478-484 (1996).

132. Xie,J. *et al.* Activating Smoothened mutations in sporadic basal-cell carcinoma. *Nature* **391**, 90-92 (1998).

133. Reifenberger,J. *et al.* Missense mutations in SMOH in sporadic basal cell carcinomas of the skin and primitive neuroectodermal tumors of the central nervous system. *Cancer Res.* **58**, 1798-1803 (1998).

134. Dahmane,N., Lee,J., Robins,P., Heller,P. & Altaba,A. Activation of the transcription factor Gli1 and the Sonic hedgehog signalling pathway in skin tumours. *Nature* **389**, 876-881 (1997).

135. Lench,N.J. *et al.* Characterisation of human patched germ line mutations in naevoid basal cell carcinoma syndrome. *Hum. Genet.* **100**, 497-502 (1997).

136. Hahn,H. *et al.* Rhabdomyosarcomas and radiation hypersensitivity in a mouse model of Gorlin syndrome. *Nat. Med.* **4**, 619-622 (1998).

137. Vortkamp,A., Gessler,M. & Grzeschik,K.H. GLI3 zinc-finger gene interrupted by translocations in Greig syndrome families. *Nature* **352**, 539-540 (1991).

138. Kang,S., Graham,J.M., Jr., Olney,A.H. & Biesecker,L.G. GLI3 frameshift mutations cause autosomal dominant Pallister-Hall syndrome. *Nat. Genet.* **15**, 266-268 (1997).

139. Radhakrishna,U., Wild,A., Grzeschik,K.H. & Antonarakis,S.E. Mutation in GLI3 in postaxial polydactyly type A. *Nat. Genet.* **17**, 269-271 (1997).

140. Petrij,F. *et al.* Rubinstein-Taybi syndrome caused by mutations in the transcriptional co-activator CBP. *Nature* **376**, 348-351 (1995).

141. Villavicencio,E.H., Walterhouse,D.O. & Iannaccone,P.M. The sonic hedgehog-patched-gli pathway in human development and disease. *Am. J. Hum. Genet.* **67**, 1047-1054 (2000).

142. Nusse,R. & Varmus,H.E. Many tumors induced by the mouse mammary tumor virus contain a provirus integrated in the same region of the host genome. *Cell* **31**, 99-109 (1982).

143. Cabrera,C.V., Alonso,M.C., Johnston,P., Phillips,R.G. & Lawrence,P.A. Phenocopies induced with antisense RNA identify the wingless gene. *Cell* **50**, 659-663 (1987).

144. Danielian,P.S. & McMahon,A.P. Engrailed-1 as a target of the Wnt-1 signalling pathway in vertebrate midbrain development. *Nature* **383**, 332-334 (1996).

145. Cadigan,K.M. & Nusse,R. Wnt signaling: a common theme in animal development. *Genes Dev.* **11**, 3286-3305 (1997).

146. Perrimon,N. The genetic basis of patterned baldness in Drosophila. *Cell* **76**, 781-784 (1994).

147. McMahon,A.P. & Moon,R.T. Ectopic expression of the proto-oncogene int-1 in Xenopus embryos leads to duplication of the embryonic axis. *Cell* **58**, 1075-1084 (1989).

148. Moon,R.T. *et al.* Xwnt-5A: a maternal Wnt that affects morphogenetic movements after overexpression in embryos of Xenopus laevis. *Development* **119**, 97-111 (1993).

149. He,X. *et al.* A member of the Frizzled protein family mediating axis induction by Wnt- 5A. *Science* **275**, 1652-1654 (1997).

150. Yamaguchi,T.P. Heads or tails: Wnts and anterior-posterior patterning. *Curr. Biol.* **11**, R713-R724 (2001).

151. Bhanot,P. *et al.* A new member of the frizzled family from Drosophila functions as a Wingless receptor. *Nature* **382**, 225-230 (1996).

152. Bhanot,P. *et al.* Frizzled and Dfrizzled-2 function as redundant receptors for Wingless during Drosophila embryonic development. *Development* **126**, 4175-4186 (1999).

153. Kennerdell,J.R. & Carthew,R.W. Use of dsRNA-mediated genetic interference to demonstrate that frizzled and frizzled 2 act in the wingless pathway. *Cell* **95**, 1017-1026 (1998).

154. Hsieh,J.C., Rattner,A., Smallwood,P.M. & Nathans,J. Biochemical characterization of Wnt-frizzled interactions using a soluble, biologically active vertebrate Wnt protein. *Proc. Natl. Acad. Sci. U. S. A* **96**, 3546-3551 (1999).

155. Perrimon,N. & Bernfield,M. Specificities of heparan sulphate proteoglycans in developmental processes. *Nature* **404**, 725-728 (2000).

156. Pinson,K.I., Brennan,J., Monkley,S., Avery,B.J. & Skarnes,W.C. An LDL-receptor-related protein mediates Wnt signalling in mice. *Nature* **407**, 535-538 (2000).

157. Tamai,K. *et al.* LDL-receptor-related proteins in Wnt signal transduction. *Nature* **407**, 530-535 (2000).

158. Wehrli,M. *et al.* arrow encodes an LDL-receptor-related protein essential for Wingless signalling. *Nature* **407**, 527-530 (2000).

159. Hoang,B., Moos,M., Jr., Vukicevic,S. & Luyten,F.P. Primary structure and tissue distribution of FRZB, a novel protein related to Drosophila frizzled, suggest a role in skeletal morphogenesis. *J. Biol. Chem.* **271**, 26131-26137 (1996).

160. Leyns,L., Bouwmeester,T., Kim,S.H., Piccolo,S. & De Robertis,E.M. Frzb-1 is a secreted antagonist of Wnt signaling expressed in the Spemann organizer. *Cell* **88**, 747-756 (1997).

161. Wang,S., Krinks,M. & Moos,M., Jr. Frzb-1, an antagonist of Wnt-1 and Wnt-8, does not block signaling by Wnts -3A, -5A, or -11. *Biochem. Biophys. Res. Commun.* **236**, 502-504 (1997).

162. Bradley,L. *et al.* Different activities of the frizzled-related proteins frzb2 and sizzled2 during Xenopus anteroposterior patterning. *Dev. Biol.* **227**, 118-132 (2000).

163. Pera,E.M. & De Robertis,E.M. A direct screen for secreted proteins in Xenopus embryos identifies distinct activities for the Wnt antagonists Crescent and Frzb-1. *Mech. Dev.* **96**, 183-195 (2000).

164. Hsieh,J.C. *et al.* A new secreted protein that binds to Wnt proteins and inhibits their activities. *Nature* **398**, 431-436 (1999).

165. Glinka,A., Wu,W., Onichtchouk,D., Blumenstock,C. & Niehrs,C. Head induction by simultaneous repression of Bmp and Wnt signalling in Xenopus. *Nature* **389**, 517-519 (1997).

166. Glinka,A. *et al.* Dickkopf-1 is a member of a new family of secreted proteins and functions in head induction. *Nature* **391**, 357-362 (1998).

167. Krupnik,V.E. *et al.* Functional and structural diversity of the human Dickkopf gene family. *Gene* **238**, 301-313 (1999).

168. Wu,W., Glinka,A., Delius,H. & Niehrs,C. Mutual antagonism between dickkopf1 and dickkopf2 regulates Wnt/beta- catenin signalling. *Curr. Biol.* **10**, 1611-1614 (2000).

169. Miller,J.R. & Moon,R.T. Signal transduction through beta-catenin and specification of cell fate during embryogenesis. *Genes Dev.* **10**, 2527-2539 (1996).

170. Miller,J.R., Hocking,A.M., Brown,J.D. & Moon,R.T. Mechanism and function of signal transduction by the Wnt/beta-catenin and Wnt/Ca2+ pathways. *Oncogene* **18**, 7860-7872 (1999).

171. Peifer,M., Sweeton,D., Casey,M. & Wieschaus,E. wingless signal and Zeste-white 3 kinase trigger opposing changes in the intracellular distribution of Armadillo. *Development* **120**, 369-380 (1994).

172. Siegfried,E., Chou,T.B. & Perrimon,N. wingless signaling acts through zeste-white 3, the Drosophila homolog of glycogen synthase kinase-3, to regulate engrailed and establish cell fate. *Cell* **71**, 1167-1179 (1992).

173. Siegfried,E., Wilder,E.L. & Perrimon,N. Components of wingless signalling in Drosophila. *Nature* **367**, 76-80 (1994).

174. Yost,C. *et al.* The axis-inducing activity, stability, and subcellular distribution of beta-catenin is regulated in Xenopus embryos by glycogen synthase kinase 3. *Genes Dev.* **10**, 1443-1454 (1996).

175. Behrens,J. *et al.* Functional interaction of an axin homolog, conductin, with beta- catenin, APC, and GSK3beta. *Science* **280**, 596-599 (1998).

176. Hart,M.J., de los,S.R., Albert,I.N., Rubinfeld,B. & Polakis,P. Downregulation of beta-catenin by human Axin and its association with the APC tumor suppressor, beta-catenin and GSK3 beta. *Curr. Biol.* **8**, 573-581 (1998).

177. Hsu,W., Zeng,L. & Costantini,F. Identification of a domain of Axin that binds to the serine/threonine protein phosphatase 2A and a self-binding domain. *J. Biol. Chem.* **274**, 3439-3445 (1999).

178. Yamamoto,H. *et al.* Axil, a member of the Axin family, interacts with both glycogen synthase kinase 3beta and beta-catenin and inhibits axis formation of Xenopus embryos. *Mol. Cell Biol.* **18**, 2867-2875 (1998).

179. Willert,K., Shibamoto,S. & Nusse,R. Wnt-induced dephosphorylation of axin releases beta-catenin from the axin complex. *Genes Dev.* **13**, 1768-1773 (1999).

180. Polakis,P. The adenomatous polyposis coli (APC) tumor suppressor. *Biochim. Biophys. Acta* **1332**, F127-F147 (1997).

181. Munemitsu,S., Albert,I., Souza,B., Rubinfeld,B. & Polakis,P. Regulation of intracellular beta-catenin levels by the adenomatous polyposis coli (APC) tumor-suppressor protein. *Proc. Natl. Acad. Sci. U. S. A* **92**, 3046-3050 (1995).

182. Vleminckx,K. *et al.* Adenomatous polyposis coli tumor suppressor protein has signaling activity in Xenopus laevis embryos resulting in the induction of an ectopic dorsoanterior axis. *J. Cell Biol.* **136**, 411-420 (1997).

183. Kitagawa,M. *et al.* An F-box protein, FWD1, mediates ubiquitin-dependent proteolysis of beta-catenin. *EMBO J.* **18**, 2401-2410 (1999).

184. Liu,C. *et al.* beta-Trcp couples beta-catenin phosphorylation-degradation and regulates Xenopus axis formation. *Proc. Natl. Acad. Sci. U. S. A* **96**, 6273-6278 (1999).

185. Orford,K., Crockett,C., Jensen,J.P., Weissman,A.M. & Byers,S.W. Serine phosphorylation-regulated ubiquitination and degradation of beta- catenin. *J. Biol. Chem.* **272**, 24735-24738 (1997).

186. Klingensmith,J., Nusse,R. & Perrimon,N. The Drosophila segment polarity gene dishevelled encodes a novel protein required for response to the wingless signal. *Genes Dev.* **8**, 118-130 (1994).

187. Yanagawa,S., van Leeuwen,F., Wodarz,A., Klingensmith,J. & Nusse,R. The dishevelled protein is modified by wingless signaling in Drosophila. *Genes Dev.* **9**, 1087-1097 (1995).

188. Axelrod,J.D., Matsuno,K., Artavanis-Tsakonas,S. & Perrimon,N. Interaction between Wingless and Notch signaling pathways mediated by dishevelled. *Science* **271**, 1826-1832 (1996).

189. Cadigan,K.M. & Nusse,R. wingless signaling in the Drosophila eye and embryonic epidermis. *Development* **122**, 2801-2812 (1996).

190. Kishida,S. *et al.* DIX domains of Dvl and axin are necessary for protein interactions and their ability to regulate beta-catenin stability. *Mol. Cell Biol.* **19**, 4414-4422 (1999).

191. Li,L. *et al.* Axin and Frat1 interact with dvl and GSK, bridging Dvl to GSK in Wnt- mediated regulation of LEF-1. *EMBO J.* **18**, 4233-4240 (1999).

192. Ruel,L., Stambolic,V., Ali,A., Manoukian,A.S. & Woodgett,J.R. Regulation of the protein kinase activity of Shaggy(Zeste-white3) by components of the wingless pathway in Drosophila cells and embryos. *J. Biol. Chem.* **274**, 21790-21796 (1999).

193. Yost,C. *et al.* GBP, an inhibitor of GSK-3, is implicated in Xenopus development and oncogenesis. *Cell* **93**, 1031-1041 (1998).

194. Cavallo,R., Rubenstein,D. & Peifer,M. Armadillo and dTCF: a marriage made in the nucleus. *Curr. Opin. Genet. Dev.* 7, 459-466 (1997).

195. Oosterwegel,M. *et al.* Cloning of murine TCF-1, a T cell-specific transcription factor interacting with functional motifs in the CD3-epsilon and T cell receptor alpha enhancers. *J. Exp. Med.* **173**, 1133-1142 (1991).

196. van de,W.M., Oosterwegel,M., Dooijes,D. & Clevers,H. Identification and cloning of TCF-1, a T lymphocyte-specific transcription factor containing a sequence-specific HMG box. *EMBO J.* **10**, 123-132 (1991).

197. Travis,A., Amsterdam,A., Belanger,C. & Grosschedl,R. LEF-1, a gene encoding a lymphoid-specific protein with an HMG domain, regulates T-cell receptor alpha enhancer function [corrected]. *Genes Dev.* **5**, 880-894 (1991).

198. van de,W.M. *et al.* Armadillo coactivates transcription driven by the product of the Drosophila segment polarity gene dTCF. *Cell* **88**, 789-799 (1997).

199. Brunner,E., Peter,O., Schweizer,L. & Basler,K. pangolin encodes a Lef-1 homologue that acts downstream of Armadillo to transduce the Wingless signal in Drosophila. *Nature* **385**, 829-833 (1997).

200. Cox,R.T., Pai,L.M., Kirkpatrick,C., Stein,J. & Peifer,M. Roles of the C terminus of Armadillo in Wingless signaling in Drosophila. *Genetics* **153**, 319-332 (1999).

201. Hecht,A., Litterst,C.M., Huber,O. & Kemler,R. Functional characterization of multiple transactivating elements in beta-catenin, some of which interact with the TATA-binding protein in vitro. *J. Biol. Chem.* **274**, 18017-18025 (1999).

202. Brannon,M., Gomperts,M., Sumoy,L., Moon,R.T. & Kimelman,D. A beta-catenin/XTcf-3 complex binds to the siamois promoter to regulate dorsal axis specification in Xenopus. *Genes Dev.* **11**, 2359-2370 (1997).

203. Riese,J. *et al.* LEF-1, a nuclear factor coordinating signaling inputs from wingless and decapentaplegic. *Cell* **88**, 777-787 (1997).

204. Cavallo,R.A. *et al.* Drosophila Tcf and Groucho interact to repress Wingless signalling activity. *Nature* **395**, 604-608 (1998).

205. Brannon,M., Brown,J.D., Bates,R., Kimelman,D. & Moon,R.T. XCtBP is a XTcf-3 co-repressor with roles throughout Xenopus development. *Development* **126**, 3159-3170 (1999).

206. Fan,M.J., Gruning,W., Walz,G. & Sokol,S.Y. Wnt signaling and transcriptional control of Siamois in Xenopus embryos. *Proc. Natl. Acad. Sci. U. S. A* **95**, 5626-5631 (1998).

207. Laurent,M.N., Blitz,I.L., Hashimoto,C., Rothbacher,U. & Cho,K.W. The Xenopus homeobox gene twin mediates Wnt induction of goosecoid in establishment of Spemann's organizer. *Development* **124**, 4905-4916 (1997).

208. McKendry,R., Hsu,S.C., Harland,R.M. & Grosschedl,R. LEF-1/TCF proteins mediate wnt-inducible transcription from the Xenopus nodal-related 3 promoter. *Dev. Biol.* **192**, 420-431 (1997).

209. He,T.C. *et al.* Identification of c-MYC as a target of the APC pathway. *Science* **281**, 1509-1512 (1998).

210. Shtutman,M. *et al.* The cyclin D1 gene is a target of the beta-catenin/LEF-1 pathway. *Proc. Natl. Acad. Sci. U. S. A* **96**, 5522-5527 (1999).

211. Tetsu,O. & McCormick,F. Beta-catenin regulates expression of cyclin D1 in colon carcinoma cells. *Nature* **398**, 422-426 (1999).

212. Crawford,H.C. *et al.* The metalloproteinase matrilysin is a target of beta-catenin transactivation in intestinal tumors. *Oncogene* **18**, 2883-2891 (1999).

213. Torres,M.A. *et al.* Activities of the Wnt-1 class of secreted signaling factors are antagonized by the Wnt-5A class and by a dominant negative cadherin in early Xenopus development. *J. Cell Biol.* **133**, 1123-1137 (1996).

214. Sheldahl,L.C., Park,M., Malbon,C.C. & Moon,R.T. Protein kinase C is differentially stimulated by Wnt and Frizzled homologs in a G-protein-dependent manner. *Curr. Biol.* **9**, 695-698 (1999).

215. Perrimon,N. & Mahowald,A.P. Multiple functions of segment polarity genes in Drosophila. *Dev. Biol.* **119**, 587-600 (1987).

216. Fahmy,O.G. & Fahmy,M. New mutants report. 33, 83-94. 1959. Drosophila Information Service.
Ref Type: Report

217. Boutros,M., Paricio,N., Strutt,D.I. & Mlodzik,M. Dishevelled activates JNK and discriminates between JNK pathways in planar polarity and wingless signaling. *Cell* **94**, 109-118 (1998).

218. Boutros,M. & Mlodzik,M. Dishevelled: at the crossroads of divergent intracellular signaling pathways. *Mech. Dev.* **83**, 27-37 (1999).

219. Sussman,D.J. *et al.* Isolation and characterization of a mouse homolog of the Drosophila segment polarity gene dishevelled. *Dev. Biol.* **166**, 73-86 (1994).

220. Klingensmith,J. *et al.* Conservation of dishevelled structure and function between flies and mice: isolation and characterization of Dvl2. *Mech. Dev.* **58**, 15-26 (1996).

221. Tsang,M. *et al.* Isolation and characterization of mouse dishevelled-3. *Dev. Dyn.* **207**, 253-262 (1996).

222. Zhang,Y., Neo,S.Y., Han,J. & Lin,S.C. Dimerization choices control the ability of axin and dishevelled to activate c-Jun N-terminal kinase/stress-activated protein kinase. *J. Biol. Chem.* **275**, 25008-25014 (2000).

223. Ponting,C.P. & Bork,P. Pleckstrin's repeat performance: a novel domain in G-protein signaling? *Trends Biochem. Sci.* **21**, 245-246 (1996).

224. Ponting,C.P., Phillips,C., Davies,K.E. & Blake,D.J. PDZ domains: targeting signalling molecules to sub-membranous sites. *Bioessays* **19**, 469-479 (1997).

225. Rothbacher,U. *et al.* Dishevelled phosphorylation, subcellular localization and multimerization regulate its role in early embryogenesis. *EMBO J.* **19**, 1010-1022 (2000).

226. Lijam,N. *et al.* Social interaction and sensorimotor gating abnormalities in mice lacking Dvl1. *Cell* **90**, 895-905 (1997).

227. Gavin,B.J., McMahon,J.A. & McMahon,A.P. Expression of multiple novel Wnt-1/int-1-related genes during fetal and adult mouse development. *Genes Dev.* **4**, 2319-2332 (1990).

228. Parr,B.A. & McMahon,A.P. Dorsalizing signal Wnt-7a required for normal polarity of D-V and A-P axes of mouse limb. *Nature* **374**, 350-353 (1995).

229. Levay-Young,B.K. & Navre,M. Growth and developmental regulation of wnt-2 (irp) gene in mesenchymal cells of fetal lung. *Am. J. Physiol* **262**, L672-L683 (1992).

230. Monkley,S.J., Delaney,S.J., Pennisi,D.J., Christiansen,J.H. & Wainwright,B.J. Targeted disruption of the Wnt2 gene results in placentation defects. *Development* **122** , 3343-3353 (1996).

231. Lako,M. *et al.* Isolation, characterisation and embryonic expression of WNT11, a gene which maps to 11q13.5 and has possible roles in the development of skeleton, kidney and lung. *Gene* **219**, 101-110 (1998).

232. McMahon,J.A. & McMahon,A.P. Nucleotide sequence, chromosomal localization and developmental expression of the mouse int-1-related gene. *Development* **107**, 643-650 (1989).

233. Zakin,L.D. *et al.* Structure and expression of Wnt13, a novel mouse Wnt2 related gene. *Mech. Dev.* **73**, 107-116 (1998).

234. Wang,J. & Shackleford,G.M. Murine Wnt10a and Wnt10b: cloning and expression in developing limbs, face and skin of embryos and in adults. *Oncogene* **13**, 1537-1544 (1996).

235. Katoh,M., Hirai,M., Sugimura,T. & Terada,M. Cloning, expression and chromosomal localization of Wnt-13, a novel member of the Wnt gene family. *Oncogene* **13**, 873-876 (1996).

236. Clark,C.C. *et al.* Molecular cloning of the human proto-oncogene Wnt-5A and mapping of the gene (WNT5A) to chromosome 3p14-p21. *Genomics* **18**, 249-260 (1993).

237. Ikegawa,S. *et al.* Isolation, characterization and chromosomal assignment of the human WNT7A gene. *Cytogenet. Cell Genet.* **74**, 149-152 (1996).

238. Reddy,S. *et al.* Characterization of Wnt gene expression in developing and postnatal hair follicles and identification of Wnt5a as a target of Sonic hedgehog in hair follicle morphogenesis. *Mech. Dev.* **107**, 69-82 (2001).

239. Lee,J.J., von Kessler,D.P., Parks,S. & Beachy,P.A. Secretion and localized transcription suggest a role in positional signaling for products of the segmentation gene hedgehog. *Cell* **71**, 33-50 (1992).

240. Crease,D.J., Dyson,S. & Gurdon,J.B. Cooperation between the activin and Wnt pathways in the spatial control of organizer gene expression. *Proc. Natl. Acad. Sci. U. S. A* **95**, 4398-4403 (1998).

241. Klein,T. & Arias,A.M. The vestigial gene product provides a molecular context for the interpretation of signals during the development of the wing in Drosophila. *Development* **126**, 913-925 (1999).

242. Attisano,L. & Wrana,J.L. Smads as transcriptional co-modulators. *Curr. Opin. Cell Biol.* **12**, 235-243 (2000).

243. Heldin,C.H., Miyazono,K. & ten Dijke,P. TGF-beta signalling from cell membrane to nucleus through SMAD proteins. *Nature* **390**, 465-471 (1997).

244. Nishita,M. *et al.* Interaction between Wnt and TGF-beta signalling pathways during formation of Spemann's organizer. *Nature* **403**, 781-785 (2000).

245. Letamendia,A., Labbe,E. & Attisano,L. Transcriptional regulation by Smads: crosstalk between the TGF-beta and Wnt pathways. *J. Bone Joint Surg. Am.* **83-A Suppl 1**, S31-S39 (2001).

246. Furuhashi,M. *et al.* Axin facilitates Smad3 activation in the transforming growth factor beta signaling pathway. *Mol. Cell Biol.* **21**, 5132-5141 (2001).

247. Takaku,K. *et al.* Intestinal tumorigenesis in compound mutant mice of both Dpc4 (Smad4) and Apc genes. *Cell* **92**, 645-656 (1998).

248. Wong,G.T., Gavin,B.J. & McMahon,A.P. Differential transformation of mammary epithelial cells by Wnt genes. *Mol. Cell Biol.* **14**, 6278-6286 (1994).

249. Bradley,R.S. & Brown,A.M. A soluble form of Wnt-1 protein with mitogenic activity on mammary epithelial cells. *Mol. Cell Biol.* **15**, 4616-4622 (1995).

250. Shimizu,H. *et al.* Transformation by Wnt family proteins correlates with regulation of beta-catenin. *Cell Growth Differ.* **8**, 1349-1358 (1997).

251. Young,C.S., Kitamura,M., Hardy,S. & Kitajewski,J. Wnt-1 induces growth, cytosolic beta-catenin, and Tcf/Lef transcriptional activation in Rat-1 fibroblasts. *Mol. Cell Biol.* **18**, 2474-2485 (1998).

252. Yamaguchi,T.P., Bradley,A., McMahon,A.P. & Jones,S. A Wnt5a pathway underlies outgrowth of multiple structures in the vertebrate embryo. *Development* **126**, 1211-1223 (1999).

253. Christiansen,J.H., Monkley,S.J. & Wainwright,B.J. Murine WNT11 is a secreted glycoprotein that morphologically transforms mammary epithelial cells. *Oncogene* **12**, 2705-2711 (1996).

254. Reya,T. *et al.* Wnt signaling regulates B lymphocyte proliferation through a LEF-1 dependent mechanism. *Immunity.* **13**, 15-24 (2000).

255. Chen,S. *et al.* Wnt-1 signaling inhibits apoptosis by activating beta-catenin/T cell factor-mediated transcription. *J. Cell Biol.* **152**, 87-96 (2001).

256. Orford,K., Orford,C.C. & Byers,S.W. Exogenous expression of beta-catenin regulates contact inhibition, anchorage-independent growth, anoikis, and radiation-induced cell cycle arrest. *J. Cell Biol.* **146**, 855-868 (1999).

257. Morin,P.J., Vogelstein,B. & Kinzler,K.W. Apoptosis and APC in colorectal tumorigenesis. *Proc. Natl. Acad. Sci. U. S. A* **93**, 7950-7954 (1996).

258. Ahmed,Y., Hayashi,S., Levine,A. & Wieschaus,E. Regulation of armadillo by a Drosophila APC inhibits neuronal apoptosis during retinal development. *Cell* **93**, 1171-1182 (1998).

259. Damalas,A. *et al.* Excess beta-catenin promotes accumulation of transcriptionally active p53. *EMBO J.* **18**, 3054-3063 (1999).

260. Wong,M.H., Rubinfeld,B. & Gordon,J.I. Effects of forced expression of an NH2-terminal truncated beta-Catenin on mouse intestinal epithelial homeostasis. *J. Cell Biol.* **141**, 765-777 (1998).

261. Kim,K., Pang,K.M., Evans,M. & Hay,E.D. Overexpression of beta-catenin induces apoptosis independent of its transactivation function with LEF-1 or the involvement of major G1 cell cycle regulators. *Mol. Biol. Cell* **11**, 3509-3523 (2000).

262. Strovel,E.T. & Sussman,D.J. Transient overexpression of murine dishevelled genes results in apoptotic cell death. *Exp. Cell Res.* **253**, 637-648 (1999).

263. Edwards,P.A., Hiby,S.E., Papkoff,J. & Bradbury,J.M. Hyperplasia of mouse mammary epithelium induced by expression of the Wnt-1 (int-1) oncogene in reconstituted mammary gland. *Oncogene* 7, 2041-2051 (1992).

264. Tsukamoto,A.S., Grosschedl,R., Guzman,R.C., Parslow,T. & Varmus,H.E. Expression of the int-1 gene in transgenic mice is associated with mammary gland hyperplasia and adenocarcinomas in male and female mice. *Cell* **55**, 619-625 (1988).

265. Brown,A.M., Wildin,R.S., Prendergast,T.J. & Varmus,H.E. A retrovirus vector expressing the putative mammary oncogene int-1 causes partial transformation of a mammary epithelial cell line. *Cell* **46**, 1001-1009 (1986).

266. Rijsewijk,F., van Deemter,L., Wagenaar,E., Sonnenberg,A. & Nusse,R. Transfection of the int-1 mammary oncogene in cuboidal RAC mammary cell line results in morphological transformation and tumorigenicity. *EMBO J.* **6**, 127-131 (1987).

267. Groden,J. *et al.* Identification and characterization of the familial adenomatous polyposis coli gene. *Cell* **66**, 589-600 (1991).

268. Nishisho,I. *et al.* Mutations of chromosome 5q21 genes in FAP and colorectal cancer patients. *Science* **253**, 665-669 (1991).

269. Miyoshi,Y. *et al.* Somatic mutations of the APC gene in colorectal tumors: mutation cluster region in the APC gene. *Hum. Mol. Genet.* **1**, 229-233 (1992).

270. Powell,S.M. *et al.* APC mutations occur early during colorectal tumorigenesis. *Nature* **359**, 235-237 (1992).

271. Alman,B.A., Li,C., Pajerski,M.E., Diaz-Cano,S. & Wolfe,H.J. Increased beta-catenin protein and somatic APC mutations in sporadic aggressive fibromatoses (desmoid tumors). *Am. J. Pathol.* **151**, 329-334 (1997).

272. Redston,M. *et al.* The APCI1307K allele and breast cancer risk. *Nat. Genet.* **20**, 13-14 (1998).

273. Imai,K. & D'Armiento,J. Activation of an embryonic gene product in pulmonary emphysema : identification of the secreted frizzled-related protein. *Chest* **117**, 229S (2000).

274. Imai,K. & D'Armiento,J. Differential gene expression of sFRP-1 and apoptosis in pulmonary emphysema. *Chest* **121**, 7S (2002).

275. Li,N., Wu,R. & Hao,C. [The research of pancadherin and beta-catenin expression in pulmonary tissue of mice with bleomycin-induced pulmonary fibrosis]. *Zhonghua Jie. He. He. Hu Xi. Za Zhi.* **24**, 599-601 (2001).

276. Li,W., Wu,R. & Li,N. [The role of beta-catenin in the repair of the damaged airway epithelium in smoking mice]. *Zhonghua Jie. He. He. Hu Xi. Za Zhi.* **24**, 481-483 (2001).

277. Hommura,F. *et al.* Increased expression of beta-catenin predicts better prognosis in nonsmall cell lung carcinomas. *Cancer* **94**, 752-758 (2002).

278. Coultas,D.B., Zumwalt,R.E., Black,W.C. & Sobonya,R.E. The epidemiology of interstitial lung diseases. *Am. J. Respir. Crit Care Med.* **150**, 967-972 (1994).

279. Mageto,Y.N. & Raghu,G. Genetic predisposition of idiopathic pulmonary fibrosis. *Curr. Opin. Pulm. Med.* **3**, 336-340 (1997).

280. Whyte,M. *et al.* Increased risk of fibrosing alveolitis associated with interleukin-1 receptor antagonist and tumor necrosis factor-alpha gene polymorphisms. *Am. J. Respir. Crit Care Med.* **162**, 755-758 (2000).

281. Hanley,M.E. *et al.* The impact of smoking on mechanical properties of the lungs in idiopathic pulmonary fibrosis and sarcoidosis. *Am. Rev. Respir. Dis.* **144**, 1102-1106 (1991).

282. Schwartz,D.A. *et al.* The influence of cigarette smoking on lung function in patients with idiopathic pulmonary fibrosis. *Am. Rev. Respir. Dis.* **144**, 504-506 (1991).

283. Turner-Warwick,M. In search of a cause of cryptogenic fibrosing alveolitis (CFA): one initiating factor or many? *Thorax* **53 Suppl 2**, S3-S9 (1998).

284. Ferri,C. *et al.* Interstitial lung fibrosis and rheumatic disorders in patients with hepatitis C virus infection. *Br. J. Rheumatol.* **36**, 360-365 (1997).

285. Egan,J.J., Woodcock,A.A. & Stewart,J.P. Viruses and idiopathic pulmonary fibrosis. *Eur. Respir. J.* **10**, 1433-1437 (1997).

286. Baumgartner,K.B. *et al.* Occupational and environmental risk factors for idiopathic pulmonary fibrosis: a multicenter case-control study. Collaborating Centers. *Am. J. Epidemiol.* **152**, 307-315 (2000).

287. Michaelson,J.E., Aguayo,S.M. & Roman,J. Idiopathic pulmonary fibrosis: a practical approach for diagnosis and management. *Chest* **118**, 788-794 (2000).

288. Turner-Warwick,M., Burrows,B. & Johnson,A. Cryptogenic fibrosing alveolitis: clinical features and their influence on survival. *Thorax* **35**, 171-180 (1980).

289. Crystal,R.G. *et al.* Idiopathic pulmonary fibrosis. Clinical, histologic, radiographic, physiologic, scintigraphic, cytologic, and biochemical aspects. *Ann. Intern. Med.* **85**, 769-788 (1976).

290. Renzi,G., Milic-Emili,J. & Grassino,A.E. The pattern of breathing in diffuse lung fibrosis. *Bull. Eur. Physiopathol. Respir.* **18**, 461-472 (1982).

291. Xaubet,A. *et al.* Pulmonary function tests and CT scan in the management of idiopathic pulmonary fibrosis. *Am. J. Respir. Crit Care Med.* **158**, 431-436 (1998).

292. Selman,M., King,T.E. & Pardo,A. Idiopathic pulmonary fibrosis: prevailing and evolving hypotheses about its pathogenesis and implications for therapy. *Ann. Intern. Med.* **134**, 136-151 (2001).

293. Wallace,W.A. & Lamb,D. Crytogenic fibrosing alveolitis: a clinico-pathological entity. 3, 27-34. 1996. Current Diagnostic Pathology.
Ref Type: Report

294. Yousem,S.A., Colby,T.V. & Gaensler,E.A. Respiratory bronchiolitis-associated interstitial lung disease and its relationship to desquamative interstitial pneumonia. *Mayo Clin. Proc.* **64**, 1373-1380 (1989).

295. Katzenstein,A.L., Myers,J.L. & Mazur,M.T. Acute interstitial pneumonia. A clinicopathologic, ultrastructural, and cell kinetic study. *Am. J. Surg. Pathol.* **10**, 256-267 (1986).

296. Katzenstein,A.L. & Fiorelli,R.F. Nonspecific interstitial pneumonia/fibrosis. Histologic features and clinical significance. *Am. J. Surg. Pathol.* **18**, 136-147 (1994).

297. Keogh,B.A. & Crystal,R.G. Alveolitis: the key to the interstitial lung disorders. *Thorax* **37**, 1-10 (1982).

298. Katzenstein,A.L. & Myers,J.L. Idiopathic pulmonary fibrosis: clinical relevance of pathologic classification. *Am. J. Respir. Crit Care Med.* **157**, 1301-1315 (1998).

299. Huaux,F. *et al.* Role of interleukin-10 in the lung response to silica in mice. *Am. J. Respir. Cell Mol. Biol.* **18**, 51-59 (1998).

300. Adamson,I.Y., Young,L. & Bowden,D.H. Relationship of alveolar epithelial injury and repair to the induction of pulmonary fibrosis. *Am. J. Pathol.* **130**, 377-383 (1988).

301. Haslam,P.L. *et al.* Bronchoalveolar lavage in pulmonary fibrosis: comparison of cells obtained with lung biopsy and clinical features. *Thorax* **35**, 9-18 (1980).

302. Watters,L.C. *et al.* Idiopathic pulmonary fibrosis. Pretreatment bronchoalveolar lavage cellular constituents and their relationships with lung histopathology and clinical response to therapy. *Am. Rev. Respir. Dis.* **135** , 696-704 (1987).

303. Line,B.R. *et al.* Gallium-67 citrate scanning in the staging of idiopathic pulmonary fibrosis: Correlation and physiologic and morphologic features and bronchoalveolar lavage. *Am. Rev. Respir. Dis.* **118**, 355-365 (1978).

304. Haslam,P.L. *et al.* Circulating immune complexes in patients with cryptogenic fibrosing alveolitis. *Clin. Exp. Immunol.* **37**, 381-390 (1979).

305. Mapel,D.W., Samet,J.M. & Coultas,D.B. Corticosteroids and the treatment of idiopathic pulmonary fibrosis. Past, present, and future. *Chest* **110**, 1058-1067 (1996).

306. Selman,M. *et al.* Colchicine, D-penicillamine, and prednisone in the treatment of idiopathic pulmonary fibrosis: a controlled clinical trial. *Chest* **114**, 507-512 (1998).

307. Douglas,W.W., Ryu,J.H. & Schroeder,D.R. Idiopathic pulmonary fibrosis: Impact of oxygen and colchicine, prednisone, or no therapy on survival. *Am. J. Respir. Crit Care Med.* **161**, 1172-1178 (2000).

308. Kasper,M. & Haroske,G. Alterations in the alveolar epithelium after injury leading to pulmonary fibrosis. *Histol. Histopathol.* **11**, 463-483 (1996).

309. McCormack,F.X. *et al.* Surfactant protein A predicts survival in idiopathic pulmonary fibrosis. *Am. J. Respir. Crit Care Med.* **152**, 751-759 (1995).

310. Burkhardt,A. Alveolitis and collapse in the pathogenesis of pulmonary fibrosis. *Am. Rev. Respir. Dis.* **140**, 513-524 (1989).

311. Chapman,H.A., Allen,C.L. & Stone,O.L. Abnormalities in pathways of alveolar fibrin turnover among patients with interstitial lung disease. *Am. Rev. Respir. Dis.* **133**, 437-443 (1986).

312. Kotani,I. *et al.* Increased procoagulant and antifibrinolytic activities in the lungs with idiopathic pulmonary fibrosis. *Thromb. Res.* 77, 493-504 (1995).

313. Imokawa,S. *et al.* Tissue factor expression and fibrin deposition in the lungs of patients with idiopathic pulmonary fibrosis and systemic sclerosis. *Am. J. Respir. Crit Care Med.* **156**, 631-636 (1997).

314. Antoniades,H.N. *et al.* Platelet-derived growth factor in idiopathic pulmonary fibrosis. *J. Clin. Invest* **86**, 1055-1064 (1990).

315. Kapanci,Y., Desmouliere,A., Pache,J.C., Redard,M. & Gabbiani,G. Cytoskeletal protein modulation in pulmonary alveolar myofibroblasts during idiopathic pulmonary fibrosis. Possible role of transforming growth factor beta and tumor necrosis factor alpha. *Am. J. Respir. Crit Care Med.* **152**, 2163-2169 (1995).

316. Khalil,N. *et al.* Increased production and immunohistochemical localization of transforming growth factor-beta in idiopathic pulmonary fibrosis. *Am. J. Respir. Cell Mol. Biol.* **5**, 155-162 (1991).

317. Kuhn,C. & McDonald,J.A. The roles of the myofibroblast in idiopathic pulmonary fibrosis. Ultrastructural and immunohistochemical features of sites of active extracellular matrix synthesis. *Am. J. Pathol.* **138**, 1257-1265 (1991).

318. Uhal,B.D. *et al.* Fibroblasts isolated after fibrotic lung injury induce apoptosis of alveolar epithelial cells in vitro. *Am. J. Physiol* **269**, L819-L828 (1995).

319. Uhal,B.D. *et al.* Alveolar epithelial cell death adjacent to underlying myofibroblasts in advanced fibrotic human lung. *Am. J. Physiol* **275** , L1192-L1199 (1998).

320. Raghu,G., Striker,L.J., Hudson,L.D. & Striker,G.E. Extracellular matrix in normal and fibrotic human lungs. *Am. Rev. Respir. Dis.* **131**, 281-289 (1985).

321. Selman,M. *et al.* TIMP-1, -2, -3, and -4 in idiopathic pulmonary fibrosis. A prevailing nondegradative lung microenvironment? *Am. J. Physiol Lung Cell Mol. Physiol* **279**, L562-L574 (2000).

322. Selman,M., Montano,M., Ramos,C. & Chapela,R. Concentration, biosynthesis and degradation of collagen in idiopathic pulmonary fibrosis. *Thorax* **41**, 355-359 (1986).

323. Crouch,E. Pathobiology of pulmonary fibrosis. *Am. J. Physiol* **259**, L159-L184 (1990).

324. Postlethwaite,A.E., Holness,M.A., Katai,H. & Raghow,R. Human fibroblasts synthesize elevated levels of extracellular matrix proteins in response to interleukin 4. *J. Clin. Invest* **90**, 1479-1485 (1992).

325. Gillery,P. *et al.* Interleukin-4 stimulates collagen gene expression in human fibroblast monolayer cultures. Potential role in fibrosis. *FEBS Lett.* **302**, 231-234 (1992).

326. Sempowski,G.D., Beckmann,M.P., Derdak,S. & Phipps,R.P. Subsets of murine lung fibroblasts express membrane-bound and soluble IL-4 receptors. Role of IL-4 in enhancing fibroblast proliferation and collagen synthesis. *J. Immunol.* **152**, 3606-3614 (1994).

327. Strieter,R.M. *et al.* Monocyte chemotactic protein gene expression by cytokine-treated human fibroblasts and endothelial cells. *Biochem. Biophys. Res. Commun.* **162**, 694-700 (1989).

328. Gharaee-Kermani,M., Denholm,E.M. & Phan,S.H. Costimulation of fibroblast collagen and transforming growth factor beta1 gene expression by monocyte chemoattractant protein-1 via specific receptors. *J. Biol. Chem.* **271**, 17779-17784 (1996).

329. Duncan,M.R. & Berman,B. Gamma interferon is the lymphokine and beta interferon the monokine responsible for inhibition of fibroblast collagen production and late but not early fibroblast proliferation. *J. Exp. Med.* **162**, 516-527 (1985).

330. Jaffe,H.A., Gao,Z., Mori,Y., Li,L. & Varga,J. Selective inhibition of collagen gene expression in fibroblasts by an interferon-gamma transgene. *Exp. Lung Res.* **25**, 199-215 (1999).

331. Diaz,A. & Jimenez,S.A. Interferon-gamma regulates collagen and fibronectin gene expression by transcriptional and post-transcriptional mechanisms. *Int. J. Biochem. Cell Biol.* **29**, 251-260 (1997).

332. Okamura,H., Kashiwamura,S., Tsutsui,H., Yoshimoto,T. & Nakanishi,K. Regulation of interferon-gamma production by IL-12 and IL-18. *Curr. Opin. Immunol.* **10**, 259-264 (1998).

333. Buttner,C. *et al.* Local production of interleukin-4 during radiation-induced pneumonitis and pulmonary fibrosis in rats: macrophages as a prominent source of interleukin-4. *Am. J. Respir. Cell Mol. Biol.* **17**, 315-325 (1997).

334. Gharaee-Kermani,M. & Phan,S.H. Lung interleukin-5 expression in murine bleomycin-induced pulmonary fibrosis. *Am. J. Respir. Cell Mol. Biol.* **16**, 438-447 (1997).

335. Zhang,K., Gharaee-Kermani,M., Jones,M.L., Warren,J.S. & Phan,S.H. Lung monocyte chemoattractant protein-1 gene expression in bleomycin- induced pulmonary fibrosis. *J. Immunol.* **153**, 4733-4741 (1994).

336. Gharaee-Kermani,M. *et al.* The role of IL-5 in bleomycin-induced pulmonary fibrosis. *J. Leukoc. Biol.* **64**, 657-666 (1998).

337. Smith,R.E. Chemotactic cytokines mediate leukocyte recruitment in fibrotic lung disease. *Biol. Signals* **5**, 223-231 (1996).

338. Davis,G.S., Pfeiffer,L.M. & Hemenway,D.R. Interferon-gamma production by specific lung lymphocyte phenotypes in silicosis in mice. *Am. J. Respir. Cell Mol. Biol.* **22**, 491-501 (2000).

339. Furuie,H., Yamasaki,H., Suga,M. & Ando,M. Altered accessory cell function of alveolar macrophages: a possible mechanism for induction of Th2 secretory profile in idiopathic pulmonary fibrosis. *Eur. Respir. J.* **10**, 787-794 (1997).

340. Atamas,S.P. *et al.* Production of type 2 cytokines by CD8+ lung cells is associated with greater decline in pulmonary function in patients with systemic sclerosis. *Arthritis Rheum.* **42**, 1168-1178 (1999).

341. Antoniades,H.N. *et al.* Expression of monocyte chemoattractant protein 1 mRNA in human idiopathic pulmonary fibrosis. *Proc. Natl. Acad. Sci. U. S. A* **89**, 5371-5375 (1992).

342. Suga,M. *et al.* Clinical significance of MCP-1 levels in BALF and serum in patients with interstitial lung diseases. *Eur. Respir. J.* **14**, 376-382 (1999).

343. Petkova,D. *et al.* Evaluation of CD30 as a marker for th2 lymphocytes in bronchoalveolar lavage in interstitial lung diseases. *Respir. Med.* **94**, 345-349 (2000).

344. Wallace,W.A., Ramage,E.A., Lamb,D. & Howie,S.E. A type 2 (Th2-like) pattern of immune response predominates in the pulmonary interstitium of patients with cryptogenic fibrosing alveolitis (CFA). *Clin. Exp. Immunol.* **101**, 436-441 (1995).

345. Shigehara,K. *et al.* Increased levels of interleukin-18 in patients with pulmonary sarcoidosis. *Am. J. Respir. Crit Care Med.* **162**, 1979-1982 (2000).

346. Kim,D.S. *et al.* The value of interleukin-12 as an activity marker of pulmonary sarcoidosis. *Sarcoidosis. Vasc. Diffuse. Lung Dis.* **17**, 271-276 (2000).

347. Minshall,E.M. *et al.* Cytokine mRNA gene expression in active and nonactive pulmonary sarcoidosis. *Eur. Respir. J.* **10**, 2034-2039 (1997).

348. Yamasaki,H., Ando,M., Brazer,W., Center,D.M. & Cruikshank,W.W. Polarized type 1 cytokine profile in bronchoalveolar lavage T cells of patients with hypersensitivity pneumonitis. *J. Immunol.* **163**, 3516-3523 (1999).

349. Letterio,J.J. & Roberts,A.B. TGF-beta: a critical modulator of immune cell function. *Clin. Immunol. Immunopathol.* **84**, 244-250 (1997).

350. Ziesche,R., Hofbauer,E., Wittmann,K., Petkov,V. & Block,L.H. A preliminary study of long-term treatment with interferon gamma-1b and low-dose prednisolone in patients with idiopathic pulmonary fibrosis. *N. Engl. J. Med.* **341**, 1264-1269 (1999).

351. Kelly,J. Cytokines of the Lung., pp. 101-1371993).

352. Desmouliere,A., Geinoz,A., Gabbiani,F. & Gabbiani,G. Transforming growth factor-beta 1 induces alpha-smooth muscle actin expression in granulation tissue myofibroblasts and in quiescent and growing cultured fibroblasts. *J. Cell Biol.* **122**, 103-111 (1993).

353. Phan,S.H. & Kunkel,S.L. Lung cytokine production in bleomycin-induced pulmonary fibrosis. *Exp. Lung Res.* **18**, 29-43 (1992).

354. Williams,A.O., Flanders,K.C. & Saffiotti,U. Immunohistochemical localization of transforming growth factor-beta 1 in rats with experimental silicosis, alveolar type II hyperplasia, and lung cancer. *Am. J. Pathol.* **142**, 1831-1840 (1993).

355. Rube,C.E. *et al.* Dose-dependent induction of transforming growth factor beta (TGF-beta) in the lung tissue of fibrosis-prone mice after thoracic irradiation. *Int. J. Radiat. Oncol. Biol. Phys.* **47**, 1033-1042 (2000).

356. Broekelmann,T.J., Limper,A.H., Colby,T.V. & McDonald,J.A. Transforming growth factor beta 1 is present at sites of extracellular matrix gene expression in human pulmonary fibrosis. *Proc. Natl. Acad. Sci. U. S. A* **88**, 6642-6646 (1991).

357. Jagirdar,J. *et al.* Immunohistochemical localization of transforming growth factor beta isoforms in asbestos-related diseases. *Environ. Health Perspect.* **105 Suppl 5**, 1197-1203 (1997).

358. Sime,P.J., Xing,Z., Graham,F.L., Csaky,K.G. & Gauldie,J. Adenovector-mediated gene transfer of active transforming growth factor- beta1 induces prolonged severe fibrosis in rat lung. *J. Clin. Invest* **100**, 768-776 (1997).

359. Gauldie,J., Kolb,M. & Sime,P.J. A new direction in the pathogenesis of idiopathic pumonary fibrosis? Respir.Res. 2002.
Ref Type: Electronic Citation

360. Splawski,J.B., Fu,S.M. & Lipsky,P.E. Immunoregulatory role of CD40 in human B cell differentiation. *J. Immunol.* **150**, 1276-1285 (1993).

361. Spriggs,M.K., Fanslow,W.C., Armitage,R.J. & Belmont,J. The biology of the human ligand for CD40. *J. Clin. Immunol.* **13**, 373-380 (1993).

362. Zhang,K., Clark,E.A. & Saxon,A. CD40 stimulation provides an IFN-gamma-independent and IL-4-dependent differentiation signal directly to human B cells for IgE production. *J. Immunol.* **146**, 1836-1842 (1991).

363. Fries,K.M. *et al.* CD40 expression by human fibroblasts. *Clin. Immunol. Immunopathol.* **77**, 42-51 (1995).

364. Mach,F. *et al.* Functional CD40 ligand is expressed on human vascular endothelial cells, smooth muscle cells, and macrophages: implications for CD40-CD40 ligand signaling in atherosclerosis. *Proc. Natl. Acad. Sci. U. S. A* **94**, 1931-1936 (1997).

365. Caux,C. *et al.* Activation of human dendritic cells through CD40 cross-linking. *J. Exp. Med.* **180**, 1263-1272 (1994).

366. Hollenbaugh,D. *et al.* Expression of functional CD40 by vascular endothelial cells. *J. Exp. Med.* **182**, 33-40 (1995).

367. Henn,V. *et al.* CD40 ligand on activated platelets triggers an inflammatory reaction of endothelial cells. *Nature* **391**, 591-594 (1998).

368. Zhang,Y. *et al.* CD40 engagement up-regulates cyclooxygenase-2 expression and prostaglandin E2 production in human lung fibroblasts. *J. Immunol.* **160**, 1053-1057 (1998).

369. Adawi,A. *et al.* Blockade of CD40-CD40 ligand interactions protects against radiation- induced pulmonary inflammation and fibrosis. *Clin. Immunol. Immunopathol.* **89**, 222-230 (1998).

370. Fireman,E. *et al.* Predictive value of response to treatment of T-lymphocyte subpopulations in idiopathic pulmonary fibrosis. *Eur. Respir. J.* **11**, 706-711 (1998).

371. Campbell,D.A., Poulter,L.W., Janossy,G. & du Bois,R.M. Immunohistological analysis of lung tissue from patients with cryptogenic fibrosing alveolitis suggesting local expression of immune hypersensitivity. *Thorax* **40**, 405-411 (1985).

372. Reynolds,H.Y. *et al.* Analysis of cellular and protein content of broncho-alveolar lavage fluid from patients with idiopathic pulmonary fibrosis and chronic hypersensitivity pneumonitis. *J. Clin. Invest* **59**, 165-175 (1977).

373. Weinberger,S.E. *et al.* Bronchoalveolar lavage in interstitial lung disease. *Ann. Intern. Med.* **89**, 459-466 (1978).

374. Wallace,W.A. *et al.* Circulating antibodies to lung protein(s) in patients with cryptogenic fibrosing alveolitis. *Thorax* **49**, 218-222 (1994).

375. Wallace,W.A., Schofield,J.A., Lamb,D. & Howie,S.E. Localisation of a pulmonary autoantigen in cryptogenic fibrosing alveolitis. *Thorax* **49**, 1139-1145 (1994).

376. Turner-Warwick,M., Burrows,B. & Johnson,A. Cryptogenic fibrosing alveolitis: response to corticosteroid treatment and its effect on survival. *Thorax* **35**, 593-599 (1980).

377. Johnson,M.A. *et al.* Randomised controlled trial comparing prednisolone alone with cyclophosphamide and low dose prednisolone in combination in cryptogenic fibrosing alveolitis. *Thorax* **44**, 280-288 (1989).

378. Ryu,J.H., Colby,T.V. & Hartman,T.E. Idiopathic pulmonary fibrosis: current concepts. *Mayo Clin. Proc.* **73**, 1085-1101 (1998).

379. Kolb,M., Kirschner,J., Riedel,W., Wirtz,H. & Schmidt,M. Cyclophosphamide pulse therapy in idiopathic pulmonary fibrosis. *Eur. Respir. J.* **12**, 1409-1414 (1998).

380. Dayton,C.S. *et al.* Outcome of subjects with idiopathic pulmonary fibrosis who fail corticosteroid therapy. Implications for further studies. *Chest* **103**, 69-73 (1993).

381. The Diffuse Parenchymal Lung Disease Group of the British Thoracic Society. The Diagnosis, Assessment and Treatment of Diffuse Parenchymal Lung Disease in Adults. *Thorax* **54**, (1999).

382. Nonn,R.A. & Garrity,E.R., Jr. Lung transplantation for fibrotic lung diseases. *Am. J. Med. Sci.* **315**, 146-154 (1998).

383. Gross,T.J. & Hunninghake,G.W. Idiopathic pulmonary fibrosis. *N. Engl. J. Med.* **345**, 517-525 (2001).

384. Douglas,W.W. *et al.* Colchicine versus prednisone in the treatment of idiopathic pulmonary fibrosis. A randomized prospective study. Members of the Lung Study Group. *Am. J. Respir. Crit Care Med.* **158**, 220-225 (1998).

385. Kehrer,J.P. & Margolin,S.B. Pirfenidone diminishes cyclophosphamide-induced lung fibrosis in mice. *Toxicol. Lett.* **90**, 125-132 (1997).

386. Raghu,G., Johnson,W.C., Lockhart,D. & Mageto,Y. Treatment of idiopathic pulmonary fibrosis with a new antifibrotic agent, pirfenidone: results of a prospective, open-label Phase II study. *Am. J. Respir. Crit Care Med.* **159**, 1061-1069 (1999).

387. Unemori,E.N. *et al.* Relaxin induces an extracellular matrix-degrading phenotype in human lung fibroblasts in vitro and inhibits lung fibrosis in a murine model in vivo. *J. Clin. Invest* **98**, 2739-2745 (1996).

388. Seibold,J.R. *et al.* Recombinant human relaxin in the treatment of scleroderma. A randomized, double-blind, placebo-controlled trial. *Ann. Intern. Med.* **132**, 871-879 (2000).

389. Mietz,H., Chevez-Barrios,P., Feldman,R.M. & Lieberman,M.W. Suramin inhibits wound healing following filtering procedures for glaucoma. *Br. J. Ophthalmol.* **82**, 816-820 (1998).

390. Park,S.H., Saleh,D., Giaid,A. & Michel,R.P. Increased endothelin-1 in bleomycin-induced pulmonary fibrosis and the effect of an endothelin receptor antagonist. *Am. J. Respir. Crit Care Med.* **156**, 600-608 (1997).

391. Marshall,R.P., McAnulty,R.J. & Laurent,G.J. Angiotensin II is mitogenic for human lung fibroblasts via activation of the type 1 receptor. *Am. J. Respir. Crit Care Med.* **161**, 1999-2004 (2000).

392. Behr,J., Maier,K., Degenkolb,B., Krombach,F. & Vogelmeier,C. Antioxidative and clinical effects of high-dose N-acetylcysteine in fibrosing alveolitis. Adjunctive therapy to maintenance immunosuppression. *Am. J. Respir. Crit Care Med.* **156**, 1897-1901 (1997).

393. Yi,E.S. *et al.* Keratinocyte growth factor ameliorates radia. *Am. J. Pathol.* **149**, 1963-1970 (1996).

394. Gurujeyalakshmi,G. & Giri,S.N. Molecular mechanisms of antifibrotic effect of interferon gamma in bleomycin-mouse model of lung fibrosis: downregulation of TGF-beta and procollagen I and III gene expression. *Exp. Lung Res.* **21**, 791-808 (1995).

395. Hein,R. *et al.* Treatment of systemic sclerosis with gamma-interferon. *Br. J. Dermatol.* **126**, 496-501 (1992).

396. Keane,M.P., Belperio,J.A., Arenburg,D.A., Burdick,M.D. & Strieter,R.M. IL-12 attenuates bleomycin-induced pulmonary fibrosis. 2000. Ref Type: Art Work

397. Giri,S.N., Hyde,D.M. & Hollinger,M.A. Effect of antibody to transforming growth factor beta on bleomycin induced accumulation of lung collagen in mice. *Thorax* **48**, 959-966 (1993).

398. Wang,Q. *et al.* Reduction of bleomycin induced lung fibrosis by transforming growth factor beta soluble receptor in hamsters. *Thorax* **54**, 805-812 (1999).

399. Yamaguchi,Y., Mann,D.M. & Ruoslahti,E. Negative regulation of transforming growth factor-beta by the proteoglycan decorin. *Nature* **346**, 281-284 (1990).

400. Kolb,M. *et al.* Transient transgene expression of decorin in the lung reduces the fibrotic response to bleomycin. *Am. J. Respir. Crit Care Med.* **163**, 770-777 (2001).

401. Bjoraker,J.A. *et al.* Prognostic significance of histopathologic subsets in idiopathic pulmonary fibrosis. *Am. J. Respir. Crit Care Med.* **157**, 199-203 (1998).

402. Gay,S.E. *et al.* Idiopathic pulmonary fibrosis: predicting response to therapy and survival. *Am. J. Respir. Crit Care Med.* **157**, 1063-1072 (1998).

403. Samet,J.M. Does idiopathic pulmonary fibrosis increase lung cancer risk? *Am. J. Respir. Crit Care Med.* **161**, 1-2 (2000).

404. Thrall,R.S., McCormick,J.R., Jack,R.M., McReynolds,R.A. & Ward,P.A. Bleomycin-induced pulmonary fibrosis in the rat: inhibition by indomethacin. *Am. J. Pathol.* **95**, 117-130 (1979).

405. Damiano,V.V. *et al.* Intraluminal fibrosis induced unilaterally by lobar instillation of CdCl2 into the rat lung. *Am. J. Pathol.* **137**, 883-894 (1990).

406. Stein-Streilein,J., Lipscomb,M.F., Fisch,H. & Whitney,P.L. Pulmonary interstitial fibrosis induced in hapten-immune hamsters. *Am. Rev. Respir. Dis.* **136**, 119-123 (1987).

407. Donaldson,K. *et al.* Contrasting bronchoalveolar leukocyte responses in rats inhaling coal mine dust, quartz, or titanium dioxide: effects of coal rank, airborne mass concentration, and cessation of exposure. *Environ. Res.* **52**, 62-76 (1990).

408. Roberts,S.N. *et al.* A novel model for human interstitial lung disease: hapten-driven lung fibrosis in rodents. *J. Pathol.* **176**, 309-318 (1995).

409. Christensen,P.J., Goodman,R.E., Pastoriza,L., Moore,B. & Toews,G.B. Induction of lung fibrosis in the mouse by intratracheal instillation of fluorescein isothiocyanate is not T-cell-dependent. *Am. J. Pathol.* **155**, 1773-1779 (1999).

410. Helene,M. *et al.* T cell independence of bleomycin-induced pulmonary fibrosis. *J. Leukoc. Biol.* **65**, 187-195 (1999).

411. Schrier,D.J. & Phan,S.H. Modulation of bleomycin-induced pulmonary fibrosis in the BALB/c mouse by cyclophosphamide-sensitive T cells. *Am. J. Pathol.* **116**, 270-278 (1984).

412. Schrier,D.J., Phan,S.H. & McGarry,B.M. The effects of the nude (nu/nu) mutation on bleomycin-induced pulmonary fibrosis. A biochemical evaluation. *Am. Rev. Respir. Dis.* **127**, 614-617 (1983).

413. Banchereau,J. & Steinman,R.M. Dendritic cells and the control of immunity. *Nature* **392**, 245-252 (1998).

414. Matzinger,P. Tolerance, danger, and the extended family. *Annu. Rev. Immunol.* **12**, 991-1045 (1994).

415. Turley,S.J. *et al.* Transport of peptide-MHC class II complexes in developing dendritic cells. *Science* **288**, 522-527 (2000).

416. Cella,M. *et al.* Maturation, activation, and protection of dendritic cells induced by double-stranded RNA. *J. Exp. Med.* **189**, 821-829 (1999).

417. Trinchieri,G. Interleukin-12: a cytokine at the interface of inflammation and immunity. *Adv. Immunol.* **70**, 83-243 (1998).

418. d'Ostiani,C.F. *et al.* Dendritic cells discriminate between yeasts and hyphae of the fungus Candida albicans. Implications for initiation of T helper cell immunity in vitro and in vivo. *J. Exp. Med.* **191**, 1661-1674 (2000).

419. Ingulli,E., Mondino,A., Khoruts,A. & Jenkins,M.K. In vivo detection of dendritic cell antigen presentation to CD4(+) T cells. *J. Exp. Med.* **185**, 2133-2141 (1997).

420. Kurts,C. *et al.* Constitutive class I-restricted exogenous presentation of self antigens in vivo. *J. Exp. Med.* **184**, 923-930 (1996).

421. Sallusto,F., Cella,M., Danieli,C. & Lanzavecchia,A. Dendritic cells use macropinocytosis and the mannose receptor to concentrate macromolecules in the major histocompatibility complex class II compartment: downregulation by cytokines and bacterial products. *J. Exp. Med.* **182**, 389-400 (1995).

422. Cella,M., Engering,A., Pinet,V., Pieters,J. & Lanzavecchia,A. Inflammatory stimuli induce accumulation of MHC class II complexes on dendritic cells. *Nature* **388**, 782-787 (1997).

423. Pierre,P. *et al.* Developmental regulation of MHC class II transport in mouse dendritic cells. *Nature* **388**, 787-792 (1997).

424. Albert,M.L., Sauter,B. & Bhardwaj,N. Dendritic cells acquire antigen from apoptotic cells and induce class I- restricted CTLs. *Nature* **392**, 86-89 (1998).

425. Valitutti,S., Dessing,M., Aktories,K., Gallati,H. & Lanzavecchia,A. Sustained signaling leading to T cell activation results from prolonged T cell receptor occupancy. Role of T cell actin cytoskeleton. *J. Exp. Med.* **181**, 577-584 (1995).

426. Valitutti,S. & Lanzavecchia,A. Serial triggering of TCRs: a basis for the sensitivity and specificity of antigen recognition. *Immunol. Today* **18**, 299-304 (1997).

427. Favero,J. & Lafont,V. Effector pathways regulating T cell activation. *Biochem. Pharmacol.* **56**, 1539-1547 (1998).

428. Baniyash,M., Garcia-Morales,P., Luong,E., Samelson,L.E. & Klausner,R.D. The T cell antigen receptor zeta chain is tyrosine phosphorylated upon activation. *J. Biol. Chem.* **263**, 18225-18230 (1988).

429. Osman,N., Turner,H., Lucas,S., Reif,K. & Cantrell,D.A. The protein interactions of the immunoglobulin receptor family tyrosine- based activation motifs present in the T cell receptor zeta subunits and the CD3 gamma, delta and epsilon chains. *Eur. J. Immunol.* **26**, 1063-1068 (1996).

430. Julius,M., Maroun,C.R. & Haughn,L. Distinct roles for CD4 and CD8 as co-receptors in antigen receptor signalling. *Immunol. Today* **14**, 177-183 (1993).

431. Parkin,J. & Cohen,B. An overview of the immune system. *Lancet* **357**, 1777-1789 (2001).

432. Gett,A.V. & Hodgkin,P.D. Cell division regulates the T cell cytokine repertoire, revealing a mechanism underlying immune class regulation. *Proc. Natl. Acad. Sci. U. S. A* **95**, 9488-9493 (1998).

433. Bird,J.J. *et al.* Helper T cell differentiation is controlled by the cell cycle. *Immunity.* **9**, 229-237 (1998).

434. Seder,R.A. & Paul,W.E. Acquisition of lymphokine-producing phenotype by CD4+ T cells. *Annu. Rev. Immunol.* **12**, 635-673 (1994).

435. Coffman,R.L. & Reiner,S.L. Instruction, selection, or tampering with the odds? *Science* **284**, 1283, 1285 (1999).

436. O'Garra,A. Cytokines induce the development of functionally heterogeneous T helper cell subsets. *Immunity.* **8**, 275-283 (1998).

437. Constant,S., Pfeiffer,C., Woodard,A., Pasqualini,T. & Bottomly,K. Extent of T cell receptor ligation can determine the functional differentiation of naive CD4+ T cells. *J. Exp. Med.* **182**, 1591-1596 (1995).

438. Kundig,T.M. *et al.* Duration of TCR stimulation determines costimulatory requirement of T cells. *Immunity.* **5**, 41-52 (1996).

439. Iezzi,G., Scotet,E., Scheidegger,D. & Lanzavecchia,A. The interplay between the duration of TCR and cytokine signaling determines T cell polarization. *Eur. J. Immunol.* **29**, 4092-4101 (1999).

440. Ledbetter,J.A. & Linsley,P.S. CD28 receptor crosslinking induces tyrosine phosphorylation of PLC gamma 1. *Adv. Exp. Med. Biol.* **323**, 23-27 (1992).

441. Mueller,D.L. T cells: A proliferation of costimulatory molecules. *Curr. Biol.* **10**, R227-R230 (2000).

442. Watts,T.H. & DeBenedette,M.A. T cell co-stimulatory molecules other than CD28. *Curr. Opin. Immunol.* **11**, 286-293 (1999).

443. June,C.H., Ledbetter,J.A., Linsley,P.S. & Thompson,C.B. Role of the CD28 receptor in T-cell activation. *Immunol. Today* **11**, 211-216 (1990).

444. June,C.H., Bluestone,J.A., Nadler,L.M. & Thompson,C.B. The B7 and CD28 receptor families. *Immunol. Today* **15**, 321-331 (1994).

445. Rudd,C.E. Upstream-downstream: CD28 cosignaling pathways and T cell function. *Immunity.* **4**, 527-534 (1996).

446. Lenschow,D.J., Walunas,T.L. & Bluestone,J.A. CD28/B7 system of T cell costimulation. *Annu. Rev. Immunol.* **14**, 233-258 (1996).

447. Hurwitz A.A. Cytotoxic Cells: Basic Mechanisms and Medical Applications. (1999).

448. McAdam,A.J., Schweitzer,A.N. & Sharpe,A.H. The role of B7 co-stimulation in activation and differentiation of CD4+ and CD8+ T cells. *Immunol. Rev.* **165**, 231-247 (1998).

449. Shahinian,A. *et al.* Differential T cell costimulatory requirements in CD28-deficient mice. *Science* **261**, 609-612 (1993).

450. Hutloff,A. *et al.* ICOS is an inducible T-cell co-stimulator structurally and functionally related to CD28. *Nature* **397**, 263-266 (1999).

451. Dong,C. *et al.* ICOS co-stimulatory receptor is essential for T-cell activation and function. *Nature* **409**, 97-101 (2001).

452. Tafuri,A. *et al.* ICOS is essential for effective T-helper-cell responses. *Nature* **409**, 105-109 (2001).

453. Swallow,M.M., Wallin,J.J. & Sha,W.C. B7h, a novel costimulatory homolog of B7.1 and B7.2, is induced by TNFalpha. *Immunity.* **11**, 423-432 (1999).

454. Yoshinaga,S.K. *et al.* Characterization of a new human B7-related protein: B7RP-1 is the ligand to the co-stimulatory protein ICOS. *Int. Immunol.* **12**, 1439-1447 (2000).

455. Aicher,A. *et al.* Characterization of human inducible costimulator ligand expression and function. *J. Immunol.* **164**, 4689-4696 (2000).

456. Thompson,C.B. & Allison,J.P. The emerging role of CTLA-4 as an immune attenuator. *Immunity.* **7**, 445-450 (1997).

457. Riley,J.L. *et al.* ICOS costimulation requires IL-2 and can be prevented by CTLA-4 engagement. *J. Immunol.* **166**, 4943-4948 (2001).

458. Carreno,B.M. *et al.* CTLA-4 (CD152) can inhibit T cell activation by two different mechanisms depending on its level of cell surface expression. *J. Immunol.* **165**, 1352-1356 (2000).

459. Marengere,L.E. *et al.* Regulation of T cell receptor signaling by tyrosine phosphatase SYP association with CTLA-4. *Science* **272**, 1170-1173 (1996).

460. Chuang,E. *et al.* The CD28 and CTLA-4 receptors associate with the serine/threonine phosphatase PP2A. *Immunity.* **13**, 313-322 (2000).

461. Mosmann,T.R., Cherwinski,H., Bond,M.W., Giedlin,M.A. & Coffman,R.L. Two types of murine helper T cell clone. I. Definition according to profiles of lymphokine activities and secreted proteins. *J. Immunol.* **136**, 2348-2357 (1986).

462. Mosmann,T.R. & Coffman,R.L. TH1 and TH2 cells: different patterns of lymphokine secretion lead to different functional properties. *Annu. Rev. Immunol.* 7, 145-173 (1989).

463. Allen,J.E. & Maizels,R.M. Th1-Th2: reliable paradigm or dangerous dogma? *Immunol. Today* **18**, 387-392 (1997).

464. Kerr,I.M. & Stark,G.R. The antiviral effects of the interferons and their inhibition. *J. Interferon Res.* **12**, 237-240 (1992).

465. Ullman,K.S., Northrop,J.P., Verweij,C.L. & Crabtree,G.R. Transmission of signals from the T lymphocyte antigen receptor to the genes responsible for cell proliferation and immune function: the missing link. *Annu. Rev. Immunol.* **8**, 421-452 (1990).

466. Chan,S.H. *et al.* Induction of interferon gamma production by natural killer cell stimulatory factor: characterization of the responder cells and synergy with other inducers. *J. Exp. Med.* **173**, 869-879 (1991).

467. Lotze,M.T., Frana,L.W., Sharrow,S.O., Robb,R.J. & Rosenberg,S.A. In vivo administration of purified human interleukin 2. I. Half-life and immunologic effects of the Jurkat cell line-derived interleukin 2. *J. Immunol.* **134**, 157-166 (1985).

468. Recht,M., Borden,E.C. & Knight,E., Jr. A human 15-kDa IFN-induced protein induces the secretion of IFN-gamma. *J. Immunol.* **147**, 2617-2623 (1991).

469. Farrar,M.A. & Schreiber,R.D. The molecular cell biology of interferon-gamma and its receptor. *Annu. Rev. Immunol.* **11**, 571-611 (1993).

470. Darnell,J.E., Jr., Kerr,I.M. & Stark,G.R. Jak-STAT pathways and transcriptional activation in response to IFNs and other extracellular signaling proteins. *Science* **264**, 1415-1421 (1994).

471. Ihle,J.N. STATs: signal transducers and activators of transcription. *Cell* **84**, 331-334 (1996).

472. Stark,G.R., Kerr,I.M., Williams,B.R., Silverman,R.H. & Schreiber,R.D. How cells respond to interferons. *Annu. Rev. Biochem.* **67**, 227-264 (1998).

473. Smith,K.A. Interleukin-2: inception, impact, and implications. *Science* **240**, 1169-1176 (1988).

474. Sadlack,B. *et al.* Ulcerative colitis-like disease in mice with a disrupted interleukin-2 gene. *Cell* **75**, 253-261 (1993).

475. Durand,D.B., Bush,M.R., Morgan,J.G., Weiss,A. & Crabtree,G.R. A 275 basepair fragment at the 5' end of the interleukin 2 gene enhances expression from a heterologous promoter in response to signals from the T cell antigen receptor. *J. Exp. Med.* **165**, 395-407 (1987).

476. Durand,D.B. *et al.* Characterization of antigen receptor response elements within the interleukin-2 enhancer. *Mol. Cell Biol.* **8**, 1715-1724 (1988).

477. Emmel,E.A. *et al.* Cyclosporin A specifically inhibits function of nuclear proteins involved in T cell activation. *Science* **246**, 1617-1620 (1989).

478. Verweij,C.L., Guidos,C. & Crabtree,G.R. Cell type specificity and activation requirements for NFAT-1 (nuclear factor of activated T-cells) transcriptional activity determined by a new method using transgenic mice to assay transcriptional activity of an individual nuclear factor. *J. Biol. Chem.* **265**, 15788-15795 (1990).

479. Yamaguchi,Y. *et al.* Purified interleukin 5 supports the terminal differentiation and proliferation of murine eosinophilic precursors. *J. Exp. Med.* **167**, 43-56 (1988).

480. Lopez,A.F. *et al.* Recombinant human interleukin 5 is a selective activator of human eosinophil function. *J. Exp. Med.* **167**, 219-224 (1988).

481. Bast,R.C. *et al.* Cancer Medicine. Bast,R.C. *et al.* (eds.) (BC Decker Inc,2000).

482. Sakamaki,K., Miyajima,I., Kitamura,T. & Miyajima,A. Critical cytoplasmic domains of the common beta subunit of the human GM- CSF, IL-3 and IL-5 receptors for growth signal transduction and tyrosine phosphorylation. *EMBO J.* **11**, 3541-3549 (1992).

483. Fiorentino,D.F., Bond,M.W. & Mosmann,T.R. Two types of mouse T helper cell. IV. Th2 clones secrete a factor that inhibits cytokine production by Th1 clones. *J. Exp. Med.* **170**, 2081-2095 (1989).

484. Fiorentino,D.F., Zlotnik,A., Mosmann,T.R., Howard,M. & O'Garra,A. IL-10 inhibits cytokine production by activated macrophages. *J. Immunol.* **147**, 3815-3822 (1991).

485. de Waal,M.R., Abrams,J., Bennett,B., Figdor,C.G. & de Vries,J.E. Interleukin 10(IL-10) inhibits cytokine synthesis by human monocytes: an autoregulatory role of IL-10 produced by monocytes. *J. Exp. Med.* **174**, 1209-1220 (1991).

486. del Prete,G. *et al.* Human IL-10 is produced by both type 1 helper (Th1) and type 2 helper (Th2) T cell clones and inhibits their antigen-specific proliferation and cytokine production. *J. Immunol.* **150**, 353-360 (1993).

487. Moore,K.W., O'Garra,A., de Waal,M.R., Vieira,P. & Mosmann,T.R. Interleukin-10. *Annu. Rev. Immunol.* **11**, 165-190 (1993).

488. Riffo-Vasquez,Y., Pitchford,S. & Spina,D. Cytokines in airway inflammation. *Int. J. Biochem. Cell Biol.* **32**, 833-853 (2000).

489. Enk,A.H., Saloga,J., Becker,D., madzadeh,M. & Knop,J. Induction of hapten-specific tolerance by interleukin 10 in vivo. *J. Exp. Med.* **179**, 1397-1402 (1994).

490. Groux,H. *et al.* A CD4+ T-cell subset inhibits antigen-specific T-cell responses and prevents colitis. *Nature* **389**, 737-742 (1997).

491. Steinbrink,K., Wolfl,M., Jonuleit,H., Knop,J. & Enk,A.H. Induction of tolerance by IL-10-treated dendritic cells. *J. Immunol.* **159**, 4772-4780 (1997).

492. Bellinghausen,I. *et al.* Inhibition of human allergic T-cell responses by IL-10-treated dendritic cells: differences from hydrocortisone-treated dendritic cells. *J. Allergy Clin. Immunol.* **108**, 242-249 (2001).

493. Moore,K.W., de Waal,M.R., Coffman,R.L. & O'Garra,A. Interleukin-10 and the interleukin-10 receptor. *Annu. Rev. Immunol.* **19**, 683-765 (2001).

494. Finbloom,D.S. & Winestock,K.D. IL-10 induces the tyrosine phosphorylation of tyk2 and Jak1 and the differential assembly of STAT1 alpha and STAT3 complexes in human T cells and monocytes. *J. Immunol.* **155**, 1079-1090 (1995).

495. Lai,C.F. *et al.* Receptors for interleukin (IL)-10 and IL-6-type cytokines use similar signaling mechanisms for inducing transcription through IL-6 response elements. *J. Biol. Chem.* **271**, 13968-13975 (1996).

496. Wehinger,J. *et al.* IL-10 induces DNA binding activity of three STAT proteins (Stat1, Stat3, and Stat5) and their distinct combinatorial assembly in the promoters of selected genes. *FEBS Lett.* **394**, 365-370 (1996).

497. Weber-Nordt,R.M. *et al.* Stat3 recruitment by two distinct ligand-induced, tyrosine-phosphorylated docking sites in the interleukin-10 receptor intracellular domain. *J. Biol. Chem.* **271**, 27954-27961 (1996).

498. Risso,A. *et al.* CD69 in resting and activated T lymphocytes. Its association with a GTP binding protein and biochemical requirements for its expression. *J. Immunol.* **146**, 4105-4114 (1991).

499. Marzio,R., Mauel,J. & Betz-Corradin,S. CD69 and regulation of the immune function. *Immunopharmacol. Immunotoxicol.* **21**, 565-582 (1999).

500. Ziegler,S.F., Ramsdell,F. & Alderson,M.R. The activation antigen CD69. *Stem Cells* **12**, 456-465 (1994).

501. Nakamura,S., Sung,S.S., Bjorndahl,J.M. & Fu,S.M. Human T cell activation. IV. T cell activation and proliferation via the early activation antigen EA 1. *J. Exp. Med.* **169**, 677-689 (1989).

502. Testi,R., Phillips,J.H. & Lanier,L.L. T cell activation via Leu-23 (CD69). *J. Immunol.* **143**, 1123-1128 (1989).

503. Testi,R., Pulcinelli,F., Frati,L., Gazzaniga,P.P. & Santoni,A. CD69 is expressed on platelets and mediates platelet activation and aggregation. *J. Exp. Med.* **172**, 701-707 (1990).

504. Testi,R. *et al.* Preferential involvement of a phospholipase A2-dependent pathway in CD69-mediated platelet activation. *J. Immunol.* **148**, 2867-2871 (1992).

505. Santis,A.G. *et al.* Tumor necrosis factor-alpha production induced in T lymphocytes through the AIM/CD69 activation pathway. *Eur. J. Immunol.* **22**, 1253-1259 (1992).

506. D'Ambrosio,D. *et al.* Transcriptional regulation of interleukin-2 gene expression by CD69-generated signals. *Eur. J. Immunol.* **23**, 2993-2997 (1993).

507. D'Ambrosio,D., Cantrell,D.A., Frati,L., Santoni,A. & Testi,R. Involvement of p21ras activation in T cell CD69 expression. *Eur. J. Immunol.* **24**, 616-620 (1994).

508. Hallberg,B., Rayter,S.I. & Downward,J. Interaction of Ras and Raf in intact mammalian cells upon extracellular stimulation. *J. Biol. Chem.* **269**, 3913-3916 (1994).

509. Nelson,B.H. & Willerford,D.M. Biology of the interleukin-2 receptor. *Adv. Immunol.* **70**, 1-81 (1998).

510. Willerford,D.M. *et al.* Interleukin-2 receptor alpha chain regulates the size and content of the peripheral lymphoid compartment. *Immunity.* **3**, 521-530 (1995).

511. Sharfe,N., Dadi,H.K., Shahar,M. & Roifman,C.M. Human immune disorder arising from mutation of the alpha chain of the interleukin-2 receptor. *Proc. Natl. Acad. Sci. U. S. A* **94**, 3168-3171 (1997).

512. John,S. *et al.* Regulation of cell-type-specific interleukin-2 receptor alpha-chain gene expression: potential role of physical interactions between Elf-1, HMG-I(Y), and NF-kappa B family proteins. *Mol. Cell Biol.* **15**, 1786-1796 (1995).

513. John,S., Robbins,C.M. & Leonard,W.J. An IL-2 response element in the human IL-2 receptor alpha chain promoter is a composite element that binds Stat5, Elf-1, HMG-I(Y) and a GATA family protein. *EMBO J.* **15**, 5627-5635 (1996).

514. Sperisen,P. *et al.* Mouse interleukin-2 receptor alpha gene expression. Interleukin-1 and interleukin-2 control transcription via distinct cis-acting elements. *J. Biol. Chem.* **270**, 10743-10753 (1995).

515. Cacalano,N.A. & Johnston,J.A. Interleukin-2 signaling and inherited immunodeficiency. *Am. J. Hum. Genet.* **65**, 287-293 (1999).

516. Nakajima,H. *et al.* An indirect effect of Stat5a in IL-2-induced proliferation: a critical role for Stat5a in IL-2-mediated IL-2 receptor alpha chain induction. *Immunity.* **7**, 691-701 (1997).

517. Shevach,E.M., McHugh,R.S., Piccirillo,C.A. & Thornton,A.M. Control of T-cell activation by CD4+ CD25+ suppressor T cells. *Immunol. Rev.* **182**, 58-67 (2001).

518. Read,S. & Powrie,F. CD4(+) regulatory T cells. *Curr. Opin. Immunol.* **13**, 644-649 (2001).

519. Papiernik,M. Natural CD4+ CD25+ regulatory T cells. Their role in the control of superantigen responses. *Immunol. Rev.* **182**, 180-189 (2001).

520. Thornton,A.M. & Shevach,E.M. CD4+CD25+ immunoregulatory T cells suppress polyclonal T cell activation in vitro by inhibiting interleukin 2 production. *J. Exp. Med.* **188**, 287-296 (1998).

521. Gilboa,E. Retroviral gene transfer: applications to human therapy. *Prog. Clin. Biol. Res.* **352**, 301-311 (1990).

522. Miller,A.D. Retroviral vectors. *Curr. Top. Microbiol. Immunol.* **158**, 1-24 (1992).

523. Miller,D.G., Adam,M.A. & Miller,A.D. Gene transfer by retrovirus vectors occurs only in cells that are actively replicating at the time of infection. *Mol. Cell Biol.* **10**, 4239-4242 (1990).

524. Kaplan,J.M. *et al.* Characterization of factors involved in modulating persistence of transgene expression from recombinant adenovirus in the mouse lung. *Hum. Gene Ther.* **8**, 45-56 (1997).

525. Schofield,J.P. & Caskey,C.T. Non-viral approaches to gene therapy. *Br. Med. Bull.* **51**, 56-71 (1995).

526. Glasser,S.W., Korfhagen,T.R., Wert,S.E. & Whitsett,J.A. Transgenic models for study of pulmonary development and disease. *Am. J. Physiol* **267**, L489-L497 (1994).

527. Strayer,M.S., Guttentag,S.H. & Ballard,P.L. Targeting type II and Clara cells for adenovirus-mediated gene transfer using the surfactant protein B promoter. *Am. J. Respir. Cell Mol. Biol.* **18**, 1-11 (1998).

528. Kistner,A. *et al.* Doxycycline-mediated quantitative and tissue-specific control of gene expression in transgenic mice. *Proc. Natl. Acad. Sci. U. S. A* **93**, 10933-10938 (1996).

529. No,D., Yao,T.P. & Evans,R.M. Ecdysone-inducible gene expression in mammalian cells and transgenic mice. *Proc. Natl. Acad. Sci. U. S. A* **93**, 3346-3351 (1996).

530. Parks,R.J. *et al.* A helper-dependent adenovirus vector system: removal of helper virus by Cre-mediated excision of the viral packaging signal. *Proc. Natl. Acad. Sci. U. S. A* **93**, 13565-13570 (1996).

531. Fisher,K.J., Choi,H., Burda,J., Chen,S.J. & Wilson,J.M. Recombinant adenovirus deleted of all viral genes for gene therapy of cystic fibrosis. *Virology* **217**, 11-22 (1996).

532. Mitani,K., Graham,F.L., Caskey,C.T. & Kochanek,S. Rescue, propagation, and partial purification of a helper virus- dependent adenovirus vector. *Proc. Natl. Acad. Sci. U. S. A* **92**, 3854-3858 (1995).

533. Schiedner,G. *et al.* Genomic DNA transfer with a high-capacity adenovirus vector results in improved in vivo gene expression and decreased toxicity. *Nat. Genet.* **18**, 180-183 (1998).

534. Yang,Y., Trinchieri,G. & Wilson,J.M. Recombinant IL-12 prevents formation of blocking IgA antibodies to recombinant adenovirus and allows repeated gene therapy to mouse lung. *Nat. Med.* **1**, 890-893 (1995).

535. Wilson,C. & Kay,M.A. Immunomodulation to enhance gene therapy. *Nat. Med.* **1**, 887-889 (1995).

536. Wilson,C.B. *et al.* Transient inhibition of CD28 and CD40 ligand interactions prolongs adenovirus-mediated transgene expression in the lung and facilitates expression after secondary vector administration. *J. Virol.* **72** , 7542-7550 (1998).

537. Ilan,Y. *et al.* Oral tolerization to adenoviral antigens permits long-term gene expression using recombinant adenoviral vectors. *J. Clin. Invest* **99**, 1098-1106 (1997).

538. Zsengeller,Z.K. *et al.* Anti-T cell receptor antibody prolongs transgene expression and reduces lung inflammation after adenovirus-mediated gene transfer. *Hum. Gene Ther.* **8**, 935-941 (1997).

539. Jooss,K., Turka,L.A. & Wilson,J.M. Blunting of immune responses to adenoviral vectors in mouse liver and lung with CTLA4Ig. *Gene Ther.* **5**, 309-319 (1998).

540. Bergelson,J.M. *et al.* Isolation of a common receptor for Coxsackie B viruses and adenoviruses 2 and 5. *Science* **275**, 1320-1323 (1997).

541. Tomko,R.P., Xu,R. & Philipson,L. HCAR and MCAR: the human and mouse cellular receptors for subgroup C adenoviruses and group B coxsackieviruses. *Proc. Natl. Acad. Sci. U. S. A* **94**, 3352-3356 (1997).

542. Bai,M., Harfe,B. & Freimuth,P. Mutations that alter an Arg-Gly-Asp (RGD) sequence in the adenovirus type 2 penton base protein abolish its cell-rounding activity and delay virus reproduction in flat cells. *J. Virol.* **67**, 5198-5205 (1993).

543. Wickham,T.J., Mathias,P., Cheresh,D.A. & Nemerow,G.R. Integrins alpha v beta 3 and alpha v beta 5 promote adenovirus internalization but not virus attachment. *Cell* **73**, 309-319 (1993).

544. Wickham,T.J., Filardo,E.J., Cheresh,D.A. & Nemerow,G.R. Integrin alpha v beta 5 selectively promotes adenovirus mediated cell membrane permeabilization. *J. Cell Biol.* **127**, 257-264 (1994).

545. Mizuguchi,H., Kay,M.A. & Hayakawa,T. Approaches for generating recombinant adenovirus vectors. *Adv. Drug Deliv. Rev.* **52**, 165-176 (2001).

546. Bett,A.J., Haddara,W., Prevec,L. & Graham,F.L. An efficient and flexible system for construction of adenovirus vectors with insertions or deletions in early regions 1 and 3. *Proc. Natl. Acad. Sci. U. S. A* **91**, 8802-8806 (1994).

547. Graham,F.L., Smiley,J., Russell,W.C. & Nairn,R. Characteristics of a human cell line transformed by DNA from human adenovirus type 5. *J. Gen. Virol.* **36**, 59-74 (1977).

548. Bett,A.J., Prevec,L. & Graham,F.L. Packaging capacity and stability of human adenovirus type 5 vectors. *J. Virol.* **67**, 5911-5921 (1993).

549. Xing,Z., Ohkawara,Y., Jordana,M., Graham,F. & Gauldie,J. Transfer of granulocyte-macrophage colony-stimulating factor gene to rat lung induces eosinophilia, monocytosis, and fibrotic reactions. *J. Clin. Invest* **97**, 1102-1110 (1996).

550. Sallenave,J.M., Xing,Z., Simpson,A.J., Graham,F.L. & Gauldie,J. Adenovirus-mediated expression of an elastase-specific inhibitor (elafin): a comparison of different promoters. *Gene Ther.* **5**, 352-360 (1998).

551. Ashcroft,T., Simpson,J.M. & Timbrell,V. Simple method of estimating severity of pulmonary fibrosis on a numerical scale. *J. Clin. Pathol.* **41**, 467-470 (1988).

552. Higuchi,R., Dollinger,G., Walsh,P.S. & Griffith,R. Simultaneous amplification and detection of specific DNA sequences. *Biotechnology (N. Y.)* **10**, 413-417 (1992).

553. Holland,P.M., Abramson,R.D., Watson,R. & Gelfand,D.H. Detection of specific polymerase chain reaction product by utilizing the 5'----3' exonuclease activity of Thermus aquaticus DNA polymerase. *Proc. Natl. Acad. Sci. U. S. A* **88**, 7276-7280 (1991).

554. Meyer,K.B., Thompson,M.M., Levy,M.Y., Barron,L.G. & Szoka,F.C., Jr. Intratracheal gene delivery to the mouse airway: characterization of plasmid DNA expression and pharmacokinetics. *Gene Ther.* **2**, 450-460 (1995).

555. Curiel,D.T., Pilewski,J.M. & Albelda,S.M. Gene therapy approaches for inherited and acquired lung diseases. *Am. J. Respir. Cell Mol. Biol.* **14**, 1-18 (1996).

556. Stewart,G.A. *et al.* Sonic hedgehog signaling modulates activation of and cytokine production by human peripheral CD4(+) T cells. *J. Immunol.* **169**, 5451-5457 (2002).

557. Chtanova,T., Kemp,R.A., Sutherland,A.P., Ronchese,F. & Mackay,C.R. Gene microarrays reveal extensive differential gene expression in both CD4(+) and CD8(+) type 1 and type 2 T cells. *J. Immunol.* **167**, 3057-3063 (2001).

558. Granucci,F., Vizzardelli,C., Virzi,E., Rescigno,M. & Ricciardi-Castagnoli,P. Transcriptional reprogramming of dendritic cells by differentiation stimuli. *Eur. J. Immunol.* **31**, 2539-2546 (2001).

559. Charrier,J.B., Lapointe,F., Le Douarin,N.M. & Teillet,M.A. Anti-apoptotic role of Sonic hedgehog protein at the early stages of nervous system organogenesis. *Development* **128**, 4011-4020 (2001).

560. Britto,J.M., Tannahill,D. & Keynes,R.J. Life, death and Sonic hedgehog. *Bioessays* **22**, 499-502 (2000).

561. Fan,H., Oro,A.E., Scott,M.P. & Khavari,P.A. Induction of basal cell carcinoma features in transgenic human skin expressing Sonic Hedgehog. *Nat. Med.* **3**, 788-792 (1997).

562. Jain,J., Loh,C. & Rao,A. Transcriptional regulation of the IL-2 gene. *Curr. Opin. Immunol.* 7, 333-342 (1995).

563. Cantrell,D. T cell antigen receptor signal transduction pathways. *Annu. Rev. Immunol.* **14**, 259-274 (1996).

564. Sloan-Lancaster,J. & Allen,P.M. Altered peptide ligand-induced partial T cell activation: molecular mechanisms and role in T cell biology. *Annu. Rev. Immunol.* **14**, 1-27 (1996).

565. Kenney,A.M. & Rowitch,D.H. Sonic hedgehog promotes G(1) cyclin expression and sustained cell cycle progression in mammalian neuronal precursors. *Mol. Cell Biol.* **20** , 9055-9067 (2000).

566. Gradl,D., Kuhl,M. & Wedlich,D. The Wnt/Wg signal transducer beta-catenin controls fibronectin expression. *Mol. Cell Biol.* **19**, 5576-5587 (1999).

567. Wagner,U. *et al.* Overexpression of the mouse dishevelled-1 protein inhibits GSK-3beta-mediated phosphorylation of tau in transfected mammalian cells. *FEBS Lett.* **411**, 369-372 (1997).

568. Xing,Z. *et al.* Adenovirus-mediated cytokine gene transfer at tissue sites. Overexpression of IL-6 induces lymphocytic hyperplasia in the lung. *J. Immunol.* **153**, 4059-4069 (1994).

569. Baecher-Allan,C.M. & Barth,R.K. PCR analysis of cytokine induction profiles associated with mouse strain variation in susceptibility to pulmonary fibrosis. *Reg Immunol.* **5**, 207-217 (1993).

570. McBride,S. *et al.* Characterisation of lectin binding patterns of mouse bronchiolar and rat alveolar epithelial cells in culture. *Histochem. J.* **32**, 33-40 (2000).